CHAPTER 1
INTRODUCTION

1.1 Description of Column-Supported Embankments

Infrastructure renewal projects often require placement of roadway embankments on soft, compressible ground. Several options are available for controlling stability and mitigating settlement problems. One option is to provide columnar support through the soft ground. This technique is especially useful when the allowable construction time is short and when applying embankment loads to the soft ground would induce damage to other facilities, such as existing adjacent embankments. Three classifications of columnar foundations include (Han and Wayne 2000):

- flexible columns (such as stone columns and lime columns),
- semi-rigid columns (such as lime-cement and soil-cement columns constructed by deep mixing or grouting), and
- rigid piles (such as concrete piles, timber piles, and vibro-concrete piles).

The columns are installed at a spacing determined by the design engineer, with lower costs for construction of the columns if they are widely spaced. Columns are typically spaced in a square or triangular pattern, and may or may not have caps. When the columns are lime-cement or soil-cement or stone columns, they typically have large enough diameters that no caps are needed in most cases. A geosynthetic-reinforced bridging layer, also know as a load-transfer platform, is often provided to transfer embankment and traffic loads to widely spaced columns. Geosynthetic reinforcement is installed within the bridging layer to increase the load transfer to the columns and reduce the required area replacement ratio of the columns (Lawson 1992, Russell & Pierpoint 1997, Kempton et al. 1998, , Han and Wayne 2000, Han and Gabr 2002). The bridging layer consists of several feet of compacted sand or sand and gravel, and it may include geosynthetic reinforcement. The geosynthetic reinforcement consists of one or more layers of planar polymeric material, typically a woven geotextile or, more often, a geogrid. A schematic of a geosynthetic-reinforced column-supported embankment is shown in Figure 1.1.

Geosynthetic-reinforced column-supported embankments are in widespread use in Japan, the United Kingdom, and Scandinavia, and they are becoming more common in the U.S. and other

countries. The geosynthetic-reinforced column-supported embankment technology has potential application at many soft-ground sites, including coastal areas where existing embankments are being widened and new embankments are being constructed.

The scope of this research is limited to embankments supported on lime-cement columns, soil-cement columns, and driven piles, though the results of the research may prove applicable to other columnar foundation systems. The term "column" used herein refers not only to columns installed by various soil improvement techniques, such as the deep soil mixing method, but also to conventional driven piles.

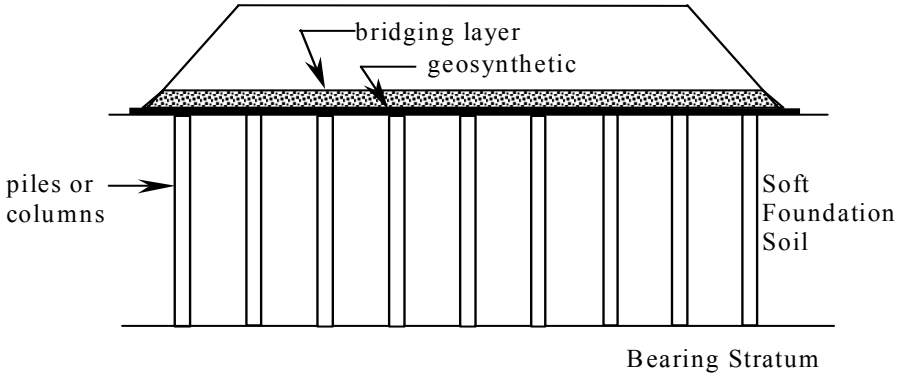

Figure 1.1. Schematic of pile-supported embankment with geosynthetic reinforcement

1.2 Need for Research on Column-Supported Embankments

Current methods used to calculate the settlements of lime-cement and soil-cement columns are empirical and based on simplified assumptions regarding the column-soil interaction. For simplicity, an "equal strain" method is often used to proportion the load between the soft clay and the columns when geosynthetic reinforcement is not used and the columns are lime-cement columns, or soil-cement columns (Broms 1999, Kaiqiu 2000; CDIT 2002). The equal strain method is not rational because it is not compatible with the requirement for the differential settlements that are necessary to mobilize stress concentrations in deformable materials and structures above the columns. Correct evaluation of the stress concentration to the columns is necessary for calculating settlements.

Several different methods exist for calculating the magnitude of loads applied to geosynthetic reinforcement in bridging layers for column-supported embankments. These methods take into account such factors as the column or pile cap size, column spacing, embankment height, embankment unit weight, and embankment friction angle. These methods produce loads that differ by an order of magnitude or more for typical examples. Furthermore, only two of these methods attempt to account for the compressibility of the soft ground between the columns, and the approaches taken are not well developed. Consequently, research is needed to improve the state of knowledge so that reliable and cost-effective geosynthetic-reinforced bridging layers can be designed using simple and practical methodology.

1.3 Objectives and Scope of Research

The primary purpose of this research is to develop a set of consistent and reliable procedures that geotechnical engineers can use to design bridging layers in column-supported geosynthetic-reinforced embankments. The specific issues addressed by this research are settlement and load transfer in the bridging layer.

The scope of the research included completing the following tasks:

(a) Perform a literature review and evaluate currently available design methods

An extensive literature review was performed to compile information on the applications and limitations, installation procedures, typical laboratory and field material properties, and current design methods of deep mixing method foundation systems. A literature review was also performed to compile information on load transfer mechanisms and the currently available methods of designing the geosynthetic-reinforced bridging layer.

(b) Verify numerical modeling methods

The numerical analyses performed within the scope of this research consisted of two- and three-dimensional finite difference analyses performed using FLAC3D and FLAC (ITASCA 2002a, ITASCA 2002b). Verification analyses were performed using FLAC3D, FLAC and the finite element program, SAGE (Bentler et al. 1999). The numerical modeling procedures were verified against instrumentation data from a full-

scale column-supported test embankment at the I-95/ Route 1 Interchange Project in Alexandria, Virginia. The numerical procedures were also verified against closed-form solutions for membranes and pilot-scale experiments.

(c) Perform numerical parametric studies

Numerical parametric studies were performed to obtain a broader understanding, and to quantitatively evaluate the factors that influence load transfer to columns beneath embankments. These parametric studies were performed using the numerical modeling methods that were verified against closed-form solutions for membranes, pilot-scale experiments, and the instrumented full-scale test embankment. Parametric studies were performed to evaluate the load transfer mechanisms of column-supported embankments, both with and without geosynthetic reinforcement. Several design factors were varied in the parametric studies, including (1) strength and modulus of the deep-mixing-method (DMM) columns, (2) density of the embankment fill, (3) embankment height, (4) thickness of an existing upper sand layer, (5) density of a base sand layer, (6) compressibility and thickness of the soft soil, (7) column diameter and column spacing, and where geosynthetic reinforcement was included (8) geosynthetic reinforcement location, and (9) geosynthetic stiffness.

(d) Develop recommendations for the design of geosynthetic-reinforced column-supported embankments to control settlement

Based on the results of the literature review and numerical analyses, practical recommendations for the consideration of load transfer and settlement control of column-supported embankments were developed.

The scope of this research does not include slope stability for column-supported embankments.

1.4 Overview of Dissertation

This dissertation addresses the design of geosynthetic-reinforced bridging layers in embankments supported on any type of columns or piles, with or without pile caps, and is divided into ten chapters and one appendix.

A review of the current state of practice of the deep mixing method is presented in Chapter 2, which includes a summary of the installation methods, typical column geometries, typical material property values, and current design methods for settlement of embankments supported on deep mixed columns. A review of the current state of practice of the design of geosynthetic-reinforced bridging layers is presented in Chapter 3. Chapter 3 discusses the important factors that affect the load transfer mechanisms of column-supported embankments, and it presents the current state of practice for designing the geosynthetic reinforcement to enhance vertical load transfer behavior.

Chapter 4 describes the case history of the full-scale test embankment that was constructed at the I-95/Route 1 interchange in Alexandria, Virginia as part of the Woodrow Wilson Bridge Reconstruction Project. This case history was used to verify the finite difference and finite element models of a column-supported embankment. Chapter 5 discusses the verification analyses that were performed of the I-95/Route 1 test embankment. The material property values and constitutive models used for analysis of the test embankment site are described, as well as the numerical modeling methods and results of the numerical analyses.

Chapter 6 describes the numerical parameter study that was performed using the finite difference axisymmetric FLAC model for the case of a column-supported embankment without geosynthetic reinforcement. Chapter 6 provides a description of the methods used in the numerical analyses, and a discussion of the results of the numerical studies, including a discussion of the trends disclosed by the analyses.

Chapter 7 discusses the analyses that were performed to verify the use of FLAC axisymmetric models to numerically evaluate load transfer mechanisms of geosynthetic-reinforced column supported embankments. The verification analyses were compared to the published results of laboratory model scale tests performed by Zaeske (2001) and Kempfert et al. (2004). Additional numerical verification studies that include geosynthetic reinforcement are discussed in Appendix A.

Chapter 8 describes the numerical parameter study that was performed for the case of a column-supported embankment with geosynthetic reinforcement. Chapter 8 provides a brief description of the methods used in the numerical analyses and a discussion of the results of the numerical studies, including a discussion of the trends disclosed by the analyses.

Chapter 9 presents the calculation procedure developed as part of this research to evaluate the settlement and load transfer behavior of column-supported embankments, both with and without geosynthetic reinforcement. This calculation procedure includes the comprehensive consideration of all the design variables associated with geosynthetic-reinforced column-supported embankments for settlement control.

The research summary, conclusions, and recommendations for further work are presented in Chapter 10.

Three appendices are included. Appendix A presents several verification and numerical studies that were performed to evaluate the modeling of membrane behavior in the explicit finite difference programs FLAC3D and FLAC. Appendix B describes the numerical analyses that were performed to evaluate the load-deflection response of membranes subjected to vertical loads. Appendix C summarizes the procedures for calculating settlement of embankments and structures supported on stone columns.

CHAPTER 2
REVIEW OF THE CURRENT STATE OF PRACTICE OF THE DEEP MIXING METHOD

2.1 Introduction

The deep mixing method is a technology that mixes in-situ soils with cementitious materials to form a vertical stiff inclusion in the ground. The deep mixing method (DMM) utilizes quicklime, slaked lime, cement, flyash, and/or other agents. The agents, widely referred to as "binders," may be introduced in the form of either a dry powder or slurry.

In the late 1960's, Japan and Sweden independently began research and development of deep soil mixing techniques using granular quicklime. The Japanese were focusing on soil improvement techniques suited to large marine and estuarine projects, while Sweden was primarily focusing on soil improvement of soft clays for road and rail projects.

In the 1970's, the method of mixing dry unslaked lime with soft soil in-situ to create lime columns was put into practice in Sweden and Japan. Dry cement was soon added as a stabilizing agent to provide greater strengths. Lime/cement or cement columns have today almost entirely replaced lime columns (Kivelo 1998). The method in which dry powdered lime and cement are used as the stabilizing agents is generally known as the "Dry Method of Deep Mixing."

By the mid-1970's, in an effort to improve the uniformity of soil treated by deep mixing, the Japanese also began introducing stabilizing agents in a cement slurry form. The use of stabilizing agents in slurry form is referred to as the "Wet Method of Deep Mixing." The wet method was initially introduced in Japan for large-scale stabilization of marine clays but has subsequently been used for land applications. Today, the wet and dry methods of deep mixing are used in Japan.

The modern methods of deep soil mixing were introduced in the U.S. in the 1980's. Deep mixing is still considered an emerging technology in the U.S. However, with increasing

availability of equipment and experienced contractors, soil mixing is becoming a viable construction technology in the U.S.

Deep mixing procedures produce improved ground that has greater strength, lower ductility, and lower compressibility than the original ground. The degree of improvement depends on the amount and type of stabilizer, installation process, characteristics of the original ground, and the curing time and temperature. In general, the wet methods of deep mixing are designed to provide higher strengths than the dry methods; however, the material produced by the wet mixing methods may experience slower strength gain with time (Kawasaki et al. 1981).

Deep soil mixing is performed under a number of different names or acronyms worldwide, many of which are proprietary. Bruce (2000) listed and classified 24 different variations of deep mixing methods. The comprehensive name "Deep Mixing" has been used to include all deep mixing methods that use mechanical shafts to accomplish soil mixing, as opposed to jet grouting, which uses hydraulic power.

Recommendations for construction and performance monitoring, as well as construction specifications, for deep mixing technologies may be found Bruce (2000) and Elias et al. (1999), and they are not discussed here. The design and testing of lime-cement and soil-cement mixes is also beyond the scope of this chapter. Valuable references on the mix design for lime-cement and soil-cement columns include Bruce (2000), CDIT (2002), EuroSoilStab (2002), and Jacobson et al. (2003).

This chapter presents a summary of the installation methods, typical column geometries, typical material property values, and current design methods for settlement of embankments supported on deep mixed columns.

2.2 Applications and Limitations

The Japanese and Swedish methods of deep mixing vary with respect to equipment and binder types, and as a result, the achieved strengths and applications vary. The Japanese application of deep mixing was initiated to improve the stability of port facilities such as breakwaters and

revetments in which the pattern of application is massive stabilization created in-situ by overlapping columns (CDIT 2002). In Japan, the wet method of deep mixing is preferred for marine work, while both the dry and wet methods are employed for on-land work (CDIT 2002). By the end of 2001, the cumulative volume of treated soils in Japan amounted to 70 million cubic meters; the shares of the wet method offshore, wet method on-land, and dry method on-land were almost the same (Terashi 2003). For on-land applications, soil-cement columns, panels, or blocks have been installed to improve slope stability, to improve the bearing capacity of foundations, for liquefaction risk mitigation, and to increase the stability and reduce the settlements of embankments constructed on soft clays. The Japanese trends have been toward the use of large-scale equipment capable of producing relatively large diameter columns to considerable depths.

In comparison, the Scandinavians typically install deep mixed columns in groups or in rows to reduce the settlement and improve the stability of roadway embankments or dwellings. Deep mixed columns have been found to be competitive in Sweden and Finland compared with other soil stabilization methods such as driven piles, and excavation and replacement. On most projects in Sweden, dry mixed columns are used in conjunction with preloading to reduce construction time and costs (Broms 2003). The majority of embankments stabilized with lime/cement columns have heights ranging from 7 – 13 ft (2 – 4 m); however, lime/cement columns have been used successfully to improve the stability of embankments with heights up to 30 ft (9 m) (Broms 2003). The Scandinavians have generally operated with smaller and lighter equipment that is capable of transversing very soft ground. The Scandinavians typically produce shorter, smaller diameter columns.

Deep mixing methods in the U.S. have been used on several projects. The dry method of deep mixing was used during the reconstruction of I-15 in Salt Lake City, Utah to decrease predicted settlements and improve embankment stability. Soil-cement deep-mixed cells installed by the wet method were constructed beneath the Jackson Lake Dam in Wyoming for liquefaction mitigation. Wet mixing methods were used extensively on the Boston Central Artery project for excavation support, toe stabilization during tunneling, cut-off walls, and for stability buttresses.

Wet mixing methods were also used to support new embankments at the I-95/Route 1 Interchange project in Alexandria, Virginia.

In general, dry mixed stabilization is appropriate for sites with relatively deep deposits of very soft soils, and sufficient groundwater to hydrate both the lime and the cement (Esrig and MacKenna 1999). Cohesive soils with moisture contents between 60 and 200% are best suited for dry mixing, although successful examples of treatment have been recorded beyond this range. High soil sulfate contents and/or high organic contents (and therefore low pH) inhibit strength development of lime-cement columns; however, data indicate that the presence of chloride ions (as in salt water) increases strength. Little improvement can be expected in soils with over 1.5% humus content (Bruce 2000). The ground temperature of the site may affect the reaction rates and shear strength improvement of the lime-cement columns. Reaction rates are very low when the ground temperature is below 39˚F (4˚C); as ground temperatures increase, the reaction rates increase (Elias et al. 1999). The dry method of deep mixing requires a high level of field control and an experienced contractor. One factor that limits the feasibility of the dry method is the required depth of improvement, which is a function of the equipment capability and available air pressure. With the equipment currently used in the U.S., the maximum depth treatable by the dry method is approximately 80 ft (24 m) (Forte 2002).

The wet methods of deep mixing are usually designed to provide higher unconfined compressive strength values than the dry methods. However, it has been reported that the rate of strength gain for dry methods is slower for the wet method in all soil types (Bruce et al. 1999). Unlike the dry method, the wet method may be used in most soil types. The wet method also requires a high level of field control and an experienced contractor. The relatively high cost of mobilization/demobilization, plus the cost of accompanying auxiliary batch plants, makes the wet method of deep mixing uneconomical for small projects. Construction considerations include the required headroom for the equipment used during the installation process, and the spoil volumes that must be disposed of (on the order of 30 – 100% of soil volume treated) (Elias et al. 1999). Additionally, the presence of high organic content and low soil pH will reduce the column strength and increase the quantity of binder material required (Burke et al. 2001). Kawasaki et al. (1981) suggested that when the organic content of a soil is more than 2%, soil-

cement columns are not suitable. In some instances, designers simply opt to remove soils with high organic contents within zones to be stabilized (Burke 2002). The maximum depth treatable by the wet method is approximately 130 ft (40 m) (Bruce 2000).

2.3 Installation and Production of DMM Columns

The deep mixing method is a technology that mixes in-situ soils with cementitious materials, or binders, to form stabilized masses in the ground. The binder can be installed either by the wet method, where a slurry of binder and water is used, or by the dry method, where the dry binder material reacts chemically with the pore water during curing. Binders include mainly limes and cements. Lime is available either as quicklime or hydrated lime. Though some drying out of the soil occurs, cement will not change the structure of clay to the same extent as lime does. Secondary binders may include blast furnace slag, fly ash, or gypsum. Such secondary binders are not standardized and should be tested case by case to judge their suitability. (EuroSoilStab 2002).

There are many methods of deep mixing, including several proprietary methods, with variations in equipment, procedure, and materials. This section discusses in general terms the dry and wet methods of installation. The purpose of the following discussion is to provide only a general overview of typical construction methods and equipment.

2.3.1 Japanese Installation Methods

Three typical mixing machines used in Japan are shown in Figure 2.1. A conventional track-mounted crane supports the soil mixing machines, which consist of auger cutting heads, discontinuous auger flights, and mixing paddles. As the mixing augers and tools are advanced, dry cement or cement slurry is pumped through the hollow shaft and mixed with the soil. In addition to constructing single columns, panels or blocks can be created with the process as the tools are worked in overlapping configurations (Burke et al. 2001).

Typical operating parameters of the Japanese mixing machines are summarized in Table 2.1. The quality and homogeneity of the deep mixing stabilization is also greatly affected by the advance per revolution of the mixing tool during mixing, grout feed pressure, and the speed of

rotation. For the Japanese wet methods, the diameter of the mixing blade is typically 3.3 ft (1.0 m), and the maximum depth of improvement is 165 ft (50 m) from the ground surface. Larger mixing blade diameters are sometimes used to improve construction speed (Terashi 2003). For the Japanese dry methods, the diameter of the mixing blade is typically 3.3 ft (1.0 m), and the maximum depth of improvement is about 98 ft (30 m) from the ground surface.

Table 2.1: Typical Japanese mixing installation parameters (from Kaiqiu 2000)

	Single drive shaft	**Double drive shaft**	**Multibarrel drive shaft**
Depth of stabilization	49 ft (15 m)	> 49 ft (15 m)	98 – 131 ft (30 – 40 m)
Penetration velocity	2 – 3.3 ft/min (0.6 – 1.0 m/min)	0.7 – 3.3 ft/min (0.2 – 1.0 m/min)	3.3 – 6.6 ft/min (1.0 – 2.0 m/min)
Withdrawal velocity	2 – 3.3 ft/min (0.6 – 1.0 m/min)	0.7 – 3.3 ft/min (0.2 – 1.0 m/min)	3.3 – 6.6 ft/min (1.0 – 1.5 m/min)
Rotating speed	50 rpm	46 rpm	20 – 30 rpm (penetration) 40 – 60 rpm (withdrawal)

The construction of deep mixed columns is a highly automated process. During installation, a computer mounted on the equipment provides a real-time record of the following mixing parameters continuously throughout the depth of each column (VDOT 2001a):

- Drilling and mixing depth,
- Mixing tool penetration and withdrawal rates,
- Mixing tool rotation speeds,
- Grout injection rate of each auger, and
- The verticality of each mixing tool shaft in two orthogonal planes.

The uniformity and shear strength of the installed columns will vary greatly if the soil and cement are not mixed sufficiently with the soft soil. Installation obstacles include frozen ground, fill material, stumps, roots, boulders, and blasted rock.

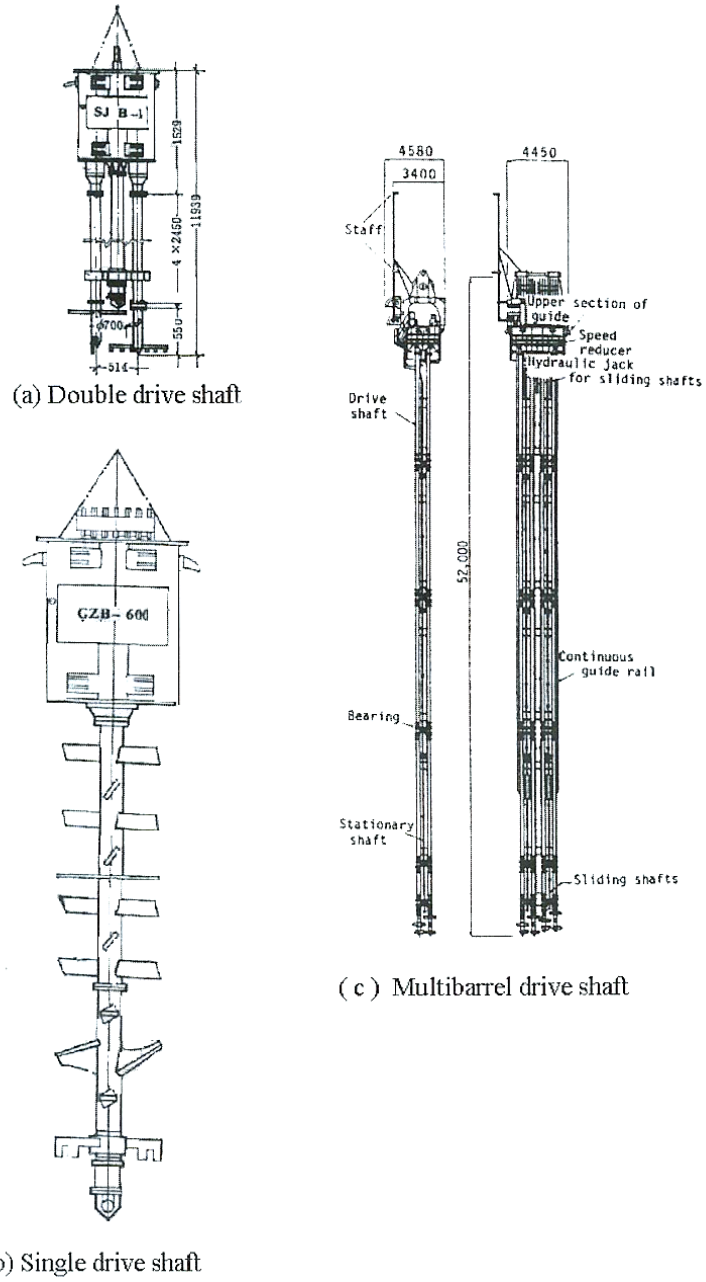

Figure 2.1. Three examples of Japanese deep mixing machines (from Kaiqiu 2000)

The wet methods of deep mixing typically require a relatively high cost of mobilization/demobilization, including the cost of accompanying auxiliary batch plants, and thus are often uneconomical for small projects. Construction considerations include the required headroom for the equipment and the spoil volumes that must be disposed.

2.3.2 Scandinavian Installation Methods

The Scandinavians typically use a mixing tool similar to the one shown in Figure 2.2. The mixing tool is rotated down to the design depth, and once the design depth is reached, the direction of rotation of the mixing tool is reversed and the tool is withdrawn at a constant rate. During withdrawal, lime and/or cement are forced into the soil using compressed air pushing through a hole located just above the mixing tool. The stabilized soil mixture is compacted by the inclined blades of the mixing tool. The dry method brings little to no spoils to the ground surface, thus avoiding the cost of disposing significant quantities of waste material.

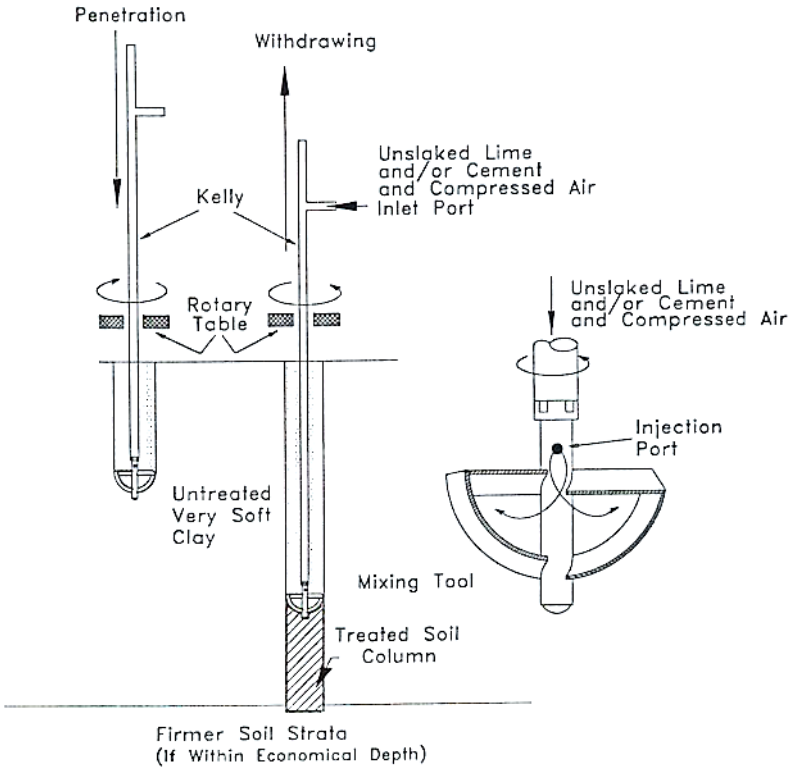

Figure 2.2. Manufacture of dry method deep mixed columns (from Schaefer 1997)

During driving, the tool is rotated at a speed of 100 to 230 revolutions per minute, with a penetration rate of about 6.5 – 10 ft/min (2 to 3 m/min). During admixture (or withdrawal), the speed of rotation is approximately 80 to 120 revolutions per minute, with a withdrawal rate of about 2 – 3 ft/min (0.6 to 0.9 m/min) (Bruce 2000). The capacity of machines used in Sweden is about 1300 to 3280 ft (400 to 1000 m) in eight hours under favorable conditions, and about 30

to 40 lime-cement columns with lengths on the order of 32 ft (10 m) can normally be installed during an eight-hour shift (Broms 2003).

For organic soils, or when the cement content is high, the rotation velocity should be increased and the retrieval rate should be reduced (Kivelo 1998). Experience has shown that by injecting one-half of the lime-cement mixture during down-driving of the mixing tool and one-half the mixture during the withdrawal, the column uniformity and the ability to adjust to different soil conditions, are improved (Saye et al. 2001, Forte 2002).

It is typically recommended that the pressure feed of dry binder be stopped 1.5 – 3 ft (0.5 – 1.0 m) below ground level to prevent the binder being blown back up along the shaft. As a result, the quality of the upper part of the columns should not be relied upon in design (Carlsten and Ekstrom 1997). The uniformity and shear strength of columns will vary greatly if the lime and cement are not mixed sufficiently with the soft soil. Installation obstacles include frost, fill material, stumps, roots, boulders, and blasted rock.

Almost all applications of dry mixed columns installed in Sweden involve the use of a surcharge prior to construction (Ruin 2002). If preloading and surcharging are not used, resulting long-term settlements should be considered in overall assessment of stabilization (Carlsten and Ekstrom 1997).

2.3.3 Typical Installation Geometries

The design spacing, diameter, and length of deep mixed elements depends on such factors as the allowable maximum total and differential settlements, and the required capacity to prevent stability failures. The geometries of deep mixed columns are determined based on several factors including (Kivelo 1998, Carlsten and Ekstrom 1997):

- the shear strength of the in-situ soil,
- the time required for pore pressure dissipation during preloading if preloading is used,
- the shear strength of the columns, and
- the height of the embankment.

Dry mixed columns are typically installed singularly or in rows, grids, or blocks. Single columns are installed on a square or triangular grid. Rows, grids, or blocks of columns should be installed without any major interruptions. Single dry mixed columns are typically spaced at 3.3 – 5.2 ft (1.0 to 1.6 m), center-to-center. Column spacings generally increase with increasing column diameter. The columns will have the same diameter as the mixing tool used during installation with typical diameters ranging from 1.2 – 3.3 ft (0.4 – 1.0 m). In Sweden and Finland, the typical diameter of deep mixed columns is 2 ft (0.6 m) (Broms 2003). The most common mixing tool used in the United States is 2.6 ft (0.8 m) in diameter (Esrig and MacKenna 1999). The maximum length of dry mixed columns is on the order of 80 to 114 ft (25 to 35 m) (Kivelo 1998); however, with the equipment used in the U.S., the maximum depth is approximately 80 ft (24 m) (Forte 2002).

Wet method techniques may utilize single columns or walls, blocks, or lattices. Singular wet mixed columns, such as soil-cement columns, are typically installed with diameters ranging from 36 inches to 8 ft (0.9 m – 2.4 m). The maximum length of the columns is on the order of 98 - 130 ft (30 to 40 m) (Bruce 2000).

2.4 Material Property Values of Soils Stabilized by Deep Mixing

The mechanical properties of soils stabilized by the deep mixing method are affected by many factors including the water, clay, and organic contents of the soil; type, proportion, and amount of binder materials; effective in-situ stress; installation mixing process; and installation sequence and geometry. Given all the factors that affect the strength of treated soils, the Coastal Development Institute of Technology (CDIT 2002) notes that presently it is not possible to predict either the laboratory strengths or the field strengths of stabilized soils within a reasonable level of accuracy. It is recognized that even relatively modest variations in the binder materials may result in greatly different properties of the soil-cement. Furthermore, the strength of soil-cement is very time dependent, due to the long-term pozzolanic process that occurs when mixing lime or cement with clay.

Laboratory tests performed on soils stabilized by deep mixing include unconfined compression, triaxial compression, direct shear, and oedometer (for one-dimensional compression).

Laboratory tests are performed on samples made in the laboratory by mixing cement grout or dry cement-lime reagent with soil from the site, and on core samples obtained from installed deep mix elements. Typical field and laboratory material property values of soils stabilized by deep mixing are discussed in this section.

2.4.1 Unconfined Compressive Strength

While several different types of laboratory tests are used to evaluate the shear strength and stiffness of deep mixed columns, the most frequently used is the unconfined compression test, mainly because of the simplicity of the test. As a result, the unconfined compressive strength is used as an index strength, and it is often the only measure of soil-cement strength on a project.

Many factors affect the unconfined compressive strength. It is well recognized in the deep mixing industry that the unconfined compressive strength of soil treated by the deep mixing methods increases with:

- increasing reagent content (cement, or lime/cement);
- increasing mixing homogeneity;
- longer curing time after installation.

The strength of soil-cement is known to decrease due to:

- increasing fines content and organic content;
- lower pH value of the native soil;
- increasing water content of the native soil;
- addition of binder substitutes, such as ash or bentonite;
- increasing air entrainment, and
- increasing water/cement ratio, except for clay soils with low natural water contents.

As an example of the last item, in the wet method of deep mixing was applied to marine clay for the Boston Central Artery/Tunnel Project (McGinn and O'Rourke 2003). At a given cement dosage rate, a threefold increase in unconfined compressive strength occurred by increasing the grout water/cement ratio from 0.7 to 0.9. This occurred because the clay was relatively stiff and the added water improved the thoroughness of mixing, which increased the strength even though

the overall average water-to-cement ratio was lower. The natural water content of the clay was 35% to 40%, which is low compared to many other clay soils treated by the deep mixing method).

A summary of contract specified values of unconfined compressive strength, q_u, for three recent projects in the U.S. are presented in Table 2.2.

Table 2.2. Specified values of q_u on deep mixing projects in the US

Project	**Soil Type / Binder Amount**	**Specified q_u**	**Reference(s)**
I-95 Route 1, Alexandria, VA	Wet mix method: Soft organic clay; 300 kg/m^3 cement (w/c 1.0)	**Average** q_u at 28 days > 160 psi (1,100 kPa), with all values capped at 220 psi (1,517 kPa) for the purpose of computing the average. **Minimum** q_u at 28 days > 100 psi (690 kPa). Values of q_u measured on cored specimens.	Shiells et al. (2003); Lambrechts et al. (2003); Lambrechts and Layhee (2003)
Central Artery Project, Boston, MA	Wet mix method: Fill, organics and Boston Blue Clay; 220 - 300 kg/m^3 cement (w/c 0.90)	**Minimum** q_u at 56 days ≥ 300 psi (2,100 kPa); **Maximum** q_u at 56 days ≤ 1,000 psi (6,900 kPa)	McGinn and O'Rourke (2003); Maswoswe (2001); Lambrechts et al. (1998)
Oakland Airport Roadway, California	Wet mix method: Loose sandy fills and soft clay; 160 – 240 kg/m^3 cement	**Average** q_u at 28 days > 150 psi (1,035 kPa). **Minimum** q_u at 28 days > 100 psi (690 kPa). Values of q_u measured on cored specimens.	Yang et al. (2001)

Many factors affect the unconfined compressive strength. For a wide variety of soil types and binder mixes, the 28-day unconfined compressive strengths for soils treated by the wet method may range from 20 to 4,000 psi (140 to 27,600 kPa) (Haley & Aldrich 2000, Japanese Geotechnical Society 2000, Kaiqiu 2000, Lin and Wong 1999, Maswoswe 2001, McGinn and O'Rourke 2003, Tatsuoka and Kobayashi 1983, VDOT 2001a). The 28-day unconfined compressive strengths for soils treated by the dry method may range from 2 to 400 psi (14 to

2,760 kPa) (Baker 2000, Esrig and MacKenna 1999, Haley and Aldrich 2000, Hebib and Farrell 2002, Jacobson et al. 2003, Kaiqiu 2000, Lin and Wong 1999, Saye et al. 2001, and VDOT 2001a).

2.4.2 Shear Strength

In the design of deep mixing for support of embankments, both the compressive and shear strength parameters of the stabilized soil are needed. The undrained shear strength, drained shear strength, and the residual, or post-peak, shear strength are discussed in the following paragraphs.

2.4.2.1 Undrained Shear Strength

The peak undrained shear strength may be determined by isotropically-consolidated undrained triaxial tests. Kivelo (1998) points out that triaxial tests and direct shear tests are often more reliable than unconfined compression tests with respect to the undrained shear strength.

For cement columns installed by the wet method, it is commonly assumed in the soil-cement design practice in Japan that the undrained shear strength is independent of normal stress and the total-stress friction angle equals zero (CDIT 2002). Takenaka and Takenaka (1995) report that the undrained shear strength is equal to one-half the unconfined compressive strength for values of unconfined compressive strength below several hundred kPa, and they also indicate that the undrained shear strength is less than one-half the unconfined compressive strength when the unconfined compressive strength becomes greater than several hundred kPa, which is usually the case for wet mixing. As a rule-of-thumb, Takenaka and Takenaka (1995) recommend that the undrained shear strength be taken as one-third of the unconfined compressive strength.

For soils treated by the dry methods, the undrained shear strength is often assumed to be equal to one-half of the unconfined compressive strength; however, based on consolidated undrained triaxial and direct shear tests, Kivelo (1997) found that the undrained shear strength can be less than one-half the unconfined compressive strength at low confining pressures. However, when the total confining pressure exceeds 22 to 36 psi (150-250 kPa), the undrained shear strength becomes almost constant at a value equal to one-half of the unconfined compressive strength. As

a result, Kivelo (1997) proposed the failure envelope for soils treated by dry lime and cement shown in Figure 2.3.

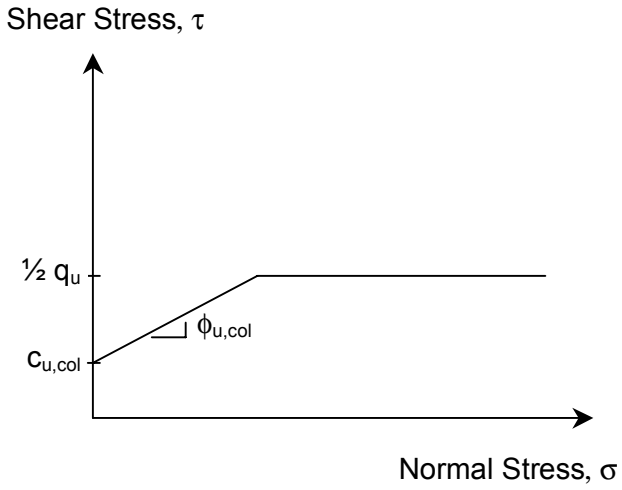

Figure 2.3. Undrained shear strength of lime/cement column (from Kivelo 1997)

The failure envelope in Figure 2.3 may be expressed as:

$$\tau_{u,col} = c_{u,col} + \sigma_n \tan \phi_{u,col} \leq \tfrac{1}{2} q_u \qquad (2.1)$$

where $\tau_{u,col}$ = undrained column shear strength,
$c_{u,col}$ = undrained cohesion of the column,
σ_n = total normal pressure, and
$\phi_{u,col}$ = undrained friction angle of the column.

Although tests results have indicated friction angles that vary generally from 25˚ to 45˚, a value of $\phi_{u,col}$ equal to 30 degrees has been recommended by Broms (1999) for normal pressures of 22 to 36 psi (150 to 250 kPa) for lime/cement columns. With this $\phi_{u,col}$ = 30 degrees, the value of the undrained cohesion, $c_{u,col}$, of the dry mixed element can be taken equal to 29% of the unconfined compressive strength. Above the range of 22 to 36 psi (150 to 250 kPa) normal stress, the undrained shear strength can be taken as half of the unconfined compressive strength. However, even though the undrained shear strength of lime-cement and cement columns

installed by the dry method can be as great as 145 psi (1000 kPa), the maximum value of undrained shear strength is typically limited in design to 15 or 22 psi (100 or 150 kPa) regardless of the results from field or laboratory tests (Kivelo 1997, EuroSoilStab 2002).

2.4.2.2 Drained Shear Strength

The peak drained shear strength can be determined from consolidated-drained triaxial tests, consolidated-drained direct shear tests, or consolidated-undrained triaxial tests with pore pressure measurements. The drained shear strength, $\tau_{d,col}$, can be determined by the following equation:

$$\tau_{d,col} = c'_{col} + \sigma'_n \tan \phi'_{col} \quad (2.2)$$

where $\tau_{d,col}$ = drained column shear strength, c'_{col} = the drained cohesion of the column, σ'_n = effective normal stress, and ϕ'_{col} = the drained (effective) friction angle of the column. According to Broms (2003), the effective friction angle may be assumed to be 35 degrees for cement/lime columns and 40 degrees when only cement has been used to make dry mix columns. Where no laboratory values are available, EuroSoilStab (2002) recommends using a drained effective stress friction angle of the column, ϕ'_{col}, equal to 30°, and estimating the drained cohesion as follows:

$$c'_{col} = \beta_s \cdot c_{u,col} = \beta_s \cdot (½)\, q_u \quad (2.3)$$

where $c_{u,col}$ = the undrained cohesion intercept (taken as one-half the unconfined compressive strength), and β_s = stability reduction factor, which is dependent on the position of the point in question along the stability analysis surface (β_s equals zero in the passive zone, 0.1 in the direct shear zone, and 0.3 in the active zone).

2.4.2.3 Residual (Post-Peak) Strength

Stabilized soils tested in triaxial conditions experience some definite decrease in strength once the peak strength is exceeded (Kivelo 1998). The peak strength is typically reached at strains of 1% to 2%. As strain continues, the shear strength reduces to a lower residual value.

The notion that soil-cement is brittle is more a manifestation of the unconfined compression test than the actual behavior of the material, and under even low confining pressures, the residual strength of soil-cement is 65% to 90% of the unconfined compressive strength (Tatsuoka and Kobayashi 1983, CDIT 2002).

Tests conducted by Ahnberg (1996) using drained triaxial conditions on specimens made by treating clay with dry lime/cement and cement, showed that at large deformations, the cementation forces are broken down, giving effective friction angles of the same magnitude as at failure, but with very low cohesion intercepts. Thus when evaluating stability of embankments using soil-cement, and combining the soil strength with that of the soil-cement, such residual conditions may have to be considered because strains for some organic soils and plastic and sensitive clays may exceed 10% to 20% before reaching their peak strength (Ahnberg 1996). In evaluating residual strength, Broms (1999) recommends that the residual value of cohesion be set to zero and the friction angles remain unchanged from the values established for peak strength conditions. In looking at undrained compressive strengths, the residual shear strength of treated soils (cement/lime dry method) has been found to typically be on the order of 80% of the peak strength (Kivelo 1997).

2.4.3 Compressibility

The compressibility of the stabilized soil is expressed in terms of both the modulus of elasticity, E, and the compression modulus, M.

Soil volumes improved by deep mixing will typically exhibit consolidation behavior similar to that of over-consolidated clays, and will possess a “yield stress,” similar to a pre-consolidation

pressure. The yield stress can be estimated to be approximately 1.0 to 1.3 times the unconfined compressive strength, as recommended by CDIT (2002).

2.4.3.1 Modulus of Elasticity, E

The most common measure of soil-cement compressibility is the undrained secant modulus of elasticity, E_{50}, which is evaluated at 50% of the peak strength. Generally, it is assumed that the relationship between the undrained modulus of elasticity, E_{50}, and the undrained shear strength of treated soils is a linear relationship, with the modulus increasing with increasing strength. Therefore, the modulus of elasticity is influenced by the same factors that control strength.

For columns installed by the dry method, the ratio of E_{50} to unconfined compressive strength ranges from 50 to 180 for lime/cement columns, and 65 to 250 for cement columns (Baker 2000, Broms 2003). Based on laboratory tests performed on three different soil types treated with dry lime/cement, Jacobson et al. (2003) showed that the ratio of E_{50} to unconfined compressive strength was approximately 75. However, for peats stabilized with dry cement, the relationship between the modulus of elasticity and the undrained shear strength is not linear, as typically assumed for other soil types (Hebib and Farrell 2000).

For cement treated soils using the wet method and prepared in the laboratory, the modulus of elasticity, E_{50}, has been reported in research done more than 20 years ago to be 350 to 1,000 times the unconfined compressive strength for a wide variety of silts and clays (Kawasaki et al. 1981). More recently, however, in a series of unconfined compressive tests performed on soils treated by cement slurry with a water/cement ratio of 1.0, Fang et al. (2001) reported that the modulus of elasticity, E_{50}, was 30 to 300 times the unconfined compressive strength. Navin and Filz (2005) found that E_{50} is about equal to 300 times q_u for soil-cement specimens obtained from both dry and wet method columns at the I-95/Route 1 interchange projects in Alexandria, Virginia, although there was a great amount of scatter in the data. The wide range in ratios of E_{50} to q_u from these various sources indicates the uncertainty and possible unreliability of estimating E_{50} by means of correlation with q_u. In addition, very little data is available on the possible changes of the modulus of elasticity with time. A summary of the published

relationships between the modulus of elasticity and the unconfined compressive strength is provided in Table 2.3.

Table 2.3. Summary of published relationships between E_{50} and q_u

Binder type	**E_{50}**	**(e) Reference**
Dry lime/cement	$50 – 180 \cdot q_u$ $75 \cdot q_u$	Baker (2000); Broms (2003) Jacobson et al. (2003)
Dry cement	$65 – 250 \cdot q_u$ $300 \cdot q_u$	Baker (2000); Broms (2003) Navin and Filz (2005)
Wet cement	$350 – 1{,}000 \cdot q_u$ $30 – 300 \cdot q_u$ $150 \cdot q_u$ $300 \cdot q_u$	Kawasaki et al. (1981) Fang et al. (2001) McGinn and O'Rourke (2003) Navin and Filz (2005)

When the modulus of elasticity is used in design analyses, the secant modulus E_{50} is typically used as the design value of the modulus of elasticity of the column, E_{col}, although that may not be appropriate if only small strains are expected.

The modulus of elasticity, E_{50}, is typically determined from unconfined compression or triaxial compression tests. The modulus of elasticity as determined by unconfined compressive tests on samples prepared in the laboratory is typically higher than the modulus determined for cores obtained in-situ from actual columns (Broms 2003).

2.4.3.2 Confined Modulus, M

The oedometer compression modulus, M_{col} (or constrained column modulus), is related to the modulus of elasticity, E_{col}, and Poisson's ratio, ν_{col}, as follows:

$$M_{col} = \frac{(1-\upsilon_{col}) \cdot E_{col}}{(1+\upsilon_{col}) \cdot (1-2 \cdot \upsilon_{col})} \qquad (2.4)$$

If the relationship between the modulus of elasticity and the strength of treated soils is a linear relationship, then it follows that the relationship between the constrained compression modulus, M_{col}, and the strength is also a linear relationship for a given value of Poisson's ratio.

In general, the Poisson's ratio of deep mixed treated soil is around 0.25 to 0.50, irrespective of the unconfined compressive strength (CDIT 2002, Terashi 2003). Therefore, the compression modulus of the column, M_{col}, is equal to 1.35 times E_{col} for a Poisson's ratio of 0.3; 1.6 times E_{col} for a Poisson's ratio of 0.35; and 2.14 times E_{col} for a Poisson's ratio of 0.40. However, for peats stabilized with dry cement, Hebib and Farrell (2000) measured Poisson's ratios on the order of 0.1 for strains less than 1%. Therefore, for peats, the constrained compression modulus of the column, M_{col}, is equal to 1.02 times E_{col} for a Poisson's ratio of 0.1 for small strains.

The compression modulus, M, can be determined by oedometer tests, where the applied load is typically increased once a day (every 24 hours), although shorter periods are also used. The compression modulus is equal to the inverse of the compressibility parameter m_v, such that:

$$M = \frac{1}{m_v} \tag{2.5}$$

The laboratory compression modulus, M, is, in general, lower than the in-situ compression modulus, and therefore, the compression modulus from oedometer tests can be considered as a lower limit (Broms 2003).

2.4.4 Unit Weight

For the dry method of deep mixing, Broms (2003) reports that the unit weight of stabilized organic soils with high initial water contents increases to be above that of the untreated soil, and becomes greater with increasing cement and lime content. However, he notes that the unit weight of inorganic soils after stabilization is often reduced. The Japanese CDIT (2002) reports that, for soils treated by the dry method of deep mixing, the total unit weight of the treated soil increases by about 3% to 15% above that of the untreated soil.

For the wet method of deep mixing, Takenaka and Takenaka (1995) report that, as the cement content increases, the unit weight of the improved soil also increases. For clayey soils, the unit weight will increase by 3 to 6 lb/ft^3 (0.5 to 1.0 kN/m^3), but in the case of sandy soil, there is little change in the unit weight. CDM (Cement Deep Mixing) (1985) generalizes by saying that, for soils treated by the wet method of deep mixing, the density change is negligible. However, at the Boston Central Artery/Tunnel Project, a substantial decrease in unit weight occurred, as reported by McGinn and O'Rourke (2003). The decrease was primarily a result of the clay initial unit weight being about 120 to 125 lb/ft^3 (20 to 21 kN/m^3) (natural water content of 35 to 40%) and there being need to add water to pre-condition the clay before wet mixing in the cement grout.

2.4.5 Tensile Strength

Takenaka and Takenaka (1995) report that the tensile strength of soil improved by the wet method is 10% to 20% of the unconfined compressive strength. EuroSoilStab (2002) states that, for the dry methods of deep mixing, columns should not be subjected to tensile stresses.

2.4.6 Permeability

The addition of lime typically increases the hydraulic conductivity of soft clay; however, the addition of lime and cement may only increase slightly or may even decrease the hydraulic conductivity of soft clay (Baker 2000).

For the dry methods of deep mixing, EuroSoilStab (2002) states that the permeability of soil treated with dry lime and cement can be assumed to be 200 to 600 times as high as that of unstabilized soil. Field tests performed by Baker (2000) indicated that the hydraulic conductivity varied between 10 and 100 times that of the original soil.

For the wet methods of deep mixing, permeabilities in the range of 3.3×10^{-7} to 3.3×10^{-8} ft/s (10^{-7} to 10^{-8} m/s) are routinely achievable but values as low 3.3×10^{-10} ft/s (10^{-10} m/s) are attainable with appropriate mix designs (and higher cost) (Bruce 2000). Increasing the cement factor and bentonite content will serve to decrease the permeability. Soil-cement elements installed by the wet method are not considered to function as vertical drains (Broms 1999).

2.4.7 Changes with Time

Depending on the type of binder, some of the chemical reactions will take place relatively quickly, but some may develop more slowly. When finely ground cement is used, the shear strength increases rapidly during the first month after the installation (Broms 2003). When using binders such as lime, gypsum, furnace slag and/or ash, the strength will continue to increase after the first month. The increase in shear strength with time is typically faster in the field than in the laboratory, mainly due to higher ground temperature and higher confining pressure, which influence the pozzolanic reactions (Bruce 2000). Designers should optimize the time schedule for construction based upon the predicted strength gains in the columns (EuroSoilStab 2002).

The design of deep mixed columns is typically based on the estimated strength 28 days after the installation of the columns. For soils stabilized by the wet method of deep mixing, the 28-day unconfined compressive strengths are generally about 1 to 2 times the 7-day values, and at least 1.6 times the 3- or 4-day values. The 60-day strengths can be 1.2 to 2.5 times the 28-day values of strength (Bruce 2000, Takenaka and Takenaka 1995). Similarly, for soils stabilized by the dry method, the 28-day unconfined compressive strengths are about 1.5 to 2.4 times the7-day values (Bruce 2000).

Generally speaking, the strength of treated soils increases almost linearly with the logarithm of time (CDIT 2002). Hayashi et al. (2003) took continuous core samples on 17-year-old columns constructed by the wet method of deep mixing. No substantial change in physical properties, such as water content and dry density, were measured; however, the strength of the columns as measured by unconfined compression testing had increased by three to seven times greater than the 28-day strength over the span of 17 years.

The available information about long-term degradation of deep mixed materials is very limited. Durability is generally linked to the same factors that control strength and permeability, and the addition of lime, bentonite, and higher cement factors each can improve durability (Bruce 2000). Deterioration caused by sulfides has been documented in subgrades stabilized with lime. For soils treated with lime/cement or cement, an increase in the volume of soil, which can reduce the bonding and shear strength, can occur with time when flowing groundwater contains sulfides.

Concern has also been expressed about the possible reduction of shear strength of lime/cement and cement columns caused by cyclic and dynamic loading (Broms 2003).

2.4.8 Laboratory Testing versus Field Testing

As described previously, the shear strength and compressibility of lime/cement and soil-cement mixtures are affected by several factors such as the water, clay, and organic contents of the soil; the type, proportion, and amount of binder materials; effective in-situ stress; installation geometry and process; and time after installation. In addition, laboratory strengths are affected by sample storage temperature, rate of shearing, degree of homogeneity, strength testing method, and type of sample. Because of the differences between conditions in the field and the laboratory, often times it is difficult to adequately predict field material values based upon laboratory testing.

On one hand, compression and strength values determined by laboratory tests may be less than the actual field values since the confining pressure of the in-situ soil is not taken into account (Kivelo 1998). According to Bruce (2000), measured strengths of core samples are generally higher than those of wet grab samples by up to 50%. The in-situ value of the compression modulus, M_{col}, may be up to five times greater than the values determined in the laboratory (Ekström et al. 1994, Broms 1999).

On the other hand, the strength values obtained from specimens prepared in the laboratory are often greater than the strength values of installed columns since the homogenous samples created in the laboratory do not adequately represent the heterogeneous mixing that occurs in the field (EuroSoilStab 2002). CDIT (2002) reports that the unconfined compressive strength of deep mixed columns in the field can be as low as one-fifth of the unconfined compressive strength of laboratory prepared samples. The Scandinavians report that the field strengths are on the order of 0.2 to 0.5 times the strengths of specimens prepared in the laboratory (EuroSoilStab 2002).

The variation of the strength and compression properties of installed deep mixed columns is often large. According to Navin and Filz (2005), values of the coefficient of variation of unconfined compressive strength range from 0.17 to 0.67, with an average value of about 0.40,

even after the influence of controllable factors such as water-to-cement ratio of the slurry and curing time were accounted for.

2.4.9 Effects of Installation Process and Sequence

For the wet methods of deep mixing, it has been shown that there is less variation and higher strengths achieved when multiple mixing shafts are used, as opposed to one (CDIT 2002, Shiells et al. 2003). Using several mixing shafts allows for opposite rotation in-situ, which provides for efficiency in mixing. Field experiments have also shown that the rotational and penetration speeds can affect strengths achieved (Dong et al. 1996). Higher strengths are achieved from faster rotation, while higher strengths and smaller variation is achieved with reduced penetration rates. Furthermore, Dong et al. (1996) noted that, for the same shape of mixing blade, a thin mixing blade contributed to greater in-situ strengths than a thick blade. Relative to the degree of mixing, or how well the soil and reagent are mixed together, Japanese researchers have shown that unconfined compressive strength decreases with decreasing mixing time and that strength variability increases with decreasing mixing time (CDIT 2002).

When stabilized columns are overlapped, the boundary surfaces between adjacent columns may become weak points in the stabilized structure. During the overlapping procedure, a stabilized column during hardening is partially scraped by the following column, and the strength in the overlapped area can be lower than that of other parts of the column (CDIT 2002).

For the dry methods of deep mixing, experience has shown that, by injecting one-half of the lime/cement mixture during down-driving of the mixing tool and one-half the mixture during the withdrawal, the column uniformity and the ability to adjust to different soil conditions, are improved (Saye et al. 2001; Forte 2002).

2.5 Existing Methods for Calculating Settlement

Although it is considered an emerging technology in the U.S., the deep mixing method has been applied extensively to the improvement of soft clays and organic soils for a wide variety of projects in both Japan and Scandinavia. This section presents a review of the methods currently

used in Japan and Scandinavia to calculate settlement of embankments and structures supported on columns installed by the deep mixing method.

2. 5.1 Definition of Terms

Deep-mixing-method columns may be installed as isolated columns constructed using single-axis equipment, elements of two or more overlapping columns constructed using multi-axis equipment, panels of overlapping columns, cells of overlapping columns, or blocks of overlapping columns. Regardless of the column arrangement, the concepts of area replacement ratio, a_s, and stress concentration ratio, n, are common to all analysis methods. For isolated columns (or elements), the area replacement ratio is defined as the ratio between the area of the deep mixed column (or element) and the total tributary area (soil and column) associated with that column (or element):

$$a_s = \frac{A_{col}}{A_{col} + A_{soil}} \tag{2.6}$$

where A_{col} = area of column (or element), A_{soil} = area of the soil associated with the column (or element), and $A_{col} + A_{soil}$ = effective area, or the total tributary area associated with each column (or element). Where panels or blocks of improvement are used, the basic meaning of the area replacement ratio remains the same.

The load applied by the embankment is carried by both the column and the soft soil between columns (although not evenly). The average stress applied by the embankment, σ, may be expressed as:

$$\sigma = \sigma_{col}(a_s) + \sigma_{soil}(1-a_s) \tag{2.7}$$

where σ_{col} and σ_{soil} = the vertical stress carried by the column and the surrounding soil, respectively. The vertical stresses induced in the column and the surrounding soil are illustrated in Figure 2.4.

The stress in the stiffer column is greater than the stress in the surrounding soil. The stress concentration ratio (or stress ratio), n, is defined as the ratio of vertical stress at the top of the column to the vertical stress at the top of the surrounding soil:

$$n = \frac{\sigma_{col}}{\sigma_{soil}} \tag{2.8}$$

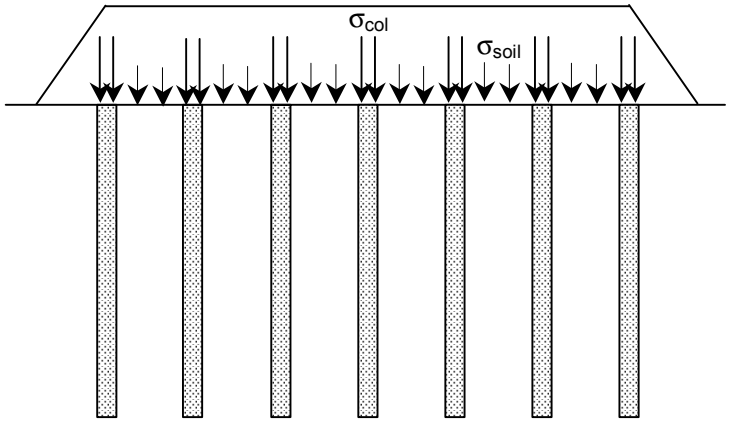

Figure 2.4. Illustration of stress-distribution for column-type deep mixed foundation

The stress concentration ratio is used in settlement calculations and to determine the loads in deep mixed columns. The vertical stresses carried by the column and the surrounding soil, as illustrated in Figure 2.4, may be calculated using Equations 2.9 and 2.10, respectively, which are obtained by combining Equations 2.7 and 2.8.

$$\sigma_{col} = \frac{n \cdot \sigma}{[1 + (n-1) \cdot a_s]} \tag{2.9}$$

$$\sigma_{soil} = \frac{\sigma}{[1 + (n-1) \cdot a_s]} \tag{2.10}$$

Values of stress concentration ratio, n, are discussed in Sections 2.5.2 and 2.5.3, respectively, for Japanese and Scandinavian practice.

2.5.2 Japanese Method for Calculating Settlement

In Japan, the deep mixing method is applied to improve soft clays and organic soils for a wide variety of applications. In this section, Japanese procedures for analyzing settlement and on deep mixed elements are discussed. Valuable references in English that discuss the state-of-practice of deep mixing in Japan include CDIT (2002), Porbaha (2000), Takenaka and Takenaka (1995), and Bergado et al. (1999).

Deep soil mixing elements are designed to carry considerably higher stress than the soft soil into which they are installed. Because the columns are much stiffer than the surrounding soft soil, embankment settlements are greatly reduced.

Typically, a grid of deep mixed columns is installed beneath the center portion of an embankment to control settlement. In Japanese practice, each deep mix element typically consists of two or three overlapping columns installed with multi-axis equipment. The distribution of load between the deep mixed elements and unstabilized soil is calculated based on the assumption that the same amount of vertical strain occurs in the columns and the soil at every level (CDIT 2002). The equal strain assumption is used for elements that bear on a deep, hard stratum, as well as for elements that are used for shallow improvement. Because the deep mix elements are stiffer than the soft soil, the equal strain assumption produces a concentration of stress in the deep mix elements. CDIT (2002) states that the stress concentration ratio for soil-cement elements installed by the wet method is typically assumed to be about 10 to 20. The stress concentration ratio for soil-cement elements installed by the dry method may be on the order of 4 to 6 (Lin and Wong 1999; Kaiqiu 2000).

In Japan, the consolidation settlement of soil stabilized by deep mixed columns is determined using the following equation (CDM 1985):

$$\Delta d_{stab} = \beta \cdot \Delta d \tag{2.11}$$

where Δd_{stab} = consolidation settlement of stabilized ground, Δd = consolidation settlement of unstabilized ground, and β = settlement reduction ratio.

The settlement reduction ratio, β, is defined as the ratio of the settlement of stabilized ground to that of the settlement predicted for the same load on unstabilized ground. The stress concentration ratio and area replacement ratio are used to determine the settlement reduction ratio as follows:

$$\beta = \frac{1}{[1 + (n-1)a_s]} = \frac{\sigma_{soil}}{\sigma} \tag{2.11a}$$

The consolidation settlement of the unstabilized ground is calculated as follows:

$$\Delta d = m_v \cdot \sigma \cdot D \tag{2.11b}$$

In Equations 2.11a and 2.11b, σ = average vertical stress applied by the embankment, σ_{soil} = stress acting on the soft soil between columns, a_s = area replacement ratio (defined in Equation 2.6), D = thickness of the stabilized clay layer (or sublayers), and m_v = coefficient of compressibility of the untreated clay. Based on Equation 2.11a, as the stress concentration ratio and area replacement ratio increase, the settlement of the stabilized ground decreases.

Alternatively, the settlement of the treated ground may be determined by proportionally combining the deep mixed elements and the soil into a single composite foundation. The total settlement of the composite foundation, S, is determined as follows (Kaiqiu 2000):

$$S = \frac{\sigma \cdot L}{E_c} \tag{2.12}$$

where σ = applied vertical stress, L = length of element (or depth of treated ground), and E_c = modulus of elasticity of the composite foundation, which is determined using the following equation:

$$E_c = a_s \cdot E_{col} + (1-a_s)\, E_{soil} \quad (2.13)$$

where E_{col} = modulus of elasticity of the deep mixed elements, and E_{soil} = modulus of elasticity of the soft clay. Equations 2.12 and 2.13 may be used for grids of isolated columns or elements, as well as for other patterns of improvement such as rows or blocks.

If n is set equal to E_{col} / E_{soil} and if E_{soil} is set equal to $1/m_v$, then Equations 2.11b and 2.12 would give the same result.

Settlement of an embankment also includes compression of soil that may be present beneath the ground treated by deep mixing. Conventional settlement calculations are performed to estimate the compression of the strata below the reinforced volume.

2.5.3 Scandinavian Method for Calculating Settlement

Lime/cement and cement columns installed by the dry method of deep mixing have been used extensively to support road and railroad embankments in Sweden and Finland. In Sweden, 85% to 90% of all columns are installed to increase the stability and reduce the settlements of embankments constructed on soft soils (Broms 2003; Holm 1999). In Scandinavia, most of the design procedures for deep mixed columns were originally developed for lime columns, but they procedures for calculating the settlement of embankments supported on deep mixed elements are discussed.

Isolated deep mixed columns are commonly installed beneath the center portions of embankments to control settlement. In Sweden, the methods used to calculate the settlement of lime/cement and cement columns are based on those developed for lime columns by Broms and Boman (1979a, 1979b). It is assumed that the same strain occurs in the columns and the soil at every level (Broms 1999). Upon loading, the concentration of stress in the stiffer column must be greater than the stress in the surrounding soil since it is assumed that the strain in the two materials is the same. The stress concentration ratio, n, between the columns and the soft soil is defined in Equation 2.8.

According Carlsten and Ekstrom (1997), a stress concentration ratio of five is often used in the design of lime/cement and soil-cement columns in Sweden and Finland. Based on large-scale field tests performed on soil-cement columns installed by the dry method, Kaiqiu (2000) reported stress concentration ratios in the range of 4.7 to 5.7 under embankment loading.

In Swedish practice, the load deformation behavior of a dry mixed column is assumed to take place as shown in Figure 2.5. The load-deformation curve is linear up to the column long-term strength, or creep strength, σ_{col}^{creep}, and the slope of the curve is equal to the modulus of elasticity of the column, E_{col}. When the creep strength is reached, it is assumed that the column would then deform without limit at constant stress. As long as the column creep strength is not reached, the vertical stresses carried by the column and the surrounding soil are calculated using Equations 2.9 and 2.10, respectively. Once, the column creep strength is reached, additional loads are carried by the soil.

The column creep strength is less than the column ultimate (or failure) strength. Broms (1999) and EuroSoilStab (2002) suggest that the column creep strength is about 65% to 90% of the ultimate strength, but they do not provide any additional guidance for determining project-specific values of creep strength.

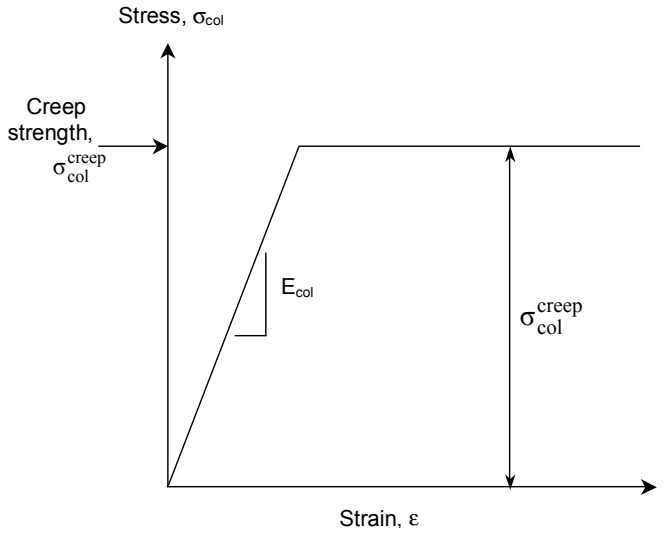

Figure 2.5. Stress-strain relationship in dry mixed columns

According to EuroSoilStab (2002), the ultimate strength can be determined using the following equation:

$$\sigma_{col}^{ult} = 2\ \tau_{u,col} + 3\ \sigma_h' \tag{2.14}$$

where $\tau_{u,col}$ = the undrained shear strength of the columns and σ_h' = the effective horizontal pressure on the columns. In Equation 2.14, EuroSoilStab (2002) states that the effective horizontal pressure should be set equal to the original effective vertical pressure in the soil. EuroSoilStab (2002) states that Equation 2.14 is empirical, and "is to some extent based on total stress analysis with $\phi = 30^o$ in the column." For the Scandinavian applications of the dry method of deep mixing, the undrained shear strength of the columns, as used in Equation 2.14, is limited to 22 psi (150 kPa) (EuroSoilStab 2002).

The method of evaluating settlement is based upon the load-deformation relationship shown in Figure 2.5. The compression of a volume of soil stabilized with columns is evaluated by considering two load cases. In the first case (Case 1), the creep strength of the columns is not reached, and the compression, S_1, and corresponding vertical strain, ε_z, within the stabilized area are calculated based on the following equations:

$$S_1 = \sum \frac{\sigma_{col}}{E_{col}} \cdot d_i = \sum \frac{\sigma_{soil}}{M_{soil}} \cdot d_i = \sum \varepsilon_v \cdot d_i \tag{2.15}$$

$$\varepsilon_v = \frac{\sigma}{a_s \cdot E_{col} + (1 - a_s) \cdot M_{soil}} \tag{2.16}$$

where S_1 = the compression of the stabilized volume for Case 1, σ = total applied vertical stress, d_i = stratum (or sublayer) thickness within the reinforced depth, a_s = area replacement ratio (as shown in Equation 2.6), E_{col} = modulus of elasticity of the column, and M_{soil} = oedometer compression modulus of the surrounding soil. Equations 2.15 and 2.16 indicate that the settlement of the stabilized volume decreases with increasing area replacement ratio and with increasing stiffness of the column.

If n is set equal to E_{col} / M_{soil} and if M_{soil} is set equal to $1/m_v$, then Equations 2.11b and 2.15 would give the same result.

In Equations 2.15 and 2.16, the modulus of elasticity of the column, E_{col}, is used instead of the constrained modulus to account for the relatively small amount of lateral restraint provided by the soft clay (Broms and Boman 1979b, Broms 1999, EuroSoilStab 2002). Broms (1999) indicates that the column stiffness may decrease with time due to creep effects; however, he also comments that the column stiffness may increase with time due to the increase of the shear strength of the stabilized soil. These effects tend to compensate, and Broms (1999) does not provide quantitative guidance for estimating changes in column stiffness with time.

In the second case (Case 2), the creep limit of the columns is reached. As the embankment is built, the columns cannot take any more load, and therefore, the subsequent loads carried by the unstabilized soil between columns governs settlement. The load that is carried by the soil is set equal to the total applied load minus the maximum load that can be carried in the columns at their creep strength. In Case 2, the compression of the stabilized volume is calculated using the following equation:

$$S_2 = \sum \frac{\sigma - \sigma_{creep}^{col} \cdot a_s}{1 - a_s} \cdot \frac{d_i}{M_{soil}} \qquad (2.17)$$

where S_2 = the compression of the stabilized volume for Case 2, σ = average applied stress, σ_{creep}^{col} = column creep strength, d_i = stratum (or sublayer) thickness within the reinforced depth, a_s = area replacement ratio, and M_{soil} = oedometer compression modulus of the surrounding soil.

Broms (2003) indicates that the observed settlement can often be larger than the calculated settlement. The difference between estimated and observed settlements generally increases with increasing column lengths (Broms 2003).

Lime/cement columns may either partly penetrate through the compressible stratum or be end-bearing. Where columns of different lengths are used in separate zones beneath an embankment,

it is recommended that settlements be calculated for each different zone (Carlsten and Ekstrom 1997). For partly penetrating columns, the compression of the stratum of thickness d* below the reinforced depth can be estimated as illustrated in Figures 2.6 and 2.7, which are from Broms (1991). For Case 1 (Figure 2.6), the applied load is assumed to be transferred directly down through the reinforced depth, after which it is distributed through the underlying material at an angle of 1H:2V. The compression of the underlying stratum, d*, is added to the result of Equation 2.15 to compute the total settlement for Case 1.

For Case 2 (Figure 2.7), when the column creep strength is reached, the maximum load that can be carried by the columns is transferred directly down through the reinforced depth, after which it is distributed through the underlying material at an angle of 1H:2V. The applied load that exceeds the creep strength of the columns is applied to the ground surface and distributed through the underlying soils at an angle of 1H:2V. The compression of the underlying stratum, d*, is added to the result of Equation 2.17 to compute the total settlement for Case 2.

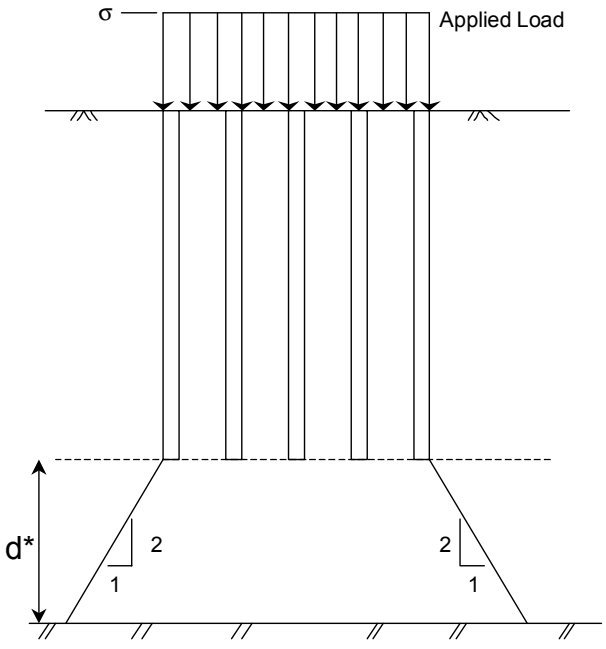

Figure 2.6. Stress distribution beneath the stabilized volume for Case 1 (from Broms 1991)

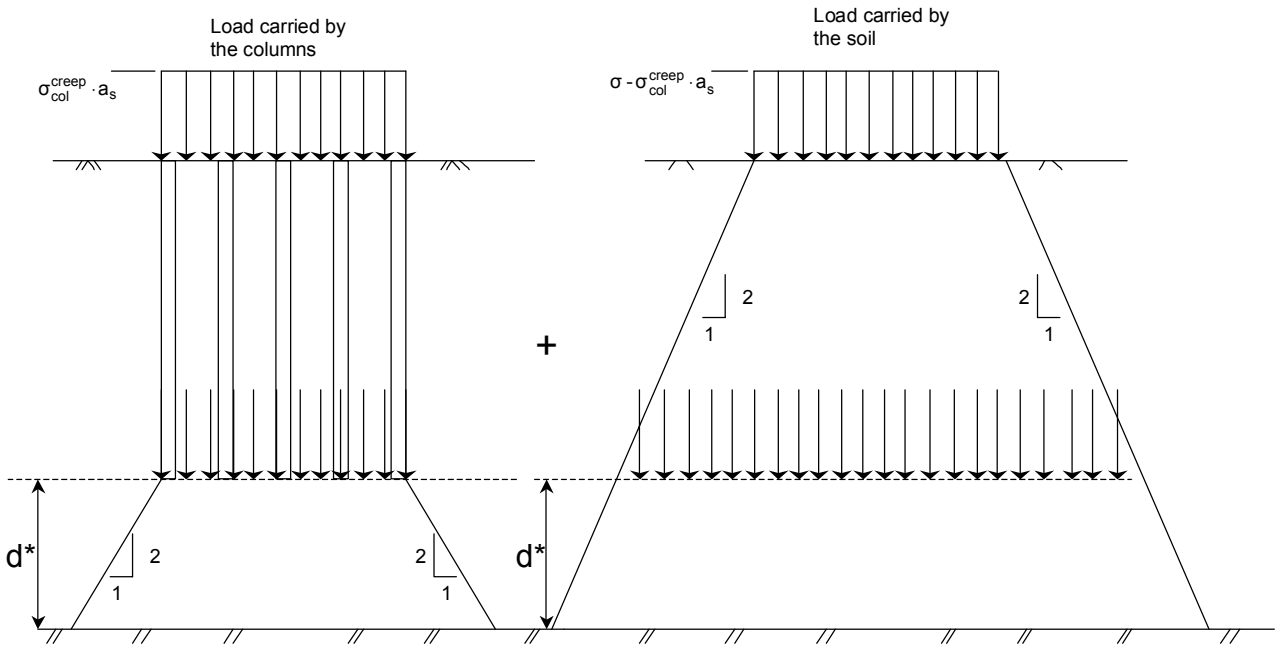

Figure 2.7. Stress distribution beneath the stabilized volume for Case 2 (from Broms 1991)

2.6 Closing Remarks

Deep mixing is still considered an emerging technology in the U.S. However, with increasing availability of equipment and experienced contractors, soil mixing is becoming a viable construction technology in the U.S. This chapter presents a summary of the deep mixing installation methods, typical column geometries, and typical material property values of soil treated by the deep mixing method. This chapter also presents the Japanese and Scandinavian methods for calculating the settlement of embankments supported on deep mixed columns.

CHAPTER 3
REVIEW OF THE CURRENT STATE OF PRACTICE FOR DESIGN OF GEOSYNTHETIC-REINFORCED BRIDGING LAYER

3.1 Introduction

The column-supported embankment technique allows for rapid construction of embankments on sites otherwise too soft and compressible to support large embankment loads. A layer of granular material reinforced with geosynthetics is often placed between the foundation columns and the embankment fill, as shown in Figure 3.1. This layer of compacted granular material is referred to as the "bridging layer" or the "load transfer platform." Geosynthetic reinforcement is installed within the bridging layer to increase the load transfer to the columns and reduce the required area replacement ratio of the columns (Lawson 1992, Russell and Pierpoint 1997, Kempton et al. 1998, Han and Wayne 2000, Han and Gabr 2002). The reinforcing material is generally a geogrid or high-strength geosynthetic, and the assigned role of the reinforcement is threefold (Kaiqiu 2000):

1. to enhance the stress concentration to the columns,
2. to restrain and counteract the horizontal thrust at the sides of the embankment, and
3. to separate the embankment fill and the foundation soils.

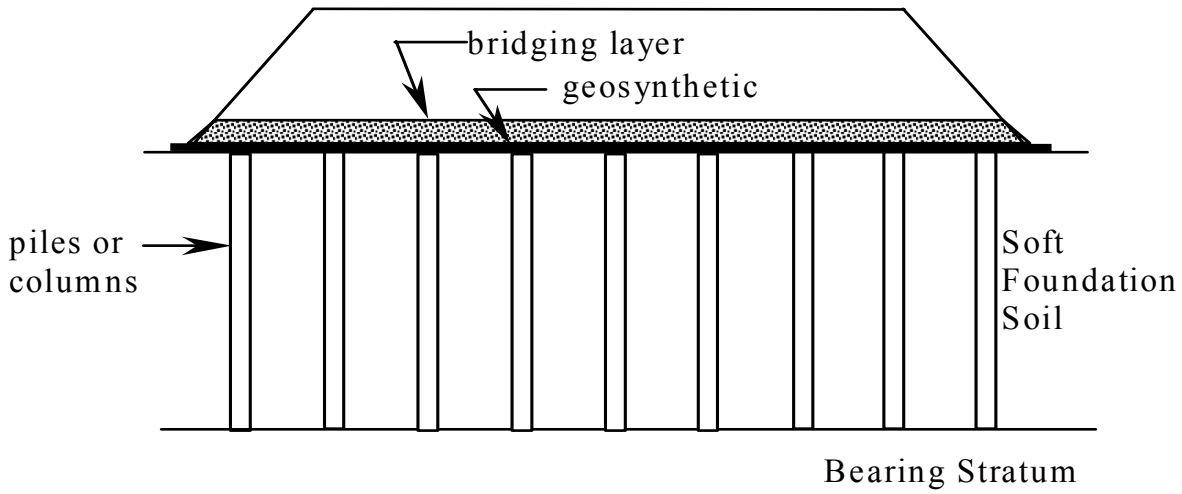

Figure 3.1. Schematic of pile-supported embankment with geosynthetic reinforcement

When one or more layers of geosynthetic reinforcement are placed in the fill above the columns, the stress that would otherwise be applied to the foundation soil between the columns is assumed to be carried by the geosynthetic. The design of the geosynthetic reinforcing material is based on the calculated strain and tension in the geosynthetic due to the vertical load from the embankment fill that is not supported by arching to the columns. This chapter discusses the important factors that affect the load transfer mechanisms in column-supported embankments, and it presents the current state of practice for designing geosynthetic reinforcement to enhance the vertical load transfer behavior.

Design of geosynthetic reinforcement to restrain and counteract the horizontal thrust at the sides of the embankment is not within the scope of this research.

The term 'column' will be used in this chapter to refer to deep-mixing method columns, driven piles, and other columnar support beneath embankments.

3.2 Arching Effects

Terzaghi demonstrated the arching effect with a layer of sand placed above a platform with a removable trap door. When the trap door was lowered slightly, the pressure exerted by the sand on the door decreased and was transferred to the adjacent stationary platforms. The sand above the lowered trap door has a tendency to move downwards; however, the relative movement within the soil is opposed by shearing resistance between the yielding and the stationary soil masses. Since the shearing resistance tends to keep the yielding mass in its original position, it reduces the pressure on the yielding part of the support and increases the pressure on the adjoining stationary part (Terzaghi 1943). Terzaghi defined the arching effect as the transfer of pressure from a yielding mass of soil onto adjacent stationary supports.

Arching effects play a significant role in the behavior of embankments supported on deep foundations. As the embankment is constructed, the soft foundation material consolidates and differential movement occurs between the relatively rigid columns or piles and the soft foundation material. Shear stresses are generated in the fill material, and through the arching effect, the vertical stresses are transferred from the soft foundation material onto the columns.

Based on field measurements, several researchers (Reid and Buchanan 1984, Ooi et al. 1987, Huat et al. 1994) have reported that the load carried by the columns increases with time, which is attributed to arching developing above the columns. The degree of arching is a function of the distance between columns, the height of the embankment, the properties of the fill material, and the rigidity of the columns in relation to the surrounding foundation soil (Lawson 1992).

To limit differential settlements at the embankment surface, the clear spacing between columns or pile caps should not be too large in comparison with the embankment height. BS8006 (1995) recommends that the embankment height should not be less than 0.7 times the clear spacing between adjacent pile caps for square pile caps in a square array. Rogbeck et al. (1998) recommend that the embankment height should be at least equal to the clear spacing between pile caps, and that the embankment should be at least three feet high. Collin (2004) recommends that the embankment height should be equal to or greater than the clear span between columns. Kempfert et al. (2004) recommend that the embankment height should not be less than 1.4 times the clear diagonal spacing between columns in a square array. Converting the diagonal clear spacing to the clear spacing between adjacent columns in a square array, the Kempert et al. (2004) recommendation for minimum embankment height is about the same as the Rogbeck et al. (1998) and Collin (2004) recommendations. Kempfert et al. (2004) also recommend that the diagonal clear spacing of columns in a square array not exceed 10 ft for static loads or 8 ft for heavy live loads. Collin (2004) recommends that the clear spacing between adjacent columns not be greater than 10 ft. Hewlett and Randolph (1988) recommend that embankment height should be at least twice the center-to-center column spacing, which is a much more conservative limitation than the others mentioned here.

Regarding area replacement ratio, Rogbeck et al. (1998) recommend that the area replacement ratio should be a least 10 percent. This is consistent with the lower limit of the trend line shown by (Han and Gabr 2002) for case histories of geosynthetic-reinforced, column-supported embankments.

According to Rogbeck et al. (1998) and Kempfert et al. (2004), the geosynthetic reinforcement should be placed as low as possible in the bridging layer to achieve greatest effectiveness, but

some distance above the columns or pile caps should be maintained to reduce the potential for damage to the geosynthetic at the edges of the columns or pile caps. Rogbeck et al. (1998) indicate that the geosynthetic should be 4 in. above pile caps, and Kempfert et al. (2004) indicate that the bottom layer of geosynthetic should not be more than 6 in. above columns or pile caps. Kempfert et al. (2004) also recommend that, at most, two layers of reinforcement be used and that the vertical distance between reinforcement layers should be in the range from 6 to 12 in.

Hewlett and Randolph (1988) recommend that well compacted fill with a friction angle of at least 30 degrees be used in the bridging layer. According to Collin (2004), select structural fill with a friction angle greater than or equal to 35 degrees should be used in the bridging layer. Kempfert et al. (2004) indicate that cohesionless fill with a friction angle of at least 30 degrees should be used, although low-cohesion fill is permitted but not preferred.

3.3 Definition of Terms

Four terms commonly used to relate the total applied embankment pressure, the pressure acting on top of the columns, and the pressure acting on the soil surface in between the columns are:

- the stress concentration ratio, n,
- the stress reduction ratio, SRR,
- the column stress ratio, CSR, or competency ratio, C, and
- efficacy, E.

The stress concentration ratio (or stress ratio), n, is defined as the ratio of vertical stress at the top of the pile to the vertical stress at the top of the surrounding soil:

$$n = \frac{\sigma_{pile}}{\sigma_{soil}} \tag{3.1}$$

The stress reduction ratio, SRR, is defined as the ratio of the stress applied to the foundation soil between the columns, σ_{soil}, to the average stress applied by the embankment plus surcharge, σ:

$$SRR = \frac{\sigma_{soil}}{\sigma} \tag{3.2}$$

The ratio between the stress on the top of the column, σ_{col}, and the average applied embankment plus surcharge stress at the level of the top of the column, σ, is referred to as the "column stress ratio," CSR:

$$CSR = \frac{\sigma_{col}}{\sigma} \tag{3.3}$$

Low et al. (1994) use the phrase "competency ratio," and the symbol, C, to refer to the same quantity defined as the column stress ratio, CSR.

Efficacy, as defined by Hewlett and Randolph (1988) and Low et al. (1994), is the fraction of the weight of the embankment fill carried by the columns:

$$E = \frac{\sigma_{col} \cdot a_s}{\sigma} \tag{3.4}$$

where a_s = area replacement ratio, which is defined as:

$$a_s = \frac{\text{area of pile}}{\text{total tributary area of column}} = \frac{A_{col}}{A_{col} + A_{soil}} \tag{3.5}$$

The stress concentration ratio, stress reduction ratio, column stress ratio, efficacy, and area replacement ratio are related as follows:

$$SRR = \frac{1}{1 + (n-1) \cdot a_s} = \frac{1 - CSR \cdot a_s}{1 - a_s} \tag{3.6}$$

$$CSR = \frac{n}{1 + (n-1) \cdot a_s} = \frac{1 - SRR \cdot (1 - a_s)}{a_s} \tag{3.7}$$

$$E = CSR \cdot a_s = 1 - SRR \cdot (1 - a_s) \tag{3.8}$$

$$SRR = \frac{1 - E}{1 - a_s} \tag{3.9}$$

Arching in the embankment plays an important role in the behavior of column-supported embankments. For the condition of no soil arching, there is no reduction of pressure on the foundation soil between the columns, and the values of CSR, n, and SRR are all equal to one. For the hypothetical condition of complete soil arching, the entire applied embankment load would be carried by the columns and no load would be carried by the soil between the columns. For complete soil arching, CSR would equal the inverse of a_s, n would approach infinity, and SRR would equal zero. The conditions of no soil arching and complete soil arching are limiting conditions, and for real embankments supported on DMM columns, the degree of arching lies between these limiting conditions. Thus, the values of SRR must lie between zero and 1, and values of CSR must lie between 1 and $1/a_s$ in all cases for which the columns are stiffer than the soft soil between columns.

The dependency of the stress reduction ratio, SRR, on the stress concentration ratio, n, and the area replacement ratio, a_s, is expressed in Equation 3.6, and is shown in Figure 3.2.

For geosynthetic-reinforced column-supported embankments, the stress reduction ratio is typically used to calculate the vertical stress carried by the geosynthetic reinforcement. However, the stress concentration ratio remains a significant unknown factor. Researchers have developed several methods to calculate the stress reduction ratio based on pile cap or column size and spacing, and embankment height. These methods are presented in Section 3.4.

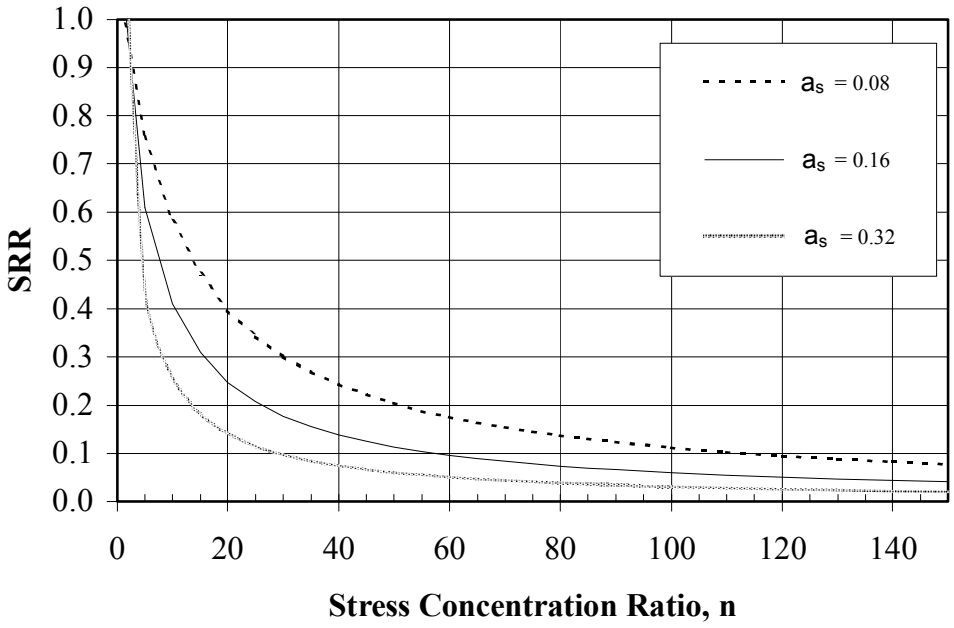

Figure 3.2. Relationship between n and SRR

3.4 Stress Reduction Ratio, SRR

When one or more layers of geosynthetic reinforcement are placed in the fill above the columns, the stress that would otherwise be applied to the foundation soil between the columns, i.e., σ_{soil}, is assumed to be carried by the geosynthetic. Thus, the SRR value can be used to represent the proportion of the embankment load carried by the geosynthetic reinforcement. The methods presented in this chapter to determine SRR values are methods frequently referenced in literature pertinent to geosynthetic-reinforced column-supported embankments. The methods described here are generally based on a square layout arrangement of columns or piles with square caps, as shown in Figure 3.3. For deep mixed columns and stone columns, pile caps are typically not installed, and the equivalent width of the column should be used instead of the width of the cap. For circular columns, the diameter of the columns, d_{col}, can be converted to an equivalent square width, a, according to $a = 0.886 \cdot d_{col}$.

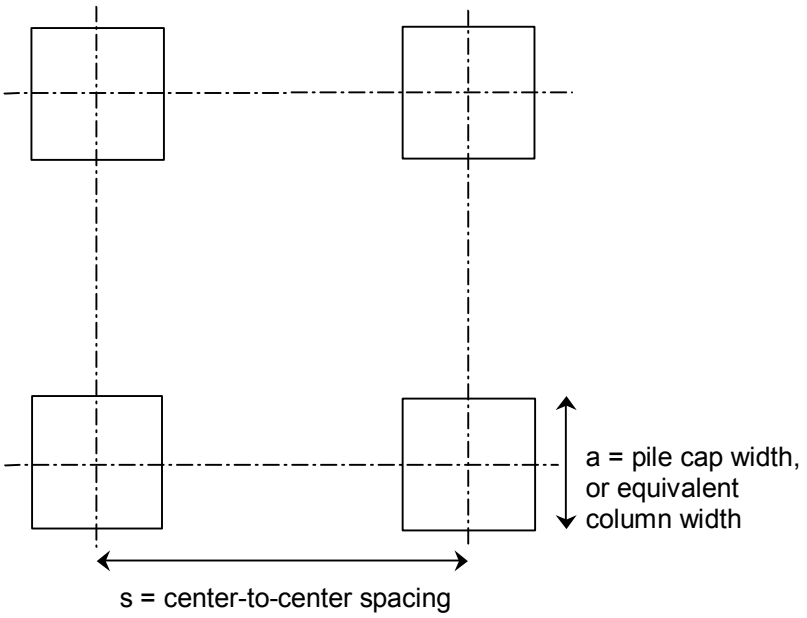

Figure 3.3. Representation of deep foundation areas supporting embankment fill

This section presents seven methods that have been used to evaluate the stress reduction ratio: the BS8006 Method, the Adapted Terzaghi's Method 1 and 2, the Hewlett and Randolph Method, the German Method, the Adapted Guido Method, and the Swedish Method. Methods of evaluating the strain and tension in the geosynthetic reinforcement are presented in Section 3.5.

3.4.1 BS8006 Method

The British Standard (BS8006 1995), "Code of practice for strengthened/reinforced soils and other fills," has adopted the empirical method developed for design of geosynthetic-reinforced column-supported embankments that was developed by Jones et al. (1990). In this method, the plan area of the unit cell is s^2 and the area not supported by columns or piles is $s^2 - a^2$, as shown in Figure 3.3. The load on the area not supported by columns is treated as a uniform vertical line load between adjacent supports for the purpose of determining the load on the geosynthetic. The BS8006 Method considers two possible cases, which are discussed in the following paragraphs.

BS8006 defines a critical embankment height equal to $1.4 \cdot (s-a)$, as shown in Figure 3.4 (where H = embankment height, s = center-to-center spacing of the columns, a = width of pile caps or columns, and (s-a) = the clear distance between supports).

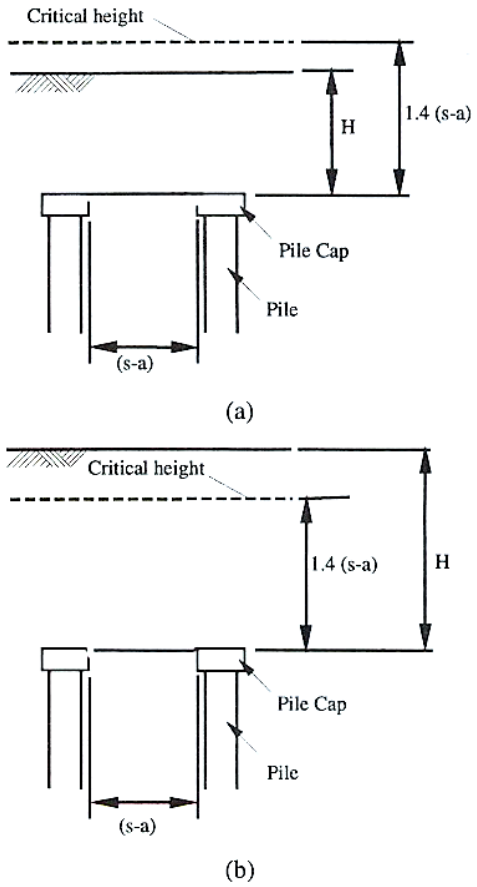

Figure 3.4. BS8006 critical height concept (from Kempton et al. 1998)

If the embankment height is below the critical height, as shown in Figure 3.4a, arching is not fully developed. The embankment and surcharge load, reduced by arching in the embankment fill, is converted to an equivalent vertical line load, W_T, between the piles or columns, as determined by using Equation 3.10:

$$W_T = \frac{s \cdot (\gamma H + q)}{s^2 - a^2}\left[s^2 - a^2 \left(\frac{p_c'}{\gamma H + q}\right)\right] \qquad \text{for } H \leq 1.4(s\text{-}a) \qquad (3.10)$$

where p_c' = vertical stress on the columns or pile caps, γ = unit weight of the embankment fill, H = embankment height, and q = embankment surcharge.

For embankment heights greater than the critical height, as shown in Figure 3.4b, BS8006 assumes that all loads above the critical height are transferred directly to the columns as a result of arching in the embankment fill (Kempton et al. 1998). The columns will also carry some portion of the fill load below the critical height due to arching. For this case, the magnitude of the vertical line load is determined using Equation 3.11:

$$W_T = \frac{1.4 \cdot s \cdot \gamma(s-a)}{s^2 - a^2}\left[s^2 - a^2 \left(\frac{p_c'}{\gamma H + q}\right) \right] \qquad \text{for } H > 1.4(s\text{-}a) \tag{3.11}$$

In Equations 3.10 and 3.11, the ratio of vertical stress concentrated on top of the columns to the average vertical stress at the base of the fill is determined based on Marston's Equation for positive projecting subsurface conduits such that:

$$\frac{p_c'}{(\gamma \cdot H + q)} = \left(\frac{C_c a}{H} \right)^2 \tag{3.12}$$

where C_c = arching coefficient, which is dependent upon the height of the fill, the width of the pile caps, and the rigidity of the piles or columns. These conditions are prescribed as follows:

- for non-yielding piles, such as steel or concrete piles founded on an incompressible stratum, $C_c = 1.95\ (H/a) - 0.18$
- for steel or concrete friction piles, or timber piles, $C_c = 1.70\ (H/a) - 0.12$ (Lawson 1992)
- for stone columns, lime columns, and sand compaction columns, $C_c = 1.5\ (H/a) - 0.07$

Based on the vertical line load between supports, the stress reduction ratio may be determined using the following equation:

$$SRR = \frac{2 \cdot W_T \cdot (s-a)}{(s^2 - a^2) \cdot (\gamma \cdot H + q)} \tag{3.13}$$

The value of W_T is obtained from Equation 3.10 or 3.11, and therefore, the stress reduction ratios for each case can be expressed as follows:

$$SRR = \frac{2 \cdot s}{(s+a) \cdot (s^2 - a^2)} \cdot \left[s^2 - a^2 \left(\frac{p_c'}{\gamma H + q} \right) \right] \qquad \text{for } H \leq 1.4(s-a) \qquad (3.14)$$

$$SRR = \frac{2.8 \cdot s \cdot \gamma}{(s+a)^2 \cdot (\gamma \cdot H + q)} \cdot \left[s^2 - a^2 \left(\frac{p_c'}{\gamma H + q} \right) \right] \qquad \text{for } H > 1.4(s-a) \qquad (3.15)$$

3.4.2 Adapted Terzaghi's Method 1 and 2

Russell and Pierpoint (1997) adapted Terzaghi's arching theory to develop a stress reduction ratio that takes into account the three-dimensional nature of column arrangements. The settling mass is assumed to be cruciform in plan, taking the shape of the soil between the columns as illustrated in Figure 3.3. The Adapted Terzaghi Method 1 stress reduction ratio presented by Russell and Pierpoint (1997) is expressed as:

$$SRR_{3D} = \frac{(s^2 - a^2)}{4 \cdot H \cdot a \cdot K \cdot \tan\phi} \cdot \left\{ 1 - \exp\left[\frac{-4 \cdot H \cdot a \cdot K \cdot \tan\phi}{(s^2 - a^2)} \right] \right\} \qquad (3.16)$$

where ϕ = angle of friction of the embankment fill, and K = coefficient of lateral earth pressure, which Russell and Pierpoint (1997) assume to be equal to one. The relationship given in Equation 3.16 is herein referred to as Adapted Terzaghi's Method 1.

Several years later, Russell et al. (2003) presented a modified version of the Adapted Terzaghi's Method. Russell et al. (2003) assume that the portion of the embankment fill that settles as a cruciform has a height of n·H, and the embankment fill above the settling cruciform is treated as a surcharge. The Adapted Terzaghi Method 2 stress reduction ratio, based on the analysis by Russell et al. (2003), is expressed as:

$$SRR = \frac{(s^2 - a^2)\gamma}{4 \cdot a \cdot (\gamma H + q) \cdot K \cdot \tan\varphi} \cdot \left[1 - \exp\left(\frac{-4 \cdot a \cdot H \cdot K\tan\phi \cdot n}{(s^2 - a^2)}\right)\right] +$$

$$\frac{\gamma \cdot (1-n) \cdot H + q}{(\gamma H + q)} \cdot \exp\left(\frac{-4 \cdot a \cdot H \cdot K\tan\phi \cdot n}{(s^2 - a^2)}\right) \qquad (3.17)$$

where q = embankment surcharge, n = 1.0 for ultimate limit state conditions and 0.8 for serviceability limit state conditions, and K = coefficient of later earth pressure, which Russell et al. (2003) assume to be equal to 0.5. The relationship given in Equation 3.17 is herein referred to as Adapted Terzaghi's Method 2. Russell et al. (2003) also provide a method for considering some support from the subgrade soil based on load transfer from the settling soil to the columns.

3.4.3 Hewlett and Randolph Method

Hewlett and Randolph (1988) presented theoretical methods for determining the embankment loads applied to columns and the foundation soil due to arching based on the limiting equilibrium of stresses in a hemispherical domed region of sand over the piles. The Hewlett and Randolph soil-arching model is illustrated in Figure 3.5. Hewlett and Randolph (1988) state that the domed regions will fail either at the crown of the arch or at the top of the column, but not elsewhere. Hewlett and Randolph (1988) evaluated the load transfer mechanisms in terms of efficacy (see Equation 3.4), and therefore, the efficacy value is calculated at both the crown of the arch and the top of the column.

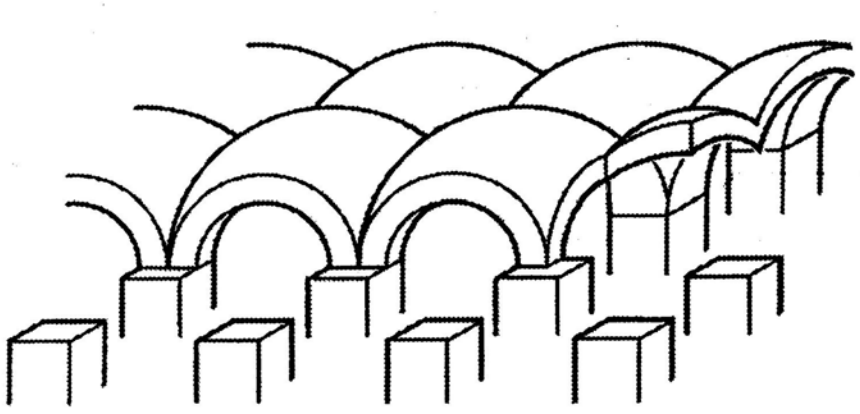

Figure 3.5: Representation of Hewlett and Randolph (1988) soil arching model

The efficacy for conditions at the arch crown is:

$$E = 1 - \left[1 - \left(\frac{a}{s}\right)^2\right] \cdot \left[\left(1 - \frac{a}{s}\right)^{2(K_p - 1)} \left(1 - \frac{s \cdot 2 \cdot (K_p - 1)}{\sqrt{2} \cdot H \cdot (2K_p - 3)}\right) + \left(\frac{(s - a) \cdot 2 \cdot (K_p - 1)}{\sqrt{2} \cdot H \cdot (2K_p - 3)}\right)\right] \qquad (3.18)$$

where K_p = the Rankine coefficient of passive earth pressure = $(1+\sin\phi')/(1-\sin\phi')$, and ϕ' = angle of friction of the embankment fill material.

The efficacy for conditions at the top of the pile is:

$$E = \frac{\beta}{1 + \beta} \qquad (3.19a)$$

$$\text{where } \beta = \left(\frac{2K_p}{K_p + 1}\right)\left(\frac{1}{1 + \frac{a}{s}}\right)\left[\left(1 - \frac{a}{s}\right)^{(-K_p)} - \left(1 + \frac{a}{s} \cdot K_p\right)\right] \qquad (3.19b)$$

Based on the relationship given in Equation 3.9, the stress reduction ratio may be determined from efficacy, and its value for conditions at the arch crown is:

$$SRR = \left(1 - \frac{a}{s}\right)^{2(K_p - 1)} \left(1 - \frac{s \cdot 2 \cdot (K_p - 1)}{\sqrt{2} \cdot H \cdot (2K_p - 3)}\right) + \left(\frac{(s - a) \cdot 2 \cdot (K_p - 1)}{\sqrt{2} \cdot H \cdot (2K_p - 3)}\right) \qquad (3.20)$$

The stress reduction ratio for conditions at the top of the pile is:

$$SRR = \frac{1}{\left(\frac{2K_p}{K_p + 1}\right)\left[\left(1 - \frac{a}{s}\right)^{(1 - K_p)} - \left(1 - \frac{a}{s}\right) \cdot \left(1 + \frac{a}{s} \cdot K_p\right)\right] + \left(1 - \frac{a^2}{s^2}\right)} \qquad (3.21)$$

Based on Equations 3.18 and 3.19, the critical efficacy is that which yields the lower value. Hewlett and Randolph (1988) explain that, at low embankment heights, the performance of the pile support is governed by the condition at the crown at each arch, and as embankment height increases, the critical region transfers to the top of the columns. The critical stress reduction ratio is that which yields the greater value, and therefore, the stress reduction ratio calculated by Equation 3.20 governs for low embankment heights, and as the embankment height increases, Equation 3.21 begins to govern. In order to make optimum use of the foundation support, Hewlett and Randolph (1988) recommend that the column spacing should not exceed three times the width of the columns, and that the pile spacing should not be greater than about half of the embankment height.

According to Equation 3.21, the pressure exerted on the area between columns increases linearly with increasing embankment height and there is no critical embankment height beyond which this pressure remains constant (Love and Milligan 2003).

Kempfert et al. (1997) indicate that the method proposed by Hewlett and Randolph (1988) is valid as long as the height of the embankment is equal to or greater than the pile spacing. Kempfert et al. (1997) recommend that, for embankment heights less than the pile spacing, efficacy be determined by linear interpolation between the values of efficacy calculated for H=s and H=0 (where H = embankment height and s = pile spacing). For H=s, the critical efficacy is the lower value from Equations 3.18 and 3.19; and as H approaches zero, the efficacy approaches the area replacement ratio. After determining the efficacy for the actual embankment height by linear interpolation, the corresponding stress reduction ratios may be determined by using Equation 3.9. An equivalent approach is to first evaluate SRR at H = s as the maximum value from Equations 3.20 and 3.21, and then evaluate SRR at the actual embankment height as $SRR_{H<s} = 1 + (H/s)(SRR_{H=s} - 1)$.

Kempfert et al. (1997) also provide for the inclusion of soil subgrade support using a bearing capacity analysis.

3.4.4 German Method

Kempfert et al. (2004) present in English the design methods that are to be adopted by the EBGEO (German Recommendations for Geosynthetic Reinforced Earth Structures) report. The recommendations provided by Kempfert et al. (2004) have been developed based upon plasticity theory, laboratory pilot scale tests, and numerical analyses. Like Hewlett and Randolph (1998), Kempfert et al. (2004) consider a domed soil arching model (see Figure 3.5).

In the German method, the vertical pressure on the soft soil in between columns is determined using the following equation:

$$\sigma_{soil} = \lambda_1^{\chi} \cdot \left(\gamma + \frac{q}{H}\right) \cdot \left[H \cdot (\lambda_1 + h_g^{\,2} \cdot \lambda_2)^{-\chi} + h_g \cdot \left(\left(\lambda_1 + \frac{h_g^{\,2} \cdot \lambda_2}{4}\right)^{-\chi} - (\lambda_1 + h_g^{\,2} \cdot \lambda_2)^{-\chi}\right)\right] \quad (3.22)$$

where s_g = the diagonal center-to-center dimension of columns installed in a square array = $s\sqrt{2}$, and

$$\lambda_1 = \frac{1}{8} \cdot (s_g - d_c)^2$$

$$\lambda_2 = \frac{s_g^{\,2} + 2 \cdot d_c \cdot s_g - d_c^{\,2}}{2 s_g^{\,2}}$$

$$K_c = \tan^2\left(45 + \frac{\phi'}{2}\right)$$

$$\chi = \frac{d_c \cdot (K_c - 1)}{\lambda_2 \cdot s_g}$$

$$h_g = \frac{s_g}{2} \quad \text{if } H \geq \frac{s_g}{2}$$

$$h_g = H \quad \text{if } H < \frac{s}{2}$$

where d_c = column diameter.

Using the vertical pressure on top of the soil calculated in Equation 3.22, the stress reduction ratio may be determined as follows:

$$SRR = \frac{1}{(1+\lambda)^{\chi}} + \frac{h_g}{H} \cdot \left[\frac{1}{\left(1+\frac{\lambda}{4}\right)^{\chi}} - \frac{1}{(1+\lambda)^{\chi}} \right] \tag{3.23}$$

where $\lambda = \frac{h_g^2 \cdot \lambda_2}{\lambda_1}$

Kempfert et al. (2004) recommend using Equation 3.22 to determine the load on the top of the geosynthetic reinforcement. Kempfert et al. (2004) also take into account some support from the subgrade soil using a modulus of subgrade reaction.

3.4.5 Adapted Guido Method

Work by Guido et al. (1987) showed that the inclusion of stiff biaxial geogrids within granular layers below spread footings could improve the bearing capacity of foundation soils. According to Bell et al. (1994), a result of the work by Guido et al. (1987) is that the angle of load spread through the geogrid reinforced cohesionless soil can conservatively be taken as 45 degrees. Bell et al. (1994) applied this finding to an embankment with two layers of geosynthetic reinforcement supported on vibro-concrete columns.

Russell and Pierpoint (1997) adapted the approach used by Bell et al. (1994) to determine an SRR value based on a single layer of reinforcement at the base of an embankment fill. Russell and Pierpoint (1997) assumed that the geosynthetic reinforcement carries a pyramid of soil that is not supported by the piles, with the ridge lines of the pyramid at an angle of 45 degrees above the horizontal. They expressed the SRR value for the Adapted Guido Method based on the interior area of the unit cell, i.e., $(s - a)^2$, rather than $s^2 - a^2$:

$$SRR = \frac{s - a}{3 \cdot \sqrt{2} \cdot H} \tag{3.24a}$$

Adapting Equation 3.24 a to the case of an embankment with a surcharge yields:

$$SRR = \frac{(s - a) \cdot \gamma}{3 \cdot \sqrt{2} \cdot (\gamma H + q)} \tag{3.24b}$$

Collin (2004) describes a refinement of the Adapted Guido Method, using approaches similar to those described by Bell et al. (1994), Jenner et al. (1998), and Card and Carter (1995). In Collin's refinement of the Adapted Guido Method, the sides rather than the ridges of the pyramid are inclined at 45 degrees above the horizontal, and at least three layers of reinforcement are necessary within the pyramid.

3.4.6 Swedish Method

Similar to the model proposed in the Adapted Guido Method, a triangular soil-arching model was also presented by Carlsson (1987). The Carlsson (1987) reference is in Swedish, but it is discussed in English by Rogbeck et al. (1998) and Horgan and Sarsby (2002). In two dimensions, the Swedish Method considers a wedge of soil whose cross-sectional area under the arching soil can be approximated by a wedge with an internal angle at the apex of the wedge equal to 30º, as shown in Figure 3.6. The Swedish Method adopts a critical height approach such that any additional overburden above the top of the wedge is transferred directly to the columns. Thus, the critical height is 1.87(s-a).

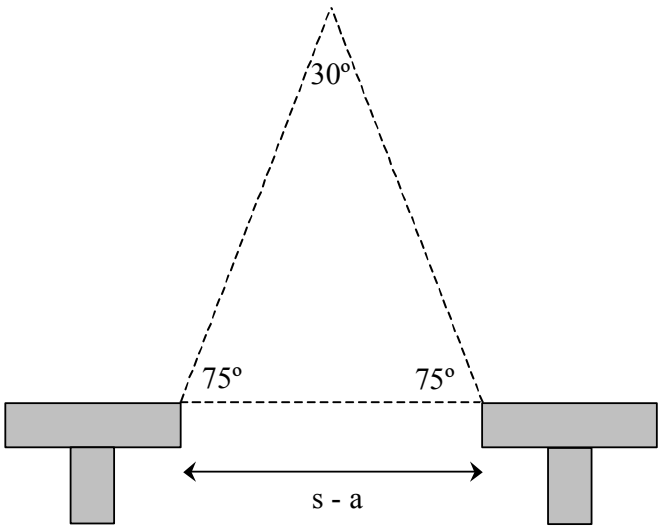

Figure 3.6. Representation of the Swedish soil arching model

The two-dimensional stress reduction ratio, SRR_{2D}, for the Swedish Method is given as:

$$SRR_{2D} = \frac{s - a}{4 \cdot H \cdot \tan 15°} \tag{3.25}$$

Rogbeck et al. (1998) provide a correction factor that is used to compute the geosynthetic tension for an embankment supported by square piles caps in a square array. The net effect of this correction factor is that the three-dimensional stress reduction ratio is the same as the two-dimensional value given in Equation 3.25. Adapting this equation to include a surcharge pressure yields:

$$SRR = \frac{(s - a) \cdot \gamma}{4 \cdot (\gamma \cdot H + q) \cdot \tan 15°} \tag{3.26}$$

Equation 3.26 is applicable for embankments greater than or equal to the critical height. For lower embankments, the upper part of the triangle shown in Figure 3.6 is truncated to calculate the stress reduction ratio.

3.4.7 Stress Reduction Ratio: Discussion of the Methods

Several researchers have demonstrated that the existing methods of determining the stress reduction ratio yield very different results (Habib et al. 2002, Horgan and Sarsby 2002, Naughton and Kempton 2005). Two case histories frequently mentioned in the literature are presented by Russell and Pierpoint (1997), who performed three-dimensional analyses, using FLAC3D, of two actual constructed geosynthetic-reinforced column-supported embankments constructed in the United Kingdom, and other authors have discussed the results of these numerical analyses (Kempton and Naughton 2002, Naughton and Kempton 2005). The Adapted Guido Method appears to consistently underpredict the stress reduction ratio compared to the numerical analyses. The current BS8006 method calculates stress concentration ratios above and below those predicted by numerical analyses for the significantly different embankment conditions used in the study. The Adapted Terzaghi Method 1 and the Hewlett and Randolph Method tend to give results similar to the numerical analyses.

Kempton et al. (1998) also performed two- and three-dimensional numerical analyses to investigate the behavior of pile-supported embankments, and confirmed the variations of the BS8006 method noted by Russell and Pierpoint (1997). Rogbeck et al. (1998) point out that the BS8006 method is not continuous, and it can be seen in Equations 5.14 and 5.15 that a discontinuity occurs at $H=1.4(s-a)$ when $q>0$. Love and Milligan (2003) also note that the BS8006 method does not satisfy vertical equilibrium.

Furthermore, although the Adapted Guido Method has reportedly been used successfully (Bell et al. 1994, Jenner et al. 1998, Habib et al. 2002), Love and Milligan (2003) point out that, in the column-supported embankment situation, gravity and the footing load are operating in the same direction, whereas, in the laboratory tests conducted by Guido et al. (1987), gravity and the column reaction force act on the geosynthetic-reinforced bridging layer in opposite directions.

Values of SRR calculated by the seven methods described above for various combinations of a/s and H/s are presented in Table 3.1. In order to make the calculations, the following assumptions were made:

1. the embankment material has an internal friction angle of 30 degrees;

2. no surcharge load was applied,
3. the piles/columns are non-yielding,
4. the foundation soil between the piles/columns provides no support to the geosynthetic, and
5. K = 1 for the Adapted Terzaghi Method 1, and K = 0.5 and n = 0.8 for the Adapted Terzaghi Method 2.

There are wide variations in the values of stress reduction ratio computed using the seven methods. The BS8006 method is more sensitive to the value of a/s than the other methods, with values of stress reduction ratio greater than unity being generated when a/s is low. The BS8006 Method can generate negative values of SRR when a/s is high. The adapted Guido method tends to generate values that are lower than those from the other methods, particularly at low a/s values. For all combinations of a/s and H/s, the Adapted Terzaghi Method 2 produces higher values of SRR than the Adapted Terzaghi Method 1

Table 3.1. SRR values from seven existing methods

	SRR							
	a/s = 0.20	**a/s = 0.20**	**a/s = 0.30**	**a/s = 0.30**	**a/s = 0.40**	**a/s = 0.40**	**a/s = 0.50**	**a/s = 0.50**
Method	**H/s = 1.5**	**H/s = 4**	**H/s = 1.5**	**H/s = 4**	**H/s = 1.5**	**H/s = 4**	**H/s = 1.5**	**H/s = 4**
BS8006	1.104	0.413	0.740	0.274	0.401	0.144	0.089	0.022
Adapted Terzaghi 1	0.712	0.444	0.596	0.313	0.490	0.225	0.390	0.162
Adapted Terzaghi 2	0.845	0.651	0.769	0.522	0.689	0.411	0.602	0.314
Hewlett & Randolph	0.723	0.723	0.529	0.506	0.425	0.330	0.337	0.205
German	0.708	0.639	0.571	0.485	0.442	0.351	0.325	0.240
Adapted Guido	0.126	0.047	0.110	0.041	0.094	0.035	0.079	0.029
Swedish	0.498	0.187	0.435	0.163	0.373	0.140	0.311	0.117

where a = column width, s = column center-to-center spacing, and H = embankment height.

3.5 Tension in Geosynthetic Reinforcement

When used between the embankment and columns, geosynthetic reinforcement helps to transfer the embankment loading directly onto the columns or piles (Lawson 1992). Under the embankment loading, the embankment fill mass between the columns has a tendency to move downwards. The shear resistance within the fill material resists the downward movement of the fill between columns. Han and Wayne (2002) state that, compared with the unreinforced case, the inclusion of a geosynthetic in the base of the fill is expected to reduce the differential movement between the yielding and stationary masses of soil. The reduction of differential displacement reduces the vertical load transferred directly to the columns by soil arching. However, the geosynthetic picks up the vertical load that does not arch directly to the piles/columns, and the geosynthetic goes into tension. Tension in the geosynthetic transfers the load to the columns by the vertical component of the tension forces (Han and Gabr 2002). The idea is that the geosynthetic bears the vertical load between columns, and then transfers that load to the columns.

The design of the reinforcing material is based on the calculated tension in the geosynthetic due to the vertical load from the embankment fill and surcharge load that is not supported by arching action. The difficulty in design is to assess the amount of vertical load that is carried by the geosynthetic and the tension that this load generates in the geosynthetic (Kempton et al. 1998). When one or more layers of geosynthetic reinforcement are placed in the fill above the columns, the stress that would otherwise be applied to the foundation soil between the columns, i.e., σ_{soil}, is assumed to be carried by the geosynthetic.

This section discusses the methods currently available to evaluate and design the geosynthetic reinforcement subjected to vertical loads for embankments supported on deep foundations, such as driven piles, stone columns, or deep mixed columns.

Geosynthetic reinforcement may be also used to provide tension resistance to the outward thrust load of the embankment, which reaches a maximum at the shoulder of the embankment (Lawson 1992). The tension due to lateral spreading in the geosynthetic reinforcement above deep foundations is not within the scope of this research.

3.5.1 BS8006 Method

The most commonly used procedures for determining the tension in the geosynthetic reinforcement due to vertical loading are those presented in BS8006 (1995). The BS8006 method assumes that the geosynthetic reinforcement is placed above columns installed in a square grid pattern, as shown in Figure 3.3. It is assumed that the embankment fill load is distributed along the horizontal span of the geosynthetic between columns. It is also assumed that the entire load between the columns is carried by the geosynthetic and that there is no support from the foundation soil. The tensile load in the geosynthetic per unit width, T, developed under the vertical line load, W_T, is calculated using the following equation, which is based on parabolic deformation of the geosynthetic:

$$T = \frac{W_T (s-a)}{2a} \cdot \sqrt{1+\frac{1}{6\varepsilon}} \tag{3.27}$$

where s = center-to-center pile/column spacing, a = width of piles or equivalent width of columns, and ε = the strain in the geosynthetic. The strain that develops in the geosynthetic is related to the deflection:

$$\varepsilon = \frac{8 \cdot d^2}{3 \cdot (s-a)^2} \tag{3.28}$$

where d = the maximum vertical deflection of the geosynthetic reinforcement between the points of foundation support. Equation 3.28 is approximate, but it provides strains in very close agreement with the exact solution for strain due to parabolic deformation provided by John (1987):

$$\varepsilon = \frac{1}{2}\sqrt{1+\frac{16d^2}{(s-a)^2}} + \frac{(s-a)}{8d} \cdot \log_e\left[\frac{4d}{(s-a)} + \sqrt{1+\frac{16d^2}{(s-a)^2}}\right] - 1 \tag{3.29}$$

The value of W_T determined by Equation 3.10 or 3.11 may be used in Equation 3.27. For compatibility with the various arching theories, the load, W_T, may also be defined in terms of the

stress reduction ratio so that other methods may also be applied. Considering columns or piles arranged in a square array, the area not supported directly by columns or piles is $(s^2 - a^2)$, and the total vertical load on the geosynthetic may be expressed as $SRR \cdot (\gamma H+q) \cdot (s^2 - a^2)$. It is assumed that one-quarter of the total load is concentrated along each of the four lines that connect the piles/columns. Because there are tributary areas on both sides of each line, equilibrium requires that:

$$W_T \cdot (s - a) = 2 \cdot [¼ \cdot SRR \cdot (\gamma H+q) \cdot (s^2 - a^2)] \tag{3.30}$$

Thus, the vertical load, W_T, may be expressed in terms of the stress reduction ratio as follows (Russell and Pierpoint 1997):

$$W_T = \frac{SRR \cdot (\gamma H + q) \cdot (s^2 - a^2)}{2(s - a)} \tag{3.31}$$

The value of the stress reduction ratio used in Equation 3.31 may be from any source. By substituting Equation 3.31 into Equation 3.27, the tension in the geosynthetic due to the vertical load is estimated as follows:

$$T = \frac{SRR \cdot (\gamma H + q) \cdot (s^2 - a^2)}{4 \cdot a} \cdot \sqrt{1 + \frac{1}{6\varepsilon}} \tag{3.32}$$

For a given geosynthetic material, the tension can also be expressed as:

$$T = E_{geo} \cdot t \cdot \varepsilon = J \cdot \varepsilon \tag{3.33}$$

where T = tension in the geosynthetic, E_{geo} = the modulus of elasticity of the geosynthetic, ε = strain in the geosynthetic, t = thickness of the geosynthetic, and $J = E_{geo} \cdot t$ = geosynthetic reinforcement stiffness.

Lawson (1992) recommends that Equations 3.27 and 3.33, or equivalently Equations 3.32 and 3.33, be solved simultaneously. Substituting Equation 3.33 in 3.32 yields:

$$96 \cdot \varepsilon^3 - 6 \cdot K_g^2 \cdot \varepsilon - K_g^2 = 0 \tag{3.34}$$

where

$$K_g = \frac{SRR \cdot (\gamma \cdot H + q) \cdot (s^2 - a^2)}{J \cdot a} \tag{3.35}$$

The solution to Equation 3.34 is shown in Figure 3.7. For a given loading, as represented by the K_g value, the geosynthetic strain can be obtained from Figure 3.7, and the geosynthetic tension can be calculated from Equation 3.33.

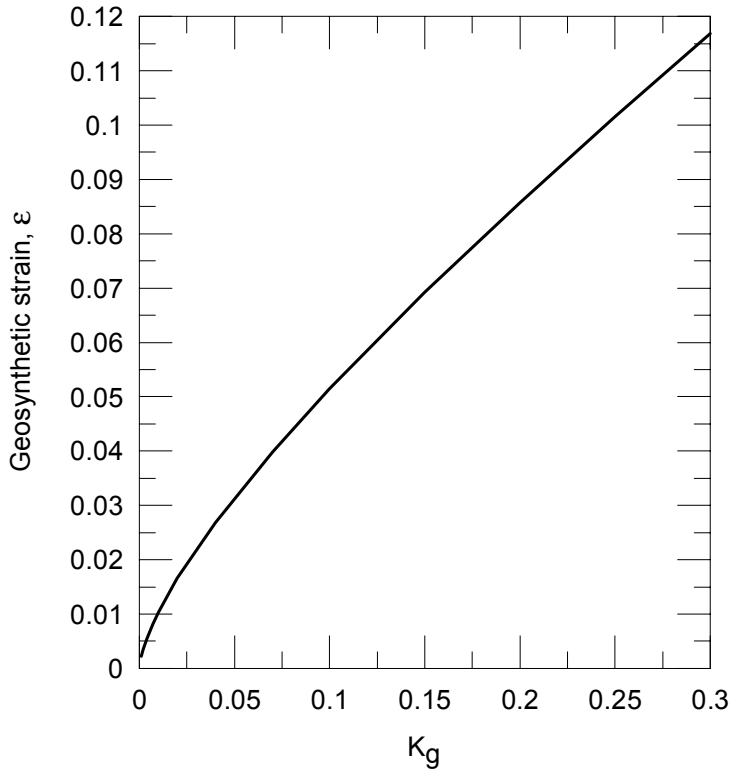

Figure 3.7. Geosynthetic strain versus dimensionless geosynthetic loading parameter, K_g

Many designers choose an upper strain limit in the geosynthetic based on the recommendations provided in BS8006 (1995), which states: "The initial tensile strain in the reinforcement is

needed to generate a tensile load. A practical upper limit of 5-6% strain should be imposed to ensure all embankment loads are transferred to the piles/columns. With shallow embankments this upper strain limit may have to be reduced to prevent differential movements at the surface of the embankment. The long-term strain (due to creep) of the reinforcement should be kept to a minimum to ensure that long-term localized deformations do not occur at the surface of the embankment. A maximum creep strain of 2% over the design life of the reinforcement should be allowed."

3.5.2 Kempfert et al. (2004) Method

Kempfert et al. (2004) present a new method for evaluating the strain and tension in geosynthetic reinforcement. In practice, the strain in the geosynthetic reinforcement is determined using dimensionless design charts, and the tension is determined by multiplying the geosynthetic stiffness by the strain. The method presented by Kempfert et al. (2004) is discussed in this section.

The first step is to calculate the stress, σ_{soil}, on the soft soil in between columns using Equation 3.22. The second step is to determine the force on the geosynthetic. The force on the geosynthetic, F_k, is equal to the stress, σ_{soil}, times a tributary area of the reinforcement associated with the strip of geosynthetic spanning directly between adjacent pile caps. Kempfert et al. (2004) provide recommendations for determining these tributary areas of reinforcement for circular columns installed in square and triangular arrays.

Kempfert et al. (2004) include the resistance of the foundation soil by using a modulus of subgrade reaction, $k_{s,k}$. The modulus of subgrade reaction is the ratio of the pressure applied to the soil over a loaded area divided by the resulting displacement.

Kempfert et al. (2004) determine the stresses in the geosynthetic reinforcement based on a theory of elastically embedded membranes. Kempfert et al. (2004) observed that a higher tension was generated in the reinforcement spanning directly between adjacent columns. In their methods, the maximum stress in the geosynthetic reinforcement occurs over a width equal to b_{Ers}, as

shown in Figure 3.8. For a round column, the value of b_{Ers} is equal to ½ $d_c\sqrt{\pi}$ = 0.886·d_c, where d_c = column diameter.

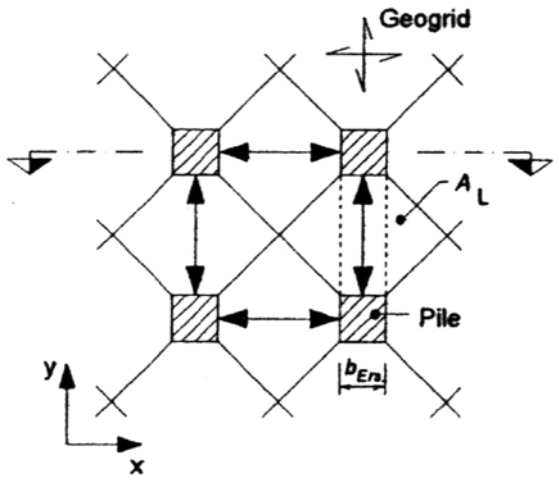

Figure 3.8. Plan view of foundation and geogrid (from Kempfert et al. 2004)

The maximum strain in the geosynthetic reinforcement is dependent upon the tensile stiffness of the geosynthetic, J_k, the modulus of subgrade reaction, the total vertical load, F_k, and the dimensions b_{Ers} and L_w, where L_w = clear spacing between columns. The value of the strain in the reinforcement, ε_k, can be determined from dimensionless design charts, as shown in Figure 3.9. The tensile force in the reinforcement can be calculated directly as a function of the strain in the geosynthetic:

$$T = \varepsilon_k \cdot J_k \tag{3.36}$$

For two layers of geosynthetic reinforcement, the calculated force is divided with respect to the ratio of their tensile moduli (Kempfert et al. 2004).

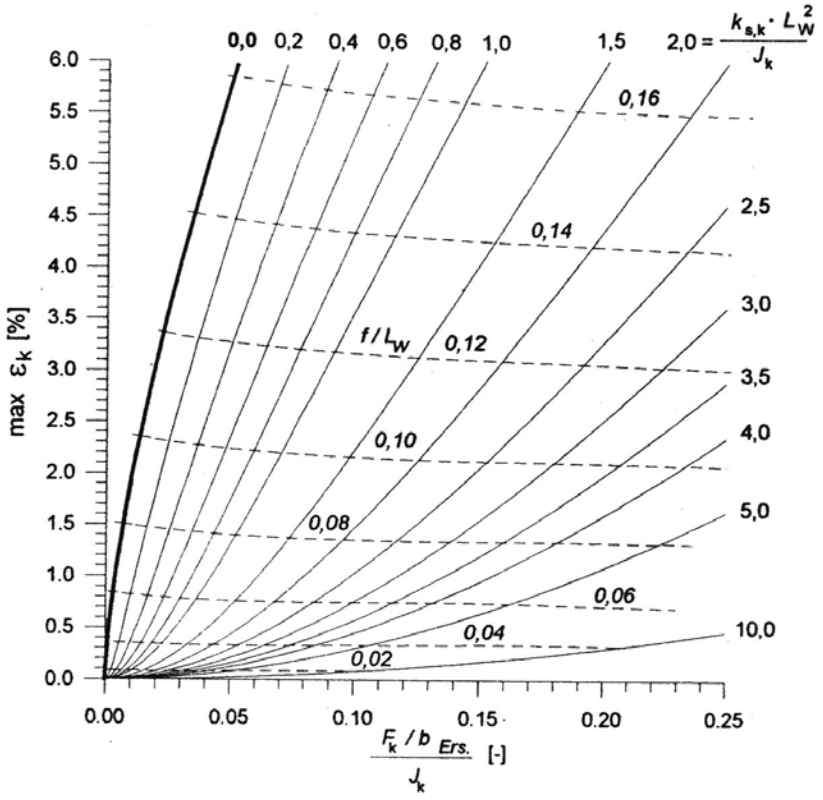

Figure 3.9. Maximum strain in geosynthetic reinforcement (from Kempfert et al. 2004)

The ratio represented on the x-axis of Figure 3.9 is the same as the value of K_g given in Equation 3.35. For a value of modulus of subgrade reaction, $k_{s,k}$, equal to zero, the dark line on the far left of Figure 3.9 may be directly compared to the relationship of K_g to geosynthetic strain as determined by the BS8006 method. This comparison is shown in Figure 3.10, where it can be seen that, for the same geometry and embankment load, the strains calculated by the Kempfert et al. (2004) Method are much higher than those calculated by the BS8006 (1995) Method. The Kempfert et al. (2004) strain is the maximum strain from a theory of embedded membranes, whereas the BS8006 (1995) strain is the uniform strain for parabolic deformation.

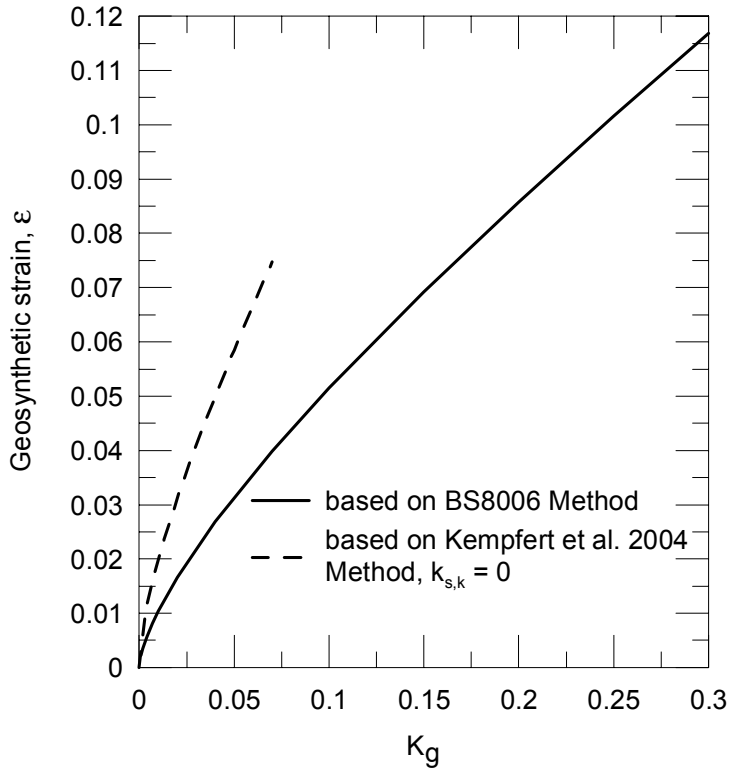

Figure 3.10. Geosynthetic strain versus dimensionless geosynthetic loading parameter, K_g

In Figure 3.9, contours are shown for various values of f/L_w, where f = the maximum vertical deflection of the geosynthetic reinforcement between the points of foundation support, and L_w = clear spacing between columns (s – a). Based on the contours given in Figure 3.9 for the Kempfert et al. (2004) Method and the relationship given in Equation 3.28 for the BS8006 Method, the geosynthetic strain is plotted against the ratio of maximum geosynthetic deflection to clear spacing between columns in Figure 3.11. It can be seen that the Kempfert et al. (2004) Method produces similar, but slightly higher, maximum deformations than the BS8006 (1995) Method at the same strain.

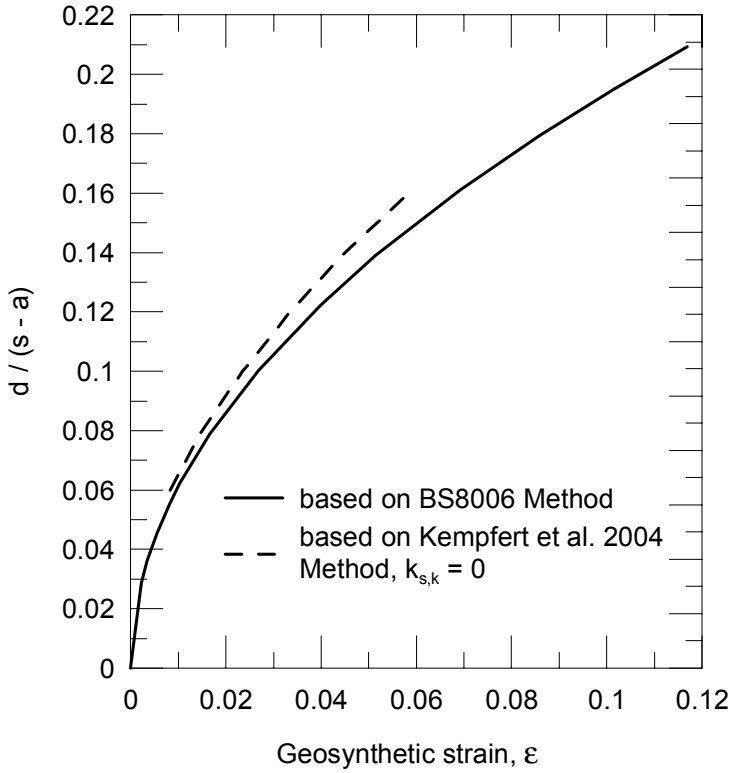

Figure 3.11. Geosynthetic strain versus $\frac{d}{(s-a)}$

3.5.3 Russell et al. (2003) Method

The numerical analyses performed by Russell and Pierpoint (1997) indicated that the reinforcement tension was concentrated in the area immediately between the pile caps. As a result, Russell et al. (2003) recommend providing two layers of geosynthetic reinforcement: (1) primary reinforcement, which is a high strength reinforcement material that spans between adjacent pile caps, and (2) secondary reinforcement, which is of lower strength but which covers the entire area beneath the embankment (Naughton and Kempton 2005). The recommended installation pattern of the geosynthetic reinforcement is shown in Figure 3.12. Separate calculations are made for the tension in the primary and secondary reinforcement, based on an approximation of the parabolic solution for geosynthetic deformation.

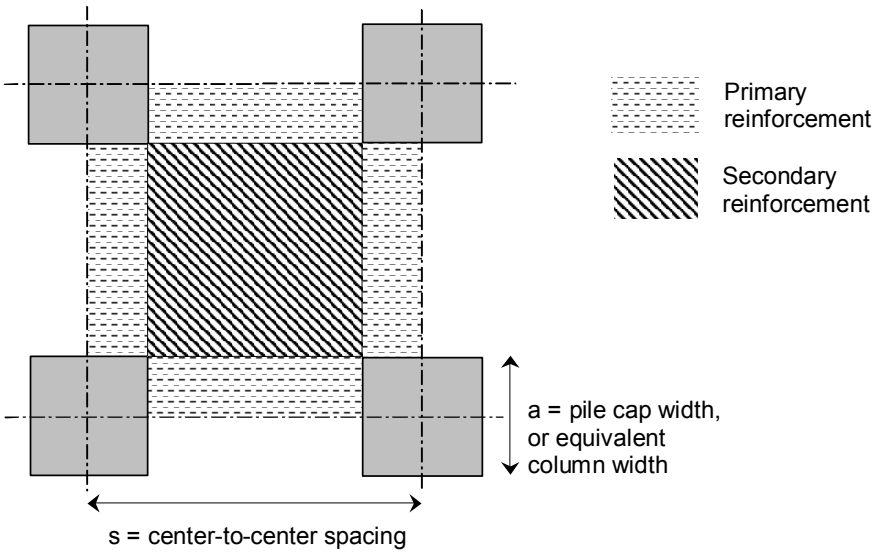

Figure 3.12. Plan view of base of embankment (from Russell et al. 2003)

3.6 Closing Remarks

The stress reduction ratio, SRR, is defined as the ratio of the stress applied to the foundation soil between the columns, σ_{soil}, to the average stress applied by the embankment. Several methods are currently available for evaluating the SRR; however, the existing methods for determining the stress reduction ratio yield very different results. There is no widespread consensus on which method should be used. This chapter presents seven methods currently available to evaluate the SRR:

(1) BS8006 Method (BS8006 1995)
(2) Adapted Terzaghi Method 1 (Russell and Pierpoint 1997)
(3) Adapted Terzaghi Method 2 (Russell et al. 2003)
(4) Hewlett & Randolph Method (Hewlett and Randolph 1998)
(5) German Method (Kempfert et al. 2004)
(6) Adapted Guido Method (Rusell and Pierpoint 1997)
(7) Swedish Method (Rogbeck et al. 1998, Horgan and Sarsby 2002)

The methods of evaluating SRR are used to evaluate the vertical stress on top of the geosynthetic reinforcement. The resulting strain and tension in the geosynthetic are most often calculated based on an assumed parabolic deflected shape, as incorporated in the BS8006 (1995) Method.

The embankment load that is not carried by direct arching to the columns or by subgrade reaction is assumed to be carried by the strands of geosynthetic spanning directly from column to column. Kempfert et al. (2004) apply a theory of elastic embedded membranes to obtain the geosynthetic strain and tension, which are determined through the use of dimensionless design charts. The strains calculated by the Kempfert et al. (2004) Method are higher than for a parabolic deflected shape. Russell et al. (2003) present a method in which strong primary geosynthetic reinforcement spans between columns and weaker secondary reinforcement may be used elsewhere.

CHAPTER 4
CASE HISTORY: FULL-SCALE TEST EMBANKMENT I-95/ROUTE 1 INTERCHANGE, WOODROW WILSON BRIDGE PROJECT

4.1 Introduction

This chapter describes a case history of a full-scale test embankment that was constructed at the I-95/Route 1 Interchange in Alexandria, Virginia as part of the Woodrow Wilson Bridge Reconstruction Project. This case history was used to calibrate the finite difference and finite element models of a column-supported embankment. An extensive subsurface exploration and laboratory testing program was conducted at the test embankment site, and the test embankment was fully instrumented. This case history provided much valuable information on the behavior of a column-supported embankment.

The Woodrow Wilson Bridge spans over a mile across the Potomac River and is a vital link between Northern Virginia and Maryland. As part of the $2.4 billion Woodrow Wilson Bridge Reconstruction Project, the existing 6-lane bridge will be replaced with a 12-lane bridge, which will require significant realignment and widening of the approach interchanges in Virginia and Maryland. On the Virginia side, the interchange between I-95 and U.S. Route 1 will be reconstructed at an estimated cost of $350 million (VDOT 2001b). A view of the interchange is shown in Figure 4.1.

Figure 4.1. View of I-95/Route 1 Interchange

Alluvial deposits of very soft and highly compressible organic silts and clays underlie the I-95/Route 1 interchange. New embankments will be constructed to widen existing embankments, which are approximately 10 feet high. Significant primary and secondary consolidation settlements on the order of 2 to 5 ft were predicted beneath the new embankments (Shiells et al. 2003). In some areas, short-term embankment stability was a primary concern. Furthermore, project requirements included maintaining existing traffic flow and meeting a tight construction schedule.

To address the construction challenges, the "wet" and "dry" methods of deep mixing were considered for support of most of the new embankments (Lambrechts et al. 2003, Shiells et al. 2003). Because this was the first large project of its type in the mid-Atlantic region and the first use of deep mixing by the Virginia Department of Transportation (VDOT), a program of laboratory mix design studies, field trials, and a test embankment were completed. Because there were more uncertainties about applicability of the dry method than the wet method at the I-95/Route 1 interchange site, the test embankment was supported on columns installed by the dry method of deep mixing. Ultimately, the wet method was selected for the production columns, but the test embankment provides an excellent case history of an instrumented embankment supported on columns installed by the dry method.

The test embankment was thoroughly instrumented, and the results of the instrumentation data were used to create and calibrate numerical models of an embankment supported on deep mixed columns. This chapter describes the site conditions and the full-scale test embankment that was constructed at the I-95/Route 1 interchange site.

4.2 History and Site Conditions

The original Woodrow Wilson Bridge and its embankments were constructed in the early 1960's. Since the project site is located above thick alluvial deposits of very soft and highly compressible organic silts, a combination of sand drains, surcharge loading, and removal of the soft soils were used during original construction. The sand drains were 18-inches in diameter, and were installed at 9 to 10-feet centers in a square pattern. Surcharges were left in place up to 13 months after installation of the sand drains. Settlements of the embankment during construction ranged

from 1.5 to 5 feet. No additional ground improvement was performed for minor widening of the existing embankment in the 1970's since the sand drains placed in the 1960's extended beyond the original toe of the embankment (VDOT 2001b).

In December 1999, URS Greiner Woodward-Clyde concluded in their Ground Improvement Feasibility Report for the Federal Highway Administration (FHWA) that prefabricated vertical drains and the deep mixing method technology were the most cost effective and practical methods of ground improvement for the embankments that were to be constructed as part of the Woodrow Wilson Bridge Reconstruction Project. URS Greiner Woodward-Clyde recommended that test embankments be constructed at the site to assess the performance of these technologies (VDOT 2001b).

In 2000, VDOT initiated the design of a test embankment program, which included further subsurface investigation, laboratory testing, bench-scale mixing tests, and field tests columns. Subsurface explorations performed in the area of the test embankment for the deep mixing method included two test borings, ten piezocone soundings, and six dilatometer soundings. Laboratory testing included moisture content, organic content, unit weight, specific gravity, Atterberg limits grain-size distribution, unconsolidated-undrained (UU) triaxial shear tests, consolidated-isotropically-undrained (CIU) triaxial tests, lab vane shear tests, consolidation tests, and flexible wall permeability tests. Detailed results of the subsurface investigation and laboratory tests are presented in the "Final Data Report on Ground Improvement for Embankment Construction at the I-95/Route 1 Interchange" by Haley & Aldrich and Virginia Geotechnical Services, P.C. (2000).

In general, the subsurface conditions consist of variable depths of man-made fill overlying extremely soft and highly compressible organic clays and silts to depths in excess of 30 feet below existing ground surface. The highly compressible organic clays and silts are underlain by sand and gravel terrace deposits, which are underlain by very stiff to hard silty clay of the Potomac Formation. The ground water table is located approximately at the surface of the soft organic clay. A typical subsurface profile beneath the test embankment is shown in Figure 4.2.

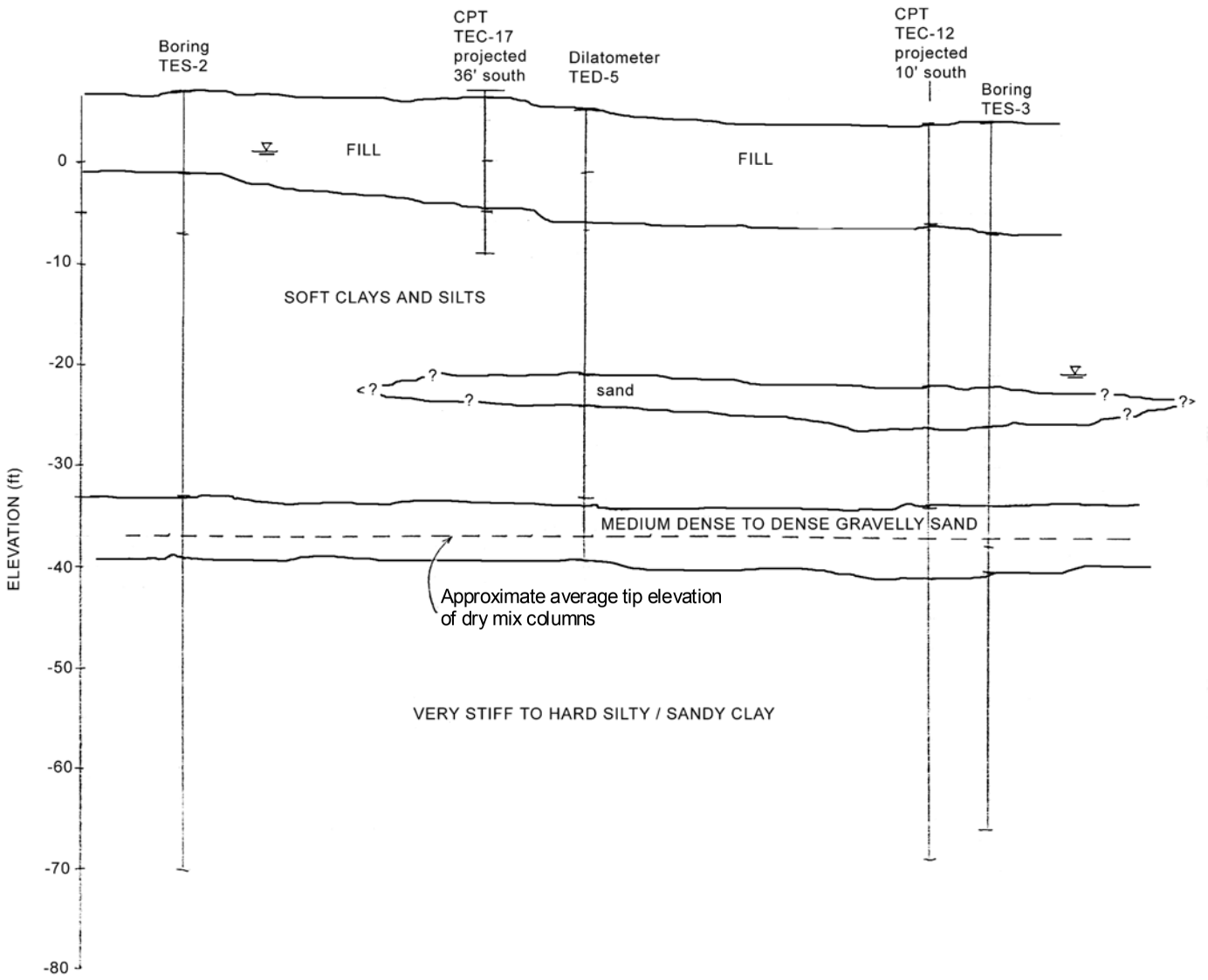

Figure 4.2: Test embankment subsurface profile

The man-made fill layer varies in thickness from 7 to 14 feet. The fill consists primarily of loose to medium dense fine sand, with some layers of medium stiff silty or sandy clay. Trace amounts of organics and gravel were encountered throughout the fill layer. Standard Penetration Test (SPT) N_{60} blow counts in this layer ranged from 6 to 22. A representative N_{60} value of 14 was used to develop material property value correlations for the fill layer. The moisture content of the fill layer ranged from 9% to 24%.

The soft and highly compressible organic clays and silts ranged in thickness from 25 to 31 feet. Blow counts in the compressible organic clays and silts ranged from 1 to 4. Organic contents ranged from 1% to 15% with most samples in the range of 5% to 10%. The natural moisture content of the alluvial clay soils ranged from 50% to 93%, with an average of about 80%. The liquid and plastic limits varied, but averaged about 80 and 25 percent, respectively, in the upper portions, and increased to 120 and 50 percent, respectively, in the deeper portions (Lambrechts and Layhee 2003). Consolidation tests indicated that the alluvial deposits are slightly overconsolidated, with an overconsolidation ratio of about 1.4 to 1.8. Typical pH values ranged from 4 to 9, with an average of about 6.5. Sulfate content ranged between 50 and 338 ppm, with an average of 120 ppm (Shiells et al. 2003).

Terrace deposits of medium dense to dense gravelly coarse to fine sand underlie the soft alluvial deposits. The terrace deposits are approximately 6 feet thick. The Potomac Formation, which consists of very stiff to hard silty and sandy clay, underlies the terrace deposits. The Potomac Formation extends beyond depths of 77 feet below the ground surface.

4.3 Test Embankment Construction

A generalized cross-section and subsurface profile of the test embankment is shown in Figure 4.3. A total of 59 dry mixed columns were installed from September 11 through September 17, 2000. The columns were 32-inches in diameter, and were installed in a triangular pattern on 6 and 10 ft center-to-center spacings, corresponding to area replacement ratios of 17.9% and 6.4%, respectively. The closer spacings were used beneath the geosynthetic-reinforced retaining wall on the south end of the embankment. The tops of the columns were generally located 3 ft below the existing ground surface, and the columns were specified to penetrate 3 ft into the medium

dense to dense terrace deposits at depths of approximately 39 to 43 feet below the original ground surface. As a result, the total length of the columns ranged from 32 to 40 ft, with an average installed length of 37 ft. Based on the results of laboratory testing, an amendment dosage rate of 9.5 lb/ft^3 with 100% cement was specified for the columns beneath the test embankment. The contract required a minimum unconfined compressive strength of 50 psi at 14 days, and 80 psi at 28 days (VDOT 2001b).

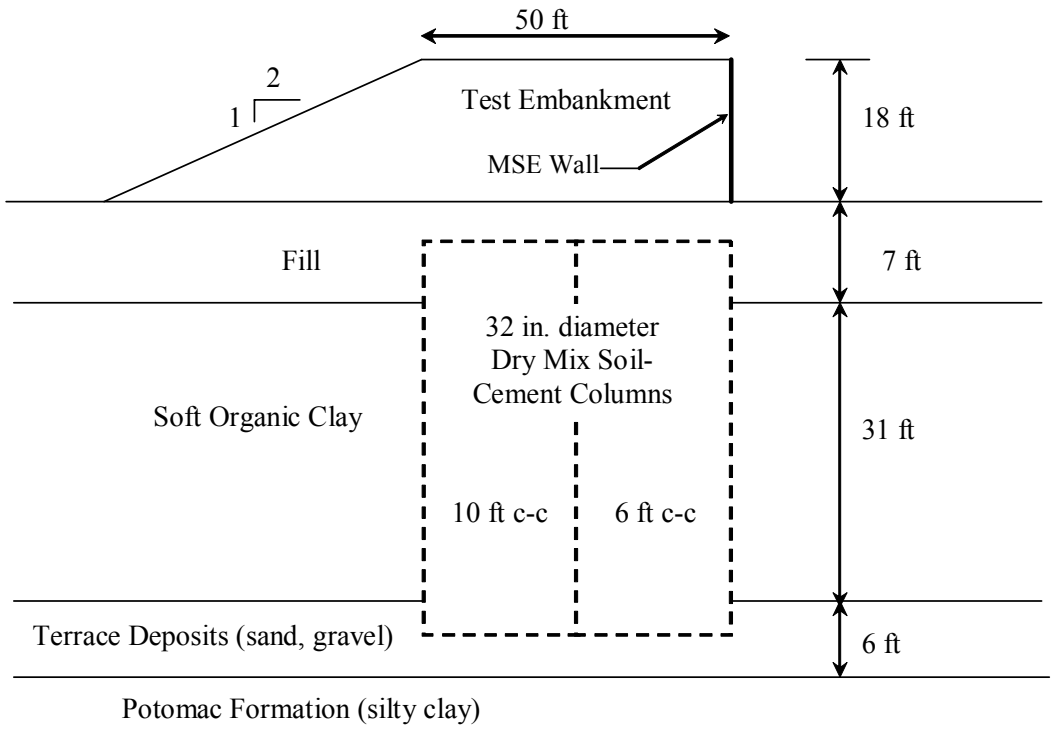

Figure 4.3. Typical section of the test embankment and subsurface conditions

The test embankment was constructed between October 4 and October 13, 2000. The embankment, which measured 50 feet square at the top, had a vertical geosynthetic-reinforced retaining wall on one side and 2H:1V slopes on the other three sides. The embankment had a height of approximately 18 ft, and was constructed with a crushed aggregate after an initial placement of approximately 3 ft of a bank run sand and gravel. The bank run sand and gravel had an average dry density of 115 pcf, and an average water content of 15%; the crushed

aggregate had an average dry density of 135 pcf, and an average water content of 5%. The test embankment was removed in November 2001.

In addition to the columns for the embankment, 23 other test columns with varying binder mixes and dosage rates were installed outside of the test embankment footprint. Three core samples, two pressuremeter tests, and three successful reverse penetration (or pullout) tests were performed on the test columns. Core sampling was performed using double tube rock core sampling procedures. Pressuremeter testing refers to conventional Menard pressuremeter tests. Reverse penetration tests were performed by installing a steel probe at the base of the column during column construction, and after a specified curing period, the probe was extracted through the column while recording the pullout force on a load cell.

For the dry mixed test columns outside the test embankment with a dosage rate of 9.5 lb/ft^3 and 100% cement, pressuremeter tests indicated an average undrained shear strength of about 2500 psf. Laboratory tests on core samples indicated an average in-situ shear strength of about 2600 psf. Reverse penetration tests indicated an average undrained shear strength of approximately 10,000 psf, which is much higher than the strengths indicated by the pressuremeter tests or core samples.

4.4 Results of Instrumentation Data

Instrumentation was installed to monitor the performance of the test embankment, which was left in place approximately 13 months. Instrumentation included eight settlement plates, eleven settlement pins, one observation well, six vertical inclinometers, a horizontal inclinometer, two vibrating-wire piezometers, two magnetic extensometers, eight pressure cells, and six thermistors.

The research described here is concerned with the settlement and load transfer behavior of columns and soil under vertical embankment loads. Of particular interest is the data generated by the horizontal inclinometer, settlement plates and pins, and the pressure cells. The settlement profile below the embankment was measured by the horizontal inclinometer. Vertical settlement was measured by the settlement plates and pins. The vertical stresses above the columns and the

soil in between columns was measured by the pressure cells. The locations of these instruments in plan view are shown in Figure 4.4.

The settlement profile below the embankment as measured by the horizontal inclinometer is shown in Figure 4.5. Settlement continued over the 13 month period the embankment was in place, with maximum settlements occurring beneath the vertical geosynthetic-reinforced retaining wall and extending back from the wall beneath the embankment. These maximum settlements were about 9.5 inches in August 2001. The embankment was removed in November 2001.

Six settlement plates were installed beneath the full height of the test embankment and two were installed beneath the embankment side slopes. In August 2001, plate settlements beneath the full height of the embankment ranged from 11 to 16 inches. The maximum settlement of 16 inches was measured by settlement plate #6. This plate was located in the region of the closely-spaced columns near the geosynthetic-reinforced retaining wall.

The pressure cells were installed in the existing fill at an elevation approximately 2 ft above the tops of the columns and 2 ft below the top of the existing fill, as shown in Figure 4.6. In the area of widely spaced columns, the two pressure cells installed directly above the columns responded nearly identically to each other, and similarly, the two pressure cells installed between columns responded nearly identically to each other. The stress measured above the widely spaced columns at the pressure cell elevation was approximately 5100 psf, and the stress measured above the soil was approximately 1980 psf (VDOT 2001b). The data from these four pressure cells is shown in Figure 4.7. In the area of the closely spaced columns, the pressure cells installed directly above the columns did not respond nearly identical to each other, nor did the pressure cells installed between columns. However, similar to the pressure cells above the widely spaced columns, stress concentrations were measured above the columns. This data is shown in Figure 4.8.

In all cases, the pressure cell readings increased rapidly as the embankment was placed, but then leveled off within a few days after embankment completion. This indicates that the local relative

deformation pattern near the top of the columns was established very quickly, even though the test embankment continued to settle for the approximately 13 months that the embankment was in place. This suggests that consolidation of the soft clay near the top of the columns occurred quickly, as would be expected near a drainage boundary, and that on-going consolidation of the soft clay at depth did not affect stress distribution at the level of the top of the columns.

4.5 Closing Remarks

The instrumentation data collected at the I-95/Route 1 test embankment shed much light on the settlement and load transfer behavior of a column-supported embankment. The results of the instrumentation data were used to calibrate numerical models of an embankment supported on deep mixed columns. These analyses are described in detail in Chapter 5.

Ultimately, the wet method was selected for the production columns, but the test embankment provides an excellent case history of an instrumented embankment supported on columns installed by the dry method. Further information on the final design of the I-95/Route 1 interchange can be found in Shiells et al. (2003) and Lambrechts and Layhee (2003).

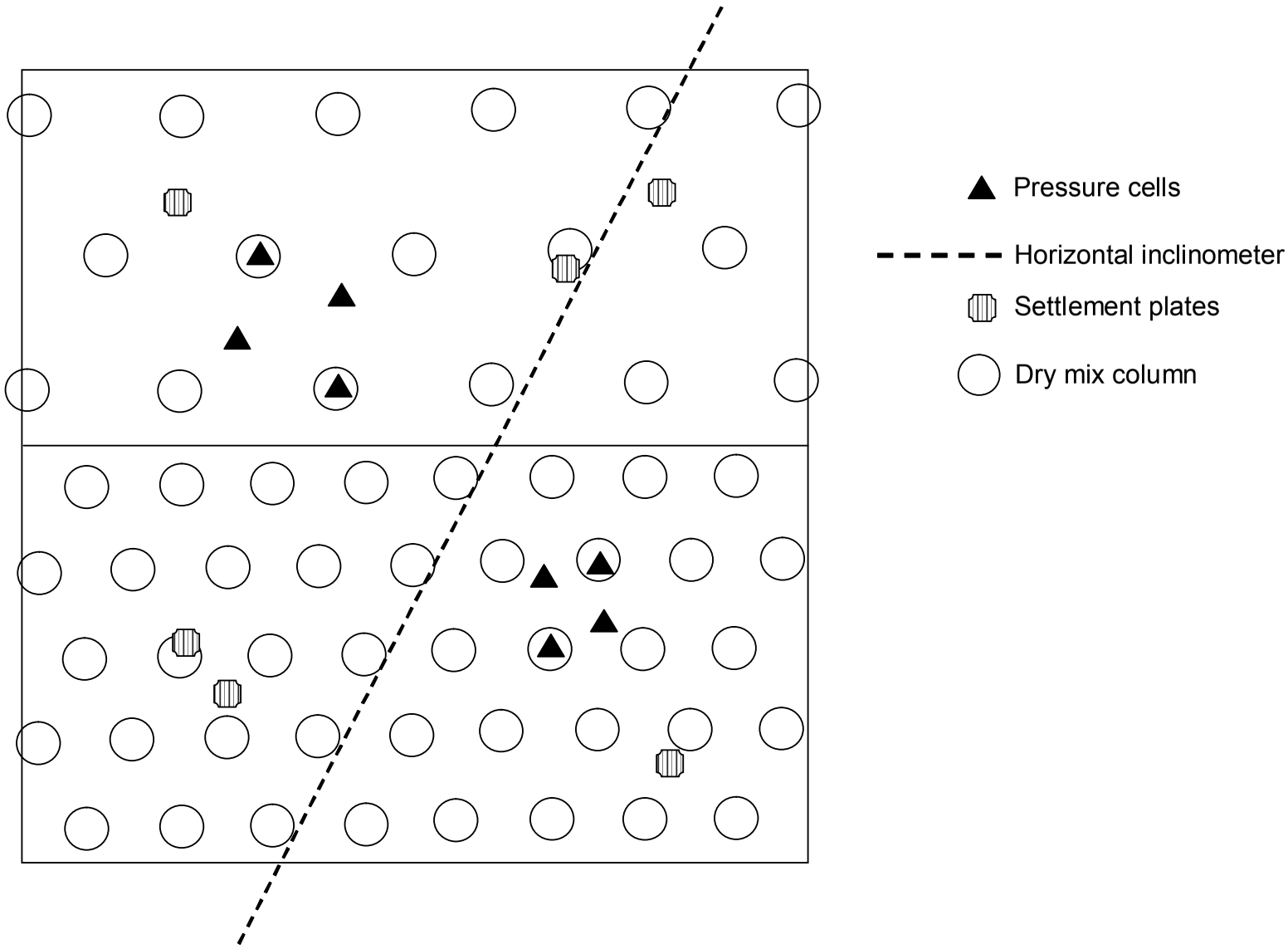

Figure 4.4: Schematic of plan view of base of test embankment with instrument and column locations

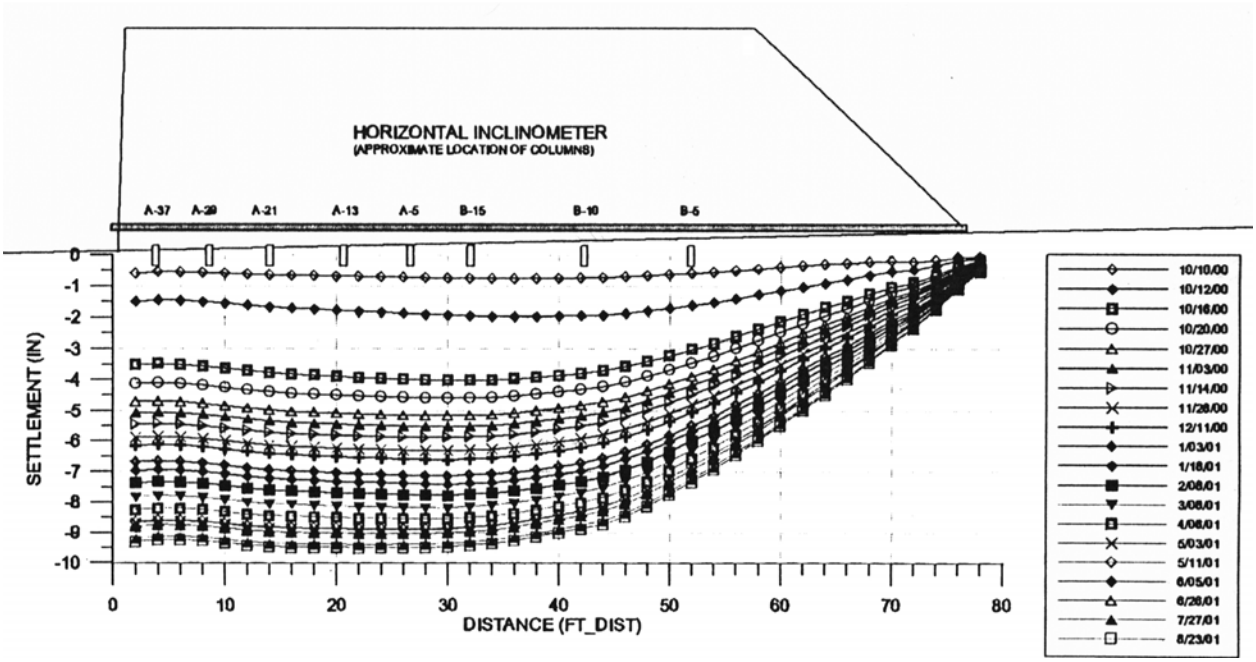

Figure 4.5: Data from horizontal inclinometer (from VDOT 2001b)

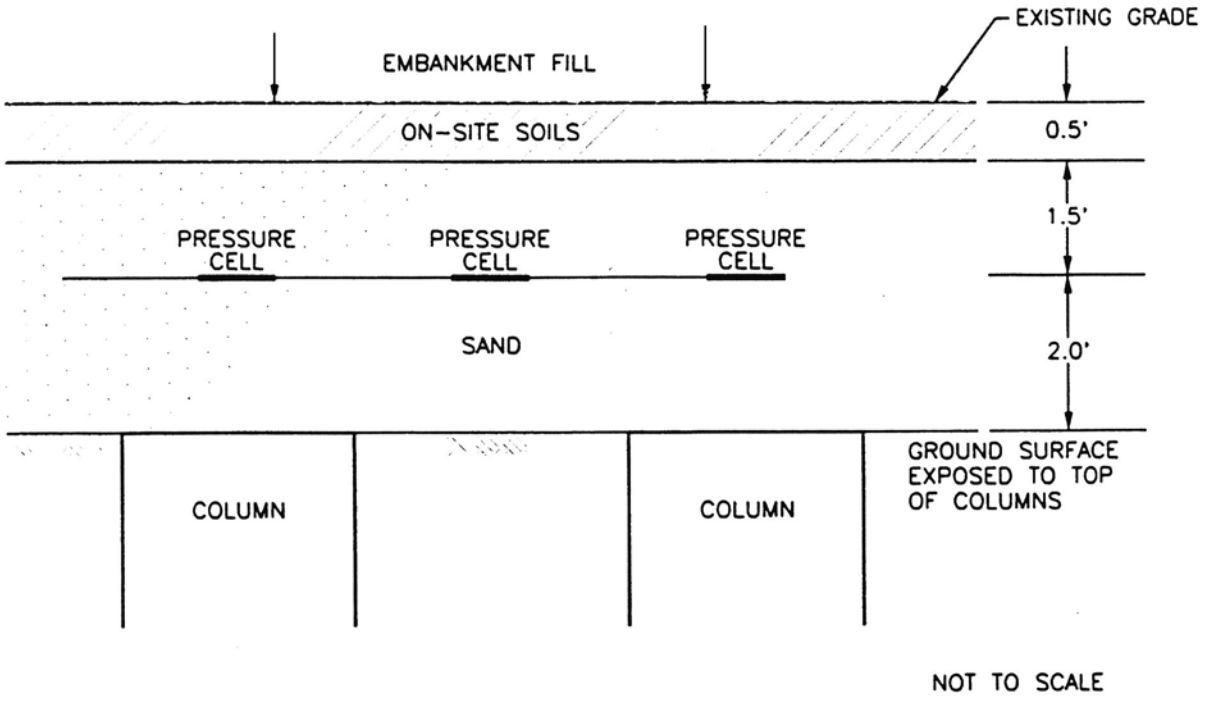

Figure 4.6: Location of pressure cells (elevation view) (from VDOT 2001b)

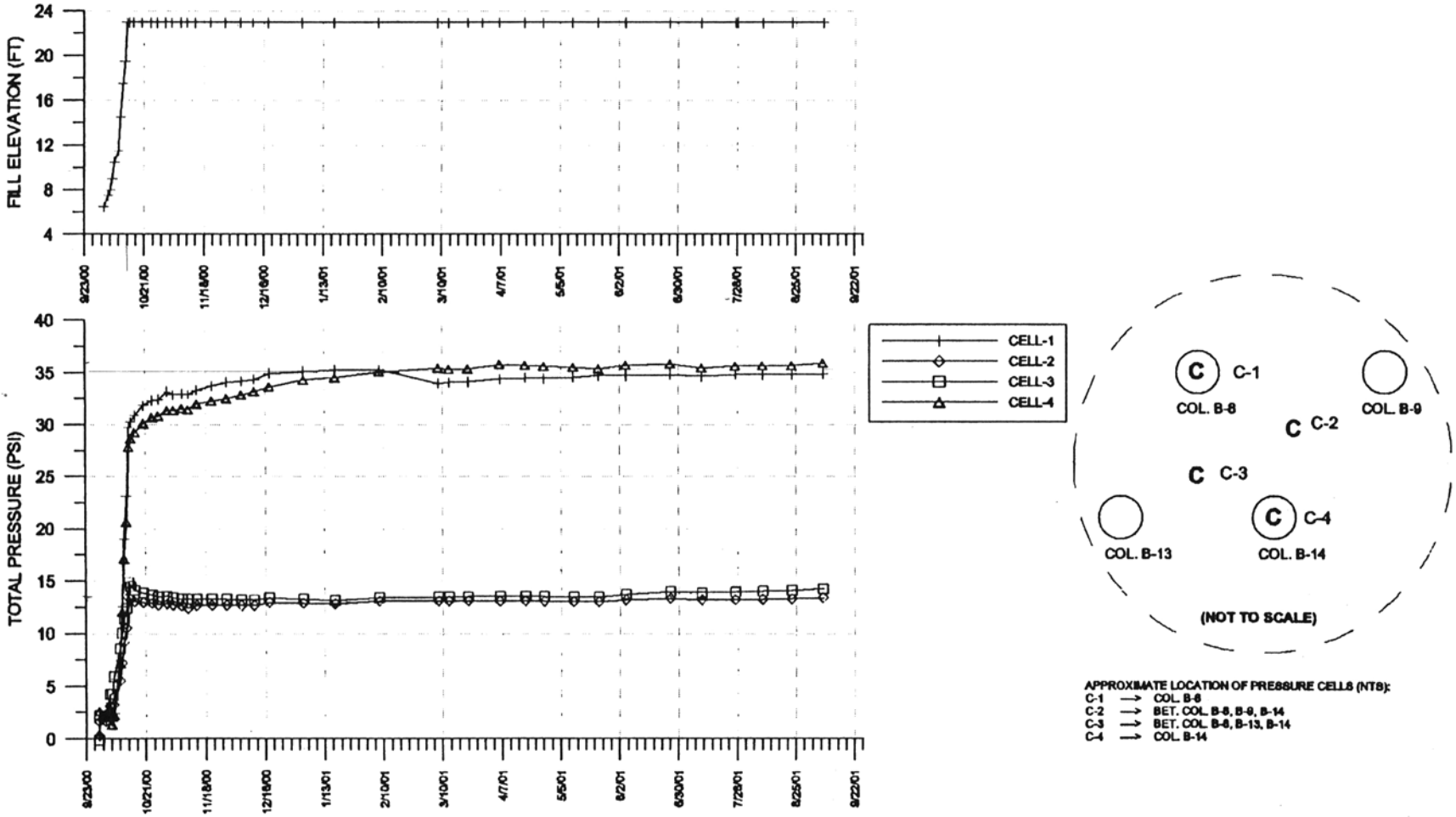

Figure 4.7. Pressure cell data from pressure cells installed above widely spaced columns (from VDOT 2001b)

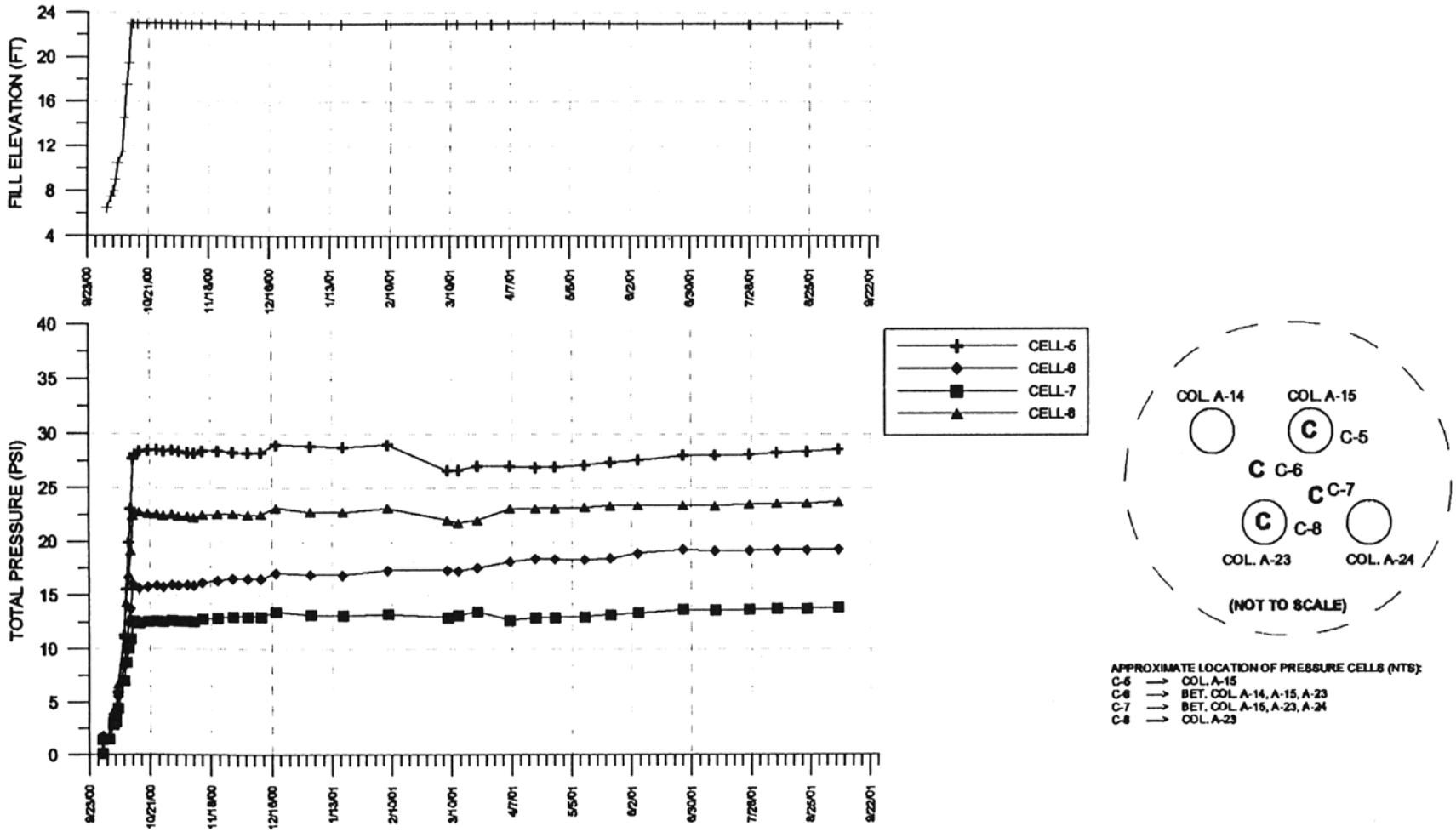

Figure 4.8: Pressure cell data from pressure cells installed above closely spaced columns (from VDOT 2001b)

CHAPTER 5
NUMERICAL MODELING OF I-95/ROUTE 1 TEST EMBANKMENT

5.1 Introduction

Verification analyses were performed to gain an understanding of appropriate numerical modeling procedures for evaluating the load transfer behavior of column-supported embankments. The results of the verification analyses were compared with measurements from the instrumented test embankment supported on deep-mixing-method (DMM) soil-cement columns installed by the dry method at the I-95/Route 1 Interchange in Alexandria, Virginia, as described in Chapter 4.

The results of the numerical analyses were compared with pressure cell readings in the test embankment. In the area of widely spaced columns, two pressure cells were installed in the existing fill directly above two columns at an elevation approximately 2 ft above the tops of the columns and 2 ft below the top of the existing fill. These two cells responded nearly identically to each other. Two pressure cells were also installed between columns at the same elevation as the cells located directly above columns, and again these cells responded nearly identically to each other. The stress measured above the columns at the pressure cell elevation was approximately 5,100 psf, and the stress measured above the soil was approximately 1980 psf (VDOT 2001b).

Three-dimensional drained analyses of the test embankment were performed using FLAC3D (Fast Lagrangian Analysis of Continua in 3 Dimensions) (ITASCA 2002a). Two-dimensional, drained axisymmetric analyses of the test embankment were also performed using FLAC (Fast Lagrangian Analysis of Continua) (ITASCA 2002b). The computer programs FLAC3D and FLAC were chosen for this research because they were readily available and have been used by other researchers to model column-supported embankments (e.g., Russell and Pierpoint 1997, Kempton et al. 1998, Han and Gabr 2002, and Han et al. 2005). The FLAC and FLAC3D analyses were performed under drained conditions. During the course of early FLAC verification efforts, problems were encountered when coupled analyses were performed in conjunction with using the modified Cam Clay material model for the soft clay, as described briefly in section 5.5. Therefore, consolidation analyses of the I-95/Route 1 test embankment

were performed using the finite element program SAGE (Static Analysis of Geotechnical Engineering Problems) (Bentler et al. 1999).

The results of the three-dimensional model produced good agreement with the pressure cell data from the I-95/Route 1 test embankment. The results of the two-dimensional model provided a good match to the pressure cell data and to the results of the FLAC3D three-dimensional analyses. The consolidation analyses performed using SAGE produced a stress distribution above the columns that was nearly identical to the results of the drained analyses performed using FLAC3D and FLAC, and that was also in good agreement with the pressure cell data.

In this chapter, the material property values and constitutive models used to model the test embankment site are described. Next, the FLAC3D, FLAC, and SAGE verification numerical analyses are described. The results of the two-dimensional and three-dimensional, as well as the drained and consolidation, analyses are compared. It was concluded that the load transfer behavior of column-supported embankments could be reasonably well modeled using axisymmetric drained analyses. After successful calibration of the axisymmetric drained model, it was used in the parametric studies described in Chapters 6 and 7.

5.2 Material Property Values and Constitutive Models

For the numerical modeling of the I-95/Route 1 test embankment, material property values were chosen for the subsurface soils, DMM columns, and embankment fill. Subsurface conditions were described in Chapter 4, and an idealized subsurface profile is shown in Figure 4.3. The profile that was used for the FLAC3D, FLAC, and SAGE verification numerical analyses is shown in Figure 5.1, and the final material property values and constitutive models that were used for all of the numerical analyses are presented in Table 5.1.

The dry density and moisture content of the embankment material were determined based on placement and compaction records of the embankment construction. The embankment was placed in compacted lifts over a time period of 10 days. Embankment material property values were chosen to correspond to those of a dense, well-graded sandy gravel. A linear-elastic,

perfectly-plastic model with a Mohr-Coulomb failure criterion was used to model the embankment fill.

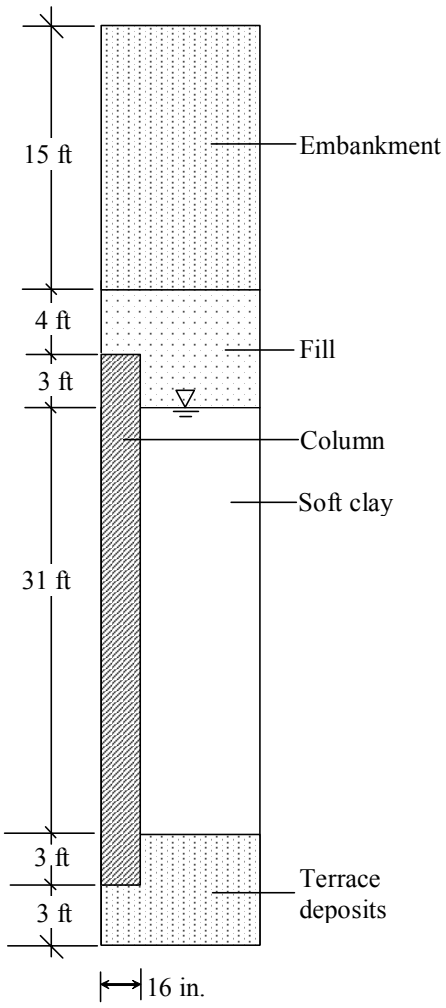

Figure 5.1. Idealized profile used in numerical analyses

Table 5.1. Material property values and models used in the numerical analyses

	Fill	Soft Clay	Base Sand	Column	Embankment
Model type	Mohr-Coulomb	Cam Clay	Mohr-Coulomb	Mohr-Coulomb	Mohr-Coulomb
Moist Density, lb/ft^3	125	-	-	-	139
Sat. Density, lb/ft^3	-	97	131	101	-
Elastic Modulus, psf	450,000	-	400,000	1,340,000	1,000,600
Poisson's Ratio	0.3	0.3	0.31	0.3	0.23
Cohesion, psf	350 / 0	-	0	6700	0
Friction Angle, deg.	35	-	34	0	45
Dilation Angle, deg.	0	-	0	0	15
Critical Shear Stress Ratio, η_{crit}	-	1.3	-	-	-
Lambda, λ	-	0.375	-	-	-
Kappa, κ	-	0.058	-	-	-
Pressure at Specific Volume, psf	-	2,100	-	-	-
Specific Volume	-	4.1	-	-	-
Preconsolidation Pressure, psf	-	see text	-	-	-
Hydraulic conductivity, cm/s	-	$1.2x10^{-6}$	$1x10^{-1}$	$1x10^{-5}$	-
Porosity	-	0.68	0.35	0.68	-

The existing man-made fill consists primarily of loose to medium dense fine sand, including some medium stiff silty clay. A representative N_{60} value of 14 was used to develop material property value correlations for the fill layer using correlations by Duncan et al. (1989), Terzaghi and Peck (1967), NAVFAC (1986), Tomlinson (1977), McGregor and Duncan (1998), and Bowles (1996). A friction angle of 35 degrees was used for the entire layer of existing man-made fill. A cohesion intercept of 350 psf was assigned to the upper four feet of fill to account for strength induced by negative pore water pressures above the water table and for the occasional occurrence of silty clay; a cohesion intercept of zero was used for the lower portion of the fill. A range of values of modulus of elasticity, E, from 300,00 to 600,000 psf were obtained using correlations by D'Appolonia et al. (1970), Mitchell and Gardner (1975), Bowles (1996), and Poulos (2002). However, an overall good model of the embankment performance was achieved using a modulus value of the existing fill equal to 450,000 psf (Stewart et al. 2004). A linear-elastic, perfectly-plastic model with a Mohr-Coulomb failure criterion was used to model the existing man-made fill.

The modified Cam Clay model was used to model the soft organic clay. The model parameter values were obtained from the results of an extensive laboratory test program performed by Haley & Aldrich, Inc. and Virginia Geotechnical Services, P.C. (2000), which included triaxial compression, 1-D consolidation, and permeability tests. The consolidation tests disclosed that the clay is overconsolidated by about 630 psf, and this was incorporated in the analyses. The base-case values of the compressibility parameters lambda and kappa listed in Table 5.1 provide a good fit to the laboratory test data.

A linear-elastic, perfectly-plastic model with a Mohr-Coulomb failure criterion was used to model the sand and gravel terrace deposits. Property values were obtained using correlations with a representative SPT N_{60} value of 19. Deformations occurring in the very stiff to hard silty clay of the Potomac Formation were assumed to be relatively unimportant compared to the deformations of the other materials, and this unit was not included in the numerical analyses.

In addition to determining property values for the existing subsurface materials, property values were also selected for the dry mixed columns. Test results were not available to directly provide effective-stress based strength parameter values for the column material. Kivelo (1998)) and Broms (2003) provide some recommendations for estimating effective-stress based strength parameter values from unconfined compression test results. McGinn and O'Rourke (2003) used an effective stress cohesion intercept of one-half the unconfined compression strength and an effective stress friction angle of zero in their numerical analyses of wet-mixing-method columns at the Central Artery project in Boston. In the analyses described in this chapter, the approach of McGinn and O'Rourke (2003) was used in these verification analyses. Subsequent parametric studies were performed to evaluate the method of modeling the strength characterization of DMM columns, and these studies are described in Chapter 6.

For the dry mixed test columns outside the test embankment, pressuremeter tests indicated an average undrained shear strength of about 2,500 psf. Laboratory tests on core samples indicated an average in-situ shear strength of about 2,600 psf. Reverse penetration tests indicated an average undrained shear strength of approximately 10,000 psf, which is much higher than the

strengths indicated by the pressuremeter tests or core samples. It was expected that the column strength and modulus values would be important in calculating the stress distribution and the vertical and horizontal displacements beneath the embankment. Consequently, an initial parameter study was performed using column shear strength values of 2500, 5000, 7500, and 10,000 psf. The modulus of elasticity, E, of cement dry-mix columns ranges from 65 to 250 times the column unconfined compression strength, $q_{u,col}$, according to Baker (2000) and Broms (2003). Laboratory test results using soil from the I-95/Route 1 site indicated a factor of about 100 may apply (Jacobson et al. 2003), and this value was selected for the base case. The parameter study described in Stewart et al. (2004) settled on a shear strength value of the columns of 7500 psf, which corresponds to a modulus value of the columns equal to 1,500,000 psf. However, based on subsequent studies, it was discovered that a shear strength value of the columns of 6700 psf, which corresponds to a modulus value of the columns equal to 1,340,000 psf, provided a better fit to the test embankment instrumentation data. Therefore, a column shear strength value of 6700 psf and a modulus value of 1,340,000 psf were used for the analyses described in this chapter.

5.3 Three-Dimensional Finite Difference Analyses Using FLAC3D

Three-dimensional drained analyses of the widely spaced columns beneath the test embankment were performed using FLAC3D. FLAC3D builds upon the capabilities of the two-dimensional finite difference program FLAC. FLAC3D is a three-dimensional explicit finite difference program. Materials are represented by polyhedral elements, or zones, within a three-dimensional grid. Additional details about FLAC3D are described in the users manual (ITASCA 2002a). The program has eleven basic built-in material models. The linear elastic, Mohr-Coulomb, and Modified Cam Clay models were used in the three-dimensional analyses.

The purpose of the 3D analyses was threefold: (1) create and verify a true three-dimensional model, (2) verify 2D axisymmetric analyses using a three-dimensional representation of an axisymmetric model, and (3) to develop recommendations/conclusions about appropriate numerical modeling methods. Descriptions of the three-dimensional finite difference analyses of the widely spaced columns beneath the test embankment are provided in this section. The profile

used in the three-dimensional analysis is shown in Figure 5.1. Material property values are listed in Table 5.1.

5.3.1 True Three-Dimensional Geometry

The results of numerical analyses based on a three-dimensional representative model of the columns beneath the center of the test embankment were compared with pressure cell readings in the test embankment. The lay-out of the widely spaced columns in a triangular pattern is shown in Figure 5.2. As can be seen in Figure 5.2, each column has a hexagon-shaped zone of influence. By utilizing planes of symmetry, the three-dimensional representation of each column may be simplified to a triangle. The plan view of the three-dimensional representation of 32-inch diameter columns installed in a triangular array on 10-foot center-to-center spacing is shown in Figure 5.3. The plan view of the symmetrical mesh is represented by a triangle with a base of 5 ft and a height of 2.89 ft. Mesh refinement in plan view employed 14 zones in the column area and 103 zones in the soil area. Vertical refinement produced 354 layers of mesh zones over the 59 ft height of the model, so that 41,418 mesh zones were used altogether. Preliminary studies indicated that such refinement was necessary to obtain convergence for analysis of the composite system. The sides of the mesh were restrained against lateral movements, but were free to move vertically; the base of the mesh was fixed against lateral and vertical movements. The embankment fill was placed all at once. The computational time on a personal computer with 1.5 GHz Pentium Processor with 256 MB RAM was approximately 15 hours.

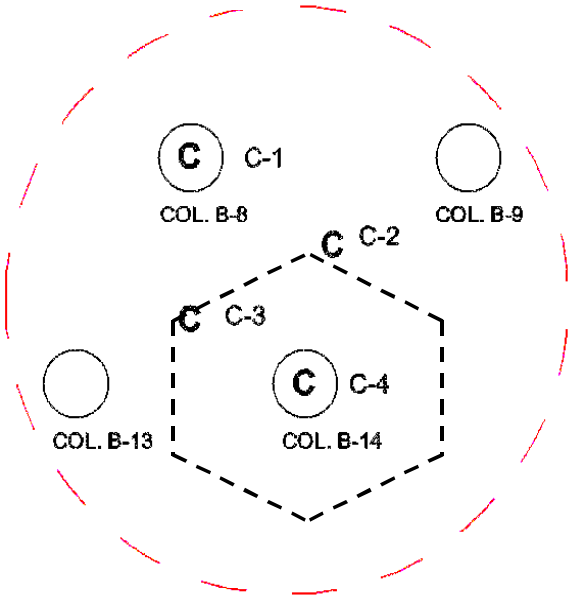

Figure 5.2. Tributary area associated with each column

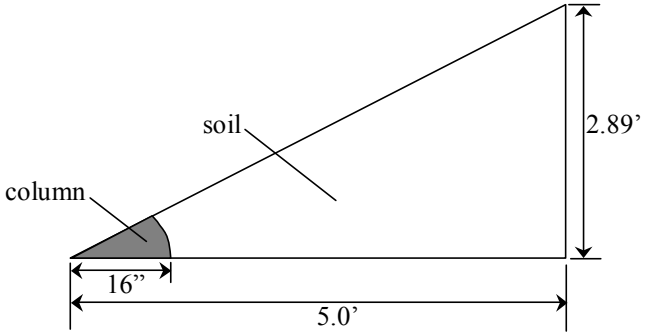

Figure 5.3. Plan view of the 3D representation of widely spaced columns

5.3.2 Three-Dimensional "Axisymmetric" Geometry

A three-dimensional "axisymmetric" model was also created, and axisymmetric results were compared against the pressure cell data and the 2D axisymmetric analysis, which is described in the following section. In axisymmetric models, the zone of influence of a column is circular and is symmetrical about the centerline. The three-dimensional "axisymmetric" representation is shown in Figure 5.4. The only difference between the three-dimensional model and 3D "axisymmetric" model is the outside edge. The 3D "axisymmetric" mesh is pie-shaped with a

radius of 5.25 ft. Mesh refinement employed 14 zones in the column area and 107 zones in the soil area. Vertical refinement produced 354 layers of mesh zones over the 59 ft height of the model, so that 42,834 mesh zones were used altogether. The embankment fill was placed all at once. The average computational time on a personal computer with 1.5 GHz Pentium Processor with 256 MB RAM was approximately 15 hours.

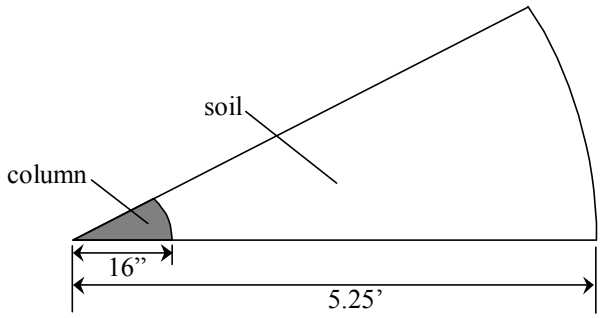

Figure 5.4. Plan view of the 3D axisymmetric representation

5.3.3 Results of Three-Dimensional Analyses

As expected, the true 3D model (shown in Figure 5.3) and the 3D “axisymmetric” model (shown in Figure 5.4) gave nearly identical results. The stresses determined by the three-dimensional analyses at an elevation of 21 inches above the top of the column are shown in Figure 5.5. At an elevation of 21 inches above the top of the column, both 3D analyses indicated that the stress above the columns was approximately 5500 psf, and the stress measured above the soil was approximately 2000 psf.

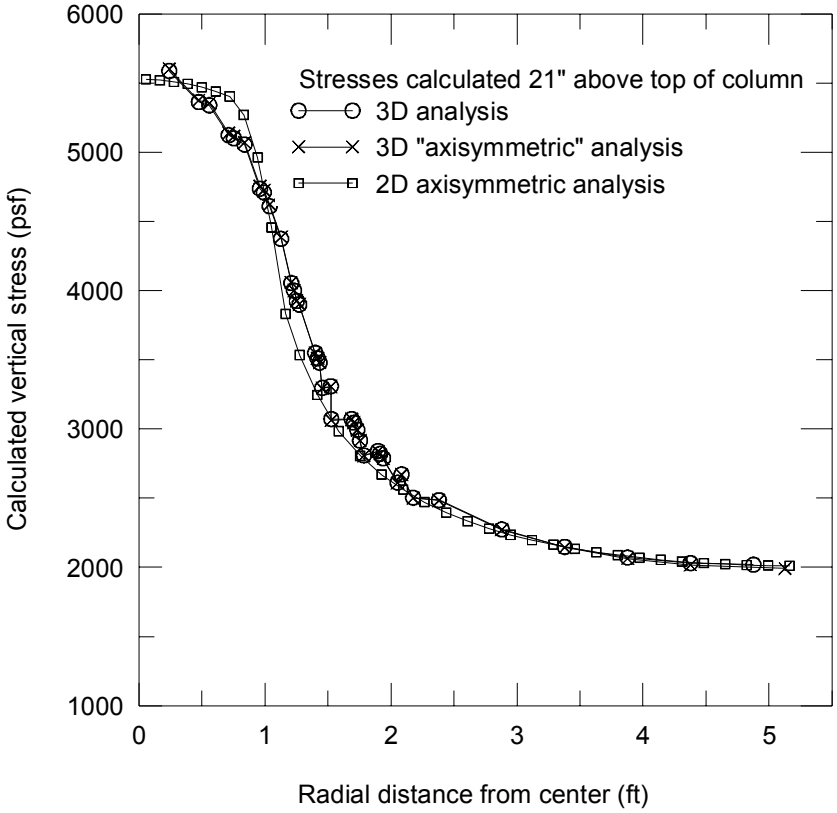

Figure 5.5. FLAC3D and FLAC calculated stresses (21" above top of column)

At an elevation of 3 inches above the top of the column, both 3D analyses indicated that the stress above the columns was approximately 8200 psf, and the stress measured above the soil was approximately 2000 psf, as shown in Figure 5.6. These stresses correspond to a stress concentration ratio of about 4 at an elevation of 3 inches above the top of the columns.

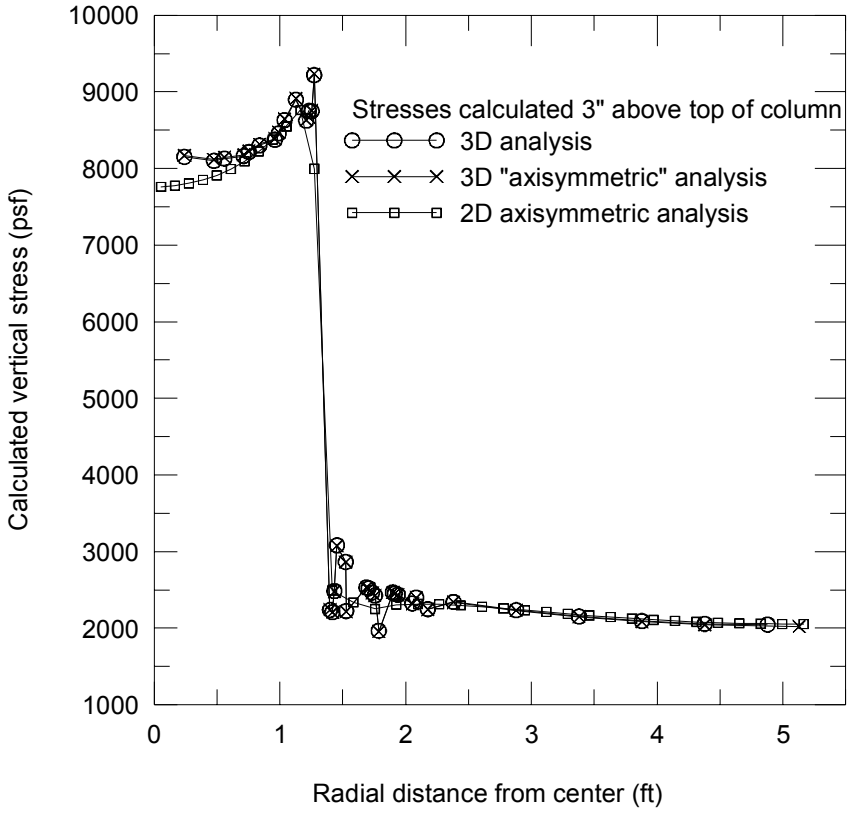

Figure 5.6. FLAC3D and FLAC calculated stresses (3" above top of column)

5.4 Two-Dimensional Finite Difference Analyses Using FLAC

Two-dimensional drained analyses of the widely spaced columns beneath the test embankment were performed using FLAC. FLAC is a two-dimensional explicit finite difference program. Materials are represented by elements, or zones, which form a grid. Additional details FLAC are described in the users manual (ITASC 2002b). The program has nine basic built-in material modes. The linear elastic, Mohr-Coulomb, and Modified Cam Clay models were used in the two-dimensional analyses. FLAC can be operated as either a menu-driven or command-driven computer program. For this research, input files were created using the command-driven mode and the FLAC "language." The profile used in the axisymmetric analyses is shown in Figure 5.1

FLAC contains plane-strain, plane-stress, and axisymmetric geometry modes. The axisymmetric model is symmetrical around its centerline, and the tributary area for a column is used to establish the radius of the axisymmetric mesh. Axisymmetric numerical analyses of the test

embankment were to investigate stress distribution between the columns and existing ground at the level of the top of the columns and above.

For the wide column spacing of 10 ft in a triangular array, the radius of the axisymmetric mesh is 5.25 ft. Mesh refinement employed 12 zones across the radius of the column, and 23 zones across half the annulus of the soil in between columns. Vertical refinement produced 354 layers of mesh zones over the 59 ft height of the model, so that 12,390 mesh zones were used altogether. Refinement studies indicated that such refinement was necessary to obtain convergence for analysis of the composite system, which is complicated in both geometry and material behavior. The sides of the mesh were restrained against lateral movements, but were free to move vertically; the base of the mesh was fixed against lateral and vertical movements. The embankment fill was placed in lifts, with an average of five feet of embankment fill per lift. The average computational time on a personal computer with a 1.5 GHz Pentium Processor with 256 MB RAM was approximately 2.5 hours.

First, an undrained analysis was performed using the axisymmetric model. As expected, this produced very little stress concentration above the columns.

Second, drained analyses were performed using the axisymmetric model. The axisymmetric FLAC model provided results that agree well with those calculated by the true 3D and the 3D "axisymmetric" analyses performed using FLAC3D, as shown in Figures 5.5 and 5.6. In Figure 5.7, the stresses calculated throughout the fill layer above the tops of the columns are shown. As seen in Figure 5.7, the stress at the top of the columns is about 8,000 psf, and the vertical stress between the columns does not show much variation at a value of about 2,000 psf. These stresses correspond to a stress concentration ratio of about 4 at the top of the columns. At the approximate elevation of the pressure cells, the FLAC numerical analyses indicated that the stress above the columns was approximately 5,100 psf, and the stress measured above the soil was approximately 2,025 psf.

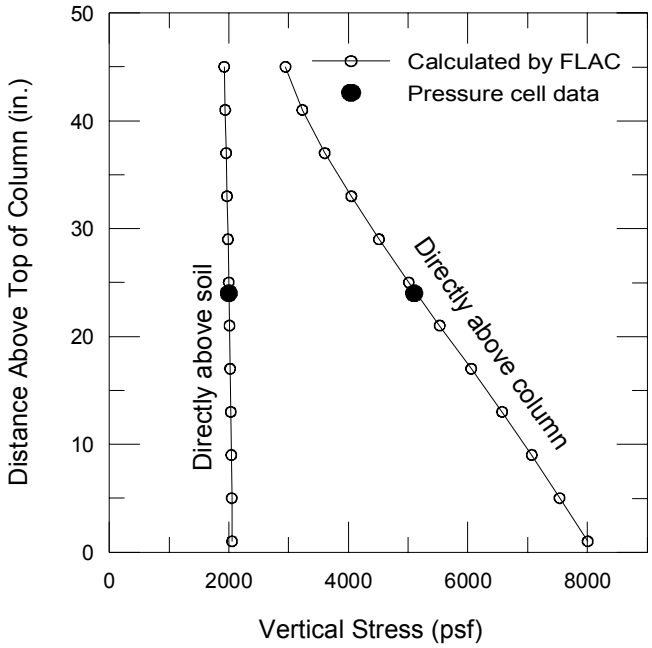

Figure 5.7. Stresses in fill layer above the columns as determined by axisymmetric analyses

A summary of the stresses determined from the FLAC3D and FLAC analyses, as compared to the pressure cell data, is provided in Table 5.2.

Table 5.2. Stresses determined by numerical analyses and measured by pressure cells (at an elevation of 24" above top of column)

	Vertical stress above column (psf)	Vertical stress above soil (psf)
Pressure cell data	5,100	1,980
2D axisymmetric analysis	5,100	2,025
True 3D analysis	5,300	1990
3D axisymmetric analysis	5,300	1990

5.5 Two-Dimensional Finite Element Analyses Using SAGE

During the course of early FLAC verification studies of consolidation analyses using the modified Cam Clay material model, it was discovered that the value of the bulk modulus of water significantly affects the results. Over a relatively small range of values of bulk modulus of water, pore pressure dissipation and calculated settlements varied erratically, and it proved

difficult to confidently select a value of the bulk modulus of water. For this reason, consolidation analyses were not performed using FLAC. Instead, the finite element computer program SAGE (Bentler et al. 1999) was used to perform consolidation analyses.

SAGE uses the 2D finite element method to solve static soil-structure interaction problems for plane-strain and axisymmetric conditions, and it has a fully coupled formulation for fluid flow and deformation. SAGE contains ten material models. The linear elastic, Mohr-Coulomb, and Modified Cam Clay models were used in the analyses described here. The capabilities of SAGE are described in detail in the users guide (Bentler et al. 1999).

The modeling goals using SAGE were to (1) compare the FLAC3D drained analyses, and FLAC axisymmetric drained analyses, and test instrumentation data with SAGE drained analyses, and (2) using the grid created for the drained analyses, perform axisymmetric consolidation analyses. The profile used in the SAGE drained and consolidation analyses is shown in Figure 5.1, and the material property values are presented in Table 5.1. The SAGE drained and consolidation analyses are described in the following sections.

5.5.1 SAGE Drained Analyses

An axisymmetric mesh was created for the SAGE drained analyses. The wide column spacing of 10 ft in a triangular array was analyzed, and the radius of the corresponding axisymmetric mesh is 5.25 ft. Mesh refinement employed 4 elements across the radius of the column, and 4 elements across half the annulus of the soil in between columns. Eight-noded quadrilateral elements were used, and the mesh consisted overall of 901 nodes and 272 elements. The sides of the finite element mesh were restrained against lateral movements, but were free to move vertically; the base of the grid was fixed against lateral and vertical movements.

The results of the SAGE drained analysis are plotted in Figure 5.8 along with the results of the FLAC drained analyses. The drained SAGE analysis agrees well with the drained FLAC analyses. Like the FLAC and FLAC3D analyses, the SAGE analyses show that the vertical stress directly above the columns increases as the top of the columns is approached, and the vertical stress between the columns does not show much variation.

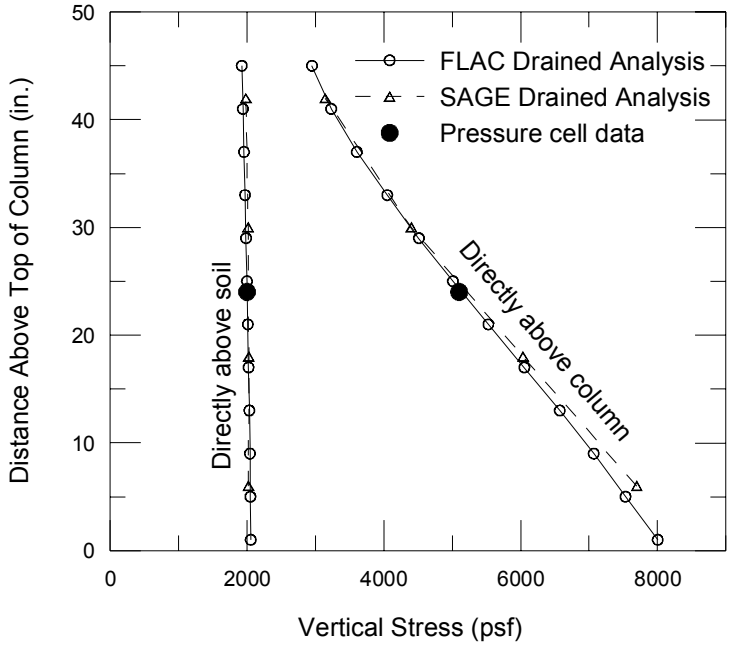

Figure 5.8. Stresses in fill layer as determined by SAGE and FLAC drained analyses

5.5.2 SAGE Consolidation Analysis

Before the consolidation analysis of the test embankment was performed, preliminary verification analyses were performed to compare the results of the coupled analyses with analytical methods. Verification studies indicated that coupled analyses could be successfully performed in conjunction with using the Modified Cam Clay material model for the soft clay using the SAGE program.

A coupled analysis was then performed of the test embankment using the same mesh created for the SAGE drained analysis. For the coupled analysis, 8-noded quadrilateral consolidation elements were used for the soft clay. Non-consolidating 8-noded quadrilateral elements were used for the base sand and fill layers since these soils were free-draining in comparison to the soft clay. Fixed pore water head boundary conditions were applied to the top and bottom of the soft clay layer to simulate double drainage conditions during consolidation. The groundwater level is located at the top of the clay layer. The construction of the test embankment was modeled using the incremental analysis capability of SAGE. The embankment fill was placed in lifts, with an average of three feet of embankment fill being placed every two days. Stresses were evaluated at the pressure cell elevation during a 10-month period.

The results of the SAGE coupled analysis at the end of the 10-month period are plotted in Figure 5.9 along with the results of the SAGE drained analysis. The SAGE coupled analysis agrees well with the SAGE drained analysis.

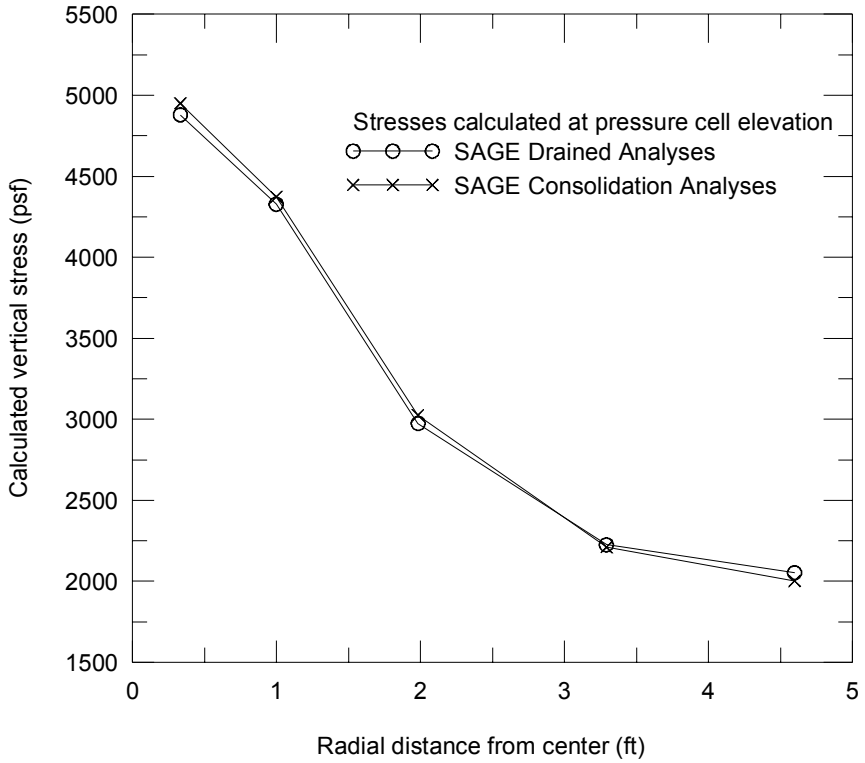

Figure 5.9. Calculated stresses from SAGE drained and consolidation analyses

The results of the SAGE couple analysis are also plotted against the pressure cell data in Figure 5.10. As previously discussed, in the area of widely spaced columns, two pressure cells were installed in the existing fill directly above two columns, and these two cells responded nearly identically to each other. Two pressure cells were also installed between columns at the same elevation as the cells located directly above columns, and again these cells responded nearly identically to each other. The stress measured by the pressure cells above the columns at the pressure cell elevation was approximately 5,100 psf, and the stress measured above the soil was approximately 1980 psf. The pressure cell readings increased rapidly as the embankment was placed, but then leveled off within a few days after embankment completion, which indicates that the local relative deformation pattern near the top of the columns was established very quickly,

even though the test embankment settlement continued for the approximately 13 months that the embankment was in place. This suggests that consolidation of the soft clay near the top of the columns occurred quickly, as would be expected near a drainage boundary, and that on-going consolidation of the soft clay at depth did not affect stress distribution at the level of the top of the columns.

The SAGE coupled analysis results agree relatively well with the pressure cell data. Some differences exist between the results of the numerical analyses and the instrumentation data early in the measurement period. The pressure cell data show a lag in response between days 3 and 10 even though no abnormalities in rate of fill placement occurred during these days. The most significant comparisons in Figure 5.10 are that (1) the calculated and measured pressure both stabilized quickly, even though the test embankment settlement continued for the approximately 13 months that the embankment was in place, and (2) the final values of calculated and measured pressure are in good agreement.

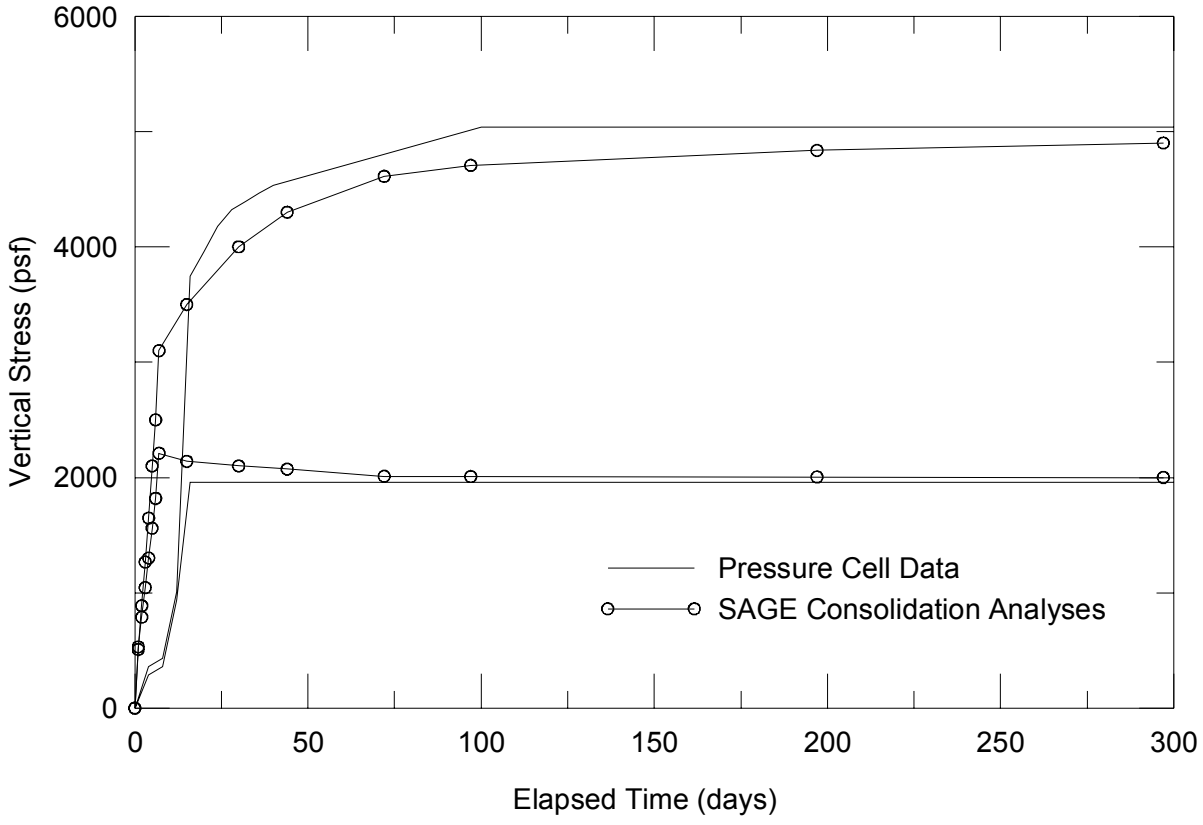

Figure 5.10. Time-dependent results of SAGE consolidation analyses

5.6 Conclusions of Verification Analyses

The 3D drained, axisymmetric drained, and axisymmetric consolidation analyses calculated nearly identical stress distributions in the material above the column. All the calculations agreed well with the pressure cell data. These results indicate that axisymmetric drained analyses can be used to accurately evaluate the stresses that developed in the material above the deep mixed columns under the test embankment loading. Since a successful calibration of the axisymmetric drained finite difference FLAC model was achieved, this approach was used to perform a parametric study, which is described in Chapter 6.

CHAPTER 6
PARAMETRIC STUDY WITHOUT GEOGRID

6.1 Introduction

The settlement of column-supported embankments depends, in part, on the portion of the embankment load that is transferred to the columns. Methods for estimating embankment loads on columns or piles have been proposed by Hewlett and Randolph (1988), BS8006 (1995), Russell and Pierpoint (1997), Rogbeck et al. (1998), and others, as described in Chapter 3; however, these methods generally take into account only a few of the system variables, such as area replacement ratio of the columns and embankment properties. Furthermore, very simplified mechanics are assumed in some of these methods.

To obtain a broader understanding, and to quantitatively evaluate the factors that influence load transfer to columns beneath embankments, a parameter study was performed using the finite difference axisymmetric FLAC model developed and verified as described in Chapter 5. Various features of the model were systematically changed in order to evaluate the influence of a wide range of design factors relevant to column supported embankments, such as: (1) strength and modulus of the deep mixing method (DMM) columns, (2) density of the embankment fill, (3) embankment height, (4) thickness of an existing upper sand layer, (5) density of a base sand layer, (6) compressibility and thickness of the soft soil, and (7) column diameter and column spacing. The analyses and results presented here and in Stewart and Filz (2005) are for the case of embankments supported on columns without overlying layers of geosynthetic reinforcement.

After the initial parametric analyses were completed, additional analyses were performed to consider combinations of design variables beyond those explored in the initial study and to provide data for the development of a calculation procedure to evaluate the settlement and load transfer behavior of column-supported embankments.

This chapter provides an overview of load transfer terminology, description of the methods used in the numerical analyses, and discussion of the results of the numerical studies, including discussion of the trends disclosed by the analyses.

Parametric studies were also performed for the case of embankments supported on columns with overlying layers of geosynthetic reinforcement. Those analyses are described in Chapter 8. Based on the results of the analyses discussed in this chapter and Chapter 8, a calculation procedure was developed to evaluate the settlement and load transfer behavior of column-supported embankments. This procedure is discussed in Chapter 10.

6.2 Review of Definition of Terms

The terms commonly used to assess the load transfer behavior of column supported embankments were discussed in Chapter 3, Section 3.3. A brief review of relevant terms is provided in this section.

The stress reduction ratio, SRR, is defined as the ratio of the stress applied to the foundation soil between the columns to the average stress applied by the embankment (Low et al. 1994, Russell and Pierpoint 1997):

$$SRR = \frac{\sigma_{soil}}{\sigma} \tag{6.1}$$

The ratio between the stress on the top of the column, σ_{col}, and the average applied embankment stress at the level of the top of the column, σ, is referred to as the "column stress ratio," CSR:

$$CSR = \frac{\sigma_{col}}{\sigma} \tag{6.2}$$

Low et al. (1994) use the phrase "competency ratio," and the symbol, C, to refer to the same quantity defined as the column stress ratio, CSR.

The stress concentration ratio, n, is defined as the ratio of vertical stress at the top of the column to the vertical stress at the top of the foundation soil, σ_{soil}, between the columns:

$$n = \frac{\sigma_{col}}{\sigma_{soil}} \tag{6.3}$$

The area replacement ratio, a_s, is defined as the ratio of the area of the column, A_{col}, to the total tributary area associated with that column, $A_{col} + A_{soil}$, such that:

$$a_s = \frac{A_{col}}{A_{col} + A_{soil}} \tag{6.4}$$

The parameters CSR, SRR, n and a_s are related as follows:

$$n = \frac{CSR}{SRR} \tag{6.5}$$

$$SRR = \frac{1}{1 + (n-1) \cdot a_s} = \frac{1 - CSR \cdot a_s}{1 - a_s} \tag{6.6}$$

$$CSR = \frac{n}{1 + (n-1) \cdot a_s} = \frac{1 - SRR \cdot (1 - a_s)}{a_s} \tag{6.7}$$

For the condition of no soil arching, there is no reduction of pressure on the foundation soil between the columns, and the values of CSR, n, and SRR are all equal to one. For the hypothetical condition of complete soil arching, the entire applied embankment load would be carried by the columns and no load would be carried by the soil between the columns. For complete soil arching, CSR would equal the inverse of a_s, n would approach infinity, and SRR would equal zero. The conditions of no soil arching and complete soil arching are limiting conditions, and for real embankments supported on DMM columns, the degree of arching lies between these limiting conditions. Thus, the values of CSR must lie between 1 and $1/a_s$ in all cases for which the columns are stiffer than the soft soil between columns.

The stress reduction ratio, SRR, and column stress ratio, CSR, are used here to present the results of numerical analyses. Knowing the value of SRR, the stress on top of the soil in between

columns is obtained from $\sigma_{soil} = (SRR)(\gamma)(H)$, where γ = the unit weight of the embankment, and H = the embankment height. Knowing the value of CSR, the stress on top of the column is obtained from $\sigma_{col} = (CSR)(\gamma)(H)$.

6.3 Base Case Description and Material Property Values

Verification analyses were performed to gain an understanding of the appropriate numerical modeling procedures and required mesh refinement. The results of verification analyses were compared with measurements from an instrumented test embankment supported on deep-mixed soil-cement columns installed by the dry method at the interchange of US I-95 and Virginia State Route 1 in Alexandria, Virginia. These analyses are described in Chapter 5.

The approach adopted for the numerical parameter studies relies on a base cases analysis, with systematic variation of parameter values from the base case. The base case geometry was chosen based on realistic values of column diameter, column spacing, and embankment height for column-supported embankments (Russell and Pierpoint 1997, Kempton et al. 1998, Han and Gabr 2002). The base case geometry and subsurface profile is shown in Figure 6.1, where it can be seen that the DMM column is 2.68 ft diameter and 31 ft long. The subsurface profile consists of an upper sand layer 2 ft thick, which is underlain by soft clay 28 ft thick, which in turn is underlain by a layer of base sand. The ground water table is located 2 ft below the original ground surface.

The reason that the layer of upper sand was included in the analyses was to represent a layer of stronger soil that often either exists or is placed to permit construction. The upper layer of stronger soil could be existing site fill, new site fill, or a desiccated crust. For simplicity, the upper layer was represented as sand in the analyses.

The total embankment fill thickness shown in Figure 6.1 is 20 ft. As discussed below, the embankment fill was placed in lifts.

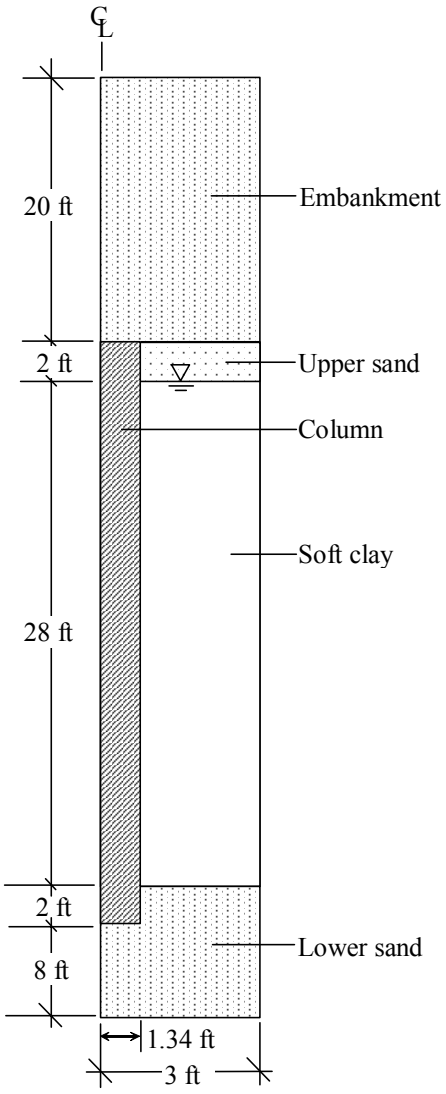

Figure 6.1. Base case profile

The material property values used for the base case analysis are listed in Table 6.1. The following parameters were systematically varied in this parametric study: (1) strength and modulus of the DMM column material, (2) density of embankment fill, (3) embankment height, (4) thickness of upper sand layer, (5) density of base sand layer, (6) compressibility and thickness of the clay, and (7) column diameter and column spacing. In most cases, each parameter was varied independently, except for the column strength and stiffness and the column diameter and spacing, as discussed below. The details of the parameter studies are described in the following sections.

Table 6.1: Base case material property values

	NC Soft Clay	Upper Sand	Base Sand	DMM Column	Embankment
Model type [(a)]	Modified Cam Clay	LEPP-MC	LEPP-MC	LEPP-MC	LEPP-MC
Moist Unit Weight, lb/ft^3	-	115	-	$= \gamma_{soil}$	125
Sat. Unit Weight, lb/ft^3	96	120	140	$= \gamma_{soil}$	-
Elastic Modulus, psf	-	250,000	1,000,000	5,400,000	625,000
Poisson's Ratio	0.35	0.33	0.26	0.35	0.30
Bulk Modulus, psf	-	245,098	694,444	6,000,000	520,833
Shear Modulus, psf	-	93,985	396,825	2,000,000	240,835
q_u, psi	-	0	0	150	0
Friction Angle, deg.	-	30	40	0	35
Dilation Angle, deg.	-	0	10	0	5, [(b)]
Critical Shear Stress Ratio	1.1	-	-	-	-
Lambda, λ	0.35	-	-	-	-
Kappa, κ	0.035	-	-	-	-
Specific Volume, v_o	3.16	-	-	-	-
Pressure at v_o, psf	100	-	-	-	-

(a) LEPP-MC: linear-elastic, perfectly plastic soil model with a Mohr-Coulomb failure criterion.
(b) Non-zero values of the dilation angle were used in the initial parametric study discussed in Sections 6.3 and 6.4. Subsequent analyses used values of dilation angle equal to zero, as discussed in Section 6.8.

6.3.1 Column Strength and Modulus

A linear-elastic, perfectly-plastic model with a Mohr-Coulomb failure criterion was used for the DMM columns. It was expected that the modulus and strength of the DMM columns would be important factors in the development of vertical stresses above the columns, and these values were varied in the parameter studies.

The unconfined compressive strength, q_u, is often the only measure of column strength on a project. Very little data exists in the literature regarding effective-stress based strength parameter values for DMM columns. The two approaches used in this study for representing the drained strength of DMM materials are presented in Figure 6.2. In Method A, which was used by McGinn and O'Rourke (2003) in their analyses of the Central Artery Project in Boston, the effective stress cohesion intercept was set equal to 0.5 times q_u, and the effective stress friction

angle was set equal to zero. In Method B, which is based on recommendations by Kivelo (1998), EuroSoilStab (2002), and Broms (2003), the effective stress cohesion intercept was set equal to 0.289 times q_u, and the effective stress friction angle was set equal to 30˚. For the compressive loading induced on the DMM material in the axisymmetric geometry, Method A is a more conservative representation of strength than Method B.

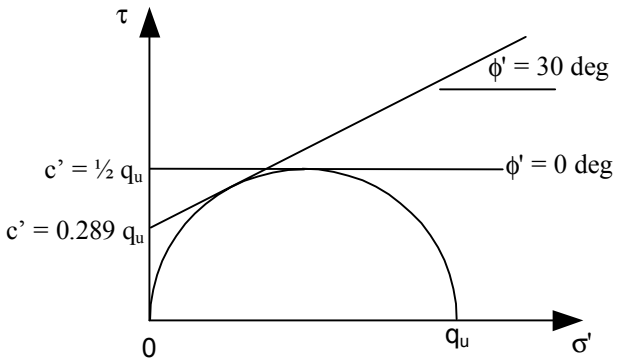

Figure 6.2. Alternative strength characterizations of DMM column material

The base case analysis used a q_u value of 150 psi and Method A to represent the column strength. In the parametric studies, four values of unconfined compressive strength ranging from 30 to 700 psi were used, and for each value, Methods A and B were both employed in separate analyses to represent the drained strength of the DMM material.

The modulus of elasticity, E, is typically assumed to increase linearly with the unconfined compressive strength, q_u, for DMM materials. For columns installed by the dry method, the ratio of E to q_u ranges from 50 to 250 (Baker 2000, Broms 2003, Jacobson et al. 2003). For columns installed by the wet method, the ratio of E to q_u ranges from about 150 to 1000 (Fang et al. 2001, CDIT 2002, McGinn and O'Rourke 2003). Analysis of a large database from the I-95/Route 1 project (Navin and Filz 2005) showed that an E/q_u ratio of about 300 is reasonable for cement-soil mixtures without lime, whether they are created by the wet or dry methods of deep mixing. For the base case, a ratio of E/q_u equal to 250 was used for the DMM columns. In the parameter studies, E/q_u ranged from 75 to 700.

The combinations of column strength and modulus that were used in the parameter studies are listed in Table 6.2. The base case values are in bold text.

Table 6.2. Values of column strength and modulus

			Method A		Method B	
q_u (psi)	**E/q_u**	**E (psi)**	**c' (psf)**	**ϕ'**	**c' (psf)**	**ϕ'**
30	250	7,500	2,160	0	1,248	30
30	400	12,000	2,160	0	1,248	30
75	75	5,625	5,400	0	3,121	30
75	250	18,750	5,400	0	3,121	30
75	400	30,000	5,400	0	3,121	30
150	75	11,250	10,800	0	6,242	30
150	**250**	**31,250**	**10,800**	**0**	6,242	30
150	700	105,000	10,800	0	6,242	30
700	250	175,000	50,400	0	29,131	30

6.3.2 Embankment Fill

A linear-elastic, perfectly-plastic soil model with a Mohr-Coulomb failure criterion was used for the embankment fill. For the base case, the embankment properties were selected to represent a medium dense sand with a moist density of 125 lb/ft^3, a friction angle of 35˚, a cohesion intercept of 0, and a dilation angle of 5˚. In the parameter studies, loose and dense conditions of the embankment fill were evaluated using the material property values given in Table 6.3.

Table 6.3. Range of material property values for embankment fill and lower sand

	Loose	**Med. Dense**	**Dense**	**Very Dense**
Moist density, lb/ft^3	115	125	135	140
Elastic Modulus, psf	250,000	625,000	1,000,000	2,000,000
Poisson's Ratio	0.33	0.30	0.26	0.23
Friction Angle, deg.	30	35	40	45
Dilation Angle, deg.	0	5	10	15

The embankment was placed using a total of ten lifts to reach a height of 20 ft, as outlined in Table 6.4. The advantage of applying the embankment in lifts is twofold: (1) greater accuracy was achieved in the numerical analyses and (2) it allowed for stresses to be recorded at intermediate embankment heights of 4, 8, 12, and 16 ft.

Table 6.4. Embankment Placement

Embankment height increment (ft)	Lift thickness (ft)
0 - 4	1
4 - 12	2
12 - 20	4

6.3.3 Upper and Lower Sand Layers

A linear-elastic, perfectly-plastic soil model with a Mohr-Coulomb failure criterion was used for the upper layer of sand. Recognizing that a high level of compaction would not normally be achieved for a fill layer directly above soft clay, the sand layer was represented as a loose material with a friction angle of 30 degrees, a cohesion intercept of zero, and a dilation angle of zero degrees. The thickness of the upper sand layer was 2 ft for the base case, and this was varied from 1 to 7 ft in the parameter study. The total thickness of the upper sand layer plus the soft clay layer was held constant at 30 ft while the thickness of the upper sand layer was varied. Thus, the column length remained constant in this part of the parameter study.

A linear-elastic, perfectly-plastic soil model with a Mohr-Coulomb failure criterion was used for the lower layer of dense sand. For the base case, the sand was represented as being in a dense condition, with a friction angle of 40 degrees, a cohesion intercept of zero, and a dilation angle of 10 degrees. In the parameter studies, medium dense and very dense conditions of the lower sand were evaluated using the material property values given in Table 6.3.

6.3.4 Clay Compressibility and Thickness

The clay between the columns was represented using the modified Cam Clay material model. According to the correlation between compressibility and water content, w_c, of clay and silt deposits in Terzaghi et al. (1996), the value of w_c in percent is approximately equal to the compression index, C_c, times 100. In Cam Clay, compressibility is represented by the

parameters lambda, λ, and kappa, κ,. The parameter λ, is equal to C_c divided by 2.3, and it was assumed in this study that κ, is equal to 0.1 times λ. Based on a range of values of w_c and a specific gravity of solids equal to 2.7, values of C_c, λ, κ, and saturated unit weight, γ_{sat}, were calculated. For the base case analysis, the clay was assumed to be normally consolidated, and the material property values were based on a water content of 80%, which produces $C_c = 0.8$, λ,= 0.35, κ, = 0.035, and γ_{sat} = 96 lb/ft^3. To evaluate the effect of clay compressibility in the parameter studies, the values of λ, κ, and γ_{sat} were varied corresponding to natural water contents of 40, 120, and 150%, as listed Table 6.5.

Table 6.5. Clay parameter values

w_c (%)	C_c	λ	κ	γ_{sat} (lb/ft^3)
40	0.4	0.17	0.017	113
80	0.8	0.35	0.035	96
120	1.2	0.52	0.052	87
150	1.5	0.65	0.065	83

Another impact on clay compressibility is the degree of overconsolidation of the clay. As part of the parameter study, the clay layer was overconsolidated by applying three different surcharge pressures (500, 1000, and 1500 psf) to the base case subsurface profile, prior to installing the column and placing the embankment.

In addition to the compressibility of the clay, the effect of varying the clay thickness, and thus the column length, was evaluated. The base case clay thickness is 28 ft, and clay thicknesses of 18 and 38 ft were also evaluated. These clay thicknesses correspond to column lengths of 32 ft for the base case, and 22 and 42 ft for the thinner and thicker clay layers, respectively.

6.3.5 Column Diameter and Spacing

As shown in Figure 6.1, the base case column diameter is 2.68 ft and the diameter of the axisymmetric model is 6 ft. These dimensions correspond to an area replacement ratio of 20%, as defined in Equation 6.4. Four values of area replacement were evaluated as part of the parameter study: a_s = 10%, 20%, 30%, and 40%. For each of the four values of a_s, three column diameters were investigated: 1.64, 2.68, and 4 ft. In axisymmetric models, the total tributary area associated with a column is represented by a circular area, and the area replacement ratio is equal to the square of the column diameter, d_{col}, divided by the square of the model diameter, d_{mod}. The values of column and model diameters and the corresponding area replacement ratios that were evaluated are given in Table 6.6.

Table 6.6. Column and model diameters

	d_{mod} (ft)			
d_{col} (ft)	a_s = 10%	a_s = 20%	a_s = 30%	a_s = 40%
1.64	5.19	3.67	3.0	2.59
2.68	8.47	6.0	4.89	4.24
4	12.65	8.94	7.30	6.32

In practice, DMM columns and driven piles are typically installed in square or triangular arrays. For the four values of column diameter and area replacement ratio evaluated, the corresponding center-to-center spacing, s, of columns installed in square and triangular arrays are given in Table 6.7.

Table 6.7: Geometries representative of columns installed in the field

	a_s = 10%		**a_s = 20%**		**a_s = 30%**		**a_s = 40%**	
	S	**T**	**S**	**T**	**S**	**T**	**S**	**T**
d_{col} (ft)	**s (ft)**	**s (ft)**	**s (ft)**	**s (ft)**	**s (ft)**	**s (ft)**	**s (ft)**	**s (ft)**
1.64	4.60	4.94	3.25	3.49	2.65	2.85	2.30	2.47
2.68	7.51	8.07	5.31	5.71	4.34	4.66	3.76	4.04
4	11.21	12.05	7.93	8.52	6.47	6.95	5.60	6.02

s = center-to-center column spacing; S = square array; T = triangular array

6.4 Results of Parametric Study Analyses

As previously mentioned, each parameter was varied independently, except for simultaneous variation of the column strength and stiffness, and the column diameter and spacing. The results of the parameter studies are discussed in this section, and are plotted in Figures 6.3 through 6.8. In Figure 6.3 and Figures 6.5 through 6.8, the thick black line with no symbols represents the results of the base case analysis.

6.4.1 Column Strength and Modulus

The influences of column strength and modulus were evaluated first, using parameter values listed in Table 6.2, with other parameter values equal to the base case values in Table 6.1 and the geometry as shown in Figure 6.1. The analysis results for the cases in which column failure did not occur are shown in Figure 6.3. Column failure did not occur for column strengths of 150 and 700 psi for any embankment height analyzed, and for column strengths of 75 psi for embankment heights not exceeding 16 ft.

Figure 6.3 shows that the values of CSR increase as the column modulus increases and as the embankment height increases. As the embankment height and column stiffness increase, the CSR values approach the upper limiting value of $1/a_s$, which is equal to 5 for the base case geometry with $a_s = 20\%$. The values of SRR decrease as the column modulus increases and as the embankment height increases. The influence of column modulus on the CSR and SRR values is most significant when the column modulus is low.

The analysis results for the cases in which column failure did occur are shown in Figure 6.4. For low strength columns ($q_u = 30$ psi), failure occurred at an embankment height of about 8 ft. For higher strength columns ($q_u = 75$ psi), failure did not become evident until an embankment height of about 20 ft was reached. When embankment failure occurs, the values of CSR decrease with increasing embankment height because the embankment load continues to increase while the column load is limited by the column strength. It can also be seen in Figure 6.4 that Method B for representing the column strength allows the columns to sustain more load than does Method A.

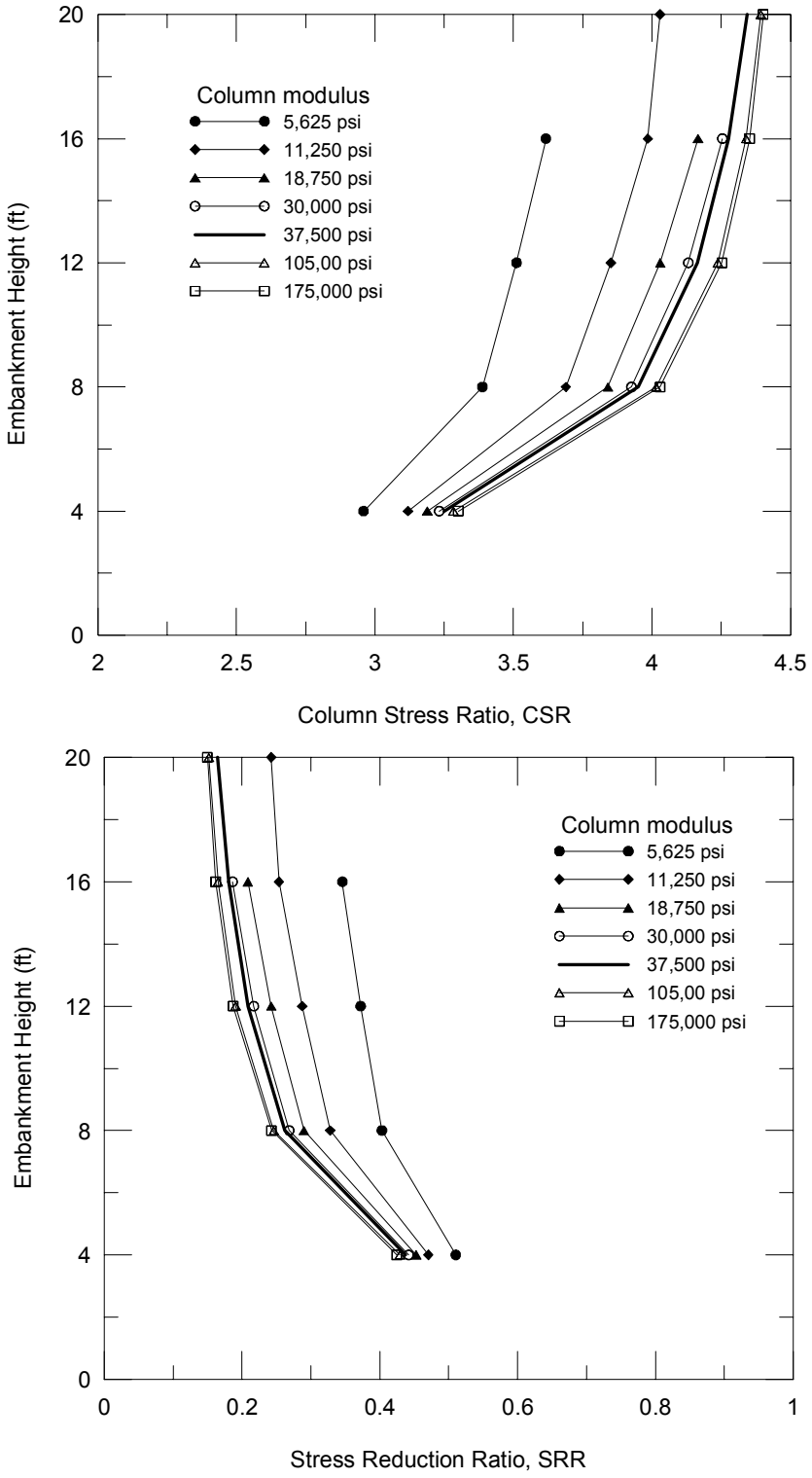

Figure 6.3. Variation of CSR and SRR with column modulus and embankment height (for columns that did not fail)

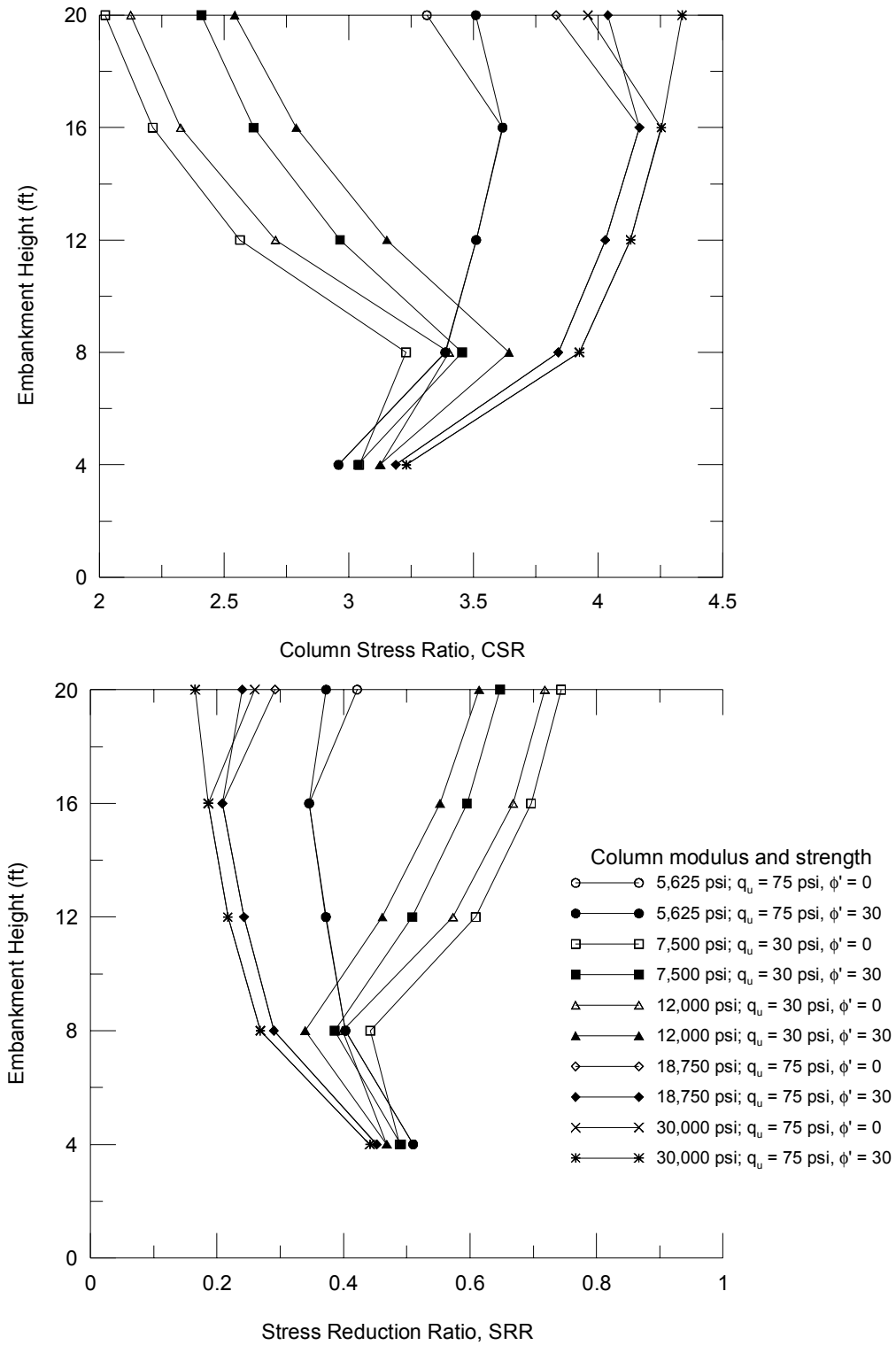

Figure 6.4. Variation of CSR and SRR with column modulus and embankment height (for columns that experienced failure)

6.4.2 Embankment Fill

As the embankment stiffness and strength increase, the embankment fill becomes a more effective bridging layer, which means that more load is transferred directly to the top of the columns. As a result, the CSR values increase and the SRR values decrease. The effect of embankment density on SRR values can be seen in Figure 6.5.

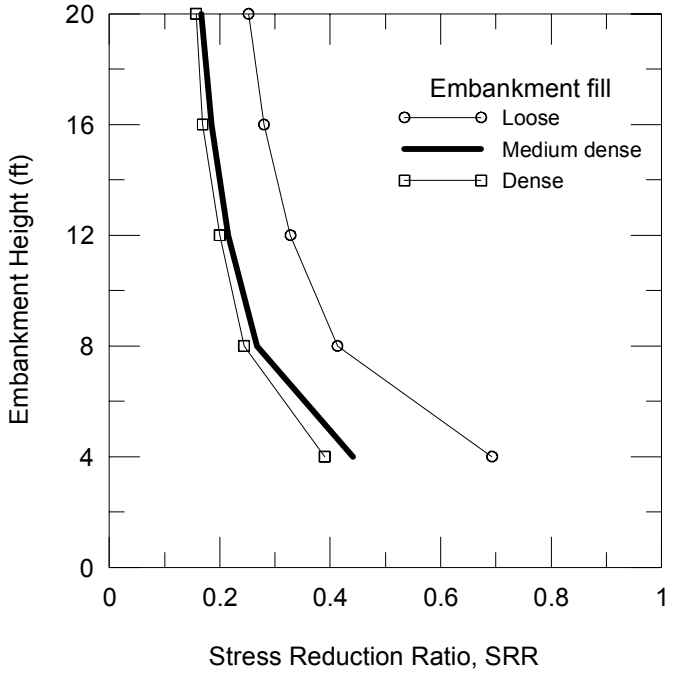

Figure 6.5. Effect of embankment fill on SRR

6.4.3 Upper and Lower Sand Layers

The upper sand layer is less compressible than the soft clay, so the presence of the upper sand means that more load is carried by the soil and less embankment load is carried by the columns at the elevation of the top of the column. As the thickness of the upper sand layer increases, the value of CSR calculated at the top of the column decreases, and the value of SRR calculated at the top of the native soil increases. The effect of thickness of the upper sand layer on SRR values is shown in Figure 6.6.

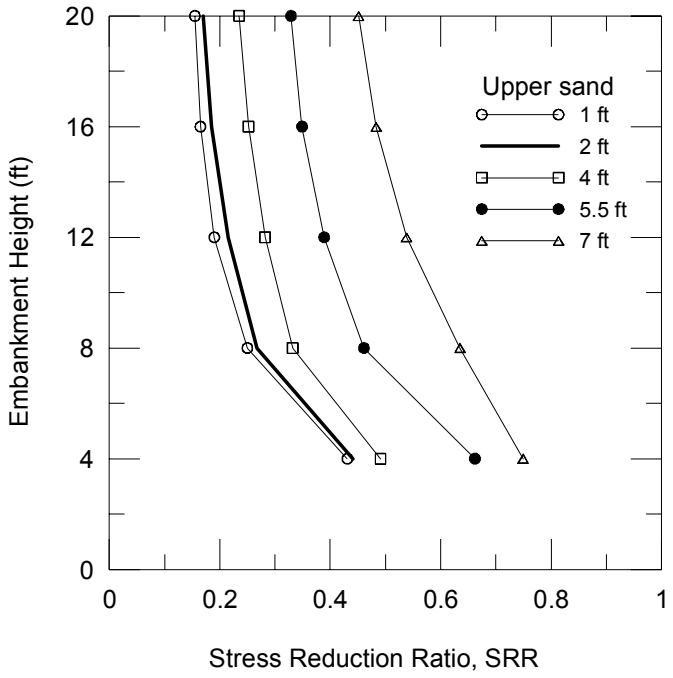

Figure 6.6. Effect of thickness of upper sand layer on SRR

However, the upper sand transfers load to the columns through friction. For comparison purposes, the load transfer to the columns was evaluated for two cases: (1) the base case thickness of 2 ft and (2) the maximum thickness of 7 ft. For both cases, at the elevation of the bottom of the clay layer, the value of CSR calculated based on the increase in stress in the columns was close to $1/a_s$. This indicates that almost 100% of the embankment load is transferred to the columns at the level of the bottom of the clay. For an embankment height of 20 ft, at the bottom of the 2-ft and 7-ft thick upper sand layers, approximately 93% and 97%, respectively, of the entire embankment load is transferred to the column within the sand layer. At the bottom of the thicker sand layer, there is more load in the column than at the same depth for the case with a thinner upper sand layer.

Analyses showed that the relative density of the lower sand layer, which was allowed to range from medium dense to very dense, with property values as listed in Table 6.3, has negligible impact on the load distribution at the elevation of the top of the column.

6.4.4 Compressibility of Normally Consolidated Clay

The analyses showed that the values of SRR decrease as the compressibility of the clay increases. However, the increase in SRR values is only a few percent, even for the approximately four-fold increase in λ from 0.17 to 0.65 that was covered in the parameter study. For all these values of λ, the normally consolidated clay is very compressible in comparison to the column stiffness. For these high values of clay compressibility, load transfer to the columns is apparently controlled by the arching that occurs in the upper sand layer and the embankment fill.

6.4.5 Degree of Overconsolidation of the Clay

The effect of overconsolidation of the clay is shown in Figure 6.7, where it can be seen that the SRR values increase as the surcharge pressure increases. The biggest incremental increase in SRR values occurs for the first increment of surcharge pressure from 0 to 500 psf. The reason this occurs is that a surcharge pressure of 500 psf is sufficient to put the clay in an overconsolidated state for most of the embankment loading. For example, the value of SRR at an embankment height of 20 ft for the 500 psf surcharge pressure is equal to 0.345 for $a_s = 20\%$, according to Figure 6.7. This implies that $\sigma_{soil} = (0.345)(2500 \text{ psf}) = 862.5$ psf. At the level of the top of the clay, the consolidation pressure is (2 ft)(115 pcf) + 500 psf = 730 psf. Thus, the clay follows recompression, which is controlled by $\kappa = 0.035$, for much of the embankment loading. Evidently, this drop in compressibility is large enough to reduce the clay compression and thereby increase the SRR value significantly.

As shown in Figure 6.7, the SRR value increases significantly when moving from the normally consolidated case to the case in which a surcharge of 500 psf was applied. For the cases in which surcharges of 1000 psf and 1500 psf were applied, the SRR value only increases a small additional amount.

Overconsolidation of the clay in these analyses had a greater effect on the load distribution than changing the compressibility parameters of the normally consolidated clay.

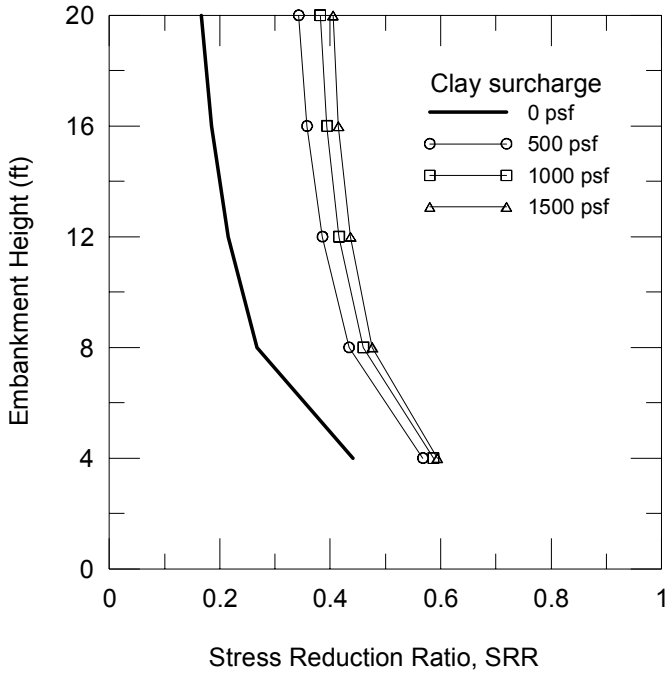

Figure 6.7. Effect of overconsolidation on SRR

6.4.6 Clay Thickness

The analyses showed that changing the thickness of the clay layer from 18 to 28 to 38 ft had negligible effect on SRR values. This result is consistent with the previously described result that the relative density of the base sand was unimportant for the SRR values at the elevation of the top of the columns. On the other hand, the thickness of the upper sand was important. It appears that the geometry and properties of materials near the top of the columns have the biggest impacts on SRR values.

6.4.7 Column Diameter and Spacing

The influence of column diameter and spacing on CSR and SRR values is shown in Figure 6.8. First, it can be seen that CSR values increase with increasing embankment height for all cases except for the smallest area replacement ratio and the greatest embankment height, for which column failure occurred. Furthermore, Figure 6.8 shows that CSR values increase as the value of the area replacement ratio, a_s, decreases. Careful examination of the figure also shows that, in every case, $1/a_s$ represents an upper bound on CSR values.

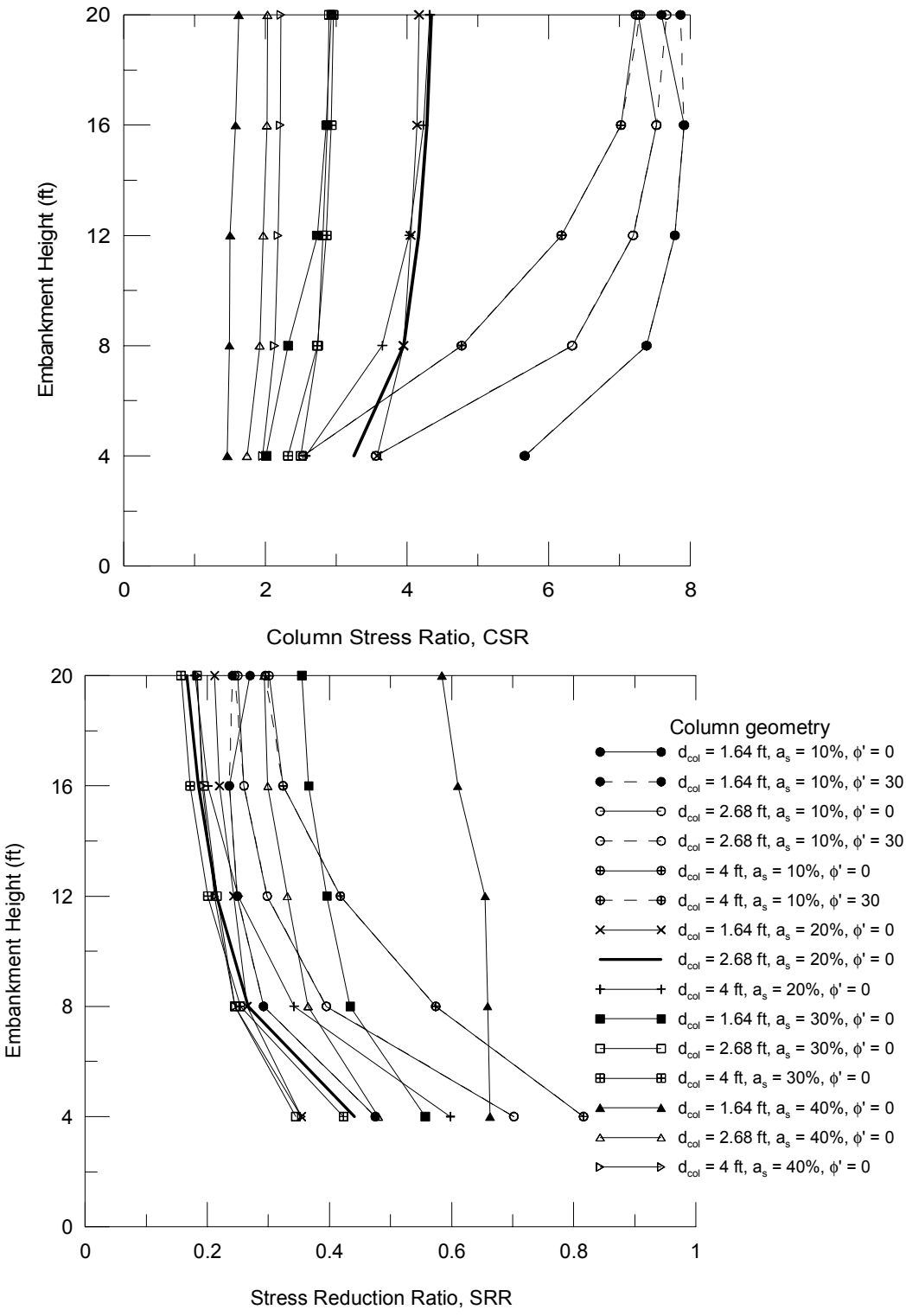

Figure 6.8. Variation of CSR and SRR with column diameter, area replacement ratio, and embankment height

As can be seen in Figure 6.8, there is no clear relationship between area replacement ratio and SRR. (As a reminder, the SRR is related to the CSR value based on the area replacement ratio as given in Equation 6.6.)

The influence of the column diameter for a constant value of a_s is complex. When a_s = 10%, CSR values decrease and SRR values increase with increasing column diameter. When a_s = 40%, CSR values increase and SRR values decrease with increasing column diameter. However, when a_s = 20% and 30%, increasing the column diameter has mixed effects on CSR and SRR values.

A possible explanation for these patterns is twofold. For low fixed values of a_s (e.g., 10%), the clear span between columns is relatively large for all column diameters studied. When the clear span is relatively large, the upper sand and clay cannot span between columns very effectively, so the CSR and SRR values are determined primarily by the interaction between the columns and the embankment. As the column diameter increases, the clear span also increases for a fixed value of a_s. As a result, for a fixed embankment height, the volume proportion of the embankment material under the arches between columns increases, and the volume of the embankment supported per unit column area decreases. Consequently, the CSR value decreases and the SRR value increases.

On the other hand, for high fixed values of a_s (e.g., 40%), the clear span between columns is small enough at small column diameters that the upper sand and clay can span between columns somewhat effectively. This provides support for the embankment between columns and reduces the load on top of the columns, and thus reduces the CSR value and increases the SRR value. As the column diameter increases, the ability of the upper sand and clay to span between columns decreases. As a result, less support is provided to the embankment between columns, which increases the load on top of the columns.

As can be seen in Figure 6.8, for the cases of a_s = 10%, column failure occurred at embankment heights of 4.8 m. For these cases, additional analyses were performed using Method B for characterizing the strength of the DMM columns. Again it can be seen that the load capacity of

the columns is greater when the DMM strength is represented by Method B than when it is represented by Method A.

6.5 Summary and Conclusions of the Initial Parametric Study

Results of the initial parameter study are expressed in terms of the stress reduction ratio, SRR, and column stress ratio, CSR. The value of CSR must lie between 1 and $1/a_s$ for columns that are stiffer than the clay between columns. The value of SRR must lie between 0 and 1.

Key findings from the analyses include:

- Where no column failure occurs, the use of Method A ($c' = 0.5q_u$ and $\phi' = 0^\circ$) and Method B ($c' = 0.289q_u$ and $\phi' = 30^\circ$) to represent DMM material strength yield the same results. When column failure does occur, DMM columns can sustain more load when their strength is characterized by Method B than by Method A.
- Where there is no column failure, CSR values increase and SRR values decrease with increasing column modulus and increasing embankment height.
- Once column failure occurs, CSR values decrease with increasing embankment height.
- As the embankment stiffness and strength increase, CSR values increase and SRR values decrease.
- As the thickness of the upper sand layer increases, SRR values calculated at the top of the native soil increase and CSR values column decrease.
- The thickness of the soft clay layer and the density of the lower sand layer have negligible effects on the load distribution at the top of the column.
- When the clay is normally consolidated, varying the clay compressibility does not have a significant effect on SRR values, because, even for the wide range of λ values in the parametric study, the clay is very compressible in comparison to the column stiffness. In this case, load transfer to the columns is controlled mostly by the arching response of the upper sand layer and the embankment fill material. Therefore, varying the compressibility of the normally consolidated clay layer has a very small effect on the load distribution at the top of the column. However, in cases where the clay is overconsolidated prior to column installation and embankment construction, subsequent loading follows recompression, which reduces the clay compressibility enough to

produce a significant difference in the load distribution at the elevation of the top of the column. As the surcharge pressure increases, the values of SRR increase.

- Values of CSR increase as the area replacement ratio, a_s, decreases.
- The influence of the column diameter for a constant value of a_s is complex, with increasing values of column diameter producing decreasing values of CSR and increasing values of SRR when the value of a_s is small, and with increasing values of column diameter producing increasing values of CSR and decreasing values of SRR when the value of a_s is large. As the clear span between columns increases, the ability of the upper sand and clay between columns to effectively span between columns is reduced, which tends to increase the stress on the top of the columns. However, the ability of the embankment to span between columns is also reduced as the clear span increases, and this tends to decrease the stress on the top of the columns. These counteracting effects produce the complex influence of column diameter on CSR and SRR values for fixed values of a_s.

6.6 Dilation Effects

The analyses performed as part of the initial parametric study discussed in the previous sections included dilation values for the sand layers and embankment fill. Dilation of granular materials can have a complex effect on the load transfer behavior of column-supported embankments. As medium dense to dense granular material shears, it has a tendency to dilate. As the embankment fill dilates, it exerts more pressure on the native soil between columns, thus increasing the load on the native soil. However, simultaneously, as the fill expands, the horizontal stresses increase, thus increasing embankment strength and potentially decreasing the load on the native soil. Also, if the upper sand layer dilates, the horizontal pressures in this layer increase as well. Analytically, quantifying the effects of dilation is difficult.

The analyses performed for the parametric study described in the previous sections were performed again with all the values of dilation angle set to zero, and the values of SRR increased. Since SRR represents the load applied to the soil between columns, it is conservative to consider increased values of SRR when such SRR values are used to design geosynthetic layers. For all subsequent analyses, the values of the dilation angles were set to zero.

6.7 Additional Numerical Analyses

An important goal of this research is to develop a calculation procedure that predicts the load transfer behavior of column-supported embankments, in which geosynethetic-reinforcement may or may not be included. To support the development of the design procedure for the case in which geosynthetic reinforcement is not included, a total of 85 axisymmetric analyses were performed. These 85 analyses included 25 of the analyses of the initial parametric study that were performed again with values of dilation angles set to zero. The remaining 60 analyses included additional system configurations and combinations of material property values.

The additional 60 axisymmetric numerical analyses built upon the knowledge gained during the first parametric study. Since the thickness of the soft clay layer and the density of the lower sand layer were shown to have negligible effects on the load distribution at the top of the column, these factors were not varied in the additional analyses. Furthermore, since varying the compressibility of a normally consolidated clay does not have a significant effect on SRR values, the material property values of the normally consolidated clay were kept constant at those given in Table 6.1.

For the 60 additional analyses, the following variables were considered:

(1) Column diameter and spacing. Column diameters ranged from 1.64 to 4 feet, and column spacings varied from 3.28 to 8 ft.
(2) Thickness of upper sand layer. Upper sand layers thicknesses ranged from 2 to 7 ft.
(3) Density of upper sand layer. Both loose and medium dense conditions of the upper sand layer were considered.
(4) Embankment fill modulus. The embankment fill was varied in accordance with Table 6.3.
(5) Column strength and modulus. The column modulus was evaluated over a range of 11,250 to 37,500 psi. The ratio of E/q_u was kept constant at 250. Method A was used to represent the column strength.
(6) Degree of consolidation of the clay. Both normally consolidated clay and clay preloaded with a surcharge of 1000 psf were considered.

The parameters of these 85 axisymmetric analyses are summarized in Table 6.8. (The first 25 analyses listed in Table 6.8 represent the parametric study analyses that were performed a second time.) For all of the 85 analyses, the value of dilation angle of the sand and embankment fill material was set to zero. The calculated values of SRR for each analysis are presented in Table 6.8 for an embankment height of 20 ft, unless otherwise noted.

6.8 Closing Remarks

A parameter study was performed using the finite difference axisymmetric FLAC model developed and verified as described in Chapter 5. Various features of the model were systematically changed in order to evaluate the influence of a wide range of factors relevant to column supported embankments. The analyses and results presented here are for the case of embankments supported on columns without overlying layers of geosynthetic reinforcement. After the parametric study was performed, additional analyses were performed to consider combinations of variables beyond those explored in the initial parametric study, and to provide data for development and evaluation of a calculation procedure to evaluate the settlement and load transfer behavior of column-supported embankments.

Parametric studies were also performed for the case of embankments supported on columns with overlying layers of geosynthetic reinforcement. Those analyses are described in Chapter 8. Based on the results of the analyses discussed in this chapter and Chapter 8, a calculation procedure was developed to evaluate the settlement and load transfer behavior of column-supported embankments. This procedure is discussed in Chapter 10.

Table 6.8. Summary of analyses performed

Run No.	r_{col} (ft)	r_{mod} (ft)	a_s (%)	Upper Sand Thickness (ft)	Upper Sand Modulus (psf)	Clay Parameters λ, κ	Surcharge/ Preload (psf)	Embankment Fill Modulus (psf)	Column Modulus (psi)	FLAC SRR (H = 20')
1	1.34	3	0.20	1	250,000	0.35, 0.035	0	625,000	37,500	0.198
2	1.34	3	0.20	2	250,000	0.35, 0.035	0	625,000	37,500	0.211
3	1.34	3	0.20	4	250,000	0.35, 0.035	0	625,000	37,500	0.263
4	1.34	3	0.20	5.5	250,000	0.35, 0.035	0	625,000	37,500	0.325
5	1.34	3	0.20	7	250,000	0.35, 0.035	0	625,000	37,500	0.440
6	1.34	3	0.20	2	250,000	0.35, 0.035	500	625,000	37,500	0.354
7	1.34	3	0.20	2	250,000	0.35, 0.035	1000	625,000	37,500	0.418
8	1.34	3	0.20	2	250,000	0.35, 0.035	1500	625,000	37,500	0.429
9	1.34	3	0.20	2	250,000	0.35, 0.035	0	250,000	37,500	0.255
10	1.34	3	0.20	2	250,000	0.35, 0.035	0	1,000,000	37,500	0.213
11	1.34	3	0.20	2	250,000	0.17, 0.017	0	625,000	37,500	0.223
12	1.34	3	0.20	2	250,000	0.52, 0.052	0	625,000	37,500	0.211
13	1.34	3	0.20	2	250,000	0.65, 0.065	0	625,000	37,500	0.210
14	0.82	1.5	0.30	2	250,000	0.35, 0.035	0	625,000	37,500	0.332
15	0.82	1.3	0.40	2	250,000	0.35, 0.035	0	625,000	37,500	0.589
16	0.82	2.6	0.10	2	250,000	0.35, 0.035	0	625,000	37,500	0.264*
17	0.82	1.84	0.20	2	250,000	0.35, 0.035	0	625,000	37,500	0.217
18	1.34	2.12	0.40	2	250,000	0.35, 0.035	0	625,000	37,500	0.272
19	1.34	4.24	0.10	2	250,000	0.35, 0.035	0	625,000	37,500	0.335*
20	1.34	2.44	0.30	2	250,000	0.35, 0.035	0	625,000	37,500	0.200
21	2	6.33	0.10	2	250,000	0.35, 0.035	0	625,000	37,500	0.450*
22	2	4.47	0.20	2	250,000	0.35, 0.035	0	625,000	37,500	0.287
23	2	3.16	0.40	2	250,000	0.35, 0.035	0	625,000	37,500	0.203
24	2	3.65	0.30	2	250,000	0.35, 0.035	0	625,000	37,500	0.205
25	3.06	4.84	0.40	2	250,000	0.35, 0.035	0	625,000	37,500	0.219
26	0.82	1.5	0.30	2	250,000	0.35, 0.035	0	250,000	11,250	0.553
27	0.82	1.5	0.30	2	250,000	0.35, 0.035	1000	250,000	11,250	0.864
28	0.82	1.5	0.30	2	250,000	0.35, 0.035	0	625,000	11,250	0.591
29	0.82	1.5	0.30	2	250,000	0.35, 0.035	1000	625,000	11,250	0.787
30	0.82	1.5	0.30	2	250,000	0.35, 0.035	0	625,000	22,500	0.406

Run No.	r_{col} (ft)	r_{mod} (ft)	a_s (%)	Upper Sand Thickness (ft)	Upper Sand Modulus (psf)	Clay Parameters λ, κ	Surcharge/ Preload (psf)	Embankment Fill Modulus (psf)	Column Modulus (psi)	FLAC SRR (H = 20')
31	0.82	1.5	0.30	2	250,000	0.35, 0.035	1000	625,000	22,500	0.628
32	0.82	1.64	0.25	2	250,000	0.35, 0.035	0	250,000	11,250	0.437
33	0.82	1.64	0.25	2	250,000	0.35, 0.035	1000	250,000	11,250	0.840
34	0.82	1.64	0.25	2	250,000	0.35, 0.035	0	625,000	11,250	0.420
35	0.82	1.64	0.25	2	250,000	0.35, 0.035	1000	625,000	11,250	0.787
36	0.82	1.64	0.25	2	250,000	0.35, 0.035	0	625,000	22,500	0.310
37	0.82	1.64	0.25	2	250,000	0.35, 0.035	1000	625,000	22,500	0.575
38	0.82	1.64	0.25	5	250,000	0.35, 0.035	0	250,000	11,250	0.883
39	0.82	1.64	0.25	5	250,000	0.35, 0.035	1000	250,000	11,250	0.883
40	0.82	1.64	0.25	5	250,000	0.35, 0.035	0	625,000	11,250	0.813
41	0.82	1.64	0.25	5	250,000	0.35, 0.035	1000	625,000	11,250	0.817
42	0.82	1.64	0.25	5	250,000	0.35, 0.035	0	625,000	22,500	0.732
43	0.82	1.64	0.25	5	250,000	0.35, 0.035	1000	625,000	22,500	0.734
44	2	3.65	0.30	4	250,000	0.35, 0.035	0	250,000	11,250	0.448
45	2	3.65	0.30	4	250,000	0.35, 0.035	1000	250,000	11,250	0.820
46	2	3.65	0.30	4	250,000	0.35, 0.035	0	625,000	11,250	0.468
47	2	3.65	0.30	4	250,000	0.35, 0.035	1000	625,000	11,250	0.747
48	2	3.65	0.30	4	250,000	0.35, 0.035	0	625,000	22,500	0.321
49	2	3.65	0.30	4	250,000	0.35, 0.035	1000	625,000	22,500	0.561
50	0.82	1.64	0.25	2	250,000	0.35, 0.035	0	250,000	37,500	0.278
51	0.82	1.64	0.25	2	250,000	0.35, 0.035	1000	250,000	37,500	0.595
52	0.82	1.5	0.30	2	250,000	0.35, 0.035	0	250,000	37,500	0.342
53	0.82	1.5	0.30	2	250,000	0.35, 0.035	1000	250,000	37,500	0.622
54	0.82	1.64	0.25	5	250,000	0.35, 0.035	0	250,000	37,500	0.764
55	0.82	1.64	0.25	5	250,000	0.35, 0.035	1000	250,000	37,500	0.767
56	0.82	1.64	0.25	2	250,000	0.35, 0.035	0	625,000	37,500	0.248
57	0.82	1.64	0.25	2	250,000	0.35, 0.035	1000	625,000	37,500	0.495
58	0.82	1.5	0.30	2	250,000	0.35, 0.035	0	625,000	37,500	0.321
59	0.82	1.5	0.30	2	250,000	0.35, 0.035	1000	625,000	37,500	0.531
60	0.82	1.64	0.25	5.5	250,000	0.35, 0.035	0	625,000	37,500	0.670
61	0.82	1.64	0.25	5.5	250,000	0.35, 0.035	1000	625,000	37,500	0.673
62	2	3.65	0.30	4	250,000	0.35, 0.035	0	250,000	37,500	0.308

Run No.	r_{col} (ft)	r_{mod} (ft)	a_s (%)	Upper Sand Thickness (ft)	Upper Sand Modulus (psf)	Clay Parameters λ, κ	Surcharge/ Preload (psf)	Embankment Fill Modulus (psf)	Column Modulus (psi)	FLAC SRR (H = 20')
63	2	3.65	0.30	4	250,000	0.35, 0.035	1000	250,000	37,500	0.595
64	2	3.65	0.30	4	250,000	0.35, 0.035	0	625,000	37,500	0.270
65	2	3.65	0.30	4	250,000	0.35, 0.035	1000	625,000	37,500	0.496
66	0.82	2.01	0.17	4	250,000	0.35, 0.035	0	625,000	22,500	0.445
67	0.82	2.01	0.17	4	250,000	0.35, 0.035	1,000	625,000	22,500	0.740
68	0.82	2.01	0.17	5	250,000	0.35, 0.035	0	625,000	22,500	0.583
69	0.82	2.01	0.17	5	250,000	0.35, 0.035	1,000	625,000	22,500	0.767
70	0.82	2.01	0.17	7	250,000	0.35, 0.035	0	625,000	22,500	0.769
71	0.82	2.01	0.17	7	250,000	0.35, 0.035	1,000	625,000	22,500	0.774
72	0.82	2.01	0.17	4	625,000	0.35, 0.035	0	625,000	22,500	0.687
73	0.82	2.01	0.17	4	625,000	0.35, 0.035	1000	625,000	22,500	0.903
74	0.82	2.01	0.17	5	625,000	0.35, 0.035	0	625,000	22,500	0.894
75	0.82	2.01	0.17	5	625,000	0.35, 0.035	1000	625,000	22,500	0.933
76	0.82	2.01	0.17	7	625,000	0.35, 0.035	0	625,000	22,500	0.913
77	0.82	2.01	0.17	7	625,000	0.35, 0.035	1000	625,000	22,500	0.914
78	0.82	1.64	0.25	5	625,000	0.35, 0.035	0	250,000	37,500	0.912
79	0.82	1.64	0.25	5	625,000	0.35, 0.035	1000	250,000	37,500	0.912
80	0.82	1.64	0.25	2	625,000	0.35, 0.035	0	625,000	37,500	0.397
81	0.82	1.64	0.25	2	625,000	0.35, 0.035	1000	625,000	37,500	0.607
82	0.82	1.5	0.30	2	625,000	0.35, 0.035	0	250,000	37,500	0.523
83	0.82	1.5	0.30	2	625,000	0.35, 0.035	1000	250,000	37,500	0.749
84	2	3.65	0.30	4	250,000	0.35, 0.035	0	625,000	37,500	0.505
85	2	3.65	0.30	4	250,000	0.35, 0.035	1000	625,000	37,500	0.599

* SRR reported for H = 16 ft

CHAPTER 7
NUMERICAL VERIFICATION STUDY WITH GEOSYNTHETIC REINFORCEMENT

7.1 Introduction

Kempfert et al. (2004) present the results of laboratory scale model tests that were performed under static loading to evaluate the load transfer mechanisms of geosynthetic-reinforced column-supported embankments. The tests were performed as part of a research project at the Institute of Geotechnics, University of Kassel. An abbreviated discussion of the model tests is provided in English by Kempfert et al. (2004), and a detailed description of the model tests is provided in the German dissertation by Zaeske (2001). In addition to the model tests, Zaeske (2001) and Kempfert et al. (2004) report the results of finite element numerical analyses that were performed to verify their model tests. Based on the results of the model tests and numerical analyses, Kempfert et al. (2004) have proposed design methods for evaluating the vertical stress carried by the geosynthetic under embankment loading and the resulting tension in the geosynthetic, as discussed in Sections 3.4.4 and 3.5.5 of Chapter 3. The design methods presented by Kempfert et al. (2004) will be adopted by the EBGEO (German Recommendations for Geosynthetic Reinforced Earth Structures) report.

The Kempfert et al. (2004) model tests were analyzed as part of this research to verify the use of FLAC axisymmetric models to numerically evaluate load transfer mechanisms of geosynthetic-reinforced column supported embankments. The FLAC verification study is discussed in this chapter. Additional numerical verification studies that include geosynthetic reinforcement are discussed in Appendix A.

7.2 Model Test Dimensions

Three-dimensional instrumented models were fabricated in a scale of 1:3 and tested at the Institute of Geotechnics, University of Kassel (Zaeske 2001, Kempfert et al. 2004). The dimensions and configuration of the model are shown in Figure 7.1. The model consisted of a group of four piles placed in a rectangular grid in a soft soil. The square piles had widths of 6.3 in. (16 cm) and center-to-center spacings of 20 in. (50 cm), which correspond to an area replacement ratio of 10%. The thickness of the soft soil was 16 in. (40 cm).

Sand was placed above the piles in two thicknesses: 14 in. (35 cm) and 28 in. (70 cm). The sand thickness is represented by the variable H in Figure 7.1. One layer of geogrid was placed approximately 1 in. (3 cm) above the tops of the piles within the sand. For each thickness of sand, three static surcharges were applied independently: 420, 1130, and 2170 psf (20, 54, and 104 kN/m^2). In the model tests, the stress distribution was recorded in the sand by pressure cells, and the geogrid displacement was measured by vertical rod extensometers.

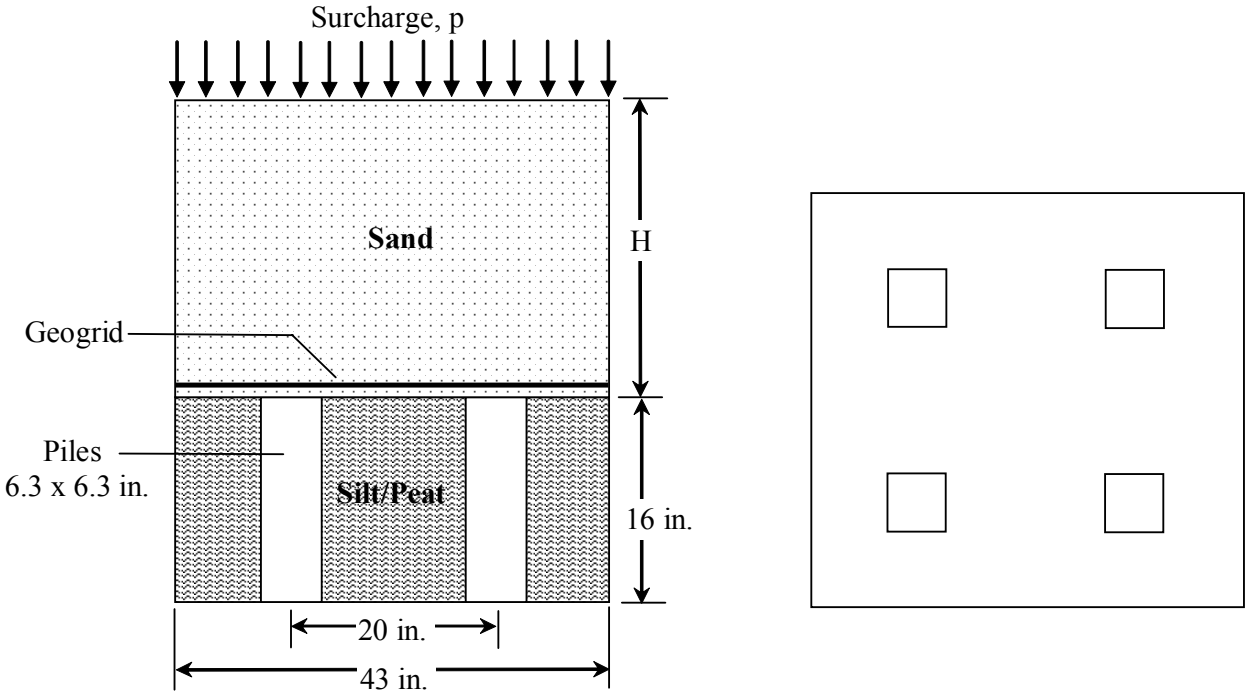

(a) Section view (a) Plan view of piles

Figure 7.1. Model test dimensions and configuration

7.3 Material Property Values

The Kempfert et al. (2004) reference does not include a discussion of the property values of the materials used in the model tests; however, a detailed description of the material property values is provided in the German dissertation by Zaeske (2001). Material property values were ascertained from the German text through the use of *Elsevier's Dictionary of Soil Mechanics in Four Languages*, and through personal conversations with Professor Rolf Katzenbach, of the Technische Universitat Darmstadt, Frankfurt, Germany.

The soft soil has been referred to as both a silt (Zaeske 2001) and a peat (Kempfert et al. 2004). The soft soil in between the piles was modeled using the Modified Cam Clay material model. Zaeske (2001) indicates the soil has a buoyant unit weight of 51 pcf (8 kN/m^3) and a water content of 300%; however, these material property values are not consistent. For this verification study, the soft soil was assigned a buoyant unit weight of 51 pcf (8 kN/m^3) and a saturated unit weight of 113 pcf (17.7 kN/m^3). A specific gravity of 2.5 was assumed for the soil, and as a result, a void ratio of 0.85 was determined for the soft soil. Zaeske (2001) also indicates that the compression and recompression indices of the soft soil are 2.48 and 0.5, respectively; these indices convert to Cam Clay factors lambda and kappa of 1.08 and 0.22, respectively. A Poisson's ratio of 0.38 was assumed for the soft soil.

A linear-elastic, perfectly-plastic model with a Mohr-Coulomb failure criterion was used to model the sand. The sand has a moist unit weight of 112 pcf (17.6 kN/m^3), a confined modulus of 585,000 psf (28,000 kN/m^2), an effective cohesion of zero, and an effective friction angle of 38 degrees (Zaeske 2001). A Poisson's ratio of 0.3 was assumed for the sand. Zaeske (2001) indicates that the sand also has a dilation angle of 11 degrees; however, as discussed below, best results were obtained in the verification study by assigning a dilation angle of zero to the sand.

The piles were assumed to be concrete and were modeled as a linear elastic material. A unit weight of 150 pcf (23.5 kN/m^3) and an Elastic Modulus of 2.6 x 10^8 psf (12.5 x 10^6 kN/m^2) were used.

The geogrid was modeled as a linear elastic material. The geogrid has a stiffness, J, of 68,540 lb/ft (1000 kN/m) (Kempfert et al. 2004). The geogrid was assigned a thickness of 0.1 in. (0.254 cm), and a Poisson's ratio of zero was assumed for the geogrid.

A summary of the material property values used in the verification study is provided in Table 7.1.

Table 7.1. Summary of material property values used in verification study

	Pile	Silt/Peat	Sand
Model type	Linear Elastic	Cam Clay	Mohr-Coulomb
Moist Density, lb/ft^3	150	-	112
Sat. Density, lb/ft^3	-	113	-
Elastic Modulus, psf	2.6×10^8	-	434,500
Poisson's Ratio	0.2	0.38	0.3
Cohesion, psf	0	-	0
Friction Angle, deg.	35	-	38
Dilation Angle, deg.	0	-	0
Critical Shear Stress Ratio, η_{crit}	-	1.1	-
Lambda, λ	-	1.08	-
Kappa, κ	-	0.22	-
Pressure at Specific Volume, psf	-	105	-
Specific Volume	-	1.85	-

7.4 FLAC Numerical Analyses

Axisymmetric analyses of the laboratory scale model tests were performed using FLAC (Fast Lagrangian Analysis of Continua) (ITASCA 2002b). The square piles were converted to circular piles with equivalent areas, and the pile spacings were converted to circular areas while maintaining the appropriate area replacement ratio. The 6.3 in. (16 cm) square pile was converted to a circular pile with a radius of 3.56 in. (9.03 cm), and the total model radius was set equal to 11.11 in. (28.22 cm).

Mesh refinement employed five zones across the radius of the column, and nine zones across half the annulus of the soil between columns. Twenty layers of mesh zones were used in the vertical direction for the soft soil. The geogrid, which has a thickness of 0.1 in. (0.254 cm), was represented with two layers of mesh zones in the vertical direction. The mesh refinement of the geogrid was chosen based on verification studies described in Appendix A. Sixteen layers of vertical mesh zones were used to represent the sand thickness of 14 in. (35 cm), and 34 layers of vertical mesh zones were used to represent the sand thickness of 28 in. (70 cm). For the full height of sand thickness of 28 in. (70 cm), a total of 826 mesh zones were used.

Results from the FLAC analyses were compared to the results of the model tests, as published by Zaeske (2001) and Kempfert et al. (2004) and as shown in Figures 7.2 through 7.4. In Figures 7.2 and 7.3, the stress distribution in the sand is plotted against the distance above the top of the piles. As can be seen in Figures 7.2 and 7.3, the axisymmetric analyses provide a good fit to the published results of the model tests, especially for the lower surcharge pressures.

In Figure 7.4, the geogrid displacement is plotted as a function of static surcharge load. Shown in Figure 7.4 are (1) the published results of the model tests, (2) the results of the analyses by Kempfert et al. (2004) of their own model tests, and (3) the results of the FLAC analyses that were performed as part of this verification study. As can be seen in Figure 7.4, the FLAC analyses predict somewhat higher geogrid displacements; however, the trends of the displacements from the FLAC analyses follow the trends from Kempfert et al. (2004) regarding sand thickness and surcharge pressure.

It was observed during the analyses that varying the dilation angle of the sand layer above the geogrid affected the stress distribution more than varying the properties of the soft soil between the piles. The best results were obtained when the dilation angle was set equal to zero for the sand, which was modeled using the Mohr Coulomb failure criteria. The results shown in Figures 7.2 through 7.4 are for the case in which the dilation angle of the sand is zero.

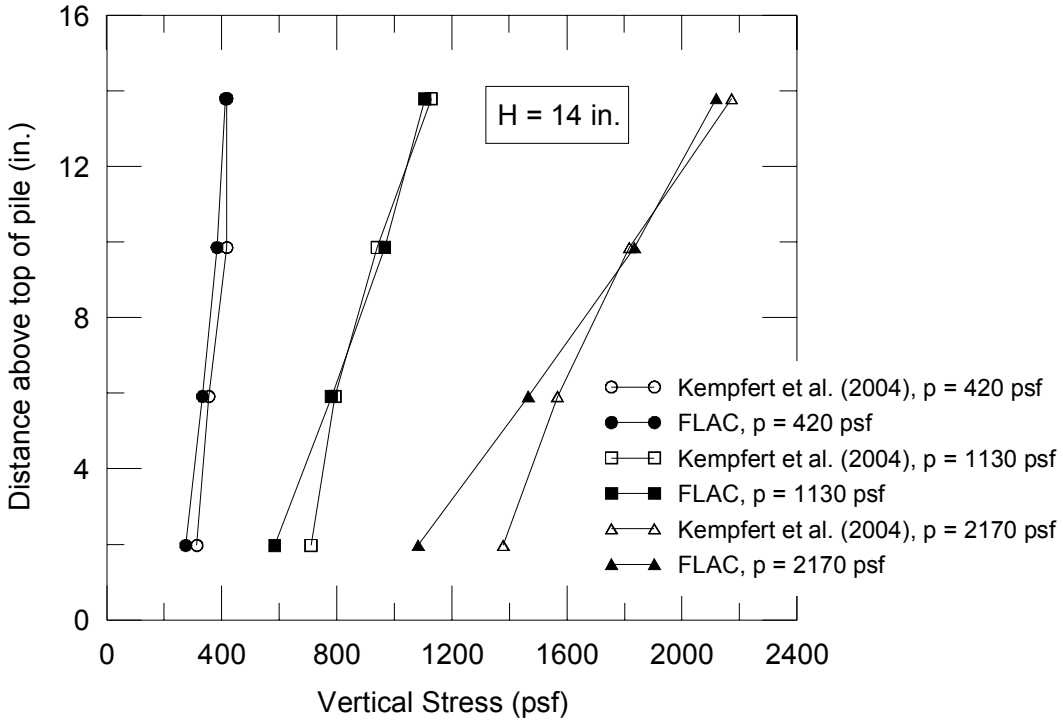

Figure 7.2. Stress distribution: FLAC versus model tests (H =14 in.)

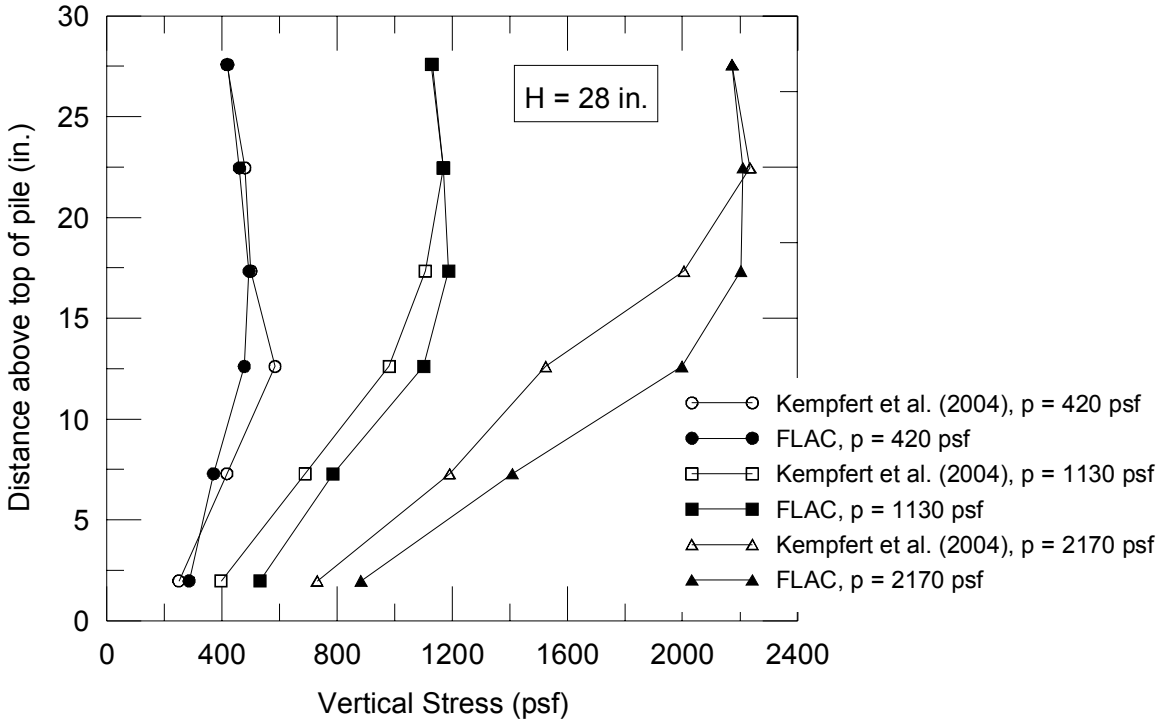

Figure 7.3. Stress distribution: FLAC versus model tests (H = 28 in.)

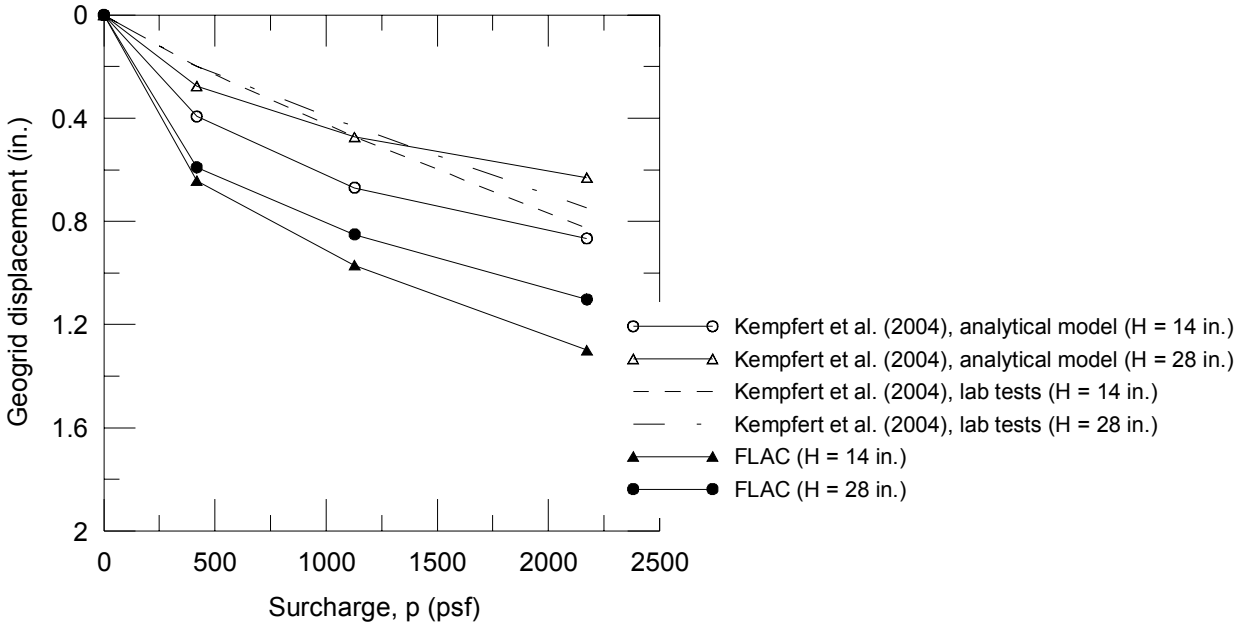

Figure 7.4. Geogrid displacement: FLAC results versus model tests

7.5 Closing Remarks

The axisymmetric FLAC analyses provided a good fit to the results of laboratory scale model tests by Zaeske (2001) and Kempfert et al. (2004) that include geosynthetic reinforcement. This verification study demonstrated that:

(1) The stress distribution in the sand layer is more appropriately captured when the dilation angle of the sand is equal to zero, and

(2) The geosynthetic reinforcement may be successfully modeled using the linear elastic material model. In the FLAC model, the geosynthetic reinforcement was assigned a thickness of 0.1 in. (0.254 cm) and was divided vertically into two layers of mesh zones.

Additional verification studies that include geosynthetic reinforcement are discussed in Appendix A. This verification study, as well as those described in Appendix A, indicate that the numerical modeling methods here are appropriate. These numerical methods were used to perform a parametric study with geosynthetic reinforcement, as described in Chapter 8.

CHAPTER 8
PARAMETRIC STUDY WITH GEOGRID

8.1 Introduction

Several different methods exist for calculating the magnitude of loads applied to geosynthetic reinforcement in bridging layers for column-supported embankments (e.g., Hewlett and Randolph 1988, BS8006 1995, Russell and Pierpoint 1997, Rogbeck et al. 1998, and others, as described in Chapter 3). These methods take into account such factors as the column or pile cap size, column spacing, embankment height, embankment unit weight, and embankment friction angle, and they produce loads that differ by an order of magnitude or more for typical examples.

To obtain a broader understanding, and to quantitatively evaluate the factors that influence load transfer to the geosynthetic reinforcement, a parameter study was performed using the finite difference axisymmetric FLAC model developed and verified as described in Chapters 5 and 7. Various features of the model were systematically changed in order to evaluate the influence of a wide range of design factors relevant to column-supported embankments, such as: (1) geosynthetic stiffness, (2) geosynthetic location, (3) density of the embankment fill, (4) embankment height, (5) thickness of an existing upper sand layer, (6) compressibility of the soft soil, and (7) column diameter and column spacing.

This chapter provides a brief description of the methods used in the numerical analyses, and a discussion of the results of the numerical studies, including discussion of the trends disclosed by the analyses.

Parametric studies were also performed for the case of embankments supported on columns without overlying layers of geosynthetic reinforcement. Those analyses are described in Chapter 6. Based on the results of the analyses discussed in this chapter and Chapter 6, a calculation procedure was developed to evaluate the settlement and load transfer behavior of column-supported embankments. This procedure is presented in Chapter 9.

8.2 Definition of Terms

The terms commonly used to assess the load transfer behavior of column-supported embankments were discussed in Chapter 3, Section 3.3. For a column-supported embankment without geosynthetic reinforcement in the bridging layer, the stress reduction ratio, SRR, is defined as the ratio of the average stress applied to the foundation soil between the columns, σ_{soil}, to the overall average stress applied by the embankment to the columns or pile caps and foundation soil (Low et al. 1994, Russell and Pierpoint 1997). When one or more layers of geosynthetic reinforcement are placed in the fill above the columns, the stress that would otherwise be applied to the foundation soil between the columns, i.e., σ_{soil}, is assumed to be carried by the geosynthetic. Thus, the SRR value can be used to represent the proportion of the embankment load on top of the geosynthetic reinforcement.

The term SRR_{net} is introduced to represent the net vertical load (i.e., the downward load on the top of the geosynthetic minus the upward load on the bottom of the geosynthetic) in the area outside the column, normalized by the weight of the embankment fill plus surcharge overlying the geosynthetic in the area outside of the column. Since SRR_{net} represents the net vertical load that causes the geosynthetic to deflect downwards, the results of this parametric study are expressed in terms of SRR_{net}.

8.3 Model Description and Material Property Values

Verification analyses were performed to gain an understanding of the appropriate numerical modeling procedures and required mesh refinement by comparison with published results of laboratory model scale tests performed by Zaeske (2001) and Kempfert et al. (2004), as described in Chapter 7. Additional numerical verification studies that include geosynthetic reinforcement are discussed in Appendix A.

The approach adopted for the numerical parameter studies relies on a systematic variation of parameter values from a given base case. Two base cases, as shown in Figure 8.1, were considered.

For both cases, the geometry was chosen based on realistic values of column diameter, column spacing, and embankment height for column-supported embankments (Russell and Pierpoint 1997, Kempton et al. 1998, Han and Gabr 2002). As shown in Figure 8.1, columns are 2.3 ft in diameter and 31 ft long for both base-case profiles. For all analyses, the geosynthetic reinforcement was placed at the elevation of six inches above the top of the column, except for three cases in which the location of the geosynthetic reinforcement was varied, as described below. The ground water table is located 2 ft below the original ground surface. The total embankment fill thickness shown in Figure 8.1 is 16 ft. As discussed below, the embankment fill was placed in lifts.

The material property values used for the base case analysis are listed in Table 8.1.

Table 8.1: Base case material property values

	NC Soft Clay	Upper Sand	Lower Sand	DMM Column	Embankment
Model type [(a)]	Modified Cam Clay	LEPP-MC	LEPP-MC	LEPP-MC	LEPP-MC
Moist Unit Weight, lb/ft^3	-	115	-	= γ_{soil}	125
Sat. Unit Weight, lb/ft^3	96	120	140	= γ_{soil}	-
Elastic Modulus, psf	-	250,000	1,000,000	5,400,000	625,000
Poisson's Ratio	0.35	0.33	0.26	0.35	0.30
Bulk Modulus, psf	-	245,098	694,444	6,000,000	520,833
Shear Modulus, psf	-	93,985	396,825	2,000,000	240,835
q_u, psi	-	0	0	150	0
Friction Angle, deg.	-	30	40	0	35
Dilation Angle, deg.	-	0	10	0	0
Critical Shear Stress Ratio	1.1	-	-	-	-
Lambda, λ	0.35	-	-	-	-
Kappa, κ	0.035	-	-	-	-
Specific Volume, v_o	3.16	-	-	-	-
Pressure at v_o, psf	100	-	-	-	-

(a) LEPP-MC: linear-elastic, perfectly plastic soil model with a Mohr-Coulomb failure criterion.

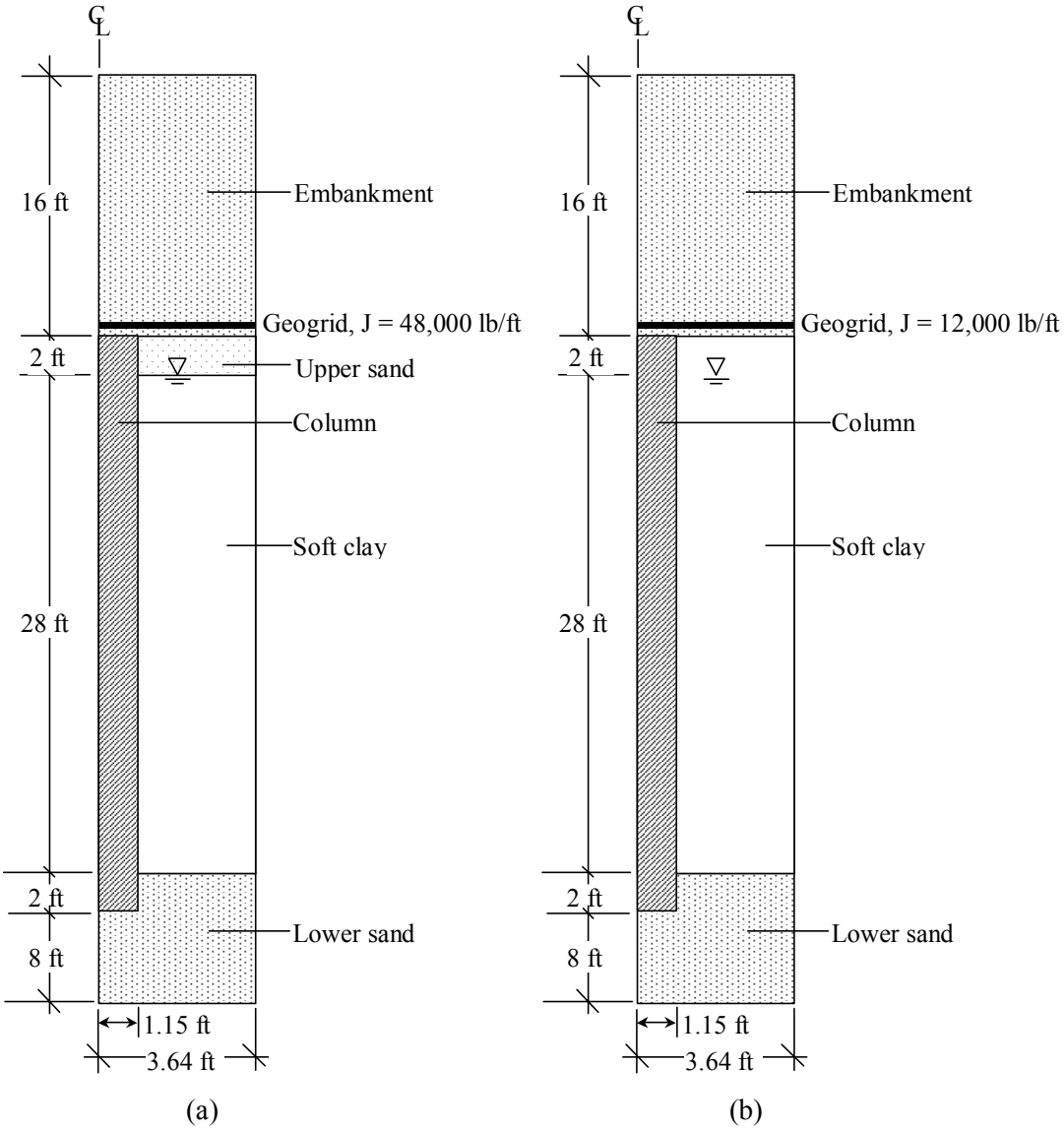

Figure 8.1: (a) Case 1 model geometry, and (b) Case 2 model geometry

The following parameters were systematically varied in this parametric study: (1) geosynthetic stiffness, (2) geosynthetic location, (3) density of the embankment fill, (4) embankment height, (5) thickness of an existing upper sand layer, (6) compressibility of the soft soil, and (7) column diameter and column spacing. In most cases, each parameter was varied independently, except for the column diameter and spacing, as discussed below. The details of the parameter studies are described in the following sections.

8.3.1 Geosynthetic Stiffness and Location

In geosynthetic-reinforced column-supported embankments, the geosynthetic reinforcement consists of one or more layers of planar polymeric material, typically a woven geotextile or, more often, a geogrid. A range of geogrid stiffness values was compiled based upon published geogrid product data (Koerner 1998, Geotechnical Fabrics Report 2002), as well as values used in numerical analyses by others (Han and Gabr 2002, Kempton and Naughton 2002, Collin et al. 2005, Han et al. 2005, Huang et al. 2005, Naughton and Kempton 2005). As can be expected, the range of geogrid stiffness values is quite large.

A linear-elastic model was used for the geosynthetic reinforcement. The geogrid was assigned a thickness of 0.1 in., and a Poisson's ratio of zero.

For Case 1, in which the subsurface profile consists of two feet of upper sand, a base case value of geogrid stiffness, J, of 48,000 lb/ft was chosen. The geosynthetic stiffness was not varied for Case 1.

For Case 2, in which normally consolidated clay extends to the original ground surface, a base case value of geogrid stiffness, J, of 12,000 lb/ft was chosen initially. Three other values of geogrid stiffnesses were evaluated for Case 2: 8,000, 16,000, and 50,000 lb/ft.

The values of geogrid stiffness used in Cases 1 and 2 are typical of many geogrids produced in the U.S. (Geotechnical Fabrics Report 2002).

Rogbeck et al. (1998) state that the reinforcement is most effective if it is installed as close as possible to the column or pile cap, but for practical purposes, it should be about 4 inches above the column or pile cap tops. Kempfert et al. (2004) recommend that the geosynthetic reinforcement be placed no higher than 6 inches above the top of the column. For both Case 1 and Case 2 analyses, the geosynthetic reinforcement was placed at the elevation of six inches above the top of the column. For Case 2, the load distribution was also evaluated for the cases in which the geogrid is located at zero, three, and nine inches above the top of the column.

8.3.2 Embankment Fill

A linear-elastic, perfectly-plastic soil model with a Mohr-Coulomb failure criterion was used for the embankment fill. For the base case, the embankment properties were selected to represent a medium dense sand with a moist density of 125 lb/ft^3, a friction angle of 35˚, a cohesion intercept of zero, and a dilation angle of zero. For the Case 1 configuration, loose and dense conditions of the embankment fill were evaluated using the material property values given in Table 8.2.

Table 8.2. Range of material property values for embankment fill and upper sand

	Loose	**Med. Dense**	**Dense**
Moist density, lb/ft^3	115	125	135
Elastic Modulus, psf	250,000	625,000	1,000,000
Poisson's Ratio	0.33	0.30	0.26
Friction Angle, deg.	30	35	40
Dilation Angle, deg.	0	0	0

The embankment was placed using a total of ten lifts to reach a height of 16 ft, as outlined in Table 8.3. The advantage of applying the embankment in lifts is twofold: (1) greater accuracy was achieved in the numerical analyses and (2) it allowed for stresses to be recorded at intermediate embankment heights of 4, 8, 12, and 16 ft.

Table 8.3. Embankment placement

Embankment height increment (ft)	Lift thickness (ft)
0 - 4	1
4 - 12	2
12 - 16	2

8.3.3 Upper and Lower Sand Layers

A linear-elastic, perfectly-plastic soil model with a Mohr-Coulomb failure criterion was used for the upper layer of sand. Recognizing that a high level of compaction would not normally be achieved for a fill layer directly above soft clay, the sand layer was represented as a loose material with a friction angle of 30 degrees, a cohesion intercept of zero, and a dilation angle of

zero degrees. The thickness of the upper sand layer was varied from zero to 4 ft for both the Case 1 and Case 2 configurations. The total thickness of the upper sand layer plus the soft clay layer was held constant at 30 ft while the thickness of the upper sand layer was varied. Thus, the column length remained constant in this part of the parameter study.

A linear-elastic, perfectly-plastic soil model with a Mohr-Coulomb failure criterion was used for the lower layer of dense sand. The lower sand was represented as being in a dense condition, with a friction angle of 40 degrees, a cohesion intercept of zero, and a dilation angle of zero degrees. Since the density of the lower sand layer was shown to have negligible effects on the load distribution at the top of the column for the case of column-supported embankments without geosynthetic reinforcement (as described in Chapter 6), it was not varied in this parametric study.

8.3.4 Clay Compressibility

The clay between the columns was represented using the modified Cam Clay material model. According to the correlation between compressibility and water content, w_c, of clay and silt deposits in Terzaghi et al. (1996), the value of w_c in percent is approximately equal to the compression index, C_c, times 100. In Cam Clay, compressibility is represented by the parameters lambda, λ, and kappa, κ,. The parameter λ, is equal to C_c divided by 2.3, and it was assumed in this study that κ is equal to 0.1 times λ. For both Case 1 and Case 2, the material property values of the clay were based on a water content of 80%, which produces $C_c = 0.8$, $\lambda = 0.35$, $\kappa = 0.035$, and $\gamma_{sat} = 96$ lb/ft^3.

It was shown in the parametric study performed for the case of a column-supported embankment without geosynthetic reinforcement that, when the clay is normally consolidated, varying the clay compressibility, C_c or λ, does not have a significant effect on SRR values. This is because, even for the wide range of λ values in the parametric study, the clay is very compressible in comparison to the column stiffness, and load transfer to the columns is controlled mostly by the arching response of the upper sand layer and the embankment fill material. Therefore, varying the compressibility of the normally consolidated clay layer had a very small effect on the load distribution at the top of the column. Consequently, for the parametric analyses with

geosynthetic reinforcement, the material property values of the normally consolidated clay were not varied from those shown in Table 8.1.

However, as also shown in the parametric study performed for the case of a column-supported embankment without geosynthetic reinforcement, the degree of overconsolidation of the soft clay does affect the load distribution at the top of the column. As discussed in Chapter 6, in cases where the clay is overconsolidated prior to column installation and embankment construction, subsequent loading follows recompression, which reduces the clay compressibility enough to produce a significant difference in the load distribution at the elevation of the top of the column. Accordingly, as part of this parameter study, the clay layer was overconsolidated by applying three different surcharge pressures (200, 500, and 1000 psf) to both the Case 1 and Case 2 subsurface profiles, prior to installing the column and placing the embankment.

Since the thickness of the clay layer was shown to have negligible effects on the load distribution at the top of the column for the case of column-supported embankments without geosynthetic reinforcement (as described in Chapter 6), it was not varied in this parametric study.

8.3.5 Column Diameter and Spacing

In axisymmetric models, the total tributary area associated with a column is represented by a circular area, and the area replacement ratio is equal to the square of the column diameter, d_{col}, divided by the square of the model diameter, d_{mod}. As shown in Figure 8.1, the base case column diameter is 2.3 ft and the diameter of the axisymmetric model is 7.28 ft, which correspond to an area replacement ratio of 10%. This geometry was based on realistic values of pile cap width, pile spacing, and embankment height for geosynthetic-reinforced, pile-supported embankments (Russell and Pierpoint 1997, Kempton et al. 1998, Han and Gabr 2002). In the parametric study, column diameters of 1.64, 2.3, and 4 ft were used, and area replacement ratios ranged from 10% to 30%, as indicated in Table 8.4.

Table 8.4. Column and model diameters, Case 2

	d_{mod} (ft)				
d_{col} (ft)	a_s = 10%	a_s = 15%	a_s = 20%	a_s = 25%	a_s = 30%
1.64	-	4.24	3.66	3.28	3
2.3	7.28	5.94	5.14	4.6	4.2
4	-	10.32	8.94	8	7.3

8.4 Results of Parametric Study Analyses

The numerical analysis results are expressed in terms of SRR_{net}, which is the normalized difference between the vertical stresses on the top and bottom of the geosynthetic in the area not supported by columns. The normalization is by the average vertical stress from the embankment calculated at the elevation of the geosynthetic. SRR_{net} represents the net vertical stress on the geosynthetic, which is the stress that causes the geosynthetic to deflect downward and develop strain and tension.

As previously mentioned, each parameter was varied independently, except for simultaneous variation of the column diameter and spacing. The results of the parameter studies are discussed in this section, and are plotted in Figures 8.2 through 8.7.

8.4.1 Geosynthetic Stiffness

The effect of geosynthetic stiffness on SRR_{net} values can be seen in Figure 8.2. As the geosynthetic stiffness increases, the geosynthetic is able to support more embankment load. As a result, values of SRR_{net} increase with increasing geosynthetic stiffness. Values of SRR_{net} decrease with increasing embankment height.

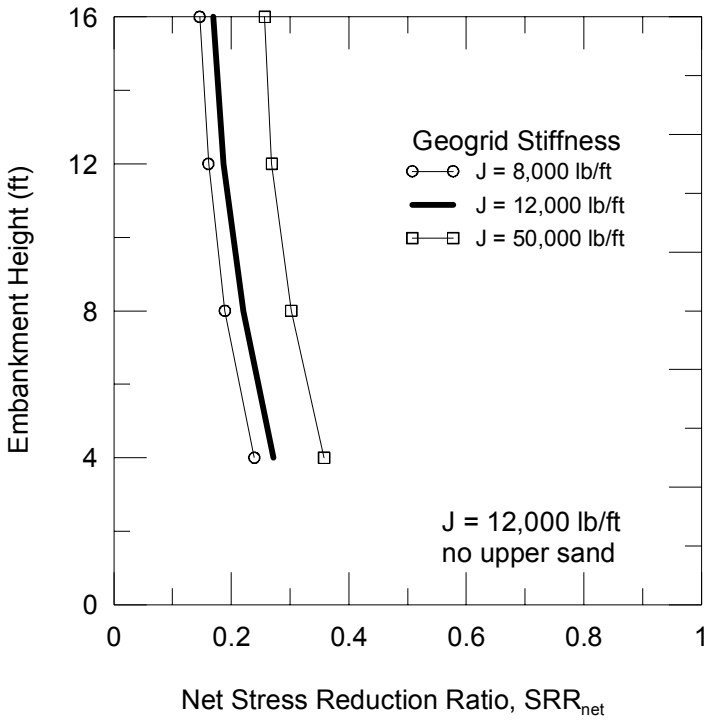

Figure 8.2. Variation of SRRnet with geogrid stiffness and embankment height

8.4.2 Geosynthetic Location

Using the Case 2 configuration, the location of the geogrid was evaluated at elevations of zero, three, six, and nine inches above the top of the column. The effect of geogrid location is shown in Figure 8.3, which indicates that SRR_{net} increases as the elevation of the geogrid approaches the top of the column. The difference in SRR_{net} values is greater for lower embankment heights, and as the embankment height increases, the values of SRR_{net} tend to decrease and appear to approach each other.

8.4.3 Embankment Fill

Using the Case 1 configuration, the effect of embankment density on SRR_{net} values was evaluated. The results can be seen in Figure 8.4, which shows that embankment density has relatively little effect on SRR_{net} values for the conditions of Case 2.

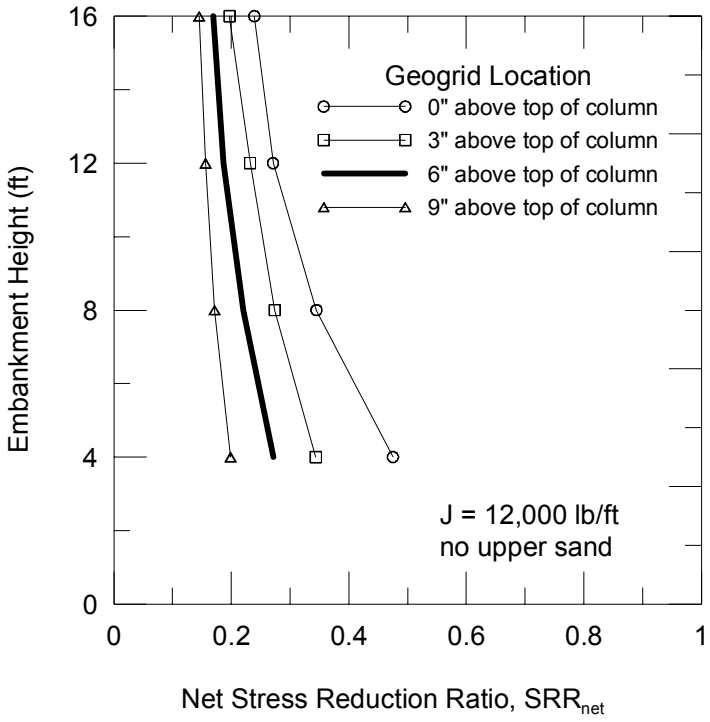

Figure 8.3. Variation of SRRnet with geogrid location and embankment height

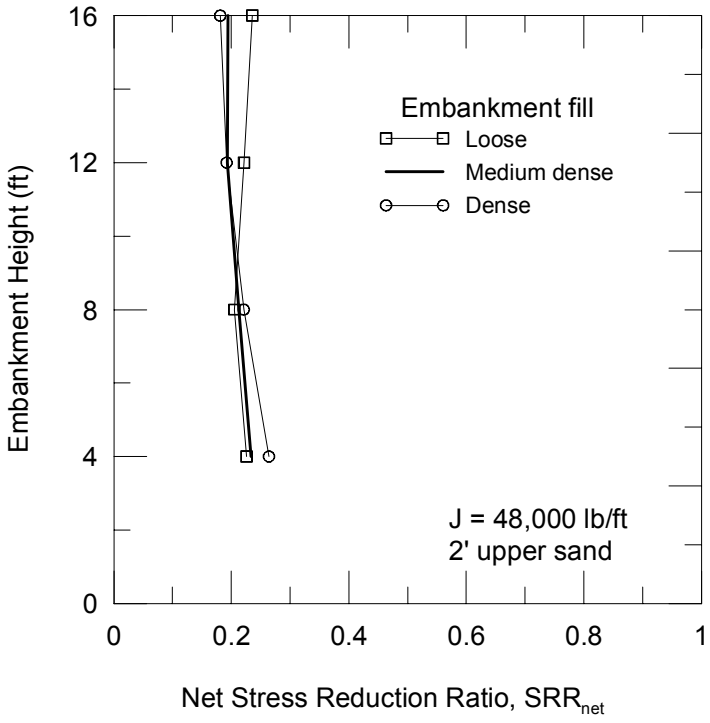

Figure 8.4. Effect of embankment fill on SRR_{net}

8.4.4 Upper Sand Layer

For both the Case 1 and 2 configurations, the effect of thickness of the upper sand layer on SRR_{net} values is shown in Figure 8.5. In all cases, the value of SRR_{net} on the geogrid decreases as the thickness of the upper sand layer increases. The upper sand layer is less compressible than the soft clay, so the presence of the upper sand means that more load is carried by the soil, which provides greater support for the geogrid. Figure 8.5 also shows that for a given sand thickness, the value of SRR_{net} is greater for the stiffer geogrid.

8.4.4 Degree of Overconsolidation of the Clay

For both the Case 1 and 2 configurations, the effect of overconsolidation of the clay is shown in Figure 8.6, which indicates that the SRR_{net} values decrease as the preload increases. For both cases, a small value of preload (i.e. 200 psf) is sufficient to cause a significant decrease in the values of SRR_{net}. As discussed in Chapter 6, even a relatively small surcharge pressure is sufficient to put the clay in an overconsolidated state for most of the embankment loading.

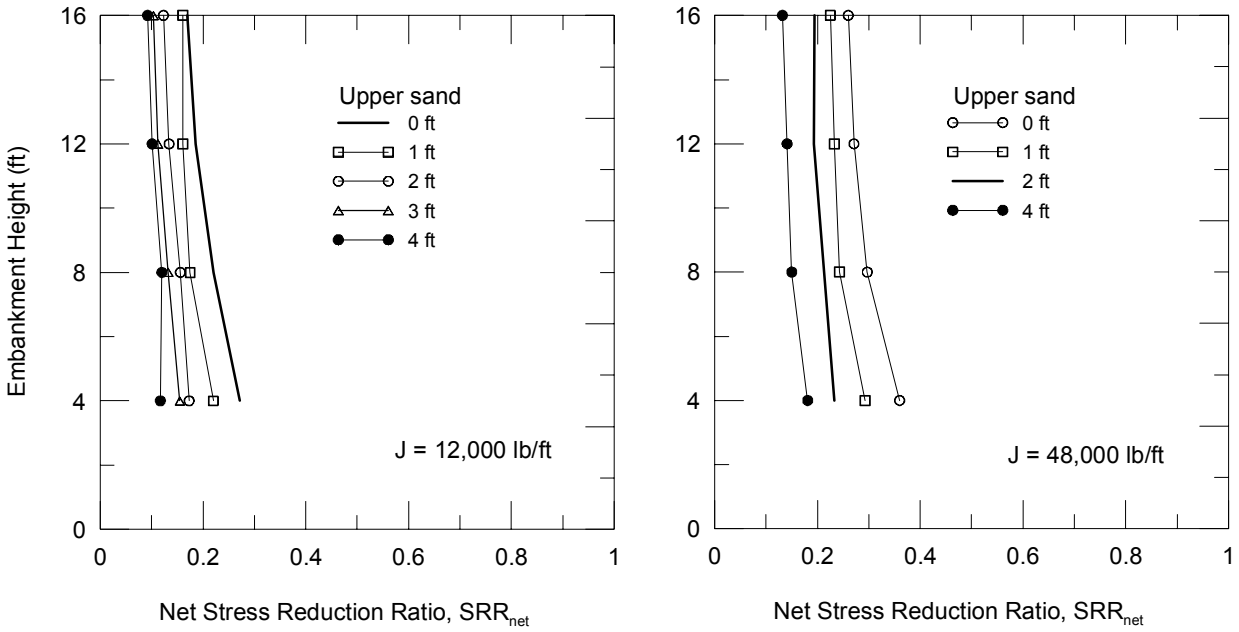

Figure 8.5. Variation of SRRnet with thickness of upper sand layer and embankment height

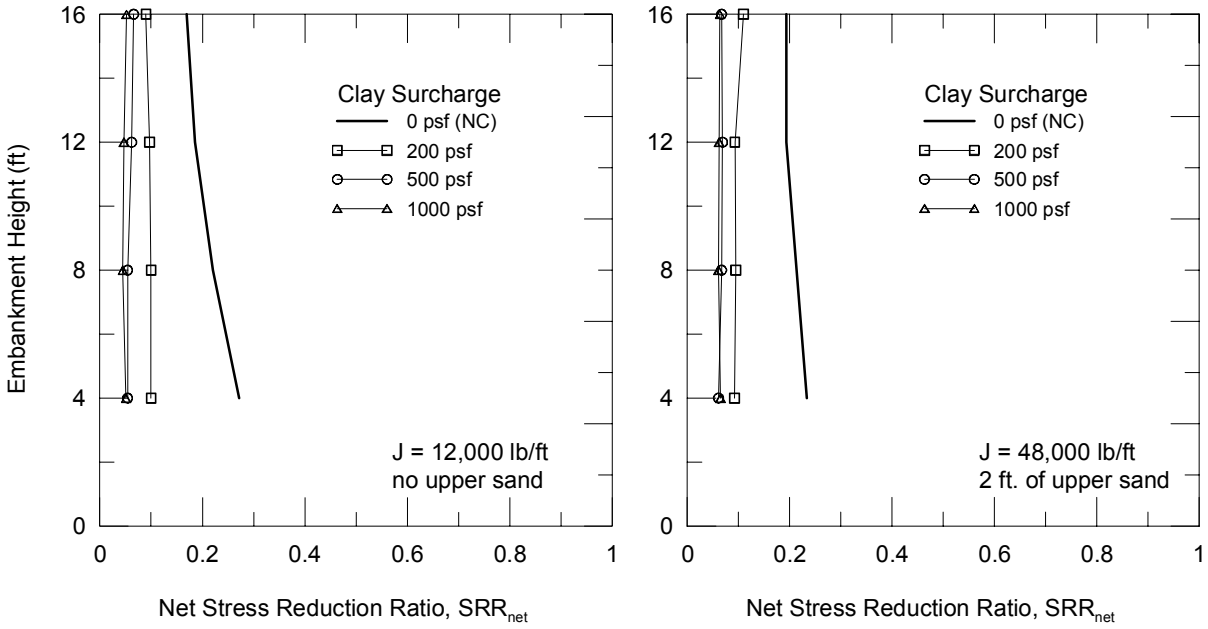

Figure 8.6. Effect of overconsolidation on SRR_{net}

8.4.5 Column Diameter and Spacing

As discussed in Chapter 6, the influence of the column diameter for a constant value of a_s has a complex effect on the load distribution behavior of column-supported embankments without geosynthetic reinforcement. As the clear span between columns increases, the ability of the upper sand and clay between columns to effectively span between columns is reduced, which tends to increase the stress on the top of the columns. However, the ability of the embankment to span between columns is also reduced as the clear span increases, and this tends to decrease the stress on the top of the columns. These counteracting effects produce the complex influence of column diameter on SRR values for fixed values of a_s.

As part of the parametric study with geosynthetic reinforcement within the bridging layer, three column diameters and four area replacement ratios were evaluated, as listed in Table 8.4. The results are shown in Figure 8.7, where the clear spacing between columns is plotted against the value of SRR_{net} at an embankment height of 16 ft. In general, as the area replacement ratio increases, the value of SRR_{net} decreases. Also, as the clear span between columns increases, the value of SRR_{net} generally increases. The increase in SRR_{net} due to an increase in clear spacing is more pronounced at smaller area replacement ratios.

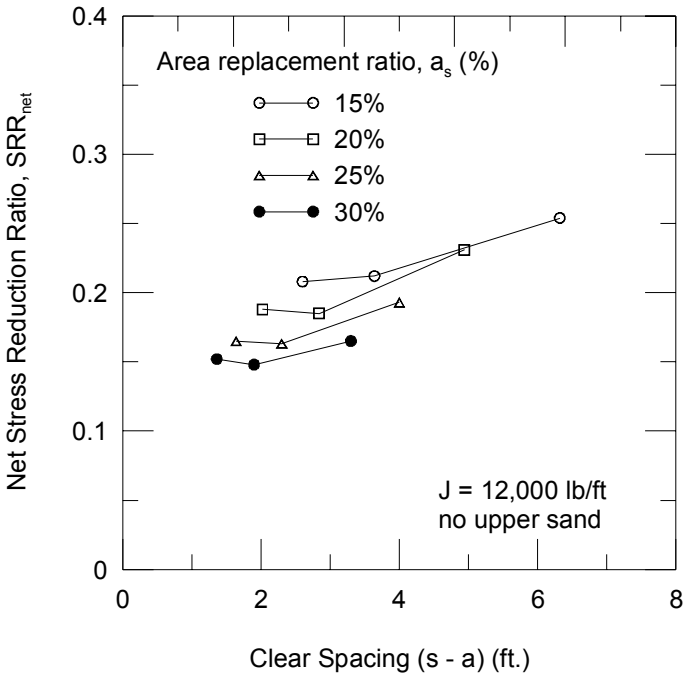

Figure 8.7. Effect of clear spacing on SRR_{net} (for H = 16 ft)

8.5 Summary and Conclusions of the Parametric Study

An important goal of this research is to develop a calculation procedure that evaluates the settlement and load transfer behavior of geosynthetic-reinforced column-supported embankments. To support development of the calculation procedure for the case in which geosynthetic reinforcement is included, a total of 36 axisymmetric analyses were performed. The parameter variations and the analysis results are summarized in Table 8.4.

Results of the parameter study for column-supported embankments with geosynthetic reinforcement in the bridging layer are expressed in terms of the net stress reduction ratio, SRR_{net}, which must lie between 0 and 1. As the value of SRR_{net} approaches zero, the geosynthetic carries less net load, and is thus less effective at transferring embankment and surcharge loads to the columns.

Key findings from the analyses include:

- As the geosynthetic stiffness increases, the geosynthetic is able to support more embankment load. As a result, values of SRR_{net} increase with increasing geosynthetic stiffness.

- As the elevation of the geogrid gets closer to the top of the column, SRR_{net} increases.
- Embankment density has a relatively small effect on SRR_{net} values.
- As the thickness of an existing upper sand layer increases, the value of SRR_{net} on the geogrid decreases.
- In cases where the clay is overconsolidated prior to column installation and embankment construction, subsequent loading follows recompression, which reduces the clay compressibility enough to produce a significant decrease in the net load on the geogrid. Even a small value of surcharge (e.g., 200 psf) produces a significant decrease in the values of SRR_{net}.
- In general, as the area replacement ratio increases, the value of SRR_{net} decreases. Also, as the clear span between columns increases, the value of SRR_{net} generally increases. The increase in SRR_{net} due to an increase in clear spacing is more pronounced at smaller area replacement ratios.

8.6 Closing Remarks

A parameter study was performed using the finite difference axisymmetric FLAC model developed and verified as described in Chapters 5 and 7. Various features of the model were systematically changed in order to evaluate the influence of a wide range of factors relevant to geosynthetic-reinforced column-supported embankments. The analyses and results presented here are for the case of embankments supported on columns with overlying layers of geosynthetic reinforcement. In general, SRR_{net} values increase with increasing clear spacing between columns and increasing geosynthetic stiffness. SRR_{net} values decrease with increasing stiffness and strength of the foundation and embankment soils, increasing elevation of the geosynthetic above the top of the columns or pile caps, and increasing area replacement ratio. The effectiveness of the geosynthetic reinforcement is greatly affected by the compressibility of the native soil, which is a factor that is typically not considered in the currently available methods of evaluating the loads applied to the geosynthetic reinforcement (e.g., Hewlett and Randolph 1988, BS8006 1995, Russell and Pierpoint 1997, Rogbeck et al. 1998, and others, as described in Chapter 3). If the subgrade support is good, geosynthetic reinforcement does not have a significant effect on system performance.

Parametric studies were also performed for the case of embankments supported on columns without overlying layers of geosynthetic reinforcement. Those analyses are described in Chapter 6. Based on the results of the analyses discussed in this chapter and Chapter 6, a calculation procedure was developed to evaluate the settlement and load transfer behavior of column-supported embankments. This calculation procedure is presented in Chapter 9.

Table 8.5. Summary of analyses performed

Run No.	r_{col} (ft)	r_{mod} (ft)	a_s (%)	Upper Sand Thickness (ft)	Upper Sand Modulus (psf)	Clay Parameters λ, κ	Surcharge/ Preload (psf)	Embankment Fill Modulus (psf)	Column Modulus (psi)	Geogrid Stiffness (lb/ft)	FLAC SRR_{net} (H = 16')
1	1.15	3.64	0.10	0	250,000	0.35, 0.035	0	625,000	5,400,000	12,000	0.169
2	1.15	3.64	0.10	0	250,000	0.35, 0.035	0	625,000	5,400,000	8,000	0.146
3	1.15	3.64	0.10	0	250,000	0.35, 0.035	0	625,000	5,400,000	50,000	0.257
4	1.15	3.64	0.10	0	250,000	0.35, 0.035	0	625,000	5,400,000	12,000	0.169
5	1.15	3.64	0.10	1	250,000	0.35, 0.035	0	625,000	5,400,000	12,000	0.161
6	1.15	3.64	0.10	2	250,000	0.35, 0.035	0	625,000	5,400,000	12,000	0.123
7	1.15	3.64	0.10	3	250,000	0.35, 0.035	0	625,000	5,400,000	12,000	0.104
8	1.15	3.64	0.10	4	250,000	0.35, 0.035	0	625,000	5,400,000	12,000	0.092
9	1.15	3.64	0.10	0	250,000	0.35, 0.035	100	625,000	5,400,000	12,000	0.133
10	1.15	3.64	0.10	0	250,000	0.35, 0.035	200	625,000	5,400,000	12,000	0.09
11	1.15	3.64	0.10	0	250,000	0.35, 0.035	500	625,000	5,400,000	12,000	0.066
12	1.15	3.64	0.10	0	250,000	0.35, 0.035	1,000	625,000	5,400,000	12,000	0.052
13	0.82	2.59	0.10	0	250,000	0.35, 0.035	0	625,000	5,400,000	12,000	0.262
14	0.82	2.12	0.15	0	250,000	0.35, 0.035	0	625,000	5,400,000	12,000	0.208
15	0.82	1.83	0.20	0	250,000	0.35, 0.035	0	625,000	5,400,000	12,000	0.188
16	0.82	1.64	0.25	0	250,000	0.35, 0.035	0	625,000	5,400,000	12,000	0.165
17	0.82	1.5	0.30	0	250,000	0.35, 0.035	0	625,000	5,400,000	12,000	0.152
18	1.15	2.97	0.15	0	250,000	0.35, 0.035	0	625,000	5,400,000	12,000	0.212
19	1.15	2.57	0.20	0	250,000	0.35, 0.035	0	625,000	5,400,000	12,000	0.185
20	1.15	2.3	0.25	0	250,000	0.35, 0.035	0	625,000	5,400,000	12,000	0.163
21	1.15	2.1	0.30	0	250,000	0.35, 0.035	0	625,000	5,400,000	12,000	0.148
22	2	5.16	0.15	0	250,000	0.35, 0.035	0	625,000	5,400,000	12,000	0.254
23	2	4.47	0.20	0	250,000	0.35, 0.035	0	625,000	5,400,000	12,000	0.231
24	2	4	0.25	0	250,000	0.35, 0.035	0	625,000	5,400,000	12,000	0.193
25	2	3.65	0.30	0	250,000	0.35, 0.035	0	625,000	5,400,000	12,000	0.165
26	1.15	3.64	0.10	2	250,000	0.35, 0.035	0	625,000	5,400,000	48,000	0.214
27	1.15	2.97	0.15	2	250,000	0.35, 0.035	0	625,000	5,400,000	48,000	0.216

Run No.	r_{col} (ft)	r_{mod} (ft)	a_s (%)	Upper Sand Thickness (ft)	Upper Sand Modulus (psf)	Clay Parameters λ, κ	Surcharge/ Preload (psf)	Embankment Fill Modulus (psf)	Column Modulus (psi)	Geogrid Stiffness (lb/ft)	FLAC SRR_{net} (H = 16')
28	1.15	2.57	0.20	2	250,000	0.35, 0.035	0	625,000	5,400,000	48,000	0.19
29	1.15	2.1	0.30	2	250,000	0.35, 0.035	0	625,000	5,400,000	48,000	0.153
30	1.15	3.64	0.10	2	250,000	0.35, 0.035	200	625,000	5,400,000	48,000	0.11
31	1.15	3.64	0.10	2	250,000	0.35, 0.035	500	625,000	5,400,000	48,000	0.067
32	1.15	3.64	0.10	2	250,000	0.35, 0.035	1,000	625,000	5,400,000	48,000	0.064
33	1.15	3.64	0.10	0	250,000	0.35, 0.035	0	625,000	5,400,000	48,000	0.26
34	1.15	3.64	0.10	1	250,000	0.35, 0.035	0	625,000	5,400,000	48,000	0.225
35	1.15	3.64	0.10	4	250,000	0.35, 0.035	0	625,000	5,400,000	48,000	0.132
36	1.15	3.64	0.10	2	250,000	0.35, 0.035	0	250,000	5,400,000	48,000	0.236
37	1.15	3.64	0.10	2	250,000	0.35, 0.035	0	1,000,000	5,400,000	48,000	0.181
38	0.82	2.12	0.15	2	250,000	0.35, 0.035	0	625,000	5,400,000	48,000	0.196
39	2	5.16	0.15	2	250,000	0.35, 0.035	0	625,000	5,400,000	48,000	0.259

CHAPTER 9
DEVELOPMENT AND IMPLEMENTATION OF CALCULATION PROCEDURE

9.1 Introduction

Based on the results of the literature review, as described in Chapters 2 and 3, and the parametric numerical analyses that were performed, as described in Chapters 6 and 8, a calculation procedure was developed to evaluate the settlement and load distribution behavior of column-supported embankments, both with and without geosynthetic reinforcement.

In this section, the practical procedures that were developed for analysis and design of geosynthetic-reinforced bridging layers in column-supported embankments are described. First, calculation procedures for SRR_{net}, geosynthetic strain, geosynthetic tension, and embankment settlement are presented. Second, a comprehensive design procedure is described. Finally, the calculation and design procedures are illustrated with examples.

9.2 Basis of Calculation Procedure

A calculation model for the net vertical load acting on the geosynthetic was developed based on placing the geosynthetic reinforcement at the bottom of the embankment because this is the most effective location for the reinforcement (Rogbeck et al. 1998, Kempfert et al. 2004) and because this is a conservative location for calculating tension in the geosynthetic. In reality, the lowest layer of geosynthetic will be placed on a lift of granular material above the columns or pile caps to prevent local damage to the geosynthetic, and if more than one layer of geosynthetic is used, a lift of soil will be placed between each adjacent layer of geosynthetic. The calculation procedures described herein are applicable to the case in which the geosynthetic reinforcement is placed approximately 6 in. above the top of the column.

To begin, definition sketches are shown in Figures 9.1 and 9.2. Figure 9.1 shows pile caps laid out in plan view. A unit cell, which consists of one pile cap and the tributary soil defined by lines of symmetry, is also shown. For piles or columns laid out in a square array with center-to-center spacing, s, the area of the unit cell, A, is equal to s^2. The area of the pile cap or column, A_c, is equal to a^2 or πd_c^2, where a = the width of a pile cap and d_c = the diameter of a column. The area of the tributary soil, A_s, is $A - A_c$. The area replacement ratio, a_s, is equal to A_c/A.

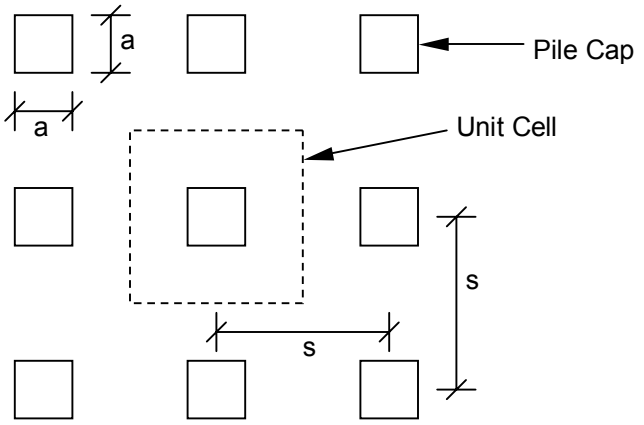

Figure 9.1. Definition sketch in plan view

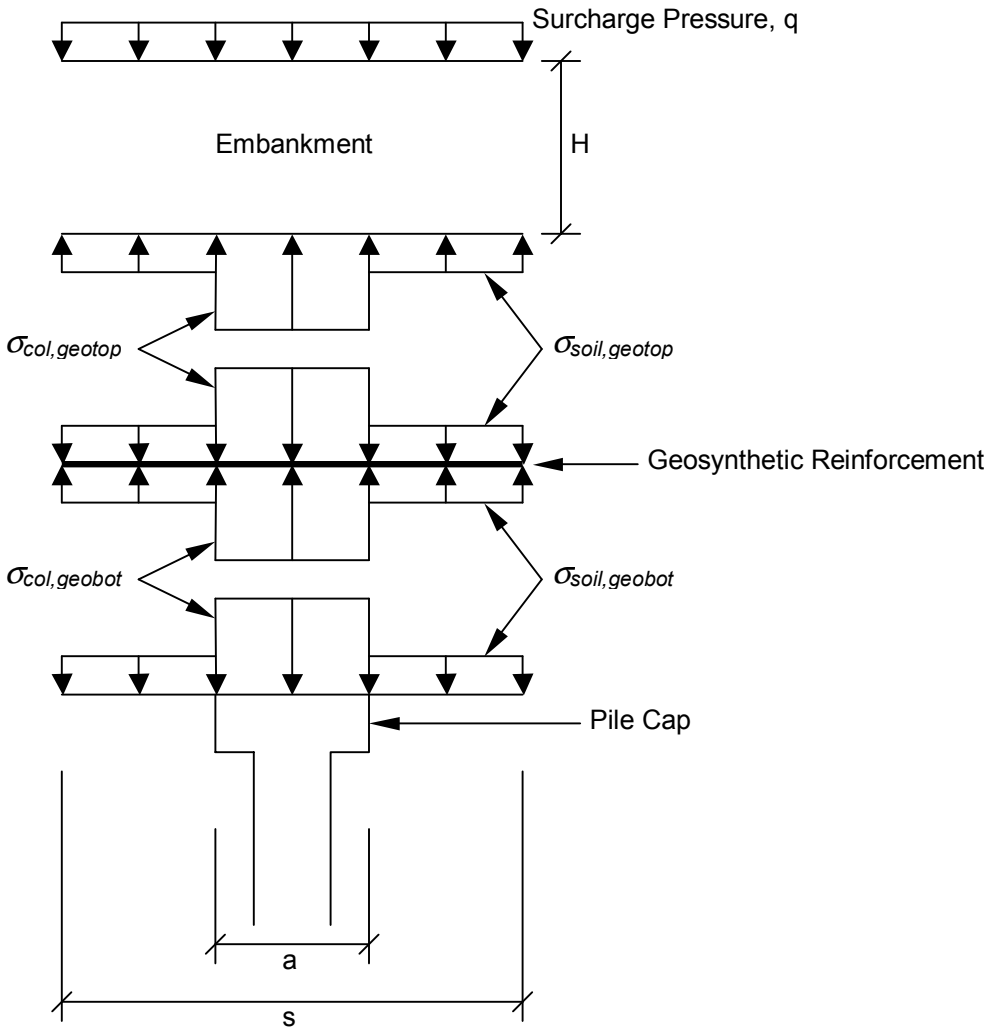

Figure 9.2. Definition sketch in profile view

Figure 9.2 shows an exploded profile view of a unit cell, including the vertical stresses at the contacts above and below the geosynthetic reinforcement. Values of stress reduction ratio applicable to the embankment, SRR_{emb}, the geogrid, SRR_{net}, and the foundation soil, SRR_{fndn}, are defined as follows:

$$SRR_{emb} = \frac{\sigma_{soil,geotop}}{\gamma H + q} \tag{9.1}$$

$$SRR_{net} = \frac{\sigma_{soil,geotop} - \sigma_{soil,geobot}}{\gamma H + q} \tag{9.2}$$

$$SRR_{fndn} = \frac{\sigma_{soil,geobot}}{\gamma H + q} \tag{9.3}$$

where $\sigma_{soil,geotop}$ = the vertical stress acting down on the top of the geosynthetic in the area underlain by the soil foundation and $\sigma_{soil,geobot}$ = the vertical stress acting up on the bottom of the geosynthetic in the area underlain by the soil foundation. From Equations 9.1 through 9.3, $SRR_{emb} = SRR_{net} + SRR_{fndn}$.

Vertical equilibrium requires that

$$\sigma_{col,geotop} = \frac{1 - (1 - a_s) \cdot SRR_{emb}}{a_s} (\gamma H + q) \tag{9.4}$$

$$\sigma_{col,geobot} = \frac{1 - (1 - a_s) \cdot SRR_{fndn}}{a_s} (\gamma H + q) \tag{9.5}$$

where $\sigma_{col,geotop}$ = the vertical stress acting down on the top of the geosynthetic in the area underlain by the column and $\sigma_{col,geobot}$ = the vertical stress acting up on the bottom of the geosynthetic in the area underlain by the column.

The procedures for obtaining the stresses on the embankment, geosynthetic reinforcement, column, and subgrade soil have several components, which are described here. First, the load-deflection relationship for the column or pile cap penetrating up, relatively, into the embankment is assumed to be linear up to the maximum load condition. The linear part is approximated using

the linear-elastic solution for displacement of a circular loaded area on a semi-infinite mass, as provided by Poulos and Davis (1974). In the terms of this application,

$$d = \frac{\sqrt{\pi A_c}(1-\nu_f)(\sigma_{col,geotop} - \sigma_{soil,geotop})}{2E_f} \tag{9.6}$$

where d = the relative displacement of the column or pile cap up into the embankment = the maximum differential settlement between the subgrade soil and the top of the column or pile cap, ν_f = the Poisson's ratio of the embankment fill, and E_f = the Young's modulus value of the embankment fill.

According to Equation 9.6, at a relative displacement of d = 0, $\sigma_{col,geotop} = \sigma_{soil,geotop}$, which corresponds to $SRR_{emb} = 1$, as shown by combining Equations 9.1 and 9.4. With increasing relative displacement d > 0, $\sigma_{col,geotop} > \sigma_{soil,geotop}$, which corresponds to $SRR_{emb} < 1$.

The limiting stress condition in the embankment above the geosynthetic reinforcement is established by setting a lower limit on the value of SRR_{emb} using the Adapted Terzaghi Method:

$$SRR_{emb} \geq SRR_{lim} = \frac{\gamma}{\alpha(\gamma H + q)}\left(1 - e^{-\alpha H}\right) + \frac{q}{\gamma H + q} \cdot e^{-\alpha H} \tag{9.7}$$

where γ = the unit weight of the embankment fill, H = the embankment height, q = the surcharge pressure on top of the embankment, $\alpha = pK\tan(\phi)/A_s$, p = the column or pile cap perimeter, K = the lateral earth pressure coefficient in the embankment fill = 1.0 according to Russell and Pierpoint (1997), ϕ = the friction angle of the embankment fill. Equation 9.7 can easily be adapted to embankments constructed of two types of fill material, as would occur when high quality soil is used in the bridging layer and lower quality soil is used above the bridging layer.

The Adapted Terzaghi Method was used to determine the limiting condition because this method provided a reasonably good fit to the results of the verified numerical analyses, as shown below in Figure 9.3. However, other realistic methods for determining a limiting SRR value, such as

the Hewlett and Randolph (1998) Method or the Kempfert et al. (2004) Method could be used in place of Equation 9.7.

By combing Equations 9.1, 9.4, 9.6, and 9.7, the differential settlement at yield, d_{yield}, can be determined:

$$d_{yield} = \frac{\sqrt{\pi A_c}\left(1-\nu_f\right)\left(1-SRR_{lim}\right)\left(\gamma H + q\right)}{2a_s E_f} \tag{9.8}$$

Thus, SRR_{emb} decreases linearly from a value of one at d = 0 to a value of SRR_{lim} at $d = d_{yield}$. For $d > d_{yield}$, SRR_{emb} remains at a value of SRR_{lim}.

The load-deflection response of the geosynthetic reinforcement was approximated by performing axisymmetric numerical analyses of a uniformly loaded annulus of membrane material with the inner boundary pinned, which represents the support provided by the column, and with the outer boundary free to move vertically but not laterally, which represents the axisymmetric approximation of lines of symmetry in the actual three-dimensional configuration of a column-supported embankment. These analyses are described in detail in Appendix B. The results are closely approximated by the following expression:

$$d = \sqrt{\frac{A}{\pi}}\left[\frac{2}{3}\left(1-\sqrt{a_s}+\left(1-\sqrt{a_s}\right)^4\right)\sqrt[3]{\Sigma_g}+\left(1-\sqrt{a_s}\right)^3\Sigma_g\right] \tag{9.9}$$

where d = the sag of the geosynthetic reinforcement = the maximum differential settlement between the subgrade soil and the top of the column or pile cap and Σ_g = the normalized vertical stress on the geosynthetic reinforcement, which is given by

$$\Sigma_g = \frac{\left(\sigma_{soil,geotop}-\sigma_{soil,geobot}\right)\sqrt{\frac{A}{\pi}}}{J_g} \tag{9.10}$$

where J_g = the stiffness of the geosynthetic reinforcement = $E_g t_g$, E_g = the modulus of the geosynthetic reinforcement, and t_g = the thickness of the geosynthetic reinforcement. Values of J_g can be obtained from tension tests on wide specimens of the geosynthetic. If more than one layer of geosynthetic reinforcement is used, J_g should be set equal to the sum of the stiffnesses of the individual layers.

The settlements of the column and the subgrade soil are determined based on the vertical stress applied to the top of the column or pile, $\sigma_{col,geobot}$, and the vertical stress applied to the subgrade soil, $\sigma_{soil,geobot}$. As the soil settles down with respect to the column, the soil sheds load to the column through shear stresses at the contact between the soil and the column along the column perimeter. The magnitude of the shear stress, τ, is calculated on an effective stress basis because this is a consolidation problem:

$$\tau = \sigma'_h \tan\delta \tag{9.11}$$

where σ'_h = the effective lateral earth pressure at the soil-column contact and δ = the effective stress interface friction angle.

The value of σ'_h is determined from

$$\sigma'_h = K_0 \sigma'_{v,0} + \Delta\sigma'_h \tag{9.12}$$

where K_0 = the initial effective stress lateral earth pressure coefficient at the soil-column contact, $\sigma'_{v,0}$ = the initial vertical effective stress in the soil, and $\Delta\sigma'_h$ = the increment in the lateral effective stress at the soil-column contract due to the applied load.

The numerical analyses disclosed that the value of $\Delta\sigma'_h$ can be higher than would be expected based on one-dimensional compression of the soil because the column can bulge laterally in response to the applied load. This effect on $\Delta\sigma'_h$ values is most significant for portions of the column that are surrounded by sand. In the simplified calculation model, the value of $\Delta\sigma'_h$, as well as the vertical strain of the column and sand layers adjacent to the column, are determined

by using the solution for an elastic solid cylinder, which represents the column, surrounded by a concentric and laterally constrained thick-walled cylinder, which represents the soil. In the terms of this application, the relationships are:

$$\Delta\sigma'_h = \frac{\nu_{col}(1+a_s-\nu_{soil}(1-a_s))E_{soil}\Delta\sigma_{col} + \nu_{soil}(1+\nu_{soil})(1-a_s)E_{col}\Delta\sigma_{soil}}{(1-\nu_{col})(1+a_s-\nu_{soil}(1-a_s))E_{soil} + (1-\nu_{soil})^2(1-a_s)E_{col}} \tag{9.13}$$

$$\varepsilon_{col} = \frac{\Delta\sigma_{col} - 2\nu_{col}\Delta\sigma'_h}{E_{col}} \tag{9.14}$$

$$\varepsilon_{soil} = \frac{(1+\nu_{soil})[(1-2\nu_{soil}+a_s)\Delta\sigma_{soil} - 2a_s\nu_{soil}\Delta\sigma'_h]}{(1-\nu_{soil}+a_s(1+\nu_{soil}))E_{soil}} \tag{9.15}$$

where ε_{col} = the vertical strain in the column, ν_{col} = the Poisson's ratio of the column, E_{col} = the Young's modulus of the column, $\Delta\sigma_{col}$ = the vertical stress increment in the column, ε_{col} = the vertical strain in the column, ν_{soil} = the Poisson's ratio of the soil, E_{soil} = the Young's modulus of the soil, and $\Delta\sigma_{soil}$ = the vertical stress increment in the soil. As mentioned above, the value of $\Delta\sigma_{col}$ increases with depth and the value of $\Delta\sigma_{soil}$ decreases with depth due to load transfer from the soil to the column.

If the soil surrounding the column is clay instead of sand, the vertical strain in the soil is determined from:

$$\varepsilon_{soil} = C_{\varepsilon c}\log\frac{p_0+\Delta\sigma_{soil}}{p_0} \qquad \text{for } p_0 = p_p \tag{9.16a}$$

$$\varepsilon_{soil} = C_{\varepsilon r}\log\frac{p_p}{p_0} + C_{\varepsilon c}\log\frac{p_0+\Delta\sigma_{soil}}{p_p} \qquad \text{for } p_0 < p_p < p_0+\Delta\sigma_{soil} \tag{9.16b}$$

$$\varepsilon_{soil} = C_{\varepsilon r}\log\frac{p_0+\Delta\sigma_{soil}}{p_0} \qquad \text{for } p_0+\Delta\sigma_{soil} < p_p \tag{9.16c}$$

where $C_{\varepsilon c}$ = the compression index, $C_{\varepsilon r}$ = and the recompression index, p_0 = initial vertical effective stress, and p_p = preconsolidation pressure of the clay.

At the elevation of the top of the columns or pile caps, $\Delta\sigma_{col} = \sigma_{col,geobot}$ and $\Delta\sigma_{soil} = \sigma_{soil,geobot}$. The value of $\Delta\sigma_{col}$ increases with depth and the value of $\Delta\sigma_{soil}$ decreases with depth due to load transfer from the soil to the column through the shear stresses around the column perimeter, as determined from Equation 9.11. This process continues with depth until the column settlement and the soil settlement are equal. At and below this depth, the settlements and strains in the column and soil are equal. The total compression of the column and the soil between columns are the integrated vertical strains over the column length.

The computational model described above is solved by requiring that the values of differential settlement, d, determined for the base of the embankment, the geosynthetic, and the underlying foundation must all be the same. The settlement profile of the subgrade soil at the level of the top of the columns is likely to be dish-shaped between columns, and the suggestion of Russell et al. (2003) that the average settlement of the foundation soil may be as small as one-half of the maximum differential settlement was adopted.

9.3 Development of Spreadsheet

A spreadsheet was set up to solve these equations and compute values of SRR for cases of column-supported embankments without geosynthetic reinforcement, and SRR_{net} for cases of column-supported embankments with geosynthetic reinforcement. The values of SRR_{net} are used to compute the strains and tension in the geosynthetic reinforcement, as described below.

One feature of the spreadsheet is that two different types of embankment fill are allowed so that lower quality fill can be used above the bridging layer. Equation 9.7 was adapted to take into account two different types of embankment fill, as shown in Figure 9.3. The modified equation for SRR_{lim} is given in Equation 9.17.

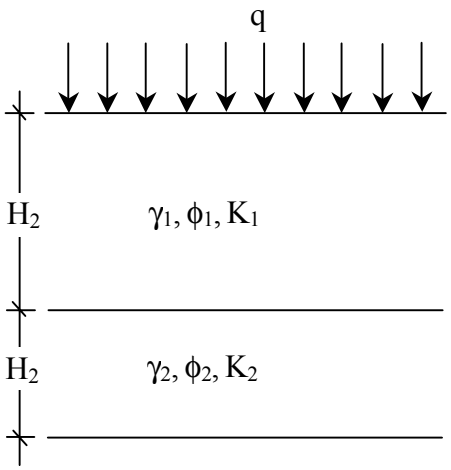

Figure 9.3. Definition of variables for case with two layers of embankment fill

$$SRR_{lim} = \frac{\frac{\gamma_2}{\alpha_2}\cdot\left(1-e^{-\alpha_2 H_2}\right)+\left[\frac{\gamma_1}{\alpha_1}\cdot\left(1-e^{-\alpha_1 H_1}\right)+q\cdot e^{-\alpha_1 H_1}\right]\cdot e^{-\alpha_2 H_2}}{\gamma_1 H_1+\gamma_2 H_2+q} \qquad (9.17)$$

where $\alpha_1 = \frac{p\cdot K_1\cdot\tan\phi_1}{A_s}$, $\alpha_2 = \frac{p\cdot K_2\cdot\tan\phi_1}{A_s}$, p = column or pile cap perimeter, A_s = area of soil.

Other features of the spreadsheet include the following:

- Analyses without geosynthetic reinforcement can be performed by setting the value of J_g equal to zero.
- The column area and properties can vary with depth so that embankments supported on piles with pile caps can be analyzed.
- The subsurface profile can include two upper sand layers and two underlying clay layers. The preconsolidation pressure for the clay can vary linearly within each clay layer.

The spreadsheet was applied to the same cases analyzed in the numerical parameter studies described in Chapters 6 and 8, using a value of K = 1. The comparisons of the resulting SRR_{fndn} values for column-supported embankments without geosynthetic reinforcement and for SRR_{net} values for column-supported embankments with geosynthetic reinforcement are shown in Figure 9.4. In both cases, it can be seen that the agreement is good.

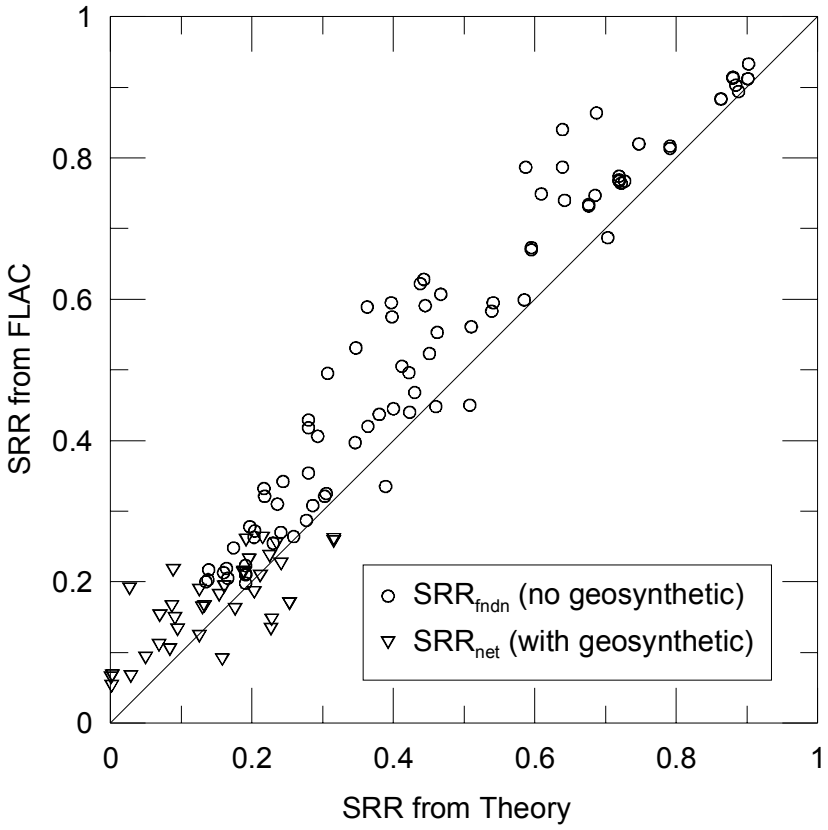

Figure 9.4. Comparison of SRR values from the simplified theory with SRR values from FLAC

For analysis of strain and tension in the geosynthetic reinforcement, the procedure presented in BS8006 (1995) is adopted. This is essentially the same procedure as employed by John (1987), Russell et al. (2003), Rogbeck et al. (1998), and others. In this approach, the load acting on the shaded area in Figure 9.5 is assumed to be carried by the portion of the geosynthetic reinforcement that spans directly between columns. This portion of the geosynthetic reinforcement is assumed to deform as a parabola. The strain in the geosynthetic reinforcement, ε_g, is obtained by solving the following cubic equation:

$$96\varepsilon_g^3 - 6K_g^2\varepsilon_g + K_g^2 = 0 \tag{9.18}$$

where $K_g = SRR_{net}(\gamma H + q)A_s/(J_g\, a)$, A_s = the area of tributary soil in a unit cell, and a = the pile cap width. If round columns or pile caps with diameter, d_c, are used, then the value of a is set equal to $0.886d_c$ when evaluating K_g.

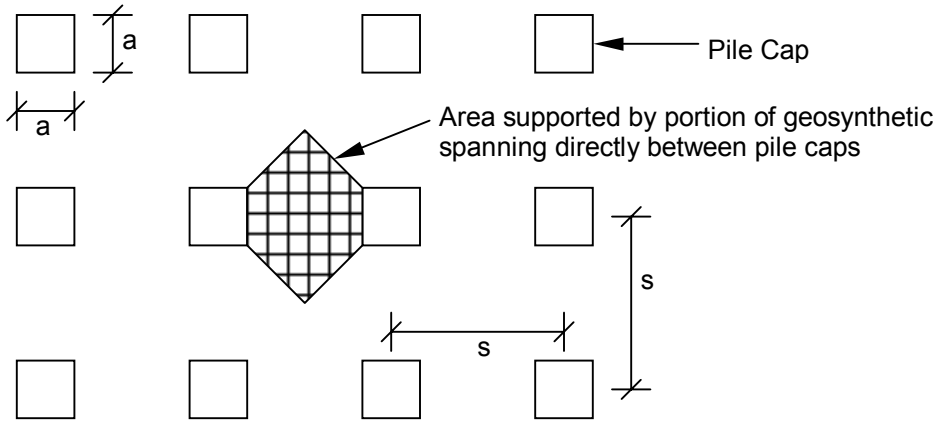

Figure 9.5. Area supported by geosynthetic spanning directly between columns

The tension in the geosynthetic reinforcement, T_g, is obtained by multiplying the strain, ε_g, by the stiffness, J_g.

A second spreadsheet, which is linked to the spreadsheet for determining SRR_{net} values, was developed to solve Equation 9.18 and compute the values of strain and tension in the geosynthetic reinforcement.

The total settlement, S, of the embankment is the sum of the embankment compliance, S_E, the compression of the columns, S_C, and the compression of underlying compressible material, S_U, if present:

$$S = S_E + S_C + S_U \tag{9.19}$$

The approach of Russell et al. (2003) can be used to account for compliance of the embankment at the level of the top of the columns. In this method, an approximation of the volume of the

settlement dish between columns or pile caps is uniformly distributed to produce an increment of embankment settlement that is due to embankment compliance, S_E, according to

$$S_E = \frac{d(1 - a_s)}{2} \tag{9.20}$$

where d = the maximum differential settlement of the settlement dish between columns or pile caps computed as described above and a_s = the area replacement ratio.

The compression of the columns, S_C, is obtained by integrating the column strains, ε_{col}.

If compressible soil exists below the bottom of the columns, the load spread method described by Broms (1991) can be used to calculate compression of this underlying material, S_U. In this method, the embankment plus surcharge load is assumed to be carried down to the bottom of the columns, and then the load is distributed across an area that increases with depth at a rate of 1H:2V. Compression of the soil below the columns is computed using the resulting stress increments in the usual way.

9.4 Design Procedure

The following step-by-step procedure is recommended for design of geosynthetic-reinforced, column-supported embankments:

1. Collect project information, including the required embankment height, H, traffic surcharge loading, q, and the maximum allowable embankment settlement, S.

2. Collect subsurface information, including stratigraphy, field test data, laboratory test results, and ground water information. Develop subsurface profile(s) for design.

3. Select trial values of the maximum center-to-center column spacing, s, of columns in a square array and the minimum column diameter, d_c, or pile cap width, a, to satisfy all

three of the following three criteria, which were obtained from a synthesis of recommendations in the literature:

a. $s - a \leq H$

b. $s - a \leq 8.5$ ft

c. $a_s \geq 0.10$

If round columns of diameter, d_c, are used, then set a equal to $0.886d_c$ when applying criteria a. and b. The area replacement ratio, a_s, is given by a^2/s^2 or $\pi d_c^2/(4s^2)$.

4. Select a clean sand or sand and gravel for the bridging layer. This should be an SP, SW, GW, or GP material, according to the Unified Soil Classification System. Estimate the values of unit weight, friction angle, modulus, and Poisson's ratio for this material. The thickness of the bridging layer fill, H_b, should satisfy both of the following criteria:

   a. $H_b \geq s - a$, except that this may be reduced using conservative engineering judgment if an upper layer of clean sand or sand and gravel exists at the site.

   b. $H_b \geq 3$ ft

5. Determine the embankment fill material that will be used above the bridging layer. This may be any suitable material for embankment construction. Estimate the values of unit weight, friction angle, modulus, and Poisson's ratio for this material.

6. Design the columns or piles to be able carry the entire load from the embankment and surcharge with an adequate factor of safety. Thus, each column should be designed to carry an allowable load of $(\gamma H + q)s^2$. Based on a conservative interpretation of the results of Chapter 6, if the columns are deep-mixing-method columns, then the unconfined compressive strength of the columns should exceed $1.5(\gamma H + q)/a_s$ by a suitable factor of safety.

7. Select a suitable layer or layers of geosynthetic reinforcement. Between one and three layers of geosynthetic reinforcement can be used. The geosynthetic reinforcement is treated as a single layer in the spreadsheets, with the value of J_g set equal to the sum of the stiffnesses of the individual layers. The geosynthetic reinforcement should be

selected to satisfy the following criteria by using the spreadsheets to calculate SRR_{net}, the strain in the geosynthetic reinforcement, ε_g, and the tension in the geosynthetic reinforcement, T_g:

a. $\varepsilon_g \leq 0.05$ using the long-term geosynthetic reinforcement stiffness, J_g

b. $T_g \leq$ the allowable geosynthetic tensile strength of the combined layers of geosynthetic reinforcement

8. Calculate the embankment settlement, S, as the sum of the embankment compliance, S_E, the compression of the columns, S_C, and the compression of underlying material, S_U, if significant. The sum of S_E and S_C is calculated in the SRR_{net} spreadsheet. The value of S_U can be determined using the approach of Broms (1991), in which the embankment load is transferred to the bottom of the columns and the load is distribute with depth using a 2V:1H load spread below the bottom of the columns.

9. If the embankment settlement is too large, the design process should be repeated using a closer column spacing, a larger area replacement ratio, a stiffer geosynthetic, and/or stiffer columns.

10. Develop the geosynthetic details:

a. The bottom layer of geosynthetic should be placed on a lift of compacted bridging layer material at an elevation of 6 in. above the top of the columns or pile caps.

b. Each additional layer of geosynthetic, if used, should be separated from the underlying layer of geosynthetic by a 6 in lift of compacted bridging layer material.

c. Sheets of geosynthetic reinforcement should be overlapped by at least 2 ft and the overlaps should be located above the columns.

9.5 Design Examples

Two design examples are presented in this section. The first example is for the case of a geosynthetic-reinforced embankment supported on deep-mixing method columns. The second example illustrates how to represent piles with pile caps in analysis of a pile-supported, geosynthetic-reinforced embankment.

Example One

1. The embankment will be 8 ft high with a traffic surcharge of 200 psf. The total embankment settlement is to be limited to 3 inches.

2. The subsurface conditions are shown in Figure 9.6. The material property values are obtained from field and laboratory data with an appropriate degree of conservatism. When the embankment plus surcharge load is applied to the foundation profile in Figure 9.6 without any improvement, the calculated settlement for a wide embankment is 24 in., which greatly exceeds the allowable settlement of 3 in.

3. Columns installed by the deep-mixing method are being considered for this project. A diameter, d_c, of 3 ft and a center-to-center spacing, s, of 7 ft are selected for trial. These dimensions satisfy the criteria provided above, as follows with $a = 0.886d_c = 2.66$ ft:

   a. $s - a = 4.34 \text{ ft} \leq H = 8 \text{ ft}$

   b. $s - a = 4.34 \text{ ft} \leq 8.5 \text{ ft}$

   c. $a_s = 0.144 \geq 0.1$

4. A GW sand and gravel is locally available for use in the bridging layer. The properties of the compacted sand and gravel are estimated to be as follows: $\gamma = 135$ pcf, $\varphi = 37$ degrees, $E = 700{,}000$ psf, $\upsilon = 0.3$. The bridging layer thickness was selected to be 4.5 ft, which is just greater than $s - a = 4.34$ ft.

5. An MH sandy silt is locally available for use above the bridging layer. The properties of the compacted silt are estimated to be as follows: $\gamma = 115$ pcf, $\varphi = 30$ degrees, $E = 300{,}000$ psf, $\upsilon = 0.33$. The thickness of the silt will be 3.5 ft to make up the total embankment height of 8 ft.

6. The columns are designed to be able to carry the full embankment and surcharge load within the area of a unit cell: $[(135 \text{ pcf})(4.5 \text{ ft}) + (115 \text{ pcf})(3.5 \text{ ft}) + 200 \text{ psf}](7 \text{ ft})^2 = 59{,}000$ lbs. This requires that the design value of the unconfined compressive strength, q_u, of the columns should be at least $1.5(\gamma H + q)/a_s$, which is equal to 88 psi for the conditions of this example. A

design value of q_u equal to 150 psi was selected. The value of E_{col} was estimated to be equal to $250q_u$, or 37,500 psi.

7. Two layers of geosynthetic with a combined long-term stiffness of 48,000 lb/ft and a combined allowable tensile strength of 2,000 lb/ft are selected for trial in the SRR_{net} spreadsheet, whose results are shown in Figure 9.7. It can be seen that the calculated value of SRR_{net} is 0.150. This value is used in the strain and tension spreadsheet, whose results are shown in Figure 9.7, to calculate a strain of 0.036 and a tension of 1,710 lb/ft in the geosynthetic reinforcement. Both values satisfy the design requirements.

8. The sum of the embankment compliance and the column compression is 3.0 inches from the SRR_{net} spreadsheet in Figure 9.7. This satisfies the design requirement.

9. Since the design requirements are satisfied, further iterations are not needed.

10. The bottom layer of geosynthetic should be placed on a layer of compacted bridging layer material at a level 6 inches above the top of the columns, and the second layer of geosynthetic should be placed on another 6-in.-thick compacted lift of bridging layer material.

An additional analysis of this example was performed with one change to the subsurface conditions: the upper layer of existing loose sand at the site is increased from 2.5 ft to 6 ft. The results from the SRR_{net} spreadsheet analysis are shown in Figure 9.8., where it can be seen that the SRR_{net} value decreases from 0.150 to 0.001. This shows the dramatic influence of subsurface conditions on SRR_{net} values. In the case of the thicker layer of existing sand, geosynthetic reinforcement does not make a significant contribution to load transfer in the bridging layer. In this case, the geosynthetic reinforcement can be eliminated from the design.

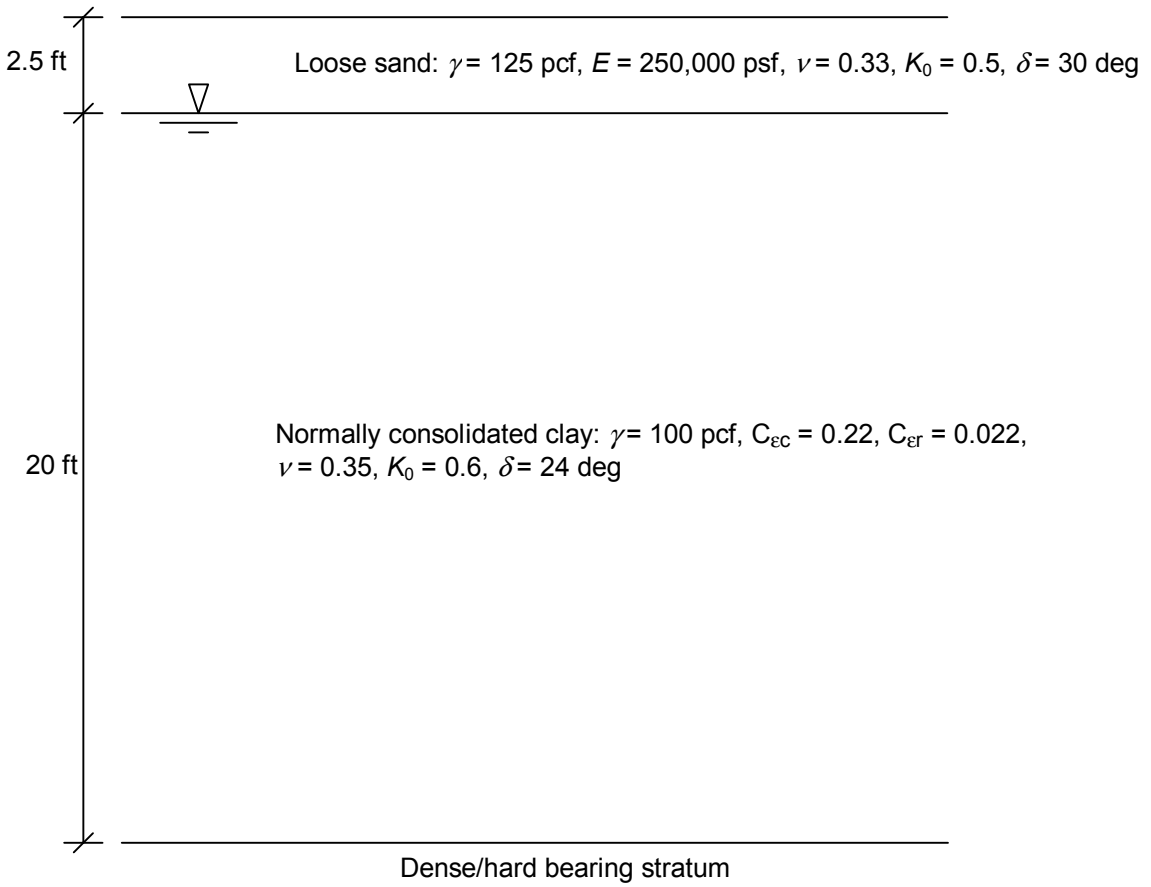

Figure 9.6. Subsurface profile for Example One.

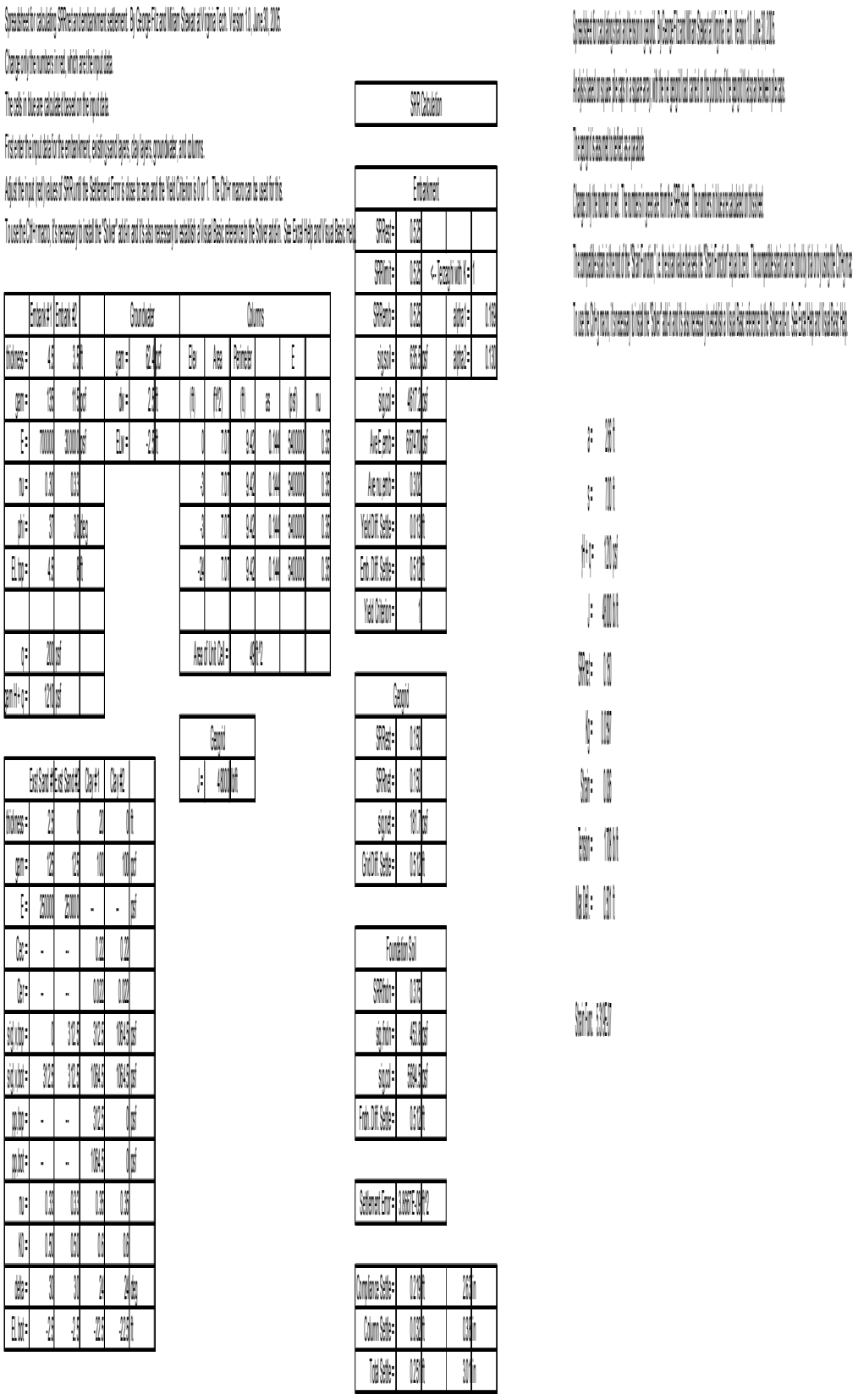

Figure 9.7. Results from spreadsheet analysis of Example One.

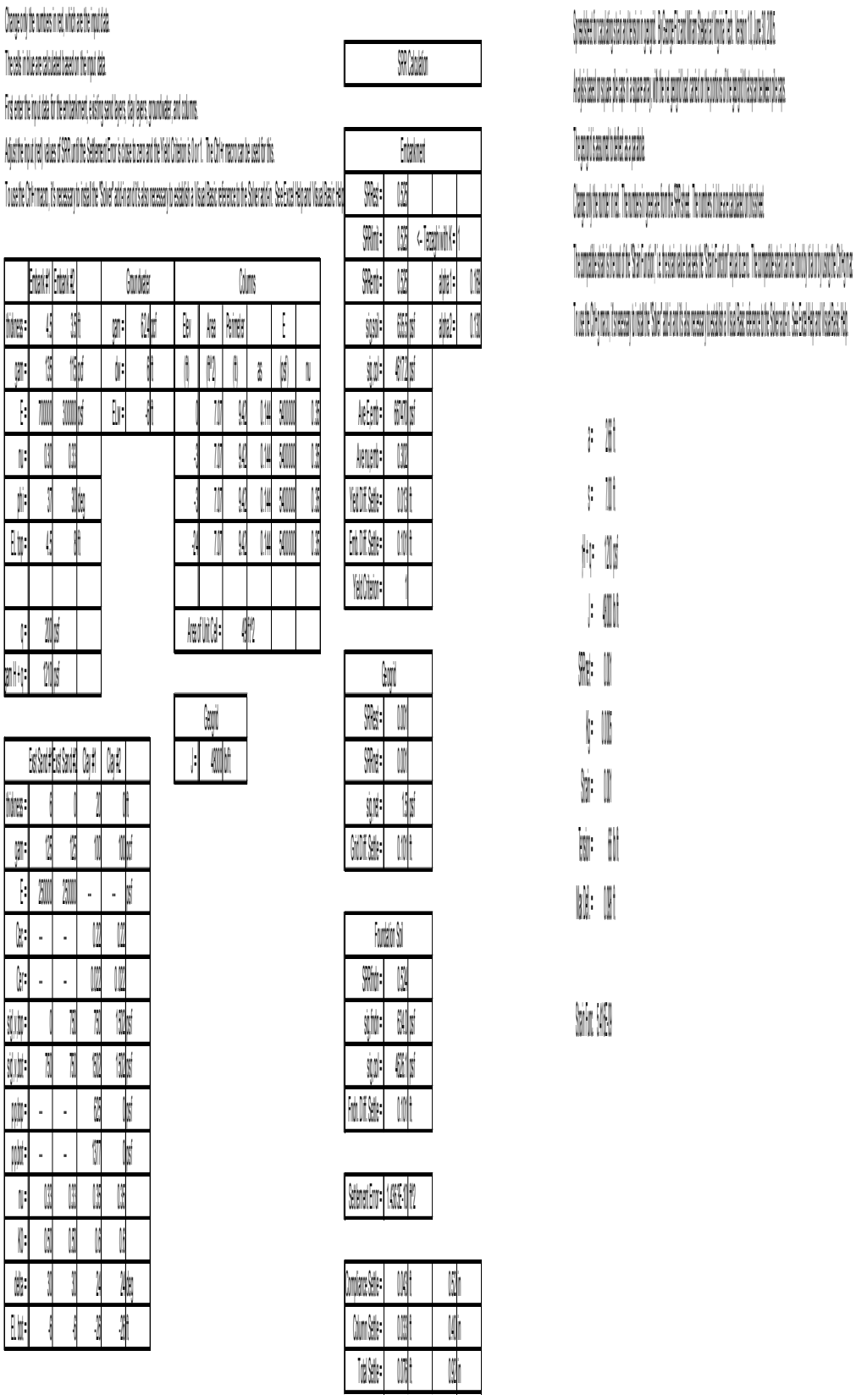

Figure 9.8. Results from spreadsheet analysis of Example One with 6-ft-thick upper sand layer.

Example Two

The following example illustrates how to represent piles with pile caps in analysis of a pile-supported, geosynthetic-reinforced embankment.

1. The embankment will be 14 ft high with a traffic surcharge of 200 psf. The total embankment settlement is to be limited to 4 inches.

2. The subsurface conditions are shown in Figure 9.9. The material property values are obtained from field and laboratory data with an appropriate degree of conservatism. When the embankment plus surcharge load is applied to the foundation profile in Figure 9.9 without any improvement, the calculated settlement for a wide embankment is 36 in., which greatly exceeds the allowable settlement of 4 in.

3. A pile cap width, a, of 4 ft and a center-to-center spacing, s, of 11 ft are selected for trial. These dimensions satisfy the criteria described above:

   a. $s - a = 7 \text{ ft} \leq H = 14 \text{ ft}$

   b. $s - a = 7 \text{ ft} \leq 8.5 \text{ ft}$

   c. $a_s = 0.132 \geq 0.1$

4. An SW sand is locally available for use in the bridging layer. The properties of the compacted sand are estimated to be as follows: $\gamma = 130$ pcf, $\varphi = 35$ degrees, $E = 600{,}000$ psf, $\upsilon = 0.3$. Because 5 ft of medium dense sand exists as the uppermost foundation soil at the site, it is judged that the bridging layer thickness can be reduced from to $s - a = 7$ ft to $H_b = 5$ ft.

5. An MH sandy silt is locally available for use above the bridging layer. The properties of the compacted silt are estimated to be as follows: $\gamma = 115$ pcf, $\varphi = 30$ degrees, $E = 300{,}000$ psf, $\upsilon = 0.33$. The thickness of the compacted silt will be 19 ft to make up the total embankment height of 14 ft.

6. The piles are designed to be able to carry the full embankment and surcharge load within the area of a unit cell: [(130 pcf)(5 ft) + (115 pcf)(9 ft) + 200 psf](11 ft)^2 = 228,000 lbs. Square, 24-in. by 24-in., prestressed concrete piles are selected.

7. Three layers of geosynthetic with a combined long-term stiffness of 72,000 lb/ft and a combined allowable tensile strength of 3,000 lb/ft are selected for trial in the SRR_{net} spreadsheet, whose results are shown in Figure 9.10. It can be seen that the calculated value of SRR_{net} is 0.071. This value is used in the strain and tension spreadsheet, whose results are shown in Figure 9.10, to calculate a strain of 0.031 and a tension of 2,215 lb/ft in the geosynthetic reinforcement. Both values satisfy the design requirements.

8. The sum of the embankment compliance and the column compression is 4.0 inches from the SRR_{net} spreadsheet in Figure 9.10. This satisfies the design requirement.

9. Since the design requirements are satisfied, further iterations are not needed.

10. The bottom layer of geosynthetic should be placed on a layer of compacted bridging layer material at a level 6 inches above the top of the columns, and the second and third layers of geosynthetic should each be placed on additional 6-in.-thick layers of compacted bridging layer material.

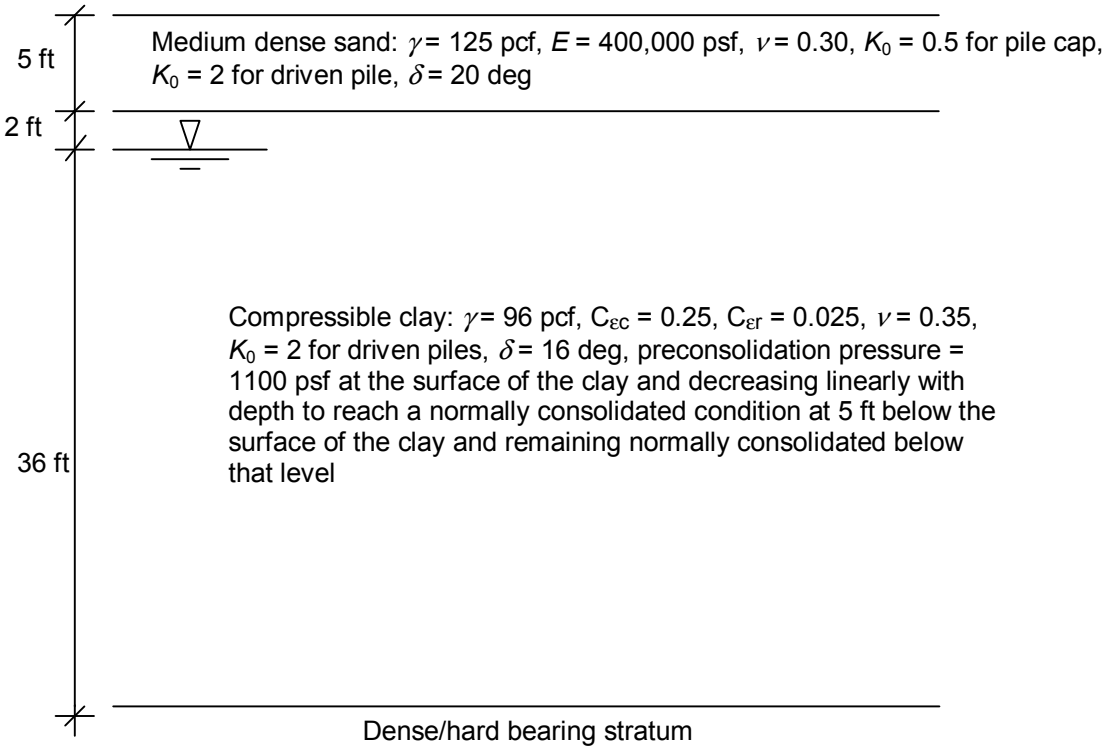

Figure 9.9. Subsurface profile for Example Two.

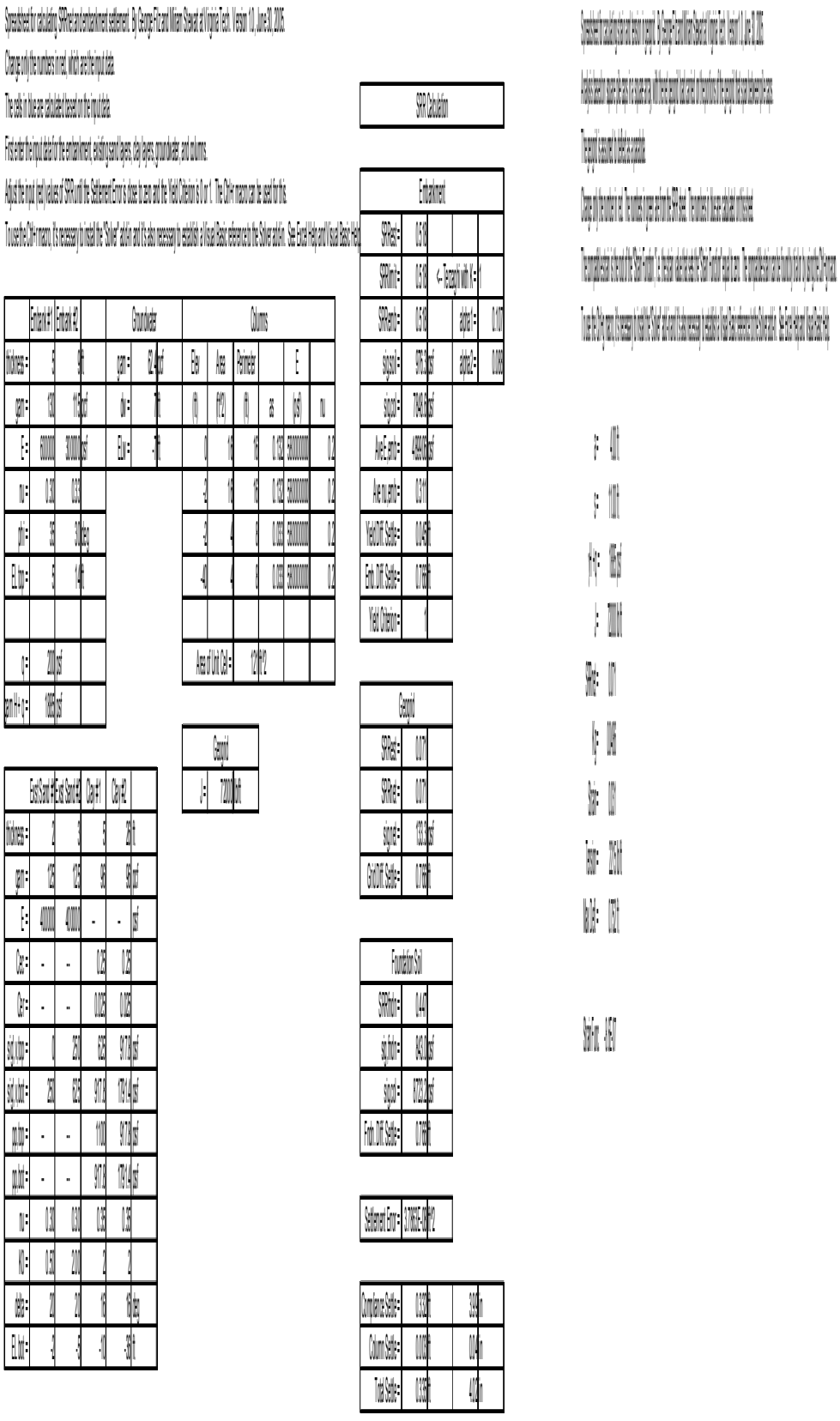

Figure 9.10. Results from spreadsheet analysis of Example Two

9.6 Closing Remarks

The chapter presents the simplified procedures that were developed for analysis and design of column-supported, geosynthetic-reinforced embankments for the control of settlement. The design procedures that were developed around the simplified computational model incorporate features of practice that have been reported in the literature for column-supported, geosynthetic-reinforced embankments. The analysis procedures were implemented in spreadsheets that permit substantial flexibility in embankment conditions, foundation conditions, and column type. The columns can be driven piles with pile caps, vibro-concrete columns, or other types of columns. The spreadsheets are easy to use, and they solve the nonlinear simultaneous equations that yield values of SRR_{net}, strain in the geosynthetic, tension in the geosynthetic, and embankment settlement.

CHAPTER 10
SUMMARY, CONCLUSIONS, AND RECOMMENDATIONS

10.1 Introduction

Column-supported geosynthetic-reinforced embankments have great potential for application in soft ground conditions when there is a need to accelerate construction and/or protect adjacent facilities from the settlement that would otherwise be induced by the new embankment load.

The columns in column-supported embankments can be driven piles, vibro-concrete columns, deep-mixing-method columns, stone columns, or any other suitable type of column. This research focused on embankments supported on lime-cement columns, soil-cement columns, and driven piles, although the results of the research are expected to be applicable to other columnar foundation systems. If driven piles are used, they are often fitted with pile caps to help transfer the embankment load to the piles. A bridging layer consisting of several feet of sand or sand and gravel is also used to help transfer the embankment load to the columns.

The cost of column-supported embankments depends, in part, on the spacing between the columns and the size of the pile caps, if used. Geosynthetic reinforcement is often employed in bridging layers to enhance load transfer to the columns and increase the spacing between columns. The number, stiffness, and strength of geosynthetic layers are selected by geotechnical design engineers based on considerations of load transfer and deformations. Several methods have been developed to calculate the load on the geosynthetic reinforcement, but the calculated loads differ by over an order of magnitude in some cases, and there is no agreement on which method is correct.

In this research, a new method was developed for calculating the load on the geosynthetic reinforcement. The new method employs one of the existing mechanistically-based approaches, and combines it with consideration of the stiffnesses of the embankment, geosynthetic, column, and subgrade soil. The new method was verified against the results of a large numerical parameter study, for which the numerical procedures themselves were verified against closed-form solutions for membranes, pilot-scale experiments, and instrumented field case histories.

This chapter presents a summary of the work accomplished, conclusions drawn from the work, recommended design procedures developed as part of the research, and recommendations for further research.

10.2 Summary of Work Accomplished

The following tasks were completed:

(a) An extensive literature review was performed to compile information on the applications and limitations, installation procedures, typical laboratory and field material properties, and current design methods of deep-mixing-method foundation systems. A literature review was also performed to compile information on load transfer mechanisms and the currently available methods for designing geosynthetic-reinforced bridging layers.

(b) Numerical modeling methods using FLAC3D (ITASCA 2002a), FLAC (ITASCA 2002b), and SAGE (Bentler et al. 1999) were verified against instrumentation data from a full-scale column-supported test embankment at the I-95/ Route 1 Interchange Project in Alexandria, Virginia. FLAC numerical modeling methods that included geosynthetic reinforcement were verified against published data from pilot-scale laboratory tests (Zaeske 2001, Kempfert et al. 2004) and closed-form solutions for membranes.

(c) Numerical parametric studies were performed to obtain a broader understanding, and to quantitatively evaluate the factors that influence load transfer to columns beneath embankments. These parametric studies were performed using the numerical modeling methods that were verified in task (b). Parametric studies were performed to evaluate the load transfer mechanisms of column-supported embankments, both with and without geosynthetic reinforcement, including variation of (1) strength and modulus of the deep-mixing-method (DMM) columns, (2) density of the embankment fill, (3) embankment height, (4) thickness of an existing upper sand layer, (5) density of a base sand layer, (6) compressibility and thickness of the soft soil, (7) column diameter and column spacing, and where geosynthetic reinforcement was included (8) geosynthetic reinforcement location, and (9) geosynthetic stiffness.

(d) Practical procedures were developed for the design of geosynthetic-reinforced column-supported embankments for load transfer and settlement control based on findings from the literature review and the results of the numerical parametric studies. The analysis procedures were implemented in spreadsheets.

10.3 Conclusions

Conclusions drawn from the literature review include the following:

(a) For embankments supported on driven piles or drilled shafts, the embankment settlement is calculated by assuming that all of the embankment load is carried by the piles or drilled shafts and using established procedures for calculating settlement of deep foundation systems. For embankments supported on deep-mixing-method columns, the settlement magnitude is determined by assuming equal strains for both the soft clay and the stiff column (Broms 1999, CDIT 2002, EuroSoilStab 2002).

(b) Russell et al. (2003) present a simple method for including the effect of compliance at the base of the embankment on overall embankment settlement. In this approach, the volume of the differential settlement depression of the soft soil between the columns is distributed across the embankment to calculate a settlement component at the embankment surface. This approach is thought to be conservative because it does not consider expansion of the embankment soil that may occur due to dilatantcy or reduction in normal stress above the foundations soil as consolidation proceeds.

(c) Several published methods for calculating the vertical loads applied by embankments and surcharges to geosynthetic reinforcement can be found in the literature. There is not widespread agreement in the literature regarding methods to calculate the vertical loads that embankments apply to geosynthetic reinforcement. However, the Adapted Terzaghi Method (Russell and Pierpoint 1997), the Hewlett and Randolph Method (1988), and the Kempfert et al. (2004) Method show the most promise because they are based on principles of mechanics and they have been verified by tests and analyses.

(d) Most methods presented in the literature for calculating geosynthetic strain and tension are very similar to the method presented in BS8006 (1995). One important exception is the method developed by Kempfert et al. (2004), which is based on a theory of an elastic embedded membrane. For the same vertical load, geometry, and geosynthetic stiffness, the Kempfert et al. (2004) method produces higher strains in the geosynthetic than does the BS8006 (1995) method. The BS8006 (1995) Method was adopted in the design procedure developed as part of this research because is has been used in practice for many years. Further measurements and analyses are warranted to determine which method best reflects performance in practice.

(e) There is some variation in recommendations in the literature regarding system details, such as limiting column spacing versus embankment height, positioning of reinforcement layers, and quality of bridging layer fill. The approaches adopted here follow the dominant usage found in the literature.

Conclusions drawn from the numerical analyses, and the analysis and design procedures include the following:

(a) The 3D drained, axisymmetric drained, and axisymmetric consolidation analyses calculated nearly identical stress distributions in the material above the column. All the calculations agreed well with the instrumentation data from a full-scale test embankment. Other numerical verification analyses demonstrated good agreement with closed form solutions for membranes, pilot-scale laboratory experiments, and other field case histories. These results indicate that axisymmetric drained analyses can be used to accurately evaluate the stresses in column-supported embankments. Although axisymmetric drained analyses can successfully calculate loads acting on geosynthetics, they cannot be expected to provide good estimates of strains and tensions in geosynthetics. Three dimensional analyses will be needed for this.

(b) The verified numerical methods were used in a parameter study that showed (1) logical increases in SRR_{net} values with increases in clear spacing between columns and increasing geosynthetic stiffness and (2) logical decreases in SRR_{net} values with

increasing stiffness and strength of the foundation and embankment soils and with increasing elevation of the geosynthetic above the top of the columns or pile caps.

(c) The numerical analyses, as well as the simplified analysis procedure, demonstrate the important impact that subgrade support has on the net vertical loads that are applied to geosynthetic reinforcement. If the subgrade support is good, geosynthetic reinforcement does not have a significant effect on system performance. If the subgrade support is poor and the clear spacing between columns or pile caps is large, it can become impossible to provide enough geosynthetic reinforcement to limit deformations to acceptable magnitudes. For intermediate conditions, geosynthetic reinforcement can enhance system performance.

(d) Simplified procedures were developed for analysis and design of column-supported, geosynthetic-reinforced embankments based on results of the literature review and the numerical analyses. The analysis procedures were implemented in spreadsheets that permit substantial flexibility in embankment conditions, foundation conditions, and column type. The columns can be driven piles with pile caps, vibro-concrete columns, or other types of columns. The spreadsheets are easy to use, and they solve the nonlinear simultaneous equations that yield values of SRR_{net}, strain in the geosynthetic, tension in the geosynthetic, and embankment settlement.

(e) The design procedures that were developed around the simplified computational model incorporate features of practice that have been reported in the literature for column-supported, geosynthetic-reinforced embankments. They included use of the BS8006 Method to calculate geosynthetic strains and tensions.

10.4 Recommendations for Further Research

It is recommended that further improvements in the state of practice be achieved by completing research on the following topics:

- An improved method should be developed to relate embankment compliance at subgrade level to total and differential settlement of the embankment surface.
- Three-dimensional numerical analyses should be performed to investigate strain and tension in the geosynthetic reinforcement.
- Reliability analyses should be performed to evaluate the effects of variability in the parameter values that influence the load transfer and settlement performance of these systems.

REFERENCES

Ahnberg, H. (1996a) Stress dependent parameters of cement and lime stabilised soils. *Grouting and Deep Mixing, Proceedings of IS-Tokyo 96, 2nd International Conference on Ground Improvement Geosystems,* May, Tokyo: 387-92.

Ahnberg, H. (1996b) Stress dependent parameters of cement stabilised soil. *Grouting and Deep Mixing, Proceedings of IS-Tokyo 96, 2nd International Conference on Ground Improvement Geosystems,* 387-92.

Bachus, R. C. and Barksdale, R. D. (1989) Design methodology for foundations on stone columns. *Foundation Engineering: Current Principles and Practices, ASCE GP 22*: 244-57.

Baker, S. (2000) "Deformation Behaviour of Lime/Cement Column Stabilized Clay." *Swedish Deep Stabilization Research Centre, Rapport 7*, Chalmers University of Technology.

Balaam, N. P. and Booker, J. R. (1981) Analysis of rigid rafts supported by granular piles. *International Journal for Numerical and Analytical Methods in Geomechanics,* 5: 379-403.

Balaam, N. P. and Booker, J. R. (1985) Effect of stone columns yield on settlement of rigid foundations in stabilized clay. *International Journal for Numerical and Analytical Methods in Geomechanics,* 9, no. 4: 331-51.

Balaam, N. P., Brown, P. T. and Poulos, H. G. (1977) Settlement analysis of soft clays reinforced with granular piles. *Proceedings of the 5th Southeast Conference on Soil Engineering,* 81-92.

Balaam, N. P. and Poulos, H. G. (1983) The behavior of foundations supported by clay stabilized by stone columns. *Proceedings, 8th European Conference on Soil Mechanics and Foundation Engineering,* 199-204.

Barksdale, R. D. and Bachus R. C. (1983) Design and Construction of Stone Columns, Vol. 1. *Federal Highway Administration, RD-83/026.*

Barksdale, R. D. and Goughnour, R. R. (1984) Settlement performance of stone columns in the U.S. *International Conference In-Situ Soil and Rock Reinforcement,* 105-10.

Bell, A. L., Jenner, C., Maddison, J.D., and Vignoles, J. (1994) Embankment support using geogrids with vibro concrete columns. *Proceedings, 5th International Conference on Geotextiles, Geomembranes, and Related Products,* 335-38.

Bentler, D.J., Morrison, C.S., Esterhuizen, J.J.B., and Duncan, J.M. (1999) SAGE User's Guide: A Finite Element Program for Static Analysis of Geotechnical Engineering Programs, *Center for Geotechnical Practice and Research*, Virginia Tech.

Bergado, D. T., Ruenkrairergsa, T., Taesiri, Y., and Balasubramaniam, A.S. (1999) Deep soil

mixing used to reduce embankment settlement. *Ground Improvement* 3: 145-62.

Bowles, J.E. (1996) *Foundation Analysis and Design*, 5th ed. McGraw-Hill, New York.

Broms, B. B. (1991) Stabilization of soil with lime columns. *Foundation Engineering Handbook* Chapter 24: 833-55.

Broms, B. B. (1999) Keynote Lecture: Design of lime, lime/cement and cement columns. *International Conference on Dry Mix Methods: Dry Mix Methods for Deep Soil Stabilization*, Rotterdam Balkema, 125-53.

Broms, B. B. (2003) *Deep soil stabilization: design and construction of lime and lime/cement columns*, Royal Institute of Technology, Stockholm, Sweden.

Broms, B. B., and Boman, P. (1979) Stabilization of soil with lime columns. *Ground Engineering* 12, no. 4: 23-32.

Bruce, D. A. (2000) "DRAFT: An Introduction to the Deep Mixing Methods as used in geotechnical applications." *Federal Highways Administration, FHWA-RD-99-138*.

Bruce, D. A., Bruce, M. E. C., and DiMillio, A. F.. (1999) Dry mix methods: a brief overview of international practice. *International Conference on Dry Mix Methods: Dry Mix Methods for Deep Soil Stabilization*, Rotterdam Balkema,15-25.

BS8006. (1995) *British Standard, Code of practice for: Strengthened/reinforced soils and other fills*.

Burke, G. (2002) Soil mixing for support of structures. *Presentation: Center for Geotechnical Practice and Research, Annual Lecture Program*, Virginia Tech.

Burke, G. (2003) Personal correspondence. Vice President –Engineering, Hayward Baker, Inc., August 1, 2003.

Burke, G. K., Brengola, A. F., and Triplett, R. E.. (2001) Soil mixing: A new approach to soft soil stabilization for structural support. *Foundations and Ground Improvement, Proceedings of Specialty Conference*, ASCE Geotechnical Special Publication No. 113, 190-203.

Card, G. B and Carter, G. R. (1995) Case history of a piled embankment in London's Docklands. *Engineering Geology of Construction* Geological Society Engineering Geology Special Publication No. 10: 79-84.

Carlsten, P. and Ekstrom, J. (1997) Lime and lime cement columns, guide for project planning, construction and inspection. *Swedish Geotechnical Society, SGF Report 4:95 E*.

CDIT (Coastal Development Institute of Technology). (2002) *The Deep Mixing Method: Principle, Design and Construction*. A.A. Balkema: The Netherlands.

CDM (Cement Deep Mixing. (1985). *Design and Construction Manual for CDM Institute, Partial English Translation*.

Charles, J. A. and Watts, K. S. (1983) Compressibility of soft clay reinforced with granular columns. *Proceedings of the 8th European Conference on Soil Mechanics and Foundation Engineering,* 347-52.

Collin, J. G. (2004) Column supported embankment design considerations. *Proceedings of the 52nd Annual Geotechnical Engineering Conference*, J.F. Labuz and J.G. Bentler (eds.), 51-78.

D'Appolonia, D.J., D'Appolonia, E., and Bisette, R.F. (1970) "Settlement of Spread Footings on Sand," *JSMFD*, ASCE, 96(2), 754-761.

Datye, K. R. (1982) Settlement and bearing capacity of foundation system with stone columns. *Symposium on Soil & Rock Improvement Techniques Including Geotextiles, Reinforced Earth and Modern Piling Methods, Southeast Asian Goetechnical Society (SEAGS)*.

DiMaggio, J. A. (1978) Stone Columns for Highway Construction. *Demonstration Report No. 46, Department of Transportation, Federal Highway Administration.*

Dong, J., Hiroi, K.,and Nakamura, K.. (1996) Experimental study on behavior of composite ground improved by deep mixing method under lateral load. *Grouting and Deep Mixing, Proceedings of IS-Tokyo 96, 2nd International Conference on Ground Improvement Geosystems*Tokyo: 585-90.

Duncan et al. (1989) Shear Strength Correlations for Geotechnical Engineering. Report, Virginia Tech, Department of Civil Engineering, Geotechnical Engineering.

Ekström, J. C., Berntsson, J. A., and Salfors, G. B. (1994) Test fills of clays stabilized with cement columns. *Proceedings, 13th International Conference on Soil Mechanics and Foundation Engineering,* 1183-86.

Elias, V., Welsh, J., Warren, J., and R. Lukas. (1999) *Ground Improvement Technical Summaries, Volume II, Demonstration Project 116*, Federal Highway Administration, FHWA-SA-98-086.

Esrig, M. I., and MacKenna, P.E. (1999) Lime cement column ground stabilization for I-15 in Salt Lake City. *34th Annual Symposium on Engineering Geology and Geotechnical Engineering*.

EuroSoilStab (2002) Development of design and construction methods to stabilise soft organic soils. *Design Guide Soft Soil Stabilization, CT97-0351* Project No.: BE 96-3177.

Fang, Y. S., Chung, Y. T., Yu, F. J., and Chen, T. J. (2001) Properties of soil-cement stabilised with deep mixing method. *Ground Improvement* 5, no. 2: 69-74.

Forte, E. (2002) Underpinning and Foundation Constructors, Inc. *Personal Conversation*.

Guido, V. A., Knueppel, J. D., and Sweeny, M. A. (1987) Plate loading tests on geogrid-reinforced earth slabs. *Geosynthetic '87 Conference* New Orleans: 216-25.

Geotechnical Fabrics Report (2002) 2003 Specifier's Guide, *GFR Engineering Solutions*, 20, no. 9.

Greenwood, D. A. (1991) Load tests on stone columns. *Deep Foundation Improvements: Design, Construction, and Testing, ASTM STP 1089*, eds. Esrig and Bachus, ASTM Philadelphia: 148-71.

Habib, H. A. A., Brugman, M. H. A., and Uijting, BG. J. (2002) Widening of Road N247 founded on a geogrid reinforced mattress on piles. *Proceedings, Geosynthetics - 7th ICG*, Delmas, Gourc, & Girard (eds), Lisse: Swets & Zeitlinger, 369-72.

Haley & Aldrich and Virginia Geotechnical Services, P.C. (2000) *Final Data Report on Ground Improvement for Embankment Construction*, I-95/Route 1 Interchange, VDOT Project No. 0095-96A-106, PE-101.

Han, J., and Gabr, M. A. (2002) Numerical analysis of geosynthetic-reinforced and pile-supported earth platforms over soft soil. *Journal of Geotechnical and Geoenvironmental Engineering* 128, no. 1: 44-53.

Han, J., Huang, J., and Porbaha, A.. (2005) 2D numerical modeling of a constructed geosynthetic-reinforced embankment over deep mixed columns. *Geo-Frontiers 2005*, ASCE.

Han, J., and Wayne, M. H. (2000) Pile-soil-geosynthetic interactions in geosynthetic reinforced platform/piled embankments over soft soil. *Paper No. 000777, Presentation at 79th Annual Transportation Research Board Meeting,* Washington D.C.

Han, J. and Gabr, M. A. (2002) Numerical Analysis of Geosynthetic-Reinforced and Pile-Supported Earth Platforms over Soft Soil. *Journal of Geotechnical and Geoenvironmental Engineering,* 128, no. 1: 44-53.

Han, J. and Ye, S. L. (2001) Simplified method for consolidation rate of stone column reinforced foundations. *Journal of Geotechnical and Geoenvironmental Engineering* 127, no. 7: 597-603.

Hayashi, H., Nishikawa, J., Ohishi, K., and Terashi, M. (2003) Field observation of long-term strength of cement treated soil. *Grouting and Ground Treatment, Proceedings of the 3rd International Conference*, ASCE Special Publication No. 120, New Orleans: 598-609.

Hebib, S., and Farrell, E. R. (2002) Deep soil mixing for organic soils. *The Engineers Journal* March: 25-29.

Hebib, S. and Farrell, R. (2000) Laboratory determination of deformation and stiffness parameters of stabilized peat. *Proceedings of the ASCE Geo-Institute Soft Ground Technology Conference, ASCE Specialty Publication No. 112,* 182-93.

Hewlett, W. J. and Randolph, M. F. (1988) Analysis of piled embankments. *Ground Engineering* 21, no. 3: 12-18.

Holm, G. (1999) Keynote lecture: Applications of dry mix methods for deep soil stabilization. *International Conference on Dry Mix Methods: Dry Mix Methods for Deep Soil Stabilization*Balkema, Rotterdam: 3-13.

Horgan, G. J., and Sarsby, R. W. (2002) The arching effect of soils over voids and piles incorporating geosynthetic reinforcement. *Proceedings, Geosynthetics - 7th ICG*, Delmas, Gourc & Girard (eds), Lisse: Swets & Zetilinger, 373-78.

Huat, B. B. K., Craig, W. H. and Ali, P. (1994) The Mechanics of Piled Embankment. *Proceedings, International Conference on Design and Construction of Deep Foundations,* 1069-82.

ITASCA Consulting Group. (2002a) *FLAC3D Fast Lagrangian Analysis of Continua in 3 Dimensions*, ITASCA Consulting Group, Minnesota, Minn., USA.

ITASCA Consulting Group. (2002b) *FLAC Fast Lagrangian Analysis of Continua*, ITASCA Consulting Group, Minnesota, Minn., USA.

Jacobson, J. R., Filz, G. M. and Mitchell, J. K. (2003) *Factors Affecting Strength Gain in Lime-Cement Columns and Development of a Laboratory Testing Procedure*, Report prepared for the Virginia Transportation Research Council, Virginia Polytechnic Institute and State University.

Japanese Geotechnical Society. (2000) "Standard practice for making and curing stabilized soil specimens without compaction (JGS 0821-2000)." *Geotechnical Test Procedure and Commentary*, Chapter 7 (in Japanese).

Jenner, C. G., Austin, R. A., and Buckland, D. (1998) Embankment support over piles using geogrids. *Proceedings of 6th International Conference on Geosynthetics* Vol. 1: 763-66.

John, N. W. M. (1987) *Geotextiles*. Glasgow and London: Blackie & Son Ltd.

Jones, C. J. F. P., Lawson, C. R., and Ayres, D. J. (1990) Geotextile reinforced piled embankments. *Proceedings, 5th International Conference on Geotextiles, Geomembranes, and Related Products,* 155-60.

Juran, I., Ider, H.M., Acar, Y.B. and Guermazi, A. (1989) "A comparative study of soil improvement reinforcement techniques for highway embankments." *Research Report*, Louisiana State University, Dept. of Civil Engineering, Baton Rouge, Louisiana Transportation Center.

Kaiqiu, L. (2000) Behaviour of DCM Columns under Highway Embankment at Bridge Approaches. *Thesis for the Degree of Doctor of Philosophy, Nanyang Technical University*.

Kawasaki, T. Niina A. Saitoh S. Suzuki Y. and Honjyo Y. (1981) Deep Mixing Method Using Cement Hardening Agent. *Proceedings of the 10th International Conference on Soil Mechanics and Foundation Engineering*Stockholm: 721-24.

Kempfert, H.-G., Gobel, C., Alexiew, D.,and Heitz, C. (2004) German recommendations for reinforced embankments on pile-similar elements. *EuroGeo3 - Thrid European Geosynthetics Conference, Geotechnical Engineering with Geosynthetics,* 279-84.

Kempfert, H.-G., Stadel, M. , and Zaeske, D. (1997) Design of geosynthetic-reinforced bearing layers over piles. *Bautechnik 74* Heft 12: 818-25.

Kempton, G., and Naughton, P. (2002) Piled embankments with basal reinforcement: development of design methods and state of the art. *Proceedings of the XV Italian Conference on Geosynthetics*.

Kempton, G., Russell D., Pierpoint, N. D., and Jones, C. J. F. P. (1998) Two- and Three-Dimensional Numerical Analysis of the Performance of Piled Embankments. *Proceedings, 6th International Conference on Geosynthetics*: 767-72.

Kivelo, M. (1997) Undrained shear strength of lime/cement columns. *Proceedings, 14th International Conference on Soil Mechanics and Foundation Engineering,* 1173-80.

Kivelo, M. (1998) "Stabilization of embankments on soft soil with lime/cement columns." Doctoral Thesis, Royal Institute of Technology.

Koerner, R.M. (1998) *Designing with Geosynthetics*. New Jersey: Prentice-Hall, Inc.

Lambrechts, J. R., Ganse, M. A., and Layhee, C. A. (2003) Soil mixing to stabilize organic clay for I-95 widening, Alexandria, VA. *Grouting and Ground Treatment, Proceedings of the 3rd International Conference*, ASCE Geotechnical Special Publication No. 120, New Orleans: 575-85.

Lambrechts, J. R., and Layhee, C. A. (2003) Stability analyses of deep soil mix buttresses in organic clay for I-95 widening, Alexandria, VA. *Proceedings 12th Panamerican Conference on Soil Mechanics and Geotechnical Engineering*, Verlag GluckaufEssen, Germany: 2097-104.

Lambrechts, J. R., Roy, P. A. and Wishart, E. (1998) Design conditions and analysis methods for soil-cement in Fort Point Channel. *Design and Construction of Earth Retaining Structures, Proceedings of Sessions of Geo-Congress '98*, ASCE Geotechnical Special Publication No. 83, Reston, Virginia: 153-74.

Lawson, C. R. (1992) Soil reinforcement with geosynthetics. *Applied Ground Improvement Techniques, Southeast Asian Geotechnical Society (SEAGS)*: 55-74.

Lin, K. Q., and Wong, I. H. (1999) Use of deep cement mixing to reduce settlements at bridge approaches. *Journal of Geotechnical and Geoenvironmental Engineering* 125, no. 4: 309-20.

Love, J. and Milligan, G. (2003) Design methods for basally reinforced pile-supported embankments over soft ground. *Ground Engineering,* March: 39-43.

Low, B. K., Tang, S. K., and Choa, V. (1994) Arching in piled embankments. *Journal of Geotechnical Engineering,* 120, no. 11: 1917-38.

McGregor, J.A. and Duncan, J.M. (1998) Performance and Use of the Standard Penetration Test in Geotechnical Engineering Practice, Center for Geotechnical Practice and Research, Virginia Tech, Blacksburg, 134 p.

Mitchell, J. K. (1981) Soil Improvement - State of the Art Report. *Proceedings of the 10th International Conference on Soil Mechanics and Foundation Engineering,* 509-65.

Mitchell, J.K., and Gardner, W.S. (1975) "In-Situ Measurement of Volume Change Characteristics, State of the Art Report," *Proc. In-Situ Measurement of Soil Properties Conference*, ASCE, 279-345.

Maswoswe, J. G. (2001) QA/QC for CA/T Deep Soil-Cement. *Foundations and Ground Improvement, Proceedings of Specialty Conference*, ASCE Geotechnical Special Publication No. 113610-624.

McGinn, A. J. and O'Rourke, T. D. (2003) "Performance of Deep Mixing Methods at Fort Point Channel." *Report to Massachusetts Turnpike Authority, Federal Highway Administration, and Bechtel/Parsons Brinckerhoff*, Cornell University.

Munfakh, G. A. (1997) Ground improvement engineering - the state of the US practice: part 2. Applications. *Ground Improvement* 1: 215-22.

Naughton, P. J. and Kempton, G. T. (2005) Comparison of analytical and numerical analysis design methods for piled embankments. *GeoFontiers 2005*.

NAVFAC (1986) Soil Mechanics. *Design Manual 7.01, Naval Facilities Engineering Command*.

Navin, M. P. and Filz, G. M. (2005) Statistical Analysis of Strength Data from Ground Improved with DMM Columns. *Proceedings of the International Conference on Deep Mixing*, Stockholm.

Ooi, T. A., Chan, S. F., and Wong, S. N. (1987) Design, Construction, and Performance of Pile Supported Embankments. *9th Southeast Asian Geotechnical Conference*: 2-1 to 2-12.

Poorooshasb, H. B. and Meyerhof, G. G. (1997) Analysis of Behavior of Stone Columns and Lime Columns. *Computers and Geotechnics* 20, no. 1: 47-70.

Porbaha, A. (2000). State of the art in deep mixing technology, Part IV. Design considerations. *Ground Improvement* 3: 111-25.

Poulos, H.G. (2002) "Simplified Design Procedure for Piled Soil Raft Foundations," *Deep Foundations 2002*, ASCE, Reston, Virginia, 441-458.

Poulos, H. GC and Davis, E. H. (1974) *Elastic Solutions for Soil and Rock Mechanics*, Wiley, New York.

Priebe, H. J. (1993) Design Criteria for Ground Improvement by Stone Columns. *Proceedings of the Fourth National Conference on Ground Improvement*.

Priebe, H. J. (1995). The design of vibro replacement. *Ground Engineering,* 28, no. 10: 31-37.

Reid, W. M. and Buchanan, N. W. (1984) Bridge approach support piling. *Piling and Ground Treatment,* Thomas Telford, London: 267-74.

Rogbeck, Y., Gustavsson, S., Sodergren, I., and Lindquist, D. (1998) Reinforced Piled Embankments in Sweden - Design Aspects. *Proceedings, Sixth International Conference on Geosynthetics*: 755-62.

Ruin, M. (2002) Scandinavian practice in deep mixing methods. *Presentation, Workshop on Geotechnical Composite Systems,* Roanoke, Virginia.

Russell, D., Naughton, P. J., and Kempton G. (2003) A new design procedure for piled embankments. *Proceedings of the 56th Canadian Geotechnical Conference and the NAGS Conference,* 858-65.

Russell, D. and Pierpoint, N. (1997) An assessment of design methods for piled embankments. *Ground Engineering* 30, no. 11: 39-44.

Saye, S. R., Esrig, M. I., Williams, J. L., Pilz, J., and Bartlett, S. F. (2001) Lime cement columns for the reconstruction of Interstate 15 in Salt Lake City, Utah. *Foundations and Ground Improvement, Proceedings of Specialty Conference, ASCE GSP No. 113,* 827-41.

Schaefer, V. R. ed. (1997) Soil improvement and geosynthetics. *Ground Improvement, Ground Reinforcement, Ground Treatment, Developments 1987-1997*, ASCE Geotechnical Special Publication No. 69, The Geo-Institute of the American Society of Civil Engineers.

Shiells, D. P., Pelnik III, T. W., and Filz, G. M. (2003) Deep Mixing: An Owner's Perspective. *Grouting and Ground Treatment, Proceedings of the 3rd International Conference*, ASCE Special Publication No. 120, New Orleans: 489-500.

Stewart, M. E., Navin, M. P., and Filz, G. M. (2004) Analysis of a column-supported test embankment at th eI-95/Route 1 interchange. *Proceedings of Geo-Trans 2004, Geotechnical Engineering for Transportation Projects,* ASCE, 1337-46.

Stewart, M. E. and Filz, G.M. (2005) Factors affecting load transfer to deep mixing columns from embankments without geosynthetic reinforcement. *Proceedings of the International Conference on Deep Mixing*, Stockholm.

Takenaka, D., and Takenaka, K. (1995) "Deep chemical mixing method - using cement as hardening agent." Takenaka Corporation, Tokyo.

Tatsuoka, F. and Kobayashi, A. (1983) Triaxial strength characteristics of cement-treated soft clay. *Proceedings of the 8th European Conference of SMFE,* 421-26.

Terashi, M. (2003) The state of practice in deep mixing methods. *Grouting and Ground Treatment, Proceedings of the 3rd International Conference*, ASCE Geotechnical Special Publication No. 120, New Orleans: 25-49.

Terzaghi, K. (1943) *Theoretical Soil Mechanics*. New York: John Wiley and Sons, Inc.

Terzaghi, K. and Peck, R. (1967) *Soil Mechanics in Engineering Practice.* New York: John Wiley and Sons, Inc.

Terzaghi, K., Peck, R.B., and Mesri, G. (1996) *Soil Mechanics in Engineering Practice*. John Wiley & Sons, Inc.

Tomlinson, M.J. (1977) *Pile design and construction practice*, London: Cement and Concrete Association.

Van Impe, W. F., Madhav, M. R. and Vandercruyssen, J. P. (1997) Considerations in stone column design. *Ground Improvement Geosystems, Densification and Reinforcement*, 190-196.

VDOT, Virginia Department of Transportation. (2001a) Special Provision for SOIL-CEMENT COLUMNS INSTALLED BY WET MIXING METHODS. *0095-96A-106, C-503*.

VDOT, Virginia Department of Transportation. (2001b) *Data Report for Deep Mixing Methods Test Embankment for I-95/Route 1 Interchange Reconstruction, Alexandria, Virginia*.

Yang, D. S., Scheibel, L. L., Lobedan, F., and Nagata, C. (2001) Oakland Airport Roadway Project. *Soil Mixing Specialty Seminar, 26th DFI Annual Conference*.

Zaeske, D. (2001) "Zur Wirkungsweise von unbewehrten und bewehrten mineralischen Tragschichten über pfahlartigen Gründungselementen." Schriftenreihe Geotechnik, Universität Gh-Kassel, Heft 10.

APPENDIX A
MEMBRANE (GEOSYNTHETIC) VERIFICATION STUDIES

A.1 Introduction

Several verification studies were performed to evaluate the modeling of membrane behavior in the explicit finite difference programs FLAC3D (Fast Lagrangian Analysis of Continua in 3 Dimensions) computer program (ITASCA 2002a) and FLAC (Fast Lagrangian Analysis of Continua) (ITASCA 2002b). The FLAC3D program contains a geogrid structural shell element; however, this element does not capture the out-of-plane behavior of a membrane subjected to normal loads, such as those installed in geosynthetic reinforced column-supported embankments. Membranes may be represented in the two-dimensional program FLAC through the use of beam or cable structural elements. However, these structural elements can not be used in axisymmetric models. As a result, verification studies were performed using FLAC3D and FLAC to investigate the use of a linear-elastic grid of zones to model membrane behavior. These analyses are described in this Appendix.

A.2 Membrane Behavior in FLAC3D

There are five finite-element shell structural elements available in FLAC3D (ITASCA 2002a): (1) CST Plane Stress Element, (2) CST Hybrid Plane Stress Element, (3) DKT Plate Bending Element, (4) DKT-CST Hybrid Shell Element, and (5) DKT-CST Shell Element. Each of the shell elements behaves as an isotropic or orthotropic, linearly elastic material with no failure limit. A geogrid structural shell element is provided in FLAC3D. By default, the geogrid structural elements are assigned the CST plane stress element. The geogrid structural element does not resist bending, and a shear-directed (in the tangent plane to the geogrid surface) frictional interaction occurs between the geogrid and the FLAC3D grid. The geogrid structural element in FLAC3D is intended to model flexible membranes whose shear interaction with the soil are important (ITASCA 2002a). Since the geogrid structural element does not resist out-of-pane deformations, it is not appropriate for use in cases in which the geogrid must deform in response to loading conditions normal to the geogrid (i.e. embankment loading).

In order to model the membrane response to out-of-plane loading conditions, a linear elastic material model was used in FLAC3D to represent the geosynthetic reinforcement. The goal of

the FLAC3D verification studies was to verify that the grid of linear elastic material responded as a membrane to out-of-plane loading conditions.

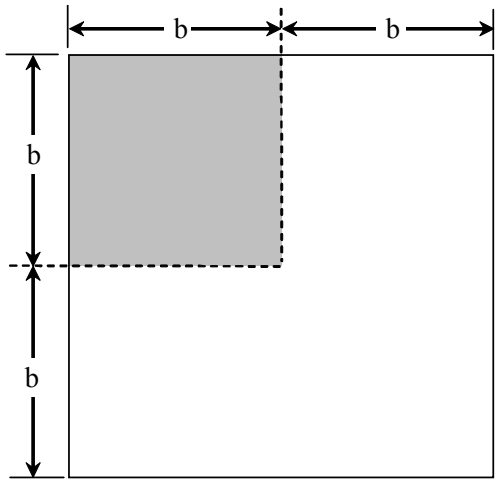

Figure A.1. FLAC 3D membrane geometry

The verification studies considered a three-dimensional square grid of linear elastic material, and based on lines of symmetry, a quarter of each square was evaluated, as shown in Figure A.1. Two of the edges were pinned, and where more than one vertical (out-of-plane) layer of mesh zones was used, the model was pinned mid-height. The remaining two edges were allowed to deflect vertically but not laterally, and the maximum deflections were measured at the center of the square. The linear elastic material was assigned an elastic modulus and Poisson's ratio. The stiffness, J, of the membrane, or geosynthetic, was represented by the product of the elastic modulus, E, and the thickness, t. The philosophy behind the use of a grid of linear elastic material is that the product of the modulus of the linear elastic material and the thickness of the grid is equal to the stiffness of the geosynthetic reinforcement. For example, a geosynthetic with a stiffness $J = E \cdot t = 8417$ lbs/in. could be modeled using a grid of linear elastic material with an elastic modulus of 16,834 psi and grid thickness of 0.5 in.

An analytical closed-form solution provided by Ugural (1999) was used to verify the results of the FLAC3D numerical analyses. The following closed-form solution calculates the deflection

at the center of a square membrane with a Poisson's ratio of 0.25 pinned along its four edges subjected to vertical loading (Ugural 1999):

$$w_{max} = 0.818 \cdot \sqrt[3]{\frac{p \cdot b}{E \cdot t}} \tag{A.1}$$

where w_{max} = the maximum deflection of the membrane that occurs at the center of the membrane, p = applied uniform vertical load, b = ½ of the square membrane width, E = membrane elastic modulus, and t = membrane thickness.

The first step was to evaluate the required thickness and refinement of the linear elastic mesh. A uniform vertical load, p, of 5 psi was applied to a square grid of linear elastic material with a dimension, b, of 18 in. and a stiffness E·t = 832 lb/in. The model thickness and the number of vertical layers, or zones, were varied. As the model thickness varied, the elastic modulus was varied accordingly to maintain a constant value of E·t. The results of the FLAC3D numerical analyses were normalized by the deflection determined using the closed-form solution given in Equation A.1. This work was performed by Dr. Meeok Kim and the results are summarized in Table A.1.

Table A.1. Required thickness and refinement of 3D geosynthetic mesh

	Normalized Deflection for Various Aspect Ratios of Mesh Zones [(a)]			
	Two layers			**One layer**
Model thickness (in.)	**4:4:1**	**2:2:1**	**1:1:1**	**2:2:1**
2	0.962	1.074	1.075	1.275
1	0.984	1.022	1.025	1.160
0.5	0.989	1.002	1.004	1.078
0.25	0.992	0.993	-	1.032

[(a)] Aspect ratios of the mesh zones are expressed in terms of H:H:V, so that 2:2:1 for a mesh zone that is 0.5 in. vertically is 1 in. by 1 in. in plan.

Based on the results summarized in Table A.1, this exercise indicated that:

(1) the grid of the linear elastic material should be divided into at least two layers,

(2) the layers should be relatively thin, such that the ratio of geosynthetic grid thickness to width, t/b, is on the order of 1/18, and

(3) the aspect ratio of the mesh zones should be 2:2:1 (H:H:V) or less.

The second step was to evaluate the effects of the elastic modulus and the mesh refinement on membrane deflections. For five different values of E·t, the thickness of the linear elastic grid was changed while keeping E·t constant. The grid thicknesses and the corresponding elastic modulus are summarized for each case in Table A.2. The values of p and b were 5 psi and 18 in., respectively, and the deflection determined from the closed-form solution is also given for each case in Table A.2.

Table A.2. Modulus and refinement of 3D geosynthetic mesh

	t = 0.5 in.[A]	**t = 1 in.**[B]	**t = 2 in.**[C]	**Closed-form Solution (in.)**
Et (lb/in.)	**E (psi)**	**E (psi)**	**E (psi)**	
8417	16834	8417	4210	3.24
13468	26936	13468	6734	2.77
16835	33670	16835	8418	2.57
20202	40404	20202	10101	2.43
30303	60606	30303	15152	2.12

[A] model consisted of one layer
[B] model consisted of two layers
[C] model consisted of four layers

For this exercise, mesh refinement was also investigated. Plots of normalized deflection versus mesh refinement are shown in Figures A.2 through A.4.

Based on the results shown in Figures A.2 through A.4, this exercise indicated that:

(1) for a wide range of values of E·t, the normalized deflections follow similar patterns,

(2) the grid thickness should be kept relatively thin, and

(3) the aspect ratio should be 2:2:1 or less.

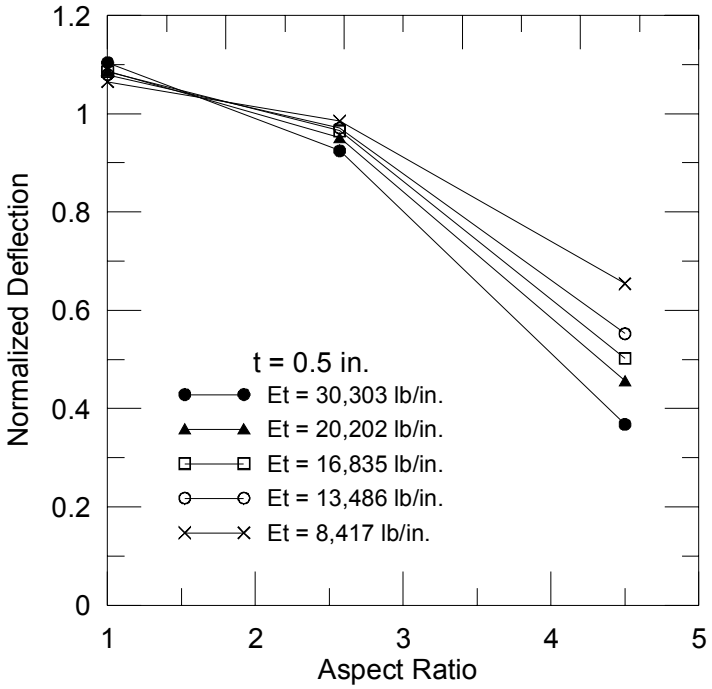

Figure A.2. FLAC3D: Aspect Ratio vs. Normalized Deflection (t = 0.5 in.)

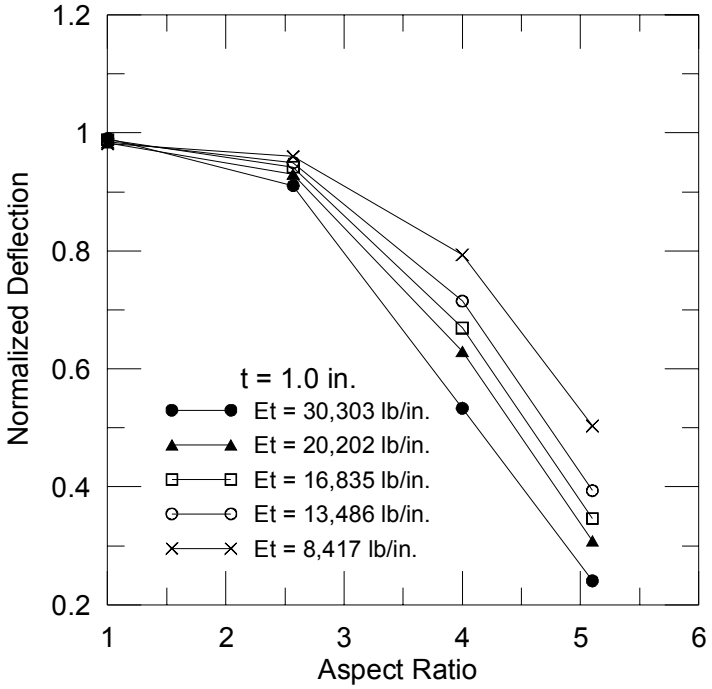

Figure A.3. FLAC3D: Aspect Ratio vs. Normalized Deflection (t = 1.0 in.)

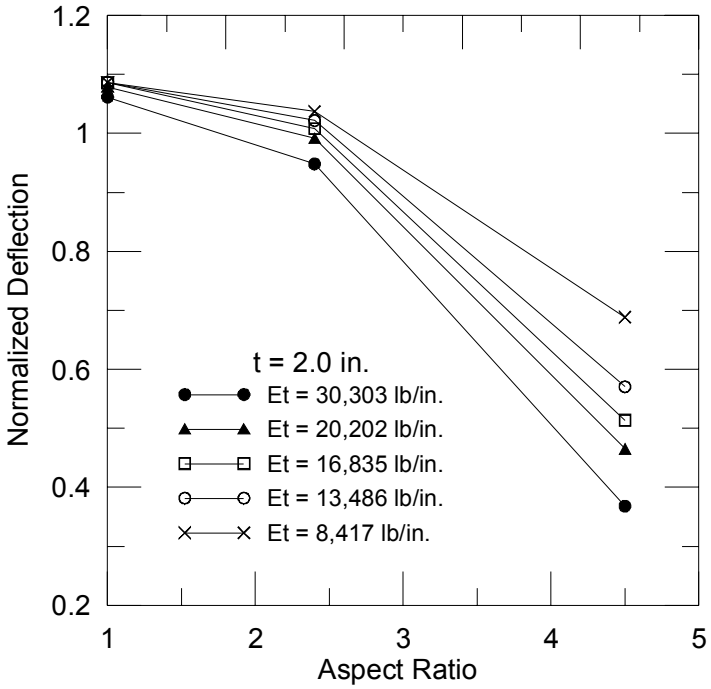

Figure A.4. FLAC3D: Aspect Ratio vs. Normalized Deflection (t = 2.0 in.)

The third step in the verification study was to investigate the behavior of the grid of linear elastic material for geometries and geosynthetic stiffnesses that are typical of geosynthetic reinforced bridging layers. The geosynthetic stiffness, E·t, was held constant at 16,835 psi. Spans of 5, 7, and 10 feet, which correspond to values of b of 30, 42, and 60 inches, respectively, were considered. Three different vertical pressures, 2, 5, and 10 psi, were applied. The grid refinement and thickness were varied, and the resulting deflections were compared to those determined by the closed-form solution. For aspect ratios of 1:1:1 and 2:2:2, and for the three values of applied vertical load, the normalized deflections are plotted against the ratio t/b in Figures A.5 through A.7. The author and Dr. Meeok Kim performed this work.

Based on the work performed in all three steps of the verification study, it was concluded that out-of-plane membrane behavior could be represented in FLAC3D by a grid of linear elastic material. For a wide range of geometries and applied vertical loads, it appears that good results are obtained when the aspect ratio is 2:2:1 or less, and the ratio of model thickness to grid width, t/b, is between 0.06 and 0.07.

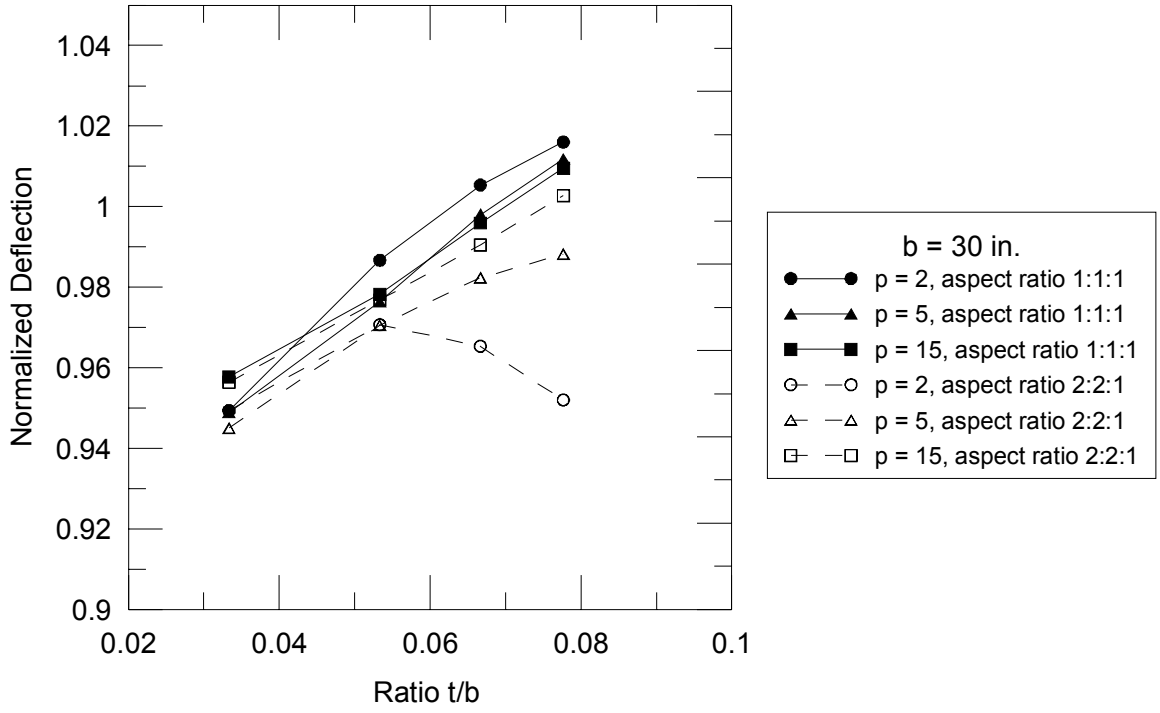

Figure A.5. FLAC3D: Ratio t/b vs. Normalized Deflection (b = 30 in.)

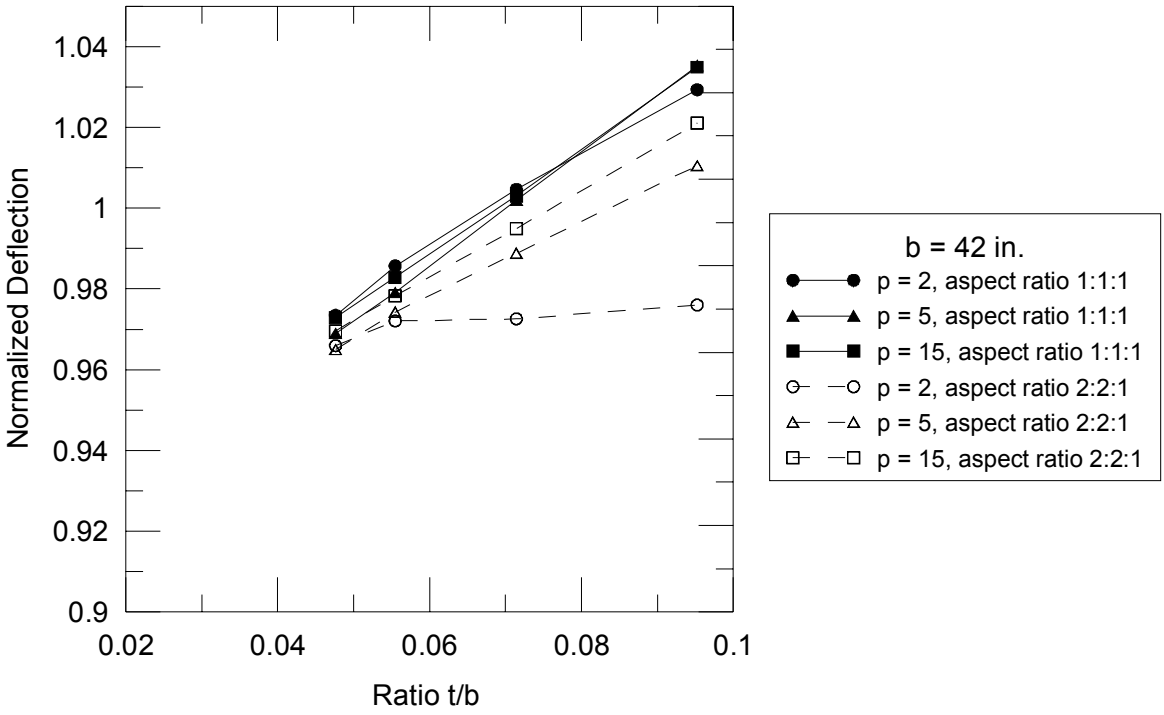

Figure A.6. FLAC3D: Ratio t/b vs. Normalized Deflection (b = 42 in.)

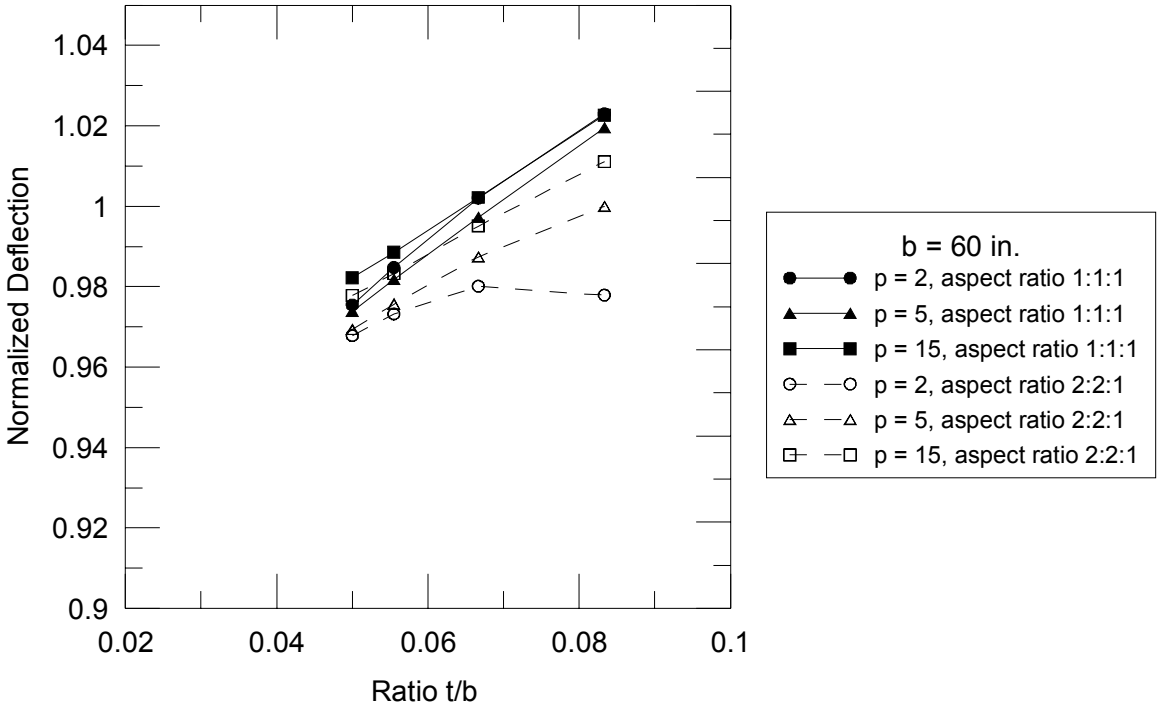

Figure A.7. FLAC3D: Ratio t/b vs. Normalized Deflection (b = 60 in.)

A.3 Membrane Behavior in FLAC

The two-dimensional finite difference computer program FLAC has four built-in structural elements: beam, cable, pile, and support elements. Beam elements are two-dimensional elements with three degree of freedom at each end node. They are used to represent a structural member in which bending resistance and limited bending moments are important. Cable elements are one-dimensional axial elements that can yield in tension or compression, but cannot sustain a bending moment. Cable elements are used to model conditions for which tensile capacity is important (Itasca 2002b). In some cases, beam and shell elements have been used to model membrane behavior in FLAC. However, these structural elements cannot be used with axisymmetric grids. Therefore, like in the FLAC3D analyses, a grid of linear elastic zones was used to model membrane behavior for the two-dimensional axisymmetric geometry. The FLAC axisymmetric membrane verification studies are described in this section.

A.3.1 FLAC analyses compared to closed-form solution

The verification studies considered an axisymmetric grid of linear elastic material. The outer diameter was pinned, and the centerline edge was allowed to deflect, as shown in Figure A.8. The maximum deflection, w_{max}, was measured at the centerline edge. The linear elastic material is assigned an elastic modulus and a Poisson's ratio. The stiffness of the membrane, or geosynthetic, is represented by the product of the elastic modulus, E, and the thickness, t. As mentioned previously, the philosophy behind the use of a grid of linear elastic material is that the product of the modulus of the linear elastic material and the thickness of the grid is equal to the stiffness of the geosynthetic reinforcement. For example, a geosynthetic with a stiffness J = E·t = 8417 lb/in. could be modeled using a grid of linear elastic material with an elastic modulus of 16,834 psi and grid thickness of 0.5 in.

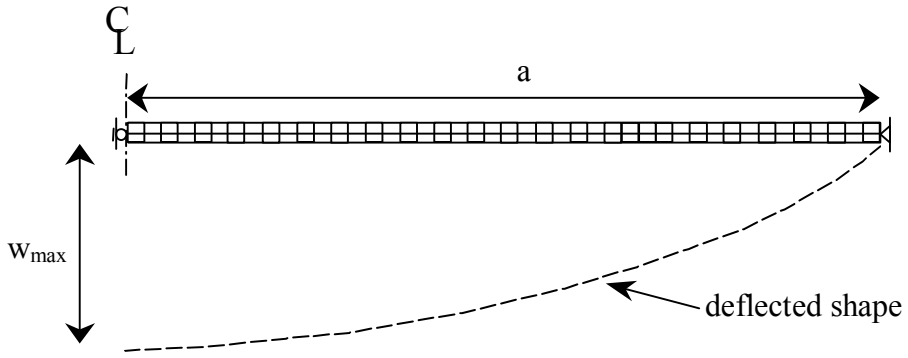

Figure A.8. Schematic of axisymmetric membrane model

An analytical closed-form solution provided by Ugural (1999) was used to verify the results of the FLAC axisymmetric numerical analyses. For a clamped circular membrane with a Poisson's ratio of 0.3 subjected to a uniform load, Ugural (1999) presents the following closed-form equation for determining the maximum deflection, w_{max}, of the membrane:

$$w_{max} = 0.704 \cdot a \cdot \sqrt[3]{\frac{p \cdot a}{E \cdot t}} \qquad (A.2)$$

where w_{max} = the maximum deflection of the membrane that occurs at the center of the membrane, p = applied uniform vertical load, a = radius of the circular membrane, E = membrane elastic modulus, and t = membrane thickness.

Similar to the FLAC3D verification studies, preliminary axisymmetric FLAC studies were focused on evaluating membrane thickness of 0.75 to 2 in. In these preliminary studies, the membrane was subjected to uniform loads of 5, 15, and 20 psi, and three values of membrane radius were evaluated: 12, 24, and 36 in. The deflections calculated by the FLAC model were in good agreement with those determined analytically from Equation A.2. However, in implementing the linear elastic geosynthetic in a numerical model, it became apparent that the thickness of the geosynthetic affected the stresses that were measured immediately above and below the geosynthetic. Therefore, it was desired to reduce the thickness of the geosynthetic as much as possible. A true geosynthetic thickness of 0.1 in. was chosen. The geosynthetic was divided into two vertical layers, and was subjected to uniform loads of 5, 15, and 20 psi. Three values of membrane radius were evaluated: 12, 24, and 36 in. The value of J or E·t was held constant at 100,000 lb/ft, or 8333 lb/in. For a thickness of 0.1 in., the elastic modulus is equal to 83,330 psi. Results of the axisymmetric FLAC verification study for a membrane with a thickness of 0.1 in. are summarized in Table A.3, which shows that results within about 5 percent of the closed form solution were obtained for all cases.

Table A.3. Results of axisymmetric membrane verification study for t = 0.1 in.

p (psi)	a (in.)	w_{max} (in.)	FLAC	Normalized deflection
Aspect Ratio 2H:1V				
5	12	1.632	1.542	0.945
15		2.353	2.253	0.958
20		2.590	2.495	0.963
5	24	4.111	3.900	0.949
15		5.929	5.762	0.972
20		6.526	6.403	0.982
5	36	7.058	6.735	0.954
15		10.180	9.995	0.982
20		11.205	11.140	0.994
Aspect Ratio 4H:1V				
5	12	1.632	1.552	0.951
15		2.353	2.261	0.961
20		2.590	2.502	0.966
5	24	4.111	3.908	0.951
15		5.929	5.764	0.972
20		6.526	6.406	0.982
5	36	7.058	6.725	0.953
15		10.180	10.030	0.985
20		11.205	11.180	0.998

A.4 FLAC analyses compared to published analyses

Another step in the verification process included performing FLAC axisymmetric analyses to analyze case histories with geosynthetic reinforcement. Two case histories found in the literature are presented by Russell and Pierpoint (1997), who performed three-dimensional analyses using FLAC3D of two actual constructed geosynthetic-reinforced column-supported embankments

constructed in the United Kingdom. Kempton and Naughton (2002) and Naughton and Kempton (2005) also discussed the results of these numerical analyses.

The goals in analyzing the two case histories presented by Russell and Pierpoint (1997) are twofold: (1) to verify the methods of using a grid of linear elastic zones to represent membrane behavior against published data, and (2) compare the results of the FLAC axisymmetric analyses to the FLAC3D analyses. It is understood that the tension in the membrane cannot be adequately evaluated using 2D axisymmetric analyses; however, as shown in Chapter 7, axisymmetric analyses can be used to evaluate the vertical stresses above the geosynthetic reinforcement.

The two embankments evaluated by Russell and Pierpoint (1997) are the A14 and Second Severn embankments. The A14 Embankment was constructed in an area underlain by compressible alluvium and peat. Driven piles were installed on a square grid with 3.3-foot square pile caps. Two layers of Terram Paralink geosynthetic reinforcement were installed at the base of the embankment. This embankment is referred to in the literature as Embankment A. The other embankment is a trial embankment constructed at the Second Severn crossing. Geotechnical parameters for the subsoil are given by Bell et al. (1994) and Maddison et al. (1996). Vibro concrete columns of 1.65 ft diameter were installed in a square array with center-to-center spacings of 8.2 ft. Two layers of Tensar SS2 were installed at the base of the embankment. This embankment is referred to in the literature as Embankment B. The geometry of the embankments and the material property values are summarized in Table A.4.

Russell and Pierpoint (1997) performed their analyses using FLAC3D. The embankment fill was modeled using the Mohr-Coulomb material model and was constructed in a single event. The reinforcement at the base of the fill, which consisted of two layers installed perpendicular to each other spanning between adjacent pile caps, were modeled using one-dimensional linear cable elements (Russell and Pierpoint 1997). The stress reduction ratio, SRR, was evaluated as the ratio of the average vertical stress carried by the reinforcement to the average vertical stress due to the embankment fill (Kempton and Naughton 2002). The foundation soil was omitted in their numerical analyses. The results of their analyses were compared with several existing methods

of evaluating the SRR (Russell and Pierpoint 1997, Kempton and Naughton 2002, Naughton and Kempton 2005).

Table A.4. Summary of geometry and material property values of Embankments A and B

Property	**Embankment A**	**Embankment B**
Height (ft)	19	14
Pile cap width (ft)	3.3	1.65
Pile spacing (ft)	8.2	8.2
Longitudinal reinforcement stiffness (lb/ft)	380,000	20,137
Transverse reinforcement stiffness (lb/ft)	650,700	50,550
Fill Poisson's Ratio	0.2	0.2
Fill Stiffness (psf)	417,800	835,600
Average fill density (pcf)	116	121
Fill angle of friction (deg)	30	40
Fill dilation (deg)	0	0
Fill cohesion (psf)	0	210

Axisymmetric FLAC analyses of Embankments A and B were performed as part of this verification study. The square pile caps were converted to circular pile caps with equivalent areas; the pile cap spacings were also converted to circular areas while maintaining the appropriate area replacement ratio. Mesh refinement was based upon knowledge gained during the numerical analyses of the I-95/Route 1 test embankment, as described in Chapter 5.

For Embankment A, the pile cap was converted to a circular cap with a radius of 1.85 ft, and the total model radius was set equal to 4.63 ft. Mesh refinement for Embankment A employed 11 zones across the radius of the column, and 17 zones across half the annulus of the soil in between columns. Vertical refinement produced 116 layers of mesh zones, so that 3,248 mesh zones were used altogether. Two layers of geosynthetic were included at the base of the actual embankment fill. Two geogrid layers were also employed in the axisymmetric numerical model. One layer was assigned the transverse stiffness from Table A.4, and the other layer was assigned

the longitudinal stiffness from Table A.4. Each layer of geosynthetic had a thickness of 0.1 in., and each geosynthetic layer was subdivided into two layers of mesh zones.

Similarly, for Embankment B, the pile cap was converted to a circular cap with a radius of 0.95 ft, and the total model radius was set equal to 4.65 ft. Mesh refinement for Embankment B employed 6 zones across the radius of the column, and 22 zones across half the annulus of the soil in between columns. Vertical refinement produced 86 layers of mesh zones, so that 2,408 mesh zones were used altogether. For the numerical modeling of the geogrid layers, the same approach used for Embankment A was also used for Embankment B.

For both axisymmetric models, the gridpoints at the pile caps were fixed in the x- and y-directions; the sides of the models were free to move downwards. No boundary conditions were applied to gridpoints that represented the space between pile caps.

The SRR was evaluated at the top of the geosynthetic reinforcement layers. The results of the axisymmetric analyses performed as part of this verification study are given in Table A.5, along with the values of SRR calculated by the FLAC3D analyses performed by Russell and Pierpoint (1997) as well as the values of SRR determined by various existing methods. The SRR value calculated using the axisymmetric FLAC model for Embankment A is very close to the value calculated by Russell and Pierpoint (1997) using FLAC3D. The SRR value from the axisymmetric FLAC model for Embankment B is 36 percent greater than that calculated by Russell and Pierpoint (1997) using FLAC3D, but is less than the average of the SRR values for this embankment calculated from seven existing methods.

Table A.5. SRR by various methods for Embankments A and B

	Embankment A	**Embankment B**
Method	**SRR**	**SRR**
BS8006	0.25	0.96
Adapted Terzaghi 1	0.36	0.58
Adapted Terzaghi 2 (Russell et al. 2003)	0.57	0.76
Hewlett & Randolph	0.36	0.55
German Method (Kempfert et al. 2004)	0.39	0.53
Adapted Guido	0.06	0.11
Swedish Method	0.24	0.44
FLAC3D numerical analyses performed by Russell and Pierpoint (1997)	0.61	0.39
FLAC axisymmetric numerical analyses performed by author	**0.64**	**0.53**

A.5 Closing Remarks

Based on the work performed in the FLAC3D verification study, it was concluded that out-of-plane membrane behavior could be represented in FLAC3D by a grid of linear elastic material. For numerical stability and reduced computation time, it was necessary in FLAC3D to represent the geosynthetic with a mesh thickness greater than the true geosynthetic thickness. Geosynthetic thicknesses of 0.25 to 2 inches were evaluated. For a wide range of geometries and applied vertical loads, good results are obtained when the aspect ratio is 2:2:1 or less, and the ratio of geosynthetic thickness to half width of the geosynthetic layer, t/b, is between 0.06 and 0.07.

Based on the work performed in the FLAC axisymmetric verification study, it was concluded that out-of-plane membrane behavior could be adequately represented in by a grid of linear elastic material. Unlike in FLAC3D, computational and run-time issues were not encountered in FLAC when the geosynthetic was assigned a very small thickness. Therefore, a geosynthetic thickness of 0.1 in. was evaluated in the parametric study. Good results were obtained by

assigning the geosynthetic grid a thickness of 0.1 in. with aspect ratios of 2H:1V or 4H:1V. Deflections of a geosynthetic with a thickness of 0.1 in. were evaluated using FLAC and were compared to a closed-form solution. These results are given in Table A.3. FLAC analyses were also performed to analyze case histories with geosynthetic reinforcement. The knowledge gained from the parametric studies described in this Appendix together with the lessons learned from the analyses of the model scale tests described in Chapter 7 were used to perform the parametric studies with geosynthetic reinforcement as described in Chapter 8.

APPENDIX B
MEMBRANE DEFLECTION STUDIES

B.1 Introduction

Axisymmetric analyses were performed to evaluate the load-deflection response of a membrane (or geosynthetic reinforcement). The goal of these analyses was to develop a relationship between the membrane deflection and the membrane geometry, membrane stiffness, and applied vertical stress. Such a relationship could then be incorporated into the calculation procedure for the evaluation of geosynthetic-reinforced column-supported embankments.

The load-deflection response of the geosynthetic reinforcement was approximated by performing axisymmetric numerical analyses of a uniformly loaded annulus of linear-elastic membrane material with the inner boundary pinned, which represents the support provided by the column, and with the outer boundary free to move vertically but not laterally, which represents the axisymmetric approximation of lines of symmetry in the actual three-dimensional configuration of a column-supported embankment.

B.2 Description of Analyses

The problem geometry and boundary conditions are shown in Figure B.1. These conditions represent the axisymmetric approximation of the actual three-dimensional configuration of a membrane installed above a columnar foundation subject to embankment loading.

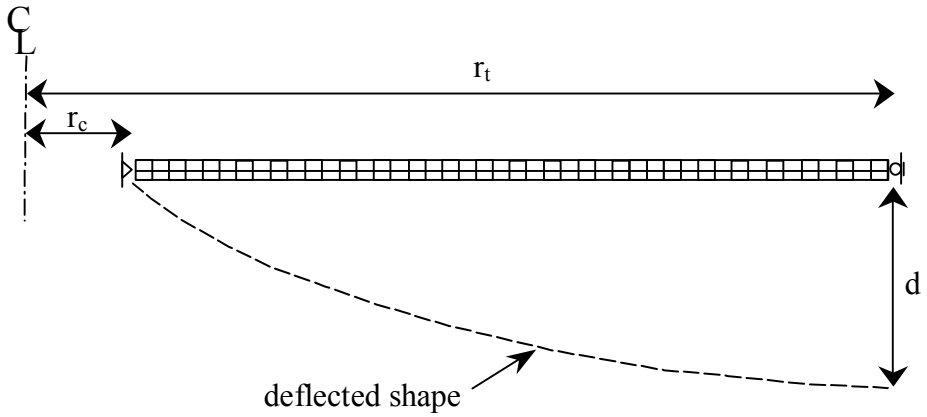

Figure B.1. Schematic of axisymmetric membrane model

The stiffness of the membrane, or geosynthetic, is represented by the product of the elastic modulus, E_g, and the thickness, t_g. The linear elastic material was assigned an elastic modulus of 4,000,000 lb/ft^2, a thickness of 0.24 in., which correspond to a membrane stiffness, J_g, of 80,000 lb/ft. The Poisson's ratio was set equal to zero to approximate the behavior of a geogrid.

The inner diameter, r_c, was varied between zero and two, and the outer diameter, r_t, was varied between one and 4.48. A summary of the geometries evaluated is provided in Table B.1. The geosynthetic was divided into two vertical layers, and the grid aspect ratio was kept constant at 2H:1V. The grid of linear elastic elements was subjected to uniform vertical loads, p, of 25, 50, 100, 200, 400, 800, 1600, and 3200 psf. The maximum deflection, d, was measured at the outer edge.

Table B.1. Inner and outer radius values used in membrane study

r_c (ft)	r_t (ft)	r_c / r_t	a_s
0	1	0	0
0.5	2.24	0.22	0.05
1	4.48	0.22	0.05
0.75	2.37	0.32	0.1
1	2.24	0.45	0.2
1	1.83	0.55	0.3
2	3.66	0.55	0.3
1	1.41	0.71	0.5

B.2 Results of Analyses

The results of the numerical analyses were plotted in terms of the normalized vertical stress, $(p*r_t)/(E*t)$ versus the normalized deflection, d/r_t, as shown in Figure B.2.

It was found that the results of the numerical analyses could be closely approximated by the following expression, which is provided in terms applicable to the column-supported embankment:

$$d = \sqrt{\frac{A}{\pi}}\left[\frac{2}{3}\left(1-\sqrt{a_s}+\left(1-\sqrt{a_s}\right)^4\right)\sqrt[3]{\Sigma_g}+\left(1-\sqrt{a_s}\right)^3\Sigma_g\right] \quad \text{(B.1)}$$

where $a_s = \frac{r_c^2}{r_t^2}$, $A = r_t^2$, and Σ_g = the normalized vertical stress on the geosynthetic reinforcement, which is given by

$$\Sigma_g = \frac{\left(\sigma_{soil,geotop} - \sigma_{soil,geobot}\right)\sqrt{\frac{A}{\pi}}}{J_g} \quad \text{(B.2)}$$

Σ_g is the same quantity as plotted on the horizontal axis of Figure B.2.

The normalized expression given in Equation B.1 is plotted for each geometry in Table B.1 by the dashed lines in Figure B.2. As can be seen in the figure, the normalized expression provides a good fit to the results of the numerical analyses.

Equations B.1 and B.2 were incorporated into the calculation procedure discussed in Chapter 9 to represent the load-deflection response of a membrane in a geosynthetic-reinforced bridging layer.

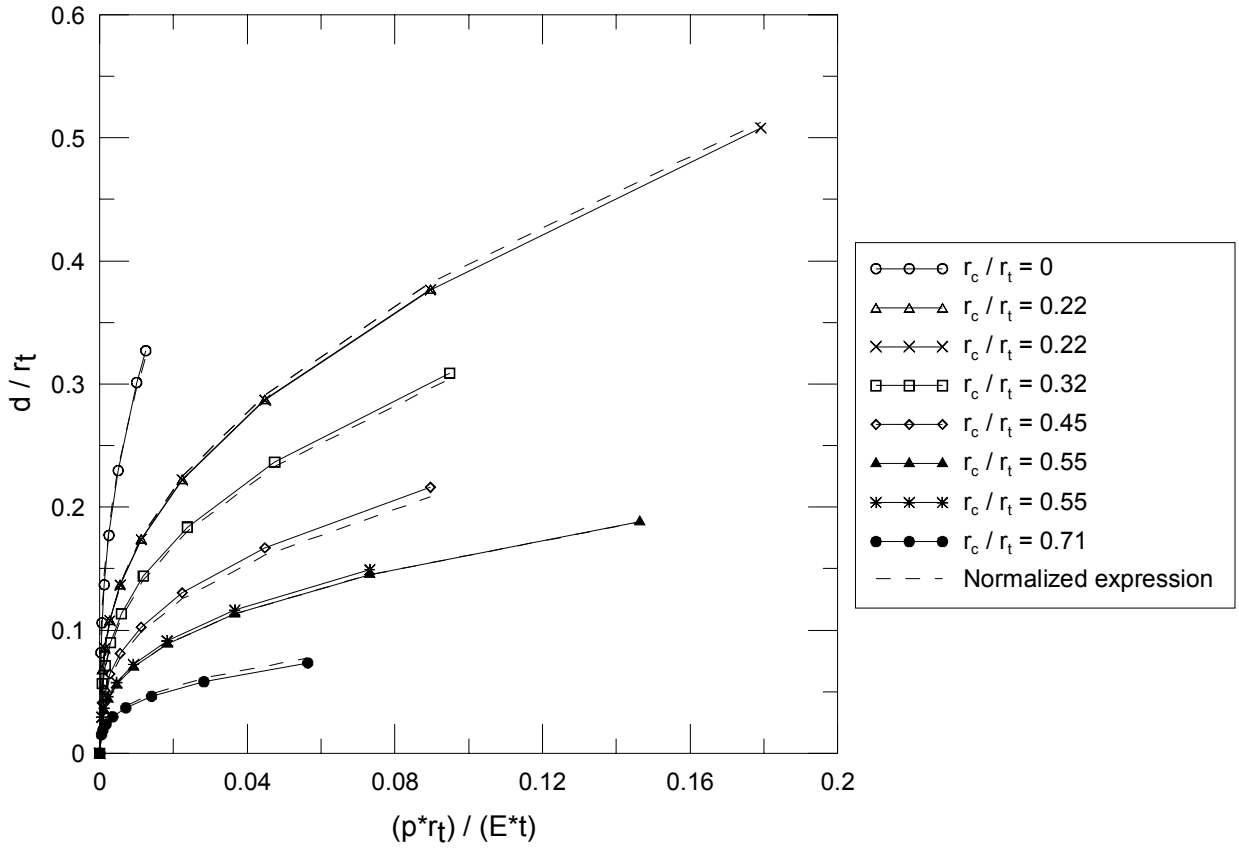

Figure B2. Results of numerical analyses compared with normalized expression

APPENDIX C
REVIEW OF THE STATE OF PRACTICE FOR STONE COLUMNS

C.1 Introduction

Stone columns are vertical columns of highly compacted gravel or aggregates constructed as inclusions within subsurface soils. Construction of stone columns is a widely used technique to increase bearing capacity, reduce settlements, and improve slope stability. In sandy soils, stone columns have been installed to mitigate potential liquefaction induced hazards. In typical applications, about 10 – 35% of the native soil is replaced with stone in the form of columns (Munfakh 1997).

This appendix presents a summary of the installation methods, typical column geometries, typical material property values, and current analysis methods for settlement of embankments supported on stone columns. Recommendations for construction, performance monitoring, and construction specifications of stone columns may be found in the following references:

- Barksdale, R. D. and Bachus R. C. (1983). "Design and Construction of Stone Columns, Vol. 1." *Federal Highway Administration, RD-83/026*.
- Elias, V., Welsh J., Warren J., and Lukas R. (1999). "Ground Improvement Technical Summaries, Volume II, Demonstration Project 116," *Federal Highway Administration.*

C.2 Applications and Limitations

Stone columns are used to support structures overlying very soft to firm cohesive soils, and loose silty sands having greater than 15% fines (Barksdale and Bachus 1983). Stone columns are installed in soft clays to provide greater bearing capacity, to reduce settlements, and to improve the stability of embankment foundations. Stone columns reduce long-term settlements of soft clays by providing stiff reinforcing elements, and they shorten consolidation time by providing increased drainage. When installed in sandy soils, stone columns may reduce liquefaction potential by increasing the overall subsurface density and providing increased drainage during a seismic event.

Stone columns are often more economical than the removal and replacement of deep soft soils, especially on larger sites where the groundwater table is close to the surface (Elias et al. 1999).

Stone columns are most effective in clays occurring near the surface with an underlying bearing stratum 18 – 30 feet (5.5 – 9 m) below the ground surface.

Stone columns will provide the most significant improvement in soft clays with shear strengths approximately 300 to 1,050 psf (15 to 50 kPa). However, stone columns have been used in clays having minimum undrained shear strengths as low as 150 psf (7 kPa) and maximum undrained shear strengths of 2,100 psf (100 kPa), which should be considered the upper limit (Elias et al. 1999).

Stone columns are not ordinarily used in sensitive clays that may lose strength during installation of the stone columns. Subsurface soils that contain significant layers of decomposable materials, such as peats, organic materials or extensive refuse, are also not typically suitable for stone columns. When thin layers of decomposable materials are encountered, a rule-of-thumb requires that the ratio of the decomposable layer thickness to the stone column diameter be less than two (Barksdale and Bachus 1983).

The vibro-replacement (wet) method is commonly used in the United States. The method is effective at sites consisting of very soft soils and a high ground water table. However, the vibro-replacement method requires a large quantity of water, which must be disposed of after construction. The water may be properly handled by constructing sediment ponds, ditches or other drainage structures, but may pose a problem at urban or contaminated sites.

The installation of stone columns requires a high level of field control and an experienced contractor. The performance of stone column systems depends primarily on the geometry of the column layout and the installation method used (Priebe 1993). The installation and geometry of stone columns are discussed in the following sections.

C.3 Installation/Production of Stone Columns

The installation of stone columns requires a high level of field control and an experienced contractor. Installation methods, typical geometries, and typical production rates of stone columns are discussed in this section.

Stone columns are typically constructed using one of the three following methods:

1.) vibro-replacement (wet) method;
2.) vibro-displacement (dry) method; or
3.) rammed column method.

In the vibro-replacement and vibro-displacement methods, a vibration probe device is used to form a vertical hole in the ground. Once the vibration device reaches the design depth of the columns, gravel backfill is placed in controlled 12 - 48 in. (30 – 120 cm) lifts. Gravel is either placed through a special duct alongside the vibrating probe or dumped into the open hole. The gravel is compacted using the vibration probe, and the process continues as the vibration probe is removed. Jetted water is used in the vibro-replacement (wet) method to erode and laterally displace the soil as the probe is advanced, as illustrated in Figure C.1. The vibro-displacement (dry) method does not use jetted water; however, compressed air is used to break the suction that develops when the vibrator is withdrawn from the hole. To use the vibro-displacement method, the vertical hole must be able to stand open.

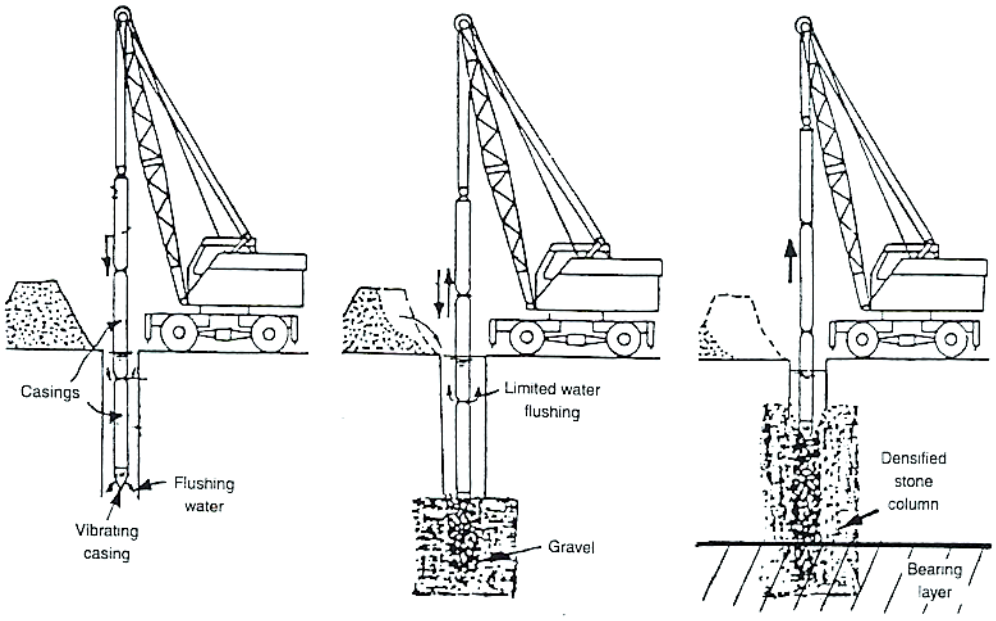

Figure C.1. Vibratory stone column installation technique (from Van Impe et al. 1997)

For the rammed column method, an open-end or closed-end casing pipe is driven, or vibrated, to the design depth of the column. For the method in which an open-ended casing is used, the soil is excavated from inside the casing and replaced with compacted gravel. For the method in which a closed-end casing is used, the soil is displaced and granular material is placed into the resulting open borehole. In both methods, the gravel is compacted in lifts by a drop weight.

Stone columns are typically formed using crushed, angular graded stones with dimensions of 0.25 to 3.0 inch (0.64 to 7.6 cm). A coarse, open-graded crushed stone is typically preferred; however, local availability may dictate what is used.

A mat of compacted gravel with a thickness of 1 to 3 feet (30 to 90 cm) is typically placed above the area of stone column installation. The granular mat, or bridging layer, serves several purposes. The bridging layer acts to distribute load over the stone columns, and it provides a drainage layer for dissipation of pore water pressure during loading. When placed prior to stone column installation, the bridging layer serves as a working platform. The use of a bridging layer also prevents shallow shear failures in the stone column (Datye 1982). Furthermore, the bridging layer forces the column to bulge at a lower depth under loading where effective stresses are greater, hence increasing the capacity of the column (Barksdale and Bachus 1983). Figure C.2 illustrates the influence of the granular mat on stone column behavior. In some cases, the bridging layer may be reinforced with one or more layers of geosynthetics. The design of the geosynthetic-reinforced bridging layer is the subject of the main body of this dissertation.

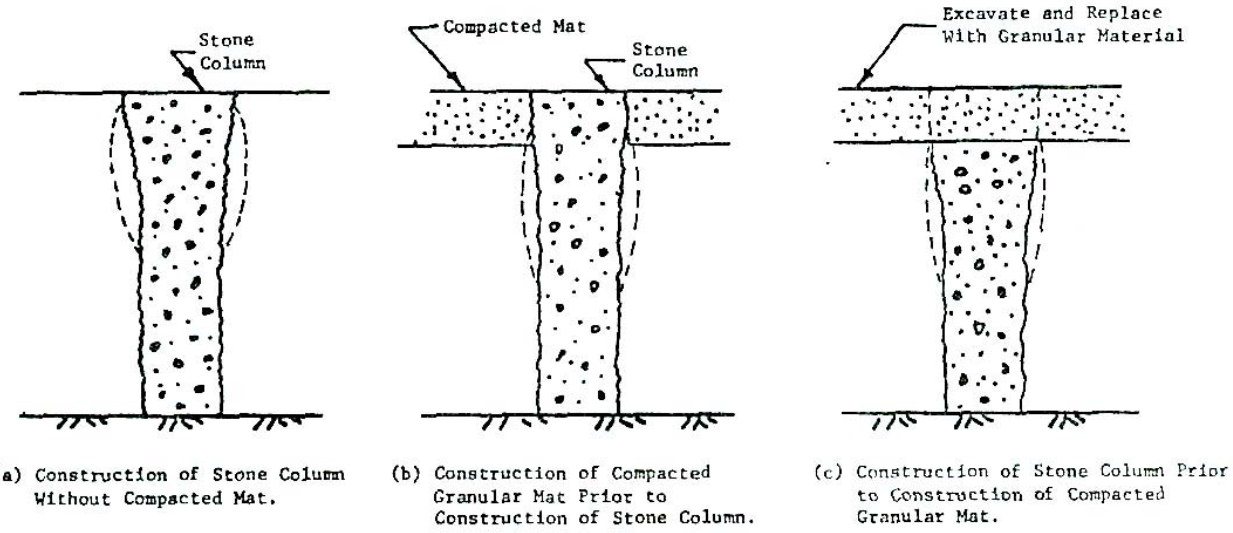

Figure C.2. Influence of granular mat on the behavior of a stone column (from Barksdale and Bachus 1983)

Stone columns are installed in triangular, square or hexagonal patterns as shown in Figure C.3. The triangular pattern is the most efficient pattern since it provides the greatest area coverage for the least number of columns, and thus is the most common pattern used (DiMaggio 1978). Columns beneath the edges of widespread loaded areas may be spaced more closely than in the center. If peripheral columns are overloaded, a progressive lateral displacement of large magnitude can occur at the surface.

Stone column spacings vary from 5 to 11.5 ft (1.5 to 3.5 m). Column spacing is the factor that is likely to influence the behavior of the stone column system the most. Column spacings larger than four diameters make the system inefficient, even under the most favorable conditions (Poorooshasb and Meyerhof 1997). If a close spacing is used, a staggered construction sequence should be developed. A minimum column spacing of 5 ft (1.5 m) is imposed because of potential construction problems (Barksdale and Bachus 1983).

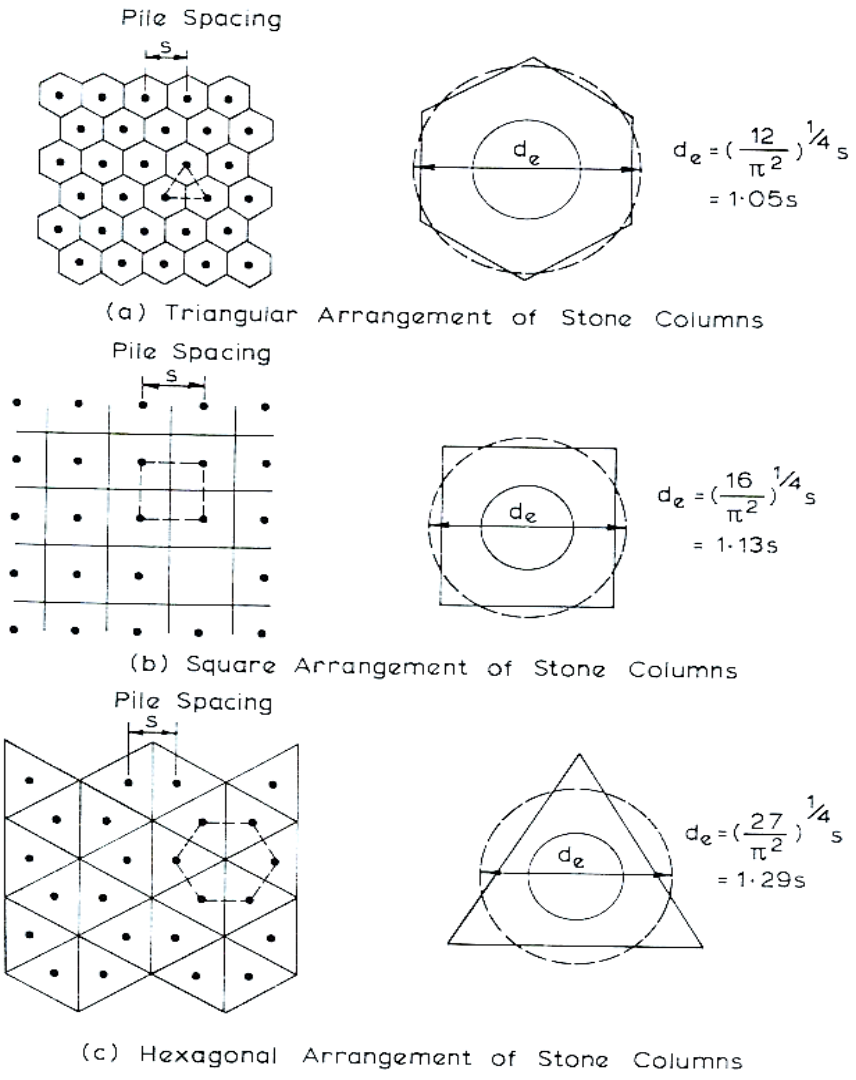

Figure C.3. Stone column layouts and corresponding effective diameters (from Balaam and Booker 1981)

Stone column diameters vary based on the method of installation and subsurface conditions. Often design dimensions are chosen based on local experience and contractor capabilities. Typical diameters of columns installed by the vibro-replacement and vibro-displacement methods range from 2.5 – 4 ft (0.8 – 1.2 m). Using the rammed method, column diameters are typically 2.5 ft (0.80 m) or less. During installation, gravel will be pushed laterally into the sides of the vertical hole. As layers of varying stiffness are encountered, the diameter of a column will fluctuate since diameters will increase in softer layers. Installed column diameters may be estimated in the field based on the amount of aggregate used or determined by excavating the

installed column. Design column diameter and spacing dimensions may be determined by field trial installations.

Each column is assumed to affect a tributary area of soil based upon column arrangement and spacing. The tributary area, or "zone of influence," of a column is represented by a circular area with an effective diameter, d_e. The effective diameter is calculated for different arrangements of stone columns in Figure C.3.

An important geometric factor involved in the design of stone columns is the area replacement ratio, a_s, which is defined as:

$$a_s = \frac{A_{col}}{A_{col} + A_{soil}} \tag{C.1}$$

where A_{col} = area of column, A_{soil} = area of the soil surrounding the column, and $A_{col} + A_{soil}$ = effective area, or the total tributary area associated with each column, which is determined using the effective diameter.

Typical area replacement ratios vary from 0.15 to 0.35. According to Charles and Watts (1983), a large area ratio is required to achieve a significant reduction in settlement; an area ratio of 0.3, which corresponds to a ratio of spacing to column diameter of about 1.7, results in approximately a 30% reduction of settlement. Generally, more reductions in settlement are achieved by reducing column spacings. However, as previously mentioned, for column spacings less than 5 ft (1.5 m), potential construction problems arise.

Stone columns typically extend to an underlying bearing stratum, and are reported to be most effective when supported by a bearing stratum 18 – 30 feet (5.5 to 9 m) below the ground surface (Juran et al. 1989). Typical stone column lengths are 13 – 33 ft (4 – 10 m). Stone columns with lengths up to 60 ft (18 m) have been constructed successfully in the past (Mitchell 1981). However, when the required column lengths exceed 33 ft (10 m), it may become more economical to use conventional deep foundations.

The average reported construction rates for stone columns are 3 – 6 ft/min (1-2 m/min) during hole excavation, and 1.5 – 3 ft/min (0.5 - 1 m/min) during backfill and compaction. Including time to move between columns, overall installation rates typically vary from 30 – 100 ft/hr (9 – 30 m/hr) (Barksdale and Bachus 1983).

It is recommended that experienced contractors be contacted to assist in estimating budget costs and project feasibility. Project budget estimates should take into account contractor mobilization/demobilization costs, stone column installation costs, and any additional costs, such as load tests or inspection.

C.4 Material Property Values of Stone Columns

Under widespread load, a group of stone columns deforms much more than a group of rigid piles and the surrounding soil is subject to compression as the stone column deforms laterally. As a result, the relative stiffness and strength of the stone column can change significantly as load is applied and the column deforms (Greenwood 1991).

The granular material of a stone column is often assumed to have an internal angle of friction value between 35 and 45 degrees and a cohesion value equal to zero. However, Barksdale and Goughnour (1984) state that a friction angle of 38 degrees is now thought to be low, and they recommend values up to 50 degrees. The modulus of elasticity, or Young's modulus, of the column material is often assumed to be 4,400 – 10,200 psi (30,000 – 70,000 kPa) (Balaam and Poulos 1983). Balaam and Booker (1981) and Balaam and Booker (1985) performed finite element analyses assuming that the ratio of modulus values between the stone and soft compressible clays is about 10 to 40. However, Barksdale and Bachus (1983) indicated that the modular ratio value is more likely to be between 40 and 100. In either case, stone columns are inherently nonhomogenous and the Young's Modulus of the stone column will increase with depth and loading (Van Impe et al. 1997).

Because the column is cohesionless, its stiffness depends upon the lateral support given by the soil around it. The modulus of elasticity of the soil may be determined by laboratory tests or

estimated. If Poisson's ratio is assumed, the modulus of the clayey soil, E_{soil}, may be estimated by Equation C.2.

$$E_{soil} = \frac{(1+\upsilon_s)(1-2\upsilon_s)}{m_v(1-\upsilon_s)} \tag{C.2}$$

where υ_s = Poisson's ratio of the soil and m_v = coefficient of compressibility of the soil as measured in an oedometer test. Typical values of Poisson's ratio for clay are provided in Table C.1 (Balaam and Poulos 1983). The Poisson's ratio of the stone column material is commonly assumed to be 0.3.

Table C.1. Typical Values of Poisson's Ratio for Clay

Clay	Poisson's Ratio
Very soft to soft NC clays	0.35 - 0.45
Medium to stiff clays	0.30 – 0.35
Stiff OC clays	0.10 – 0.30

Due to the mixing of the column material and in-situ soil during column installation, it can be difficult to determine the properties of both the column material and surrounding soil. Field tests, such as CPT or SPT, may be performed to assess installed column material property values.

C.5 Analysis Methods

The behavior of the stone column foundation is extremely complex with simultaneous and inter-dependent changes of stress ratios, pore pressures, and stiffnesses in both the soil and the column (Greenwood 1991). In general, the overall stiffness of a volume of soil stabilized with stone columns increases with reduced column spacing, increased column area, and increased column strength. The columns are stiffer than the surrounding soil and rely on the lateral support of the soil to function properly. Since the column is stiffer than the soil, it carries a larger proportion of the load. As consolidation progresses, additional load transfer to the stone column occurs until an equilibrium condition is reached (Elias et al. 1999).

Analysis methods to evaluate the bearing capacity and settlement behavior of stone column systems are discussed in this section.

C.5.1 Bearing Capacity

Design loads for stone columns are determined by experience, site-specific load tests, and empirically based equations. The ultimate capacity of a group of stone columns is frequently estimated by multiplying the capacity of a single column by the number of columns in the group. As a rough estimate, the ultimate capacity of a single stone column can be estimated as follows (Barksdale and Bachus 1983):

$$q_{ult} = c \cdot N_c \tag{C.3}$$

where q_{ult} = ultimate stress that the stone column can carry, c = undrained shear strength of the clay, N_c = bearing capacity factor for the stone column ($18 \leq N_c \leq 22$). For soils with a reasonably high initial stiffness, a bearing capacity factor of 22 is recommended, whereas for soils with a low initial stiffness, a bearing capacity factor of 18 is recommended.

Similarly, Mitchell (1981) reported that the allowable vertical stress on a single column may be expressed by the following equation:

$$\sigma_v = \frac{25 \cdot c}{FS} \tag{C.4}$$

where c = undrained shear strength of the soft ground and FS = factor of safety (typically 3). Comparing Equations C.3 and C.4, it can be seen that the value of N_c incorporated in Equation C.4 is 25, which slightly exceeds the range recommended by Barksdale and Bachus (1983).

Stone columns in groups are typically designed to carry axial loads on the order of 20 to 50 tons per column (Juran et al. 1989). The capacity of a stone column is also affected by the method of installation. During installation, the in-situ soil may mix with the column material, thus

decreasing the effective diameter of the column. During the vibro-replacement (wet) method, the jetted water flushes out fine material to prevent clogging; however, clogging is difficult to prevent using the dry, or vibro-displacement, method. The use of casing for the rammed method also prevents the intrusion of soft soil. In some cases, the electricity consumption of the vibrating device used to install the columns can be monitored and correlated to the lateral constraint that the soil provides to the column, which influences column capacity. The methods presented in Equations C.3 and C.4 for estimating column capacity do not distinguish between different construction techniques.

C.5.2 Consolidation Settlement

Generally, by reducing stone column spacing and increasing column penetration, the magnitude of settlement decreases and the rate of consolidation increases (Balaam et al. 1977). Presently available methods to estimate the magnitude of settlement of ground reinforced with stone columns range from simple approximate methods (such as the equilibrium method) to complex methods based on theories of elasticity and plasticity.

Two commonly used methods for calculating the settlement of ground reinforced with stone columns are presented in this section. These methods take into account only the anticipated primary consolidation settlements. Typically, the immediate settlement of ground reinforced with stone columns is considered to be negligible.

C.5.2.1 Equilibrium Method

The equilibrium method offers a simple analytical approach to evaluating the stress distribution and settlement of ground reinforced with stone columns based on the unit cell concept and conventional one-dimensional compression calculations. In a unit cell, the applied load is distributed between the stone column and the surrounding soil. For each stone column, a cylindrical tributary domain, which is approximated by a circle of effective diameter, d_e, is assigned. The unit-cell concept is illustrated in Figure C.4.

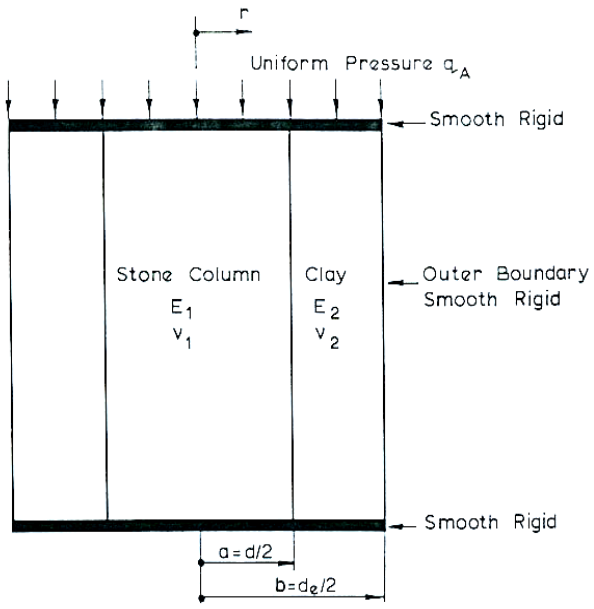

Figure C.4. Definition of terms for analysis using the "unit-cell" concept. (From Balaam and Booker 1981).

The unit cell concept assumes that the behavior of each column-unit is the same, which is valid for columns beneath the center of the large loaded areas but not for columns beneath the edges of the loaded areas. The unit cell method assumes that the deformation of the columns is equal to the deformation of the surrounding soil (equal strain condition), and disregards shear stresses between the stone column and surrounding soil. It is also assumed that the stress increase under a large loaded area is uniform with depth, and that the perimeter of each unit cell is shear-free and undergoes no lateral displacement. Based on several parametric studies, it has been shown that the settlements calculated using the unit cell analysis are insensitive to whether the base is modeled as a smooth or rough surface.

Upon loading, the concentration of stress in the stiffer stone column must be greater than the stress in the surrounding soil since the deflection in the two materials is the same. The applied load is supported by the columns and the surrounding soil in proportion to the relative stiffness of the two materials. The stress concentration ratio (or stress ratio), n, can be defined as the ratio of vertical stress in the column, σ_{col}, to the vertical stress in the surrounding clay, σ_{soil}:

$$n = \frac{\sigma_{col}}{\sigma_{soil}} \tag{C.5}$$

The stress concentration ratio is dependent on factors such as the relative stiffness between the column and the soil, the length of the stone column, the area replacement ratio, and the characteristics of the bridging layer, if used. Theory indicates the stress concentration ratio increases with time (Elias et al. 1999). The value of stress concentration used in the equilibrium analyses is either known or estimated.

Han and Ye (2001) note that the stress concentration ratio can be related to the ratio of the modulus of the column and the modulus of the soil by a Poisson ratio factor such that:

$$n = \xi \cdot \frac{E_{col}}{E_{soil}} \tag{C.6}$$

where E_{col} and E_{soil} = the modulus of the stone column and the surrounding soil, respectively, and ξ = Poisson ratio factor. This relationship is plotted for a Poisson's ratio in the columns, ν_c, of 0.15 and a Poisson's ratio in the soil, ν_s, of 0.45, along with the results from a theoretical and experimental study conducted by Barksdale and Bachus (1983), in Figure C.5.

However, based on many field studies, Mitchell (1981) reports that the stress concentration ratio for stone columns typically falls in the range of 2 to 6 with values of 3 to 4 common. Furthermore, Barksdale and Bachus (1983) recommend using a stress concentration ratio of 4 to 5 for stone column settlement calculations in soft soil.

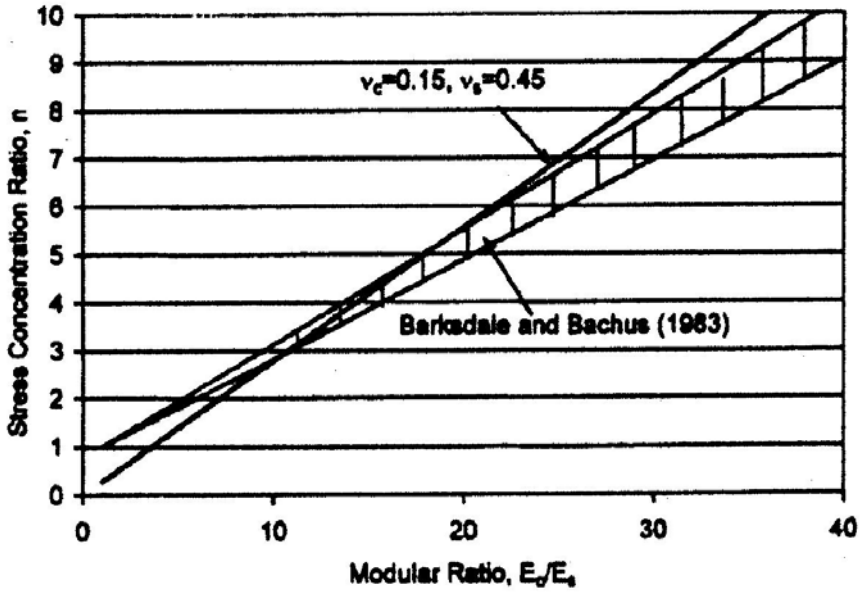

Figure C.5. Relationship between Stress Concentration Ratio and Modular Ratio (from Han and Ye 2001)

The geometry factors which contribute to the stress distribution within a volume of stabilized soil include column diameter and spacing, which are represented by the area replacement ratio, a_s, as given in Equation C.1. The vertical applied stress, σ, which occurs over a loaded area for a given area replacement ratio, is distributed as represented by the following equation:

$$\sigma = \sigma_{col} \cdot a_s + \sigma_{soil} \cdot (1-a_s) \tag{C.7}$$

where σ = total applied vertical stress, σ_{soil} = vertical stress in the clay and σ_{col} = vertical stress in the stone column.

In terms of the stress concentration ratio and the area replacement ratio, the vertical stresses induced in the column and the surrounding soil area may be estimated using the following equations:

$$\sigma_{soil} = \frac{\sigma}{[1+(n-1)a_s]} = \mu_{soil} \cdot \sigma \tag{C.8}$$

$$\sigma_{col} = \frac{n \cdot \sigma}{[1 + (n-1)a_s]} = \mu_{col} \cdot \sigma \qquad \text{(C.9)}$$

where μ_{soil} and μ_{col} are the ratio of stresses in the soil and column, respectively, to the average applied vertical stress, σ. The vertical stress distribution may be determined using Equations C.8 and C.9. Beneath loadings of limited size, the Bouissnesq or Westergaard stress distribution theories are sometimes used to determine the applied vertical stress, σ, as a function of depth.

For the Equilibrium Method, the amount of consolidation settlement of the stabilized ground is determined using Equation C.10.

$$\Delta d_{stab} = m_v \cdot \sigma_{soil} \cdot D = \beta \cdot \Delta d \qquad \text{(C.10)}$$

where Δd_{stab} = consolidation settlement of stabilized ground, Δd = consolidation settlement of unstabilized ground, and β = settlement reduction ratio, where:

$$\Delta d = m_v \cdot \sigma \cdot D \qquad \text{(C.10a)}$$

$$\beta = \frac{\sigma_{soil}}{\sigma} = \frac{1}{[1 + (n-1)a_s]} \qquad \text{(C.10b)}$$

and D = thickness of the stabilized clay layer, and m_v = coefficient of compressibility of the clay.

The settlement reduction ratio, β, is essentially defined as the ratio of the settlement of stabilized ground to that of the settlement predicted for unstabilized ground. Therefore, as the stress concentration ratio and replacement ratio increase, the settlement of the stabilized ground decreases.

C.5.2.2 Priebe's Method

The method proposed by Pribe (1995) to evaluate the settlement of stone columns is commonly used by contractors in the US (Burke 2003). The Priebe method was originally developed in the

late 1970's but has undergone several adaptations. The method refers to the improving effect of stone columns in a soil that is otherwise unaltered in comparison to the initial state. In a first step, an initial improvement factor is determined; subsequent steps modify this improvement factor. It is important to note that in Priebe's method, the improvement factor is represented by n; this improvement factor is not the same as the stress concentration ratio, which was defined in Equation C.5.

In the first step, the initial improvement factor, n_o, is determined by Equation C.11, or graphically in Figure C.6.

$$n_o = 1 + a_s \cdot \left[\frac{5 - a_s}{4 \cdot K_{o,c} \cdot (1 - a_s)} - 1 \right] \tag{C.11}$$

where a_s = area replacement ratio, and $K_{o,c} = \tan^2(45^o - \varphi_c/2)$, where φ_c = internal friction angle of the stone column aggregate. In Figure C.6, the "area ratio" is used, which is the reciprocal of the area replacement ratio, $1/a_s = A/A_c$, where A = the tributary area of the column, and A_c = area of the column. In Equation C.11, a Poisson's ratio of 0.33 is assumed for the soil, which is represented in Figure C.6 by $\mu_s = 1/3$.

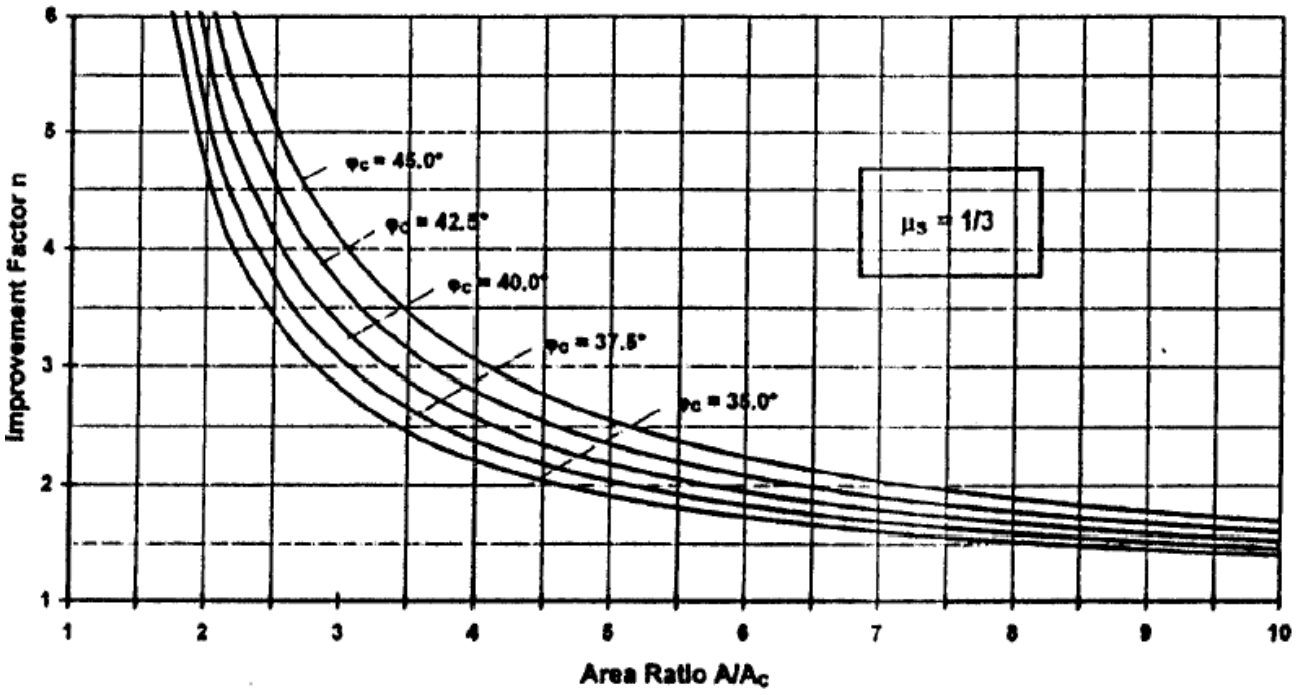

Figure C.6. Design Chart for Priebe's Method (from Priebe 1995)

In the second step, the area replacement ratio is adjusted to take into account the compressibility and bulging of the column material. In order to take into account the compressibility of the columns, the constrained moduli of the stone and surrounding soil must be known. However, the constrained modulus of the stone material is very difficult to determine and thus, its value is often assumed based on published values and previous experience. (In most soil mechanics literature, the constrained modulus is represented by M, but in Priebe's method, the constrained modulus of the column and the soil are represented by D_c and D_s, respectively.) In the second step, the area replacement ratio is revised based upon the relationships in Figure C.7. Using Figure C.7, the reciprocal of the modified area replacement ratio becomes:

$$\frac{1}{a_s} = \frac{1}{a_s} + \Delta\left(\frac{A}{A_c}\right) \tag{C.12}$$

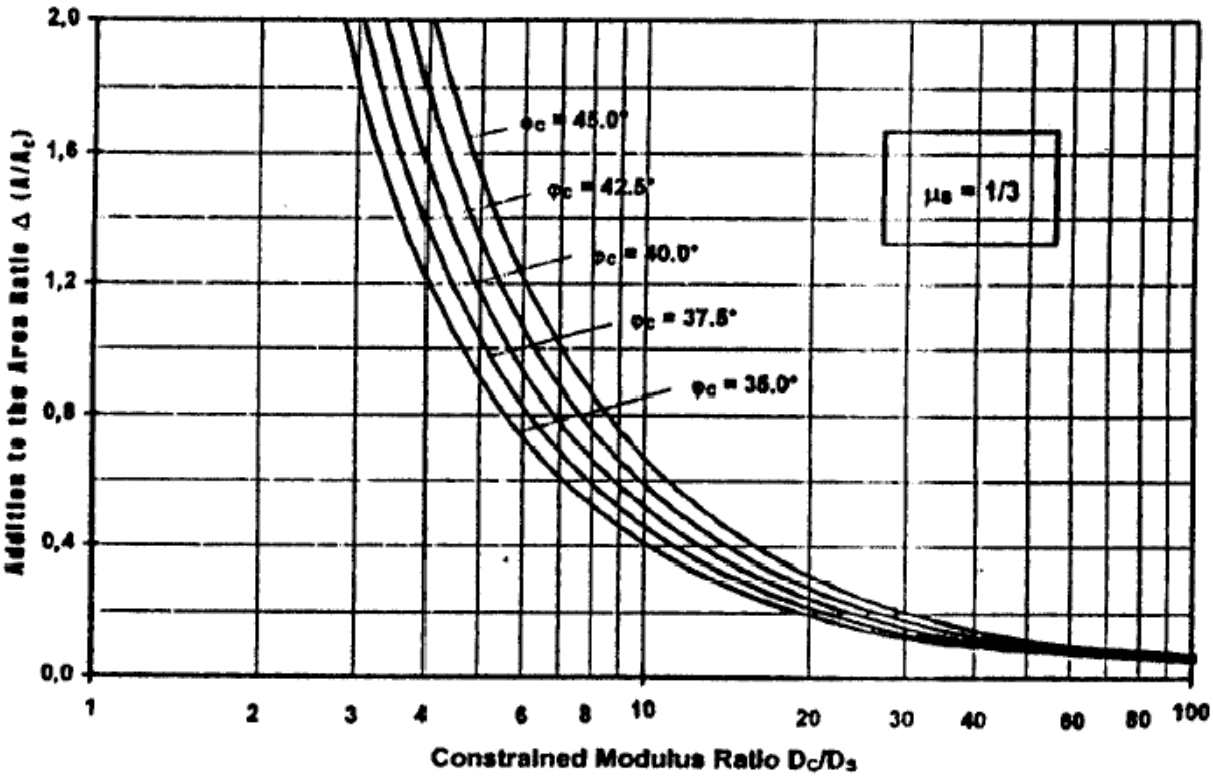

Figure C.7. Design Chart for Priebe's Method (from Priebe 1995)

The modified area replacement ratio as determined from Figure C.7 and Equation C.12, is plugged back into Equation C.11, or used in Figure C.6, and a revised value of improvement factor is determined. The new revised value of improvement factor is referred to as n_1.

As overburden increases, the columns are better supported laterally and thus, can provide more bearing capacity. To take into account the effects of overburden, as well as the bulk densities of the column and the soil, the improvement factor is adjusted, such that:

$$n_2 = f_d \cdot n_1 \qquad \text{(C.13)}$$

where n_1 = the revised improvement factor determined in the second step, and f_d = depth factor, which is represented as:

$$f_d = \frac{1}{\left[1 - \frac{y \cdot \sum(\gamma_s \cdot \Delta d)}{p}\right]} \qquad (C.14)$$

where y = an influence factor determined from Figure C.8, p = applied loading, and $\sum(\gamma_s \cdot \Delta d)$ = effective overburden stress. Priebe (1995) does not explicitly state where the effective overburden stress should be calculated. However, it appears in the design example provided by Priebe (1995) that the effective stress should be calculated at the same depth at which the vertical strain of the unimproved ground was determined for calculating the settlement of the unimproved ground. In Figure C.8, the ratio A/A_c represents the reciprocal of the area replacement ratio, $1/a_s$, after adjustment by Figure C.7.

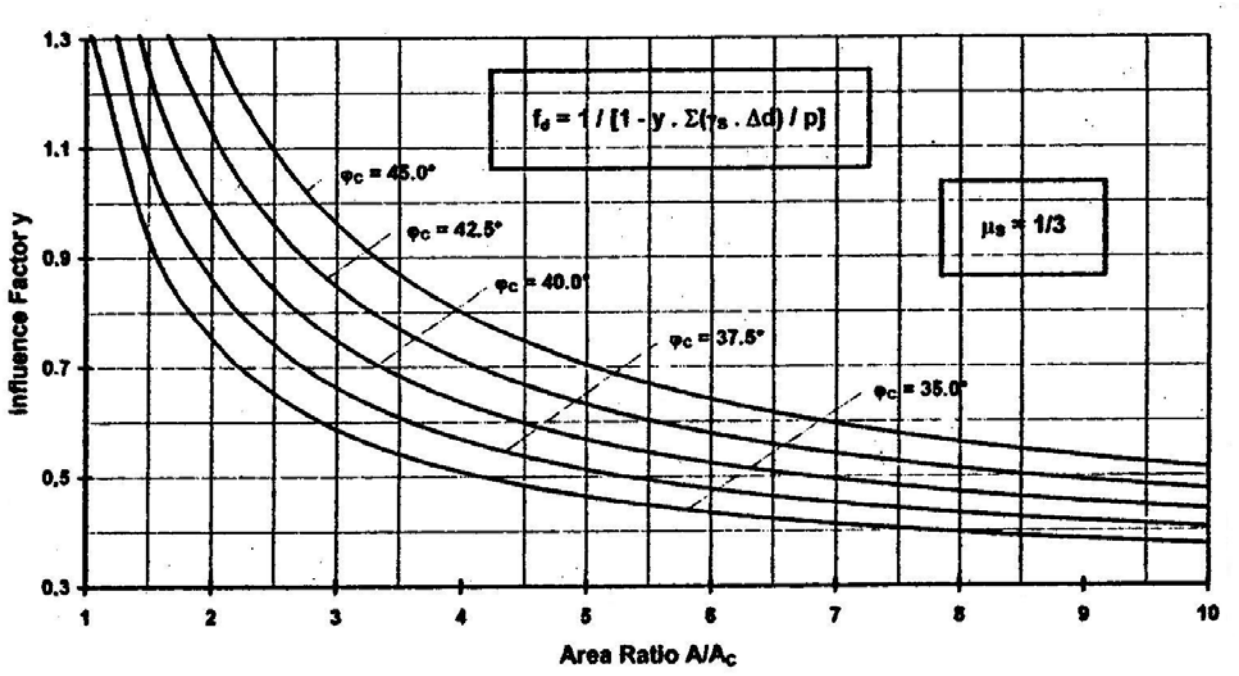

Figure C.8. Determination of the depth factor (from Priebe 1995)

A depth factor of $f_d < 1$ should not be considered, even though it may result from the calculation (Priebe 1995). Furthermore, an upper bound is applied to the depth factor, f_d. The upper bound value of the depth factor is determined based on Figure C.9.

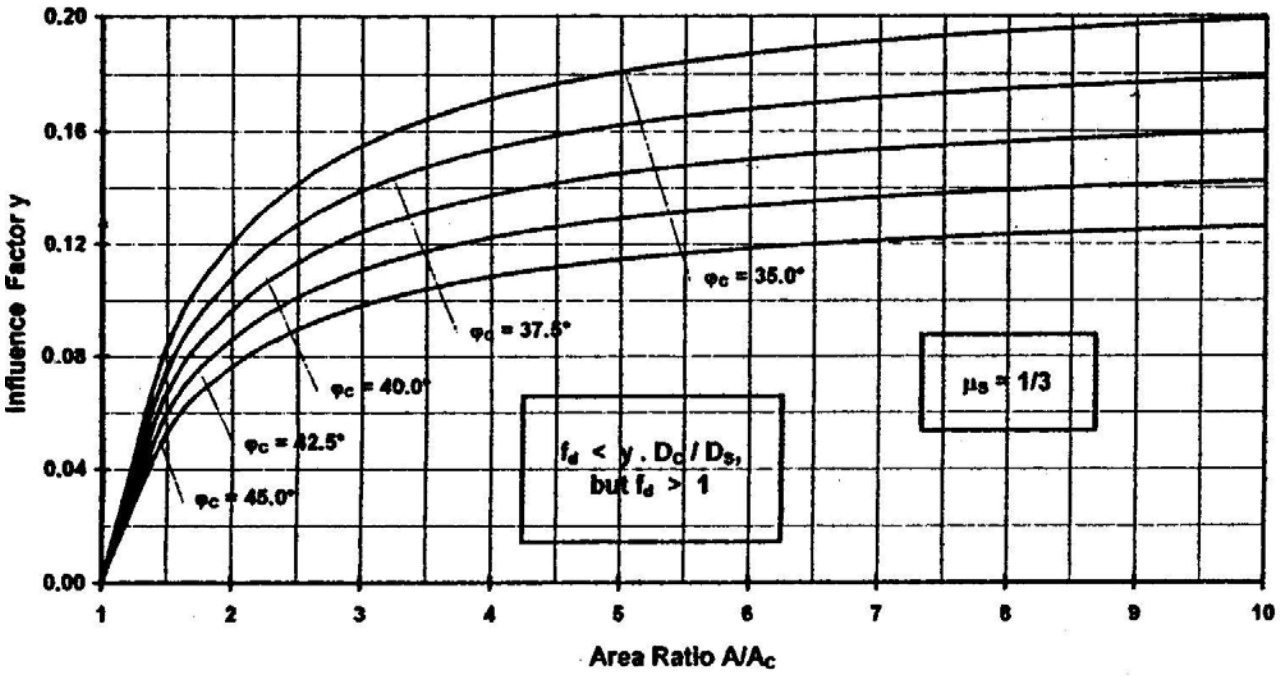

Figure C.9. Determination of upper bound depth factor (Priebe 1995)

An upper bound is also imposed on the improvement factor so that the calculated settlement of the columns does not exceed the settlement of the surrounding soil by the loads that are assigned to each (Priebe 1995). The upper bound improvement factor is given as:

$$n_{max} = 1 + a_s \cdot \left(\frac{D_c}{D_s} - 1 \right) \tag{C.15}$$

Finally, the settlement of the ground improved by stone columns, S_{imp}, is estimated by dividing the estimated settlement of the unimproved ground, S_{unimp}, by the improvement factor such that:

$$S_{imp} = \frac{S_{unimp}}{n_2} \tag{C.16}$$

C.5.2.3 Discussion of Settlement Analyses

The equilibrium method provides a simple analytical approach to estimating settlement. The effects of radial deformation, the stress-strain behavior of the column, and the increased confining pressure on the column with depth are incorporated indirectly through the use of the stress concentration ratio. The value of the stress concentration ratio, therefore, plays a large role when estimating settlement by the equilibrium method (Barksdale and Goughnour 1984). However, the value of the stress concentration ratio must be assumed.

The steps involved in Priebe's method are not connected mathematically and they contain simplifications and approximations (Priebe 1995). To fully utilize Priebe's method, a value of the ratio between the constrained modulus of the column and the soil must be assumed. With respect to the complexity of foundations improved by stone columns, the method is simple to use and is now widely recognized.

The methods presented herein to estimate settlement of ground reinforced with stone columns utilize the unit cell concept. The unit cell concept is valid for columns beneath the center of large loaded areas, but not for columns beneath the edges of the loaded areas or along the edges of a group of columns. For columns along the edges of a group of columns, Goughnour (in Barksdale and Goughnour 1984) recommends that only 75% of the actual area ratio be used since the columns are not confined on all sides.

Other researchers have provided chart-based methods to evaluate the settlement of stone columns. The incremental approach developed by Goughnour and Bayuk (1979) and Goughnour (1983) analyzes individual elements of the stone column idealized unit cell. In the incremental method, the stone column is assumed to be either elastic or elastic-perfectly plastic, and the clay soil is assumed to be elastic. Barksdale and Bachus (1983) performed a finite element study and created simplified design curves for estimating the settlement of stone columns in compressible cohesive soils. The finite element study featured a nonlinear analysis using Mohr-Coulomb failure criteria. These chart-based approaches for evaluating the settlement of stone columns are presented in detail by Barksdale and Bachus (1983).

C.5.3 Time Rate of Settlement

Stone columns may substantially increase the rate of consolidation since radial drainage is provided. The time rate of settlement calculations for stone columns are the same as those for sand drains. The effect of disturbance, or smear, during installation may be accounted for by decreasing the diameter of the column by 50 to 80% (Elias et al. 1999).

However, Barksdale and Bachus (1983) report that stone columns do not accelerate the time for secondary settlements, which can be significant in some very soft clays. Secondary settlements are difficult to predict, although they may be roughly estimated based on the secondary compression characteristics of the native clay. Secondary settlement may be an important consideration in many stone column projects. In many cases, the magnitude of secondary settlement may be reduced by surcharge loading (Elias et al. 1999).